AD-A125 810 APPLICATION OF THE WAVY MECHANICAL FACE SEAL TO SUBMARINE SEAL DESIGN(U) NEW MEXICO UNIV ALBUQUERQUE COLL OF ENGINEERING A O LEBECK ET AL. JUL 82 1/3

UNCLASSIFIED ME-117(82)ONR-414-1 N00014-76-C-0071 F/G 11/1 NL

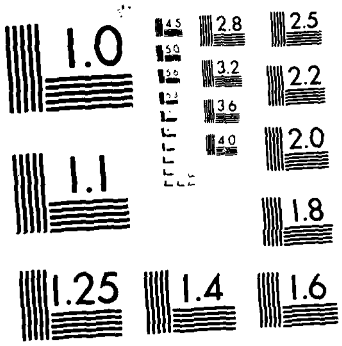

MICROCOPY RESOLUTION TEST CHART
NATIONAL BUREAU OF STANDARDS 1963 A

(12)

THE UNIVERSITY OF NEW MEXICO
COLLEGE OF ENGINEERING

AD A125810

BUREAU OF ENGINEERING RESEARCH

APPLICATION OF THE WAVY MECHANICAL FACE SEAL
TO SUBMARINE SEAL DESIGN

BY

A. O. LEBECK, L. A. YOUNG, K. L. WONG, AND J. KNOWLTON

REPORT NO. ME-117(82)ONR-414-1

WORK PERFORMED UNDER CONTRACT NO. ONR-N-00014-76-C-0071

JULY 1982

APPLICATION OF THE WAVY MECHANICAL FACE SEAL

TO SUBMARINE SEAL DESIGN

by

A. O. Lebeck
Professor of Mechanical Engineering

and

L. A. Young
Staff Engineer

K. L. Wong
Research Assistant

and

J. Knowlton
Research Assistant

The University of New Mexico
Department of Mechanical Engineering
and
Bureau of Engineering Research
Albuquerque, New Mexico 87131

Summary Report ME-117(82)ONR-414-1

July 1982

Prepared for the Office of Naval Research under
Contract Number ONR-N-00014-76-C-0071

SECURITY CLASSIFICATION OF THIS PAGE (When Data Entered)

REPORT DOCUMENTATION PAGE

READ INSTRUCTIONS BEFORE COMPLETING FORM

1. REPORT NUMBER	2. GOVT ACCESSION NO. AD-A125810	3. RECIPIENT'S CATALOG NUMBER
4. TITLE (and Subtitle) APPLICATION OF THE WAVY MECHANICAL FACE SEAL TO SUBMARINE SEAL DESIGN		5. TYPE OF REPORT & PERIOD COVERED Summary Report Dec. 1, 1980-July 31, 1982
		6. PERFORMING ORG. REPORT NUMBER ME-117(82)ONR-414-1
7. AUTHOR(s) A. O. Lebeck, L. A. Young, K. L. Wong, and J. Knowlton		8. CONTRACT OR GRANT NUMBER(s) ONR-N-00014-76-C-0071
9. PERFORMING ORGANIZATION NAME AND ADDRESS The University of New Mexico Albuquerque, New Mexico 87131		10. PROGRAM ELEMENT, PROJECT, TASK AREA & WORK UNIT NUMBERS
11. CONTROLLING OFFICE NAME AND ADDRESS Director, Power Program Dept. of the Navy - Office of Naval Research Arlington, Virginia 22217		12. REPORT DATE July 1982
		13. NUMBER OF PAGES 205
14. MONITORING AGENCY NAME & ADDRESS (if different from Controlling Office)		15. SECURITY CLASS. (of this report) Unclassified
		15a. DECLASSIFICATION/DOWNGRADING SCHEDULE

16. DISTRIBUTION STATEMENT (of this Report)

Approved for public release; distribution unlimited.

17. DISTRIBUTION STATEMENT (of the abstract entered in Block 20, if different from Report)

18. SUPPLEMENTARY NOTES

19. KEY WORDS (Continue on reverse side if necessary and identify by block number)

Mechanical Seals, Seals, Face Seals, Lubrication, Wear, Friction, Waviness

20. ABSTRACT (Continue on reverse side if necessary and identify by block number)

In this report the results of theoretical and experimental investigations on the effects of waviness on mechanical seal performance are presented. In addition, the design techniques, design, and test results for a nine-wave small scale submarine seal are presented.

(continued on reverse)

DD FORM 1 JAN 73 1473 EDITION OF 1 NOV 65 IS OBSOLETE

SECURITY CLASSIFICATION OF THIS PAGE (When Data Entered)

The nine-wave seal has been shown to operate satisfactorily in preliminary testing. Problems with fabrication, stiffness, bonding, and oil system sealing were encountered and solved. Test results show friction to be somewhat higher than predicted. Leakage is very low. Further tests are being conducted. Further testing on balanced parallel face seals is reported. Details of test machine modifications required to operate in a simulated submarine environment are given.

Complete details of the design methodology and the details of the nine-wave seal design are given. The design of a device to create variable mis-alignment during testing is also given.

The moving waviness concept has been applied to the design of a gas seal. Certain advantages of using moving waviness compared to other designs are noted. A complete theoretical-numerical analysis of moving wave gas seal performance is made. Parameter studies are performed. Results show very low leakage and friction. Potential problems are discussed.

Progress was made on solving the general problem of determining the precise contact pattern of two seal rings pressed together. This problem is important in assessing seal leakage problems. A new, general, coupled (in- and out-of-plane), ring finite element was developed and checked. Simple beam contact problems were solved using finite element methods. The final solution requires combining the finite element and the contact problem.

Conclusions and recommendations are made.

APPLICATION OF RESEARCH TO THE NEEDS OF THE U.S. NAVY

Mechanical face seals are used in numerous applications in Naval machinery. These applications range from propeller shaft seals to boiler feed pump seals. In such equipment the mechanical seal plays a vital role. When such seals fail, repair is costly both in terms of lost time and direct costs, so any improvement in seal life and reliability would be of significant benefit.

As more advanced equipment is designed, it is sometimes difficult to achieve desired performance in more severe service environments with the present state of the art of seal design. Thus, an improvement in seal technology would serve this important application.

One objective of the research herein is to further the understanding of mechanical face seal lubrication phenomena. Another objective is to develop the capability of designing contacting face seals having a longer life, greater reliability, and for extreme environments. The immediate objective herein is to apply the knowledge gained to the design of a small scale submarine type seal. Thus, the objectives of this research are compatible with mechanical face seal needs for Naval machinery.

TABLE OF CONTENTS

TABLE OF CONTENTS (continued)

LIST OF FIGURES

LIST OF FIGURES (continued)

LIST OF TABLES

LIST OF SYMBOLS

a	Ring cross sectional area - m^2
$A = \frac{EJ_x}{GJ_\theta}$	Stiffness ratio - dimensionless or area - m^2
b	Fraction of seal subject to fluid pressure
$B = \frac{r_o^2 - r_b^2}{r_o^2 - r_i^2}$	Balance ratio for an outside pressurized seal
c	One-half maximum roughness height - m
d	Diameter of gas pressure hole and parameter as defined - m
e	Distance between gas pressure hole center and centroid - m
$e_1 e_2$	Eccentricities as defined - m
E	Youngs modulus - N/m^2
$E(\ )$	Expectancy operator
$f(h_s)$	Roughness distribution function
F	Force - N
G	Shear modulus - N/m^2
h	Nominal film thickness - m
h_n	Amplitude of the nth harmonic - m
$\bar{h} = \frac{h}{c}$	Dimensionless film thickness
h_o	Nominal film thickness or minimum film thickness (between mean roughness heights) - m
H	Film thickness in difference equation - m

I_x, I_y, I_{xy}	Approximate values of J_x J_y J_{xy} based on straight beam theory
$J_x = \int_A \frac{y^2}{1 - x/r_c} dA$	Stiffness constant about x axis for ring cross section - m^4
$J_y = \int_A \frac{x^2}{1 - x/r_c} dA$	Stiffness constant about the y axis for ring cross section - m^4
$J_{xy} = \int_A \frac{xy}{1 - x/r_c} dA$	Stiffness constant - m^2
J_θ	Torsional stiffness constant for ring cross section - m^4
K	Ratio of contact radius to inside radius or stiffness matrix
ℓ	Length of beam element - m
m_θ, m_{θ_o}	Distributed moment and amplitude on seal ring - N • m/m
m_r, m_θ, m_v	Mass flow rates kg/s
M_x, M_y, M_θ	Ring moments - N • m
n	Number of the harmonic or number of waves around seal face or normal direction
N_θ	Ring normal force - N
p, P	Fluid pressure - N/m^2
p_c	Cavity pressure - N/m^2
p_g	Gas pressure amplitude causing waviness - N/m^2
p_i, P_i	Seal inside pressure - N/m^2
p_m, P_m	Pressure at asperity contact--equals compressive strength - N/m^2
p_{m_a}	Average mechanical contact pressure - N/m^2
p_o, P_o	Seal outside pressure - N/m^2

p_s, P_s	Shear strength of asperities - N/m^2
p_{sp}, P_{sp}	Spring pressure on face - N/m^2
Q	Total leakage for the seal - m^3/s
$Q = p^2$	Pressure squared used in A.D.I. method
$\tilde{Q}$	Assumed known value at previous time step
Q_{in}	Fluid leakage across the inside face
Q_{out}	Fluid leakage across the outside face
r	Radial coordinate
r, θ, z	Seal coordinates
r_b, R_b	Seal balance radius - m
r_c	Radius to centroid of seal ring - m
r_f	Friction radius - m
r_i, R_i	Inside radius of seal - m
r_o, R_o	Outside radius of seal - m
R	Radius to centroid of seal ring - m
R	Radius of the control volume center - m
S_u, S_y, S'_e	Ultimate strength, yield strength, fatigue strength - N/m^2
S	Stiffness of the gas seal - N/m
SCFM	Standard cubic feet per minute
SCMM	Standard cubic meter per minute
t	time - s, bond thickness - m
T_q	Seal friction torque - N $\cdot$ m
u, v, w, ϕ	Ring displacements
U	Velocity - m/s or energy - N $\cdot$ m

v, v_o	Ring centroid di· ·lacement and amplitude - m
V_x, V_y	Ring shear forces - N
$V_{r,\theta,z}$	Velocity components
x, y, θ	Ring coordinates
$w(r)$	Seal wear as a function of radius
W	Total load support - N
W^*	Required load support - N
$\alpha_1\alpha_2$	Angle as defined
$\beta_1\beta_2$	Angle as defined
Δa	Differential area of control volume
ΔA	Differential area in difference form
$\Delta\theta$	Differential change in angle of control volume
ΔR	Differential change in radius in finite difference form
ΔT	Time step in A.D.I. method
∇	Gradient
γ	Angle as defined
δ	Displacements
η	Viscosity - N · s/m^2
θ	Angular coordinate or flow variable
ϑ	Angular coordinate
Λ	6 $\omega\eta$
μ	Friction coefficient or Poisson's Ratio
ξ, ξ'	Angles as defined
ρ	Density - kg/m^3

τ_a	Asperity shear stress - N/m^2
τ_f	Fluid shear stress - N/m^2
ϕ	Rotation of seal ring about its centroid
ϕ_o	The maximum rotation of the seal
ω	Angular speed
Ω	Angular speed of waviness - 1/s
%	Percent of load supported by fluid pressure
-	All symbols with bar are dimensionless as defined.

CHAPTER 1
INTRODUCTION

Mechanical Face Seals

Applications of face seals range from water pumps to compressors, to power pumps, to propeller shafts. In many applications the reliability of the mechanical seal is of the greatest importance to the reliability of the equipment itself.

Mechanical face seal technology has been steadily improving over the past several decades. However there still remain demands for seal performance which have not been met. One such application of note is the submarine propeller shaft.

Such demands on a particular technology can often be satisfied by first improving the technology. In the case of mechanical face seals, the main barrier to advancement has been that the mechanics of seal operation are not well enough understood to be able to reasonably anticipate seal performance as a function design parameters.

During the past five years of this research program, much has been learned about controlling the hydrostatic and hydrodynamic mechanisms which enhance face seal operation. In this work, this knowledge is applied to the design of an improved small scale submarine shaft seal. Theory, design, and test results are presented. The results show promise that significant improvements in submarine shaft seal design are possible, and the application of such designs could greatly increase the length of trouble-free shaft seal service.

Seal Lubrication

As background, the mechanical face seal consists basically of two annular rings which rotate relative to each other and which are pressed together by spring and fluid pressures (see Figure 1-1). In conventional seals, the surfaces that rub

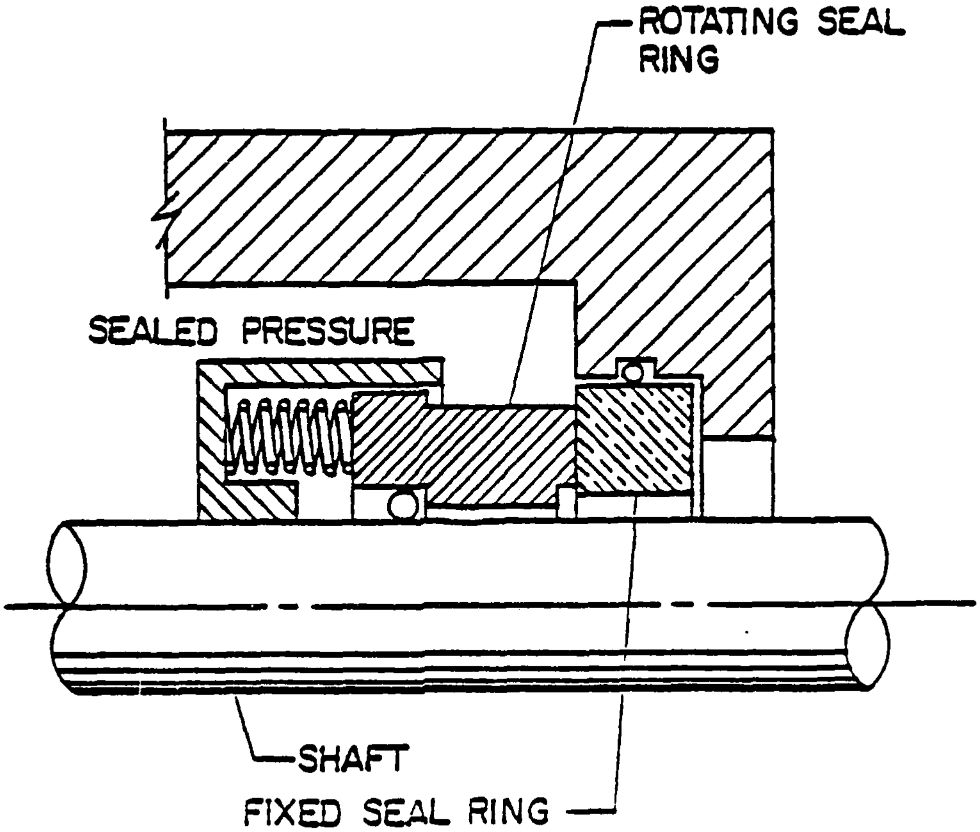

Figure 1-1. Mechanical Face Seal.

together are generally manufactured as flat as possible initially so as to minimize leakage. The effective gap between the faces is ideally quite small (order of 1 μm) so that leakage flow across the faces will be quite small. The difficulty in designing a mechanical seal is in maintaining the gap at a very low value while at the same time providing a definite lubricant film between the faces.

The load that must be supported at the faces of a mechanical seal is due primarily to loading caused by the sealed pressure. The load support at the faces is derived from fluid pressure and mechanical pressure. If the fluid pressure at the faces is large enough to support all of the load, then there will be no contact and no adhesive wear.* If none of the load is supported by fluid pressure, the load must be carried by mechanical contact, and the wear rate will be large.

In practice, conventional seals often operate at one of two extremes. At one extreme, a large gap will be created by hydrostatic or hydrodynamic pressure or distortion, all of the load will be supported by fluid pressure, and the seal will leak a lot and wear very little. At the opposite extreme, the gap will close completely. Leakage will be low but only a fraction of the load will be carried by fluid pressure, and wear and heat generation will increase.

Based on the above, it can be concluded that an effective seal should operate between these two extremes--having both adequate fluid pressure load support and low leakage. The seal should operate so that it just touches to minimize leakage but such that the load is carried by fluid pressure. To do this

---

*There may still be abrasive or corrosive wear even if the surfaces do not touch.

requires that any fluid pressure generation mechanism used to provide load support to the seal must be very carefully controlled. At present in commercial seals, this is left primarily to chance and sometimes seals operate at one of the undesirable extremes mentioned.

In this research program, attention has been devoted toward studying the effects of waviness as a source of controlled hydrodynamic and hydrostatic load support. Waviness was selected because it is controllable. In this present work, waviness has been applied as the basis for the design of an improved small scale submarine shaft seal.

Background

ONR-sponsored research on mechanical seals had been conducted for five years prior to the beginning of the submarine seal design phase described herein. The work being reported evolved from various discoveries over this five year period, and the past work must be reviewed to better understand the nature of the current work.

As a starting point for this Navy research program, the effects of waviness on seal performance were modeled in some detail. In the first annual report for this project, Reference [1], this general problem was solved using a one-dimensional theory. In the second annual report, [2], the much more complex two-dimensional solution to the above problem was solved. The effects of waviness, roughness, asperity contact, wear, cavitation, and elastic deflection were included in this model. Using this model, predictions were made for the relative wear rate, friction, and leakage as a function of roughness, waviness, speed, size, pressure, viscosity, and material.

A number of conclusions were reached based on these first two annual reports:

1) The effects of roughness on hydrodynamic lubrication are not completely understood. Certain fundamental questions remain concerning the roughness model used.
2) As to the potential of utilizing hydrodynamic effects caused by parallel face waviness to advantage by design, the results show that wear rate and friction can be greatly reduced while maintaining leakage at acceptable levels.
3) While a comparison of predicted results to experimental results given in the literature is generally good, data contained in the literature is incomplete, so more complete experimental data are needed for comparison.
4) In low viscosity or heavily loaded applications where some touching is expected to occur, waviness will wear away with time and any benefit derived will be lost unless something is done to counteract this effect.
5) Based upon data for some commercial seals and using the model, it was determined that there was insufficient accidentally caused waviness to produce significant hydrodynamic effects in water. One cannot generalize to say that such effects do not occur in commerical seals. However, using the model the question can be answered on a case by case basis.

Item 1) was treated extensively in the third annual report [3]. Even after this analysis certain fundamental questions remain concerning how to deal with roughness in lubrication problems. However, this thorough analysis led to conclusions allowing certain simplifying assumptions discussed in the fourth annual report [4].

Item 2) was also treated extensively in the third annual report [3]. A methodology for the design of a wavy face seal was developed and applied. Theoretical results showed large reduction in friction and wear rate compared to conventional designs whereas leakage could be controlled.

Concerning Item 3), the second and third annual reports [2,3] describe a test apparatus designed to test the wavy seal theory. This apparatus has been in operation for more than three years and many tests have been conducted. These test results are reported in the fourth and fifth annual reports [4,5].

Early in the test program it was observed that the type of waviness which can be practically applied is not of the radially parallel type. Waviness generally consists of alternating tilt plus radially parallel waviness. Based on these considerations, a new model for predicting performance was developed and appears in the fourth annual report [4].

Concerning Item 4) above, a solution to this problem was first proposed in the first annual report [1]. It was proposed to move the waviness slowly around the seal so that whatever wear occurred would be uniformly distributed. Then the shape of the wave would be preserved and tests using a constant wave could be made. The concept is illustrated in Figure 1-2. This concept was incorporated into the test apparatus and is described in detail in References [2] and [3]. In the fifth annual report [5], a new concept to move the waviness with no internal moving parts is described in detail.

In the fifth annual report [5], additional experimental results using waviness are presented, the wavy seal model is further improved, and theory and experiment are compared. The results using a new concept, that of a self-generating seal profile, are reported. Results from tests of the effects of radial taper and high temperature environment are also reported and compared to theory.

In summary, both the theoretical and experimental basis for applying waviness to a mechanical seal to reduce friction and wear were well established during these first five years. In the present work, the waviness concept is applied to the design of a long life submarine shaft seal as described later.

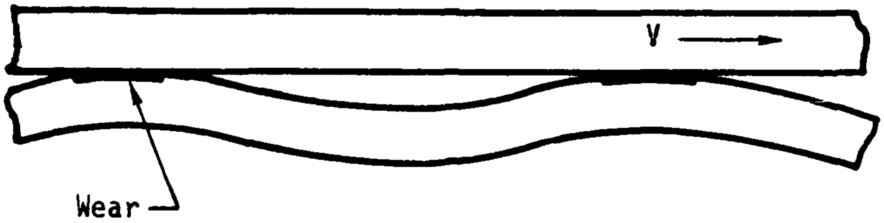

Distorted Ring

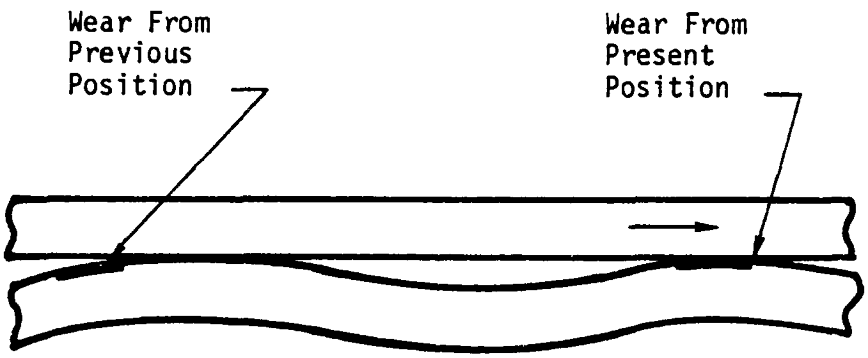

Distorted Ring After Wave Has Moved

Figure 1-2. Moving Waviness Concept.

The results developed to date and discussed in the five annual reports are also presented in several papers and theses [6-24].

Wavy Face Seal

The concept of waviness is that the film thickness varies in some fashion circumferentially around the seal. Generally speaking, film thickness may vary radially as well as tangentially.

$$h = h(r, \theta) \; . \tag{1-1}$$

In the present work interest is focused upon film thickness shapes of the following functional form

$$h = h_0 + f(r) \cos n\theta \; . \tag{1-2}$$

At any particular radius r the film shape is periodic with n waves around the seal and is therefore wavy. However, film shape can also vary in some general manner with r.

If $f(r) = \text{const}$ then the faces are always radially parallel. This component of film thickness variation is commonly termed waviness. If $f(r) \neq \text{const}$, then the faces are not in general radially parallel. $f(r)$ is referred to as tilt. Thus, the film thickness shapes of interest are combinations of waviness and tilt. Since at any radius the film thickness is wavy, the combination of waviness and tilt defined above will also be called a wavy film shape.

The reason for choosing film shapes as described by Equation (1-2) as a subject for study is that these shapes can conveniently be generated by planned mechanical distortions in a seal ring, and the shapes also include common modes of unplanned distortion found in operating seals. For example, generally seals undergo a uniform tilt due to pressure and thermal deformation. When rings are loaded by any nonaxisymmetrical load they become wavy as described by Equation (1-2).

Now, for the sake of illustration, assume a seal has a wavy film thickness shape given by Equation (1-2) where $f(r)$ is a linear function of r. This gives a film shape as shown in Figure 1-3 where for each of the n periods the seal touches all across at one point and is radially convergent π/n radians away. At any radius, the seal is wavy circumferentially. The waviness enhances hydrodynamic effects and the radial convergence enhances hydrostatic effects.

It is this shape which previous research [1-5] has shown has the greatest potential to reduce friction and wear while holding leakage at very low levels. This is the film shape used for the design of the small scale submarine seal.

Submarine Seal

The general objectives of the present three-year contract phase are:

1) to conduct further experiments using moving waviness to further the understanding of this concept.
2) to refine mathematical models already developed so as to be able to better predict performance.
3) to demonstrate in a practical way the use of the concept of moving waviness to reduce friction and wear in mechanical seals.
4) to undertake the development needed to be able to demonstrate the applicability of the concept to submarine shaft seals and to design a full scale long life seal.
5) to explore other uses of the waviness concept such as for gas seals and to create better methods by which the concept can be applied.

From these objectives, the following specific tasks have been defined.

1) Design, fabricate, and test a nine wave optimum seal. As shown in the previous annual report [5], nine waves

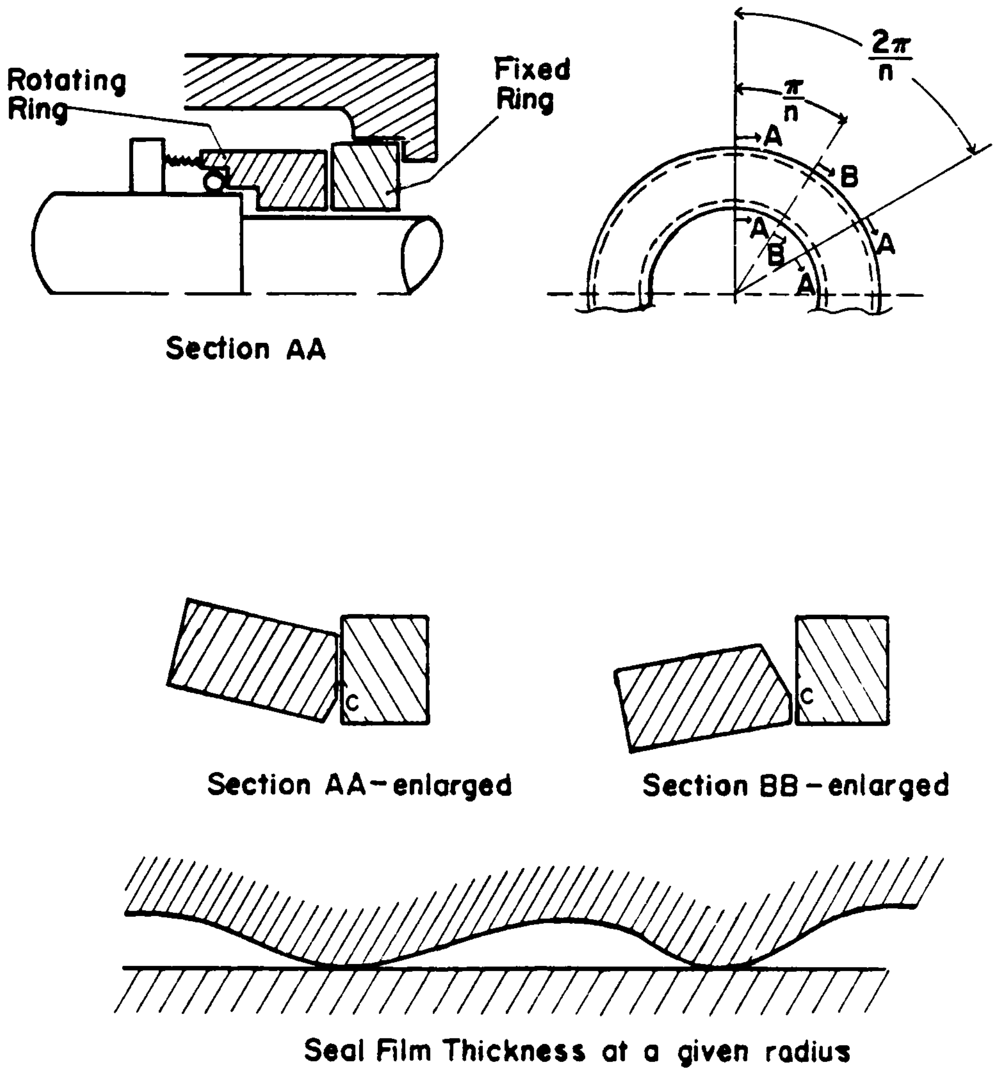

Figure 1-3. Mechanical Seal with Waviness and Tilt.

are needed to minimize changes in tilt with changes in pressure and speed.

2) Operate the seal for an extended period of time under simulated submarine operating conditions including seawater and changing speed, pressure, and alignment.
3) Evaluate compliancy of existing and proposed submarine seals.
4) Conduct friction and wear tests on carbon and hard face materials.
5) Seek alternate methods of applying moving waviness.
6) Perform analysis of a moving wave gas seal.

Progress has been made on all of these tasks, and the report to follow details the research efforts and achievements for the period December 1, 1980 through June 30, 1982.

CHAPTER 2
EXPERIMENTAL RESULTS

A nine-wave seal has been designed, fabricated, and tested during this reporting period. The test apparatus has been modified to automatically change operating conditions, and a 75 percent balance ratio test has been completed. In this chapter these results will be reported.

Nine-Wave Seal

Design--The first item to be reported is the design of the nine-wave seal (the design procedure is discussed in Chapter 3; the design itself is discussed here). Figure 2-1 shows the assembly drawing of the nine-wave seal. Starting at the left, one of three sinusoidally varying pressures generated by the waviness drive unit [5] is directed into two (180° apart) of six pressure channels 1 in the waviness cylinder 2. The pressurized fluid then passes through the pressure coupler 3 and is ported to one of three circumferential channels on the left end of the waviness adapter 4. Eighteen smaller passages, connected to each of the three circumferential channels, terminate at pressure pockets 5 located on the inside and outside diameters of the waviness adapter 4 (right-hand end). The 54 pressure pockets (three sets of eighteen) apply a waviness pressure to the 54 "fingers" of the nine-wave seal 6.

Figure 2-2 shows a modified isometric cross section of the nine-wave seal. The pads shown are labeled with a 1, 2 or 3 depending on the termination point of the three sinusoidally varying pressures, i.e., one pressure, say, P_1, exerts a wave producing load on all pads labeled with a 1. The load on all outer pads is directed outward on the inside radius and the load

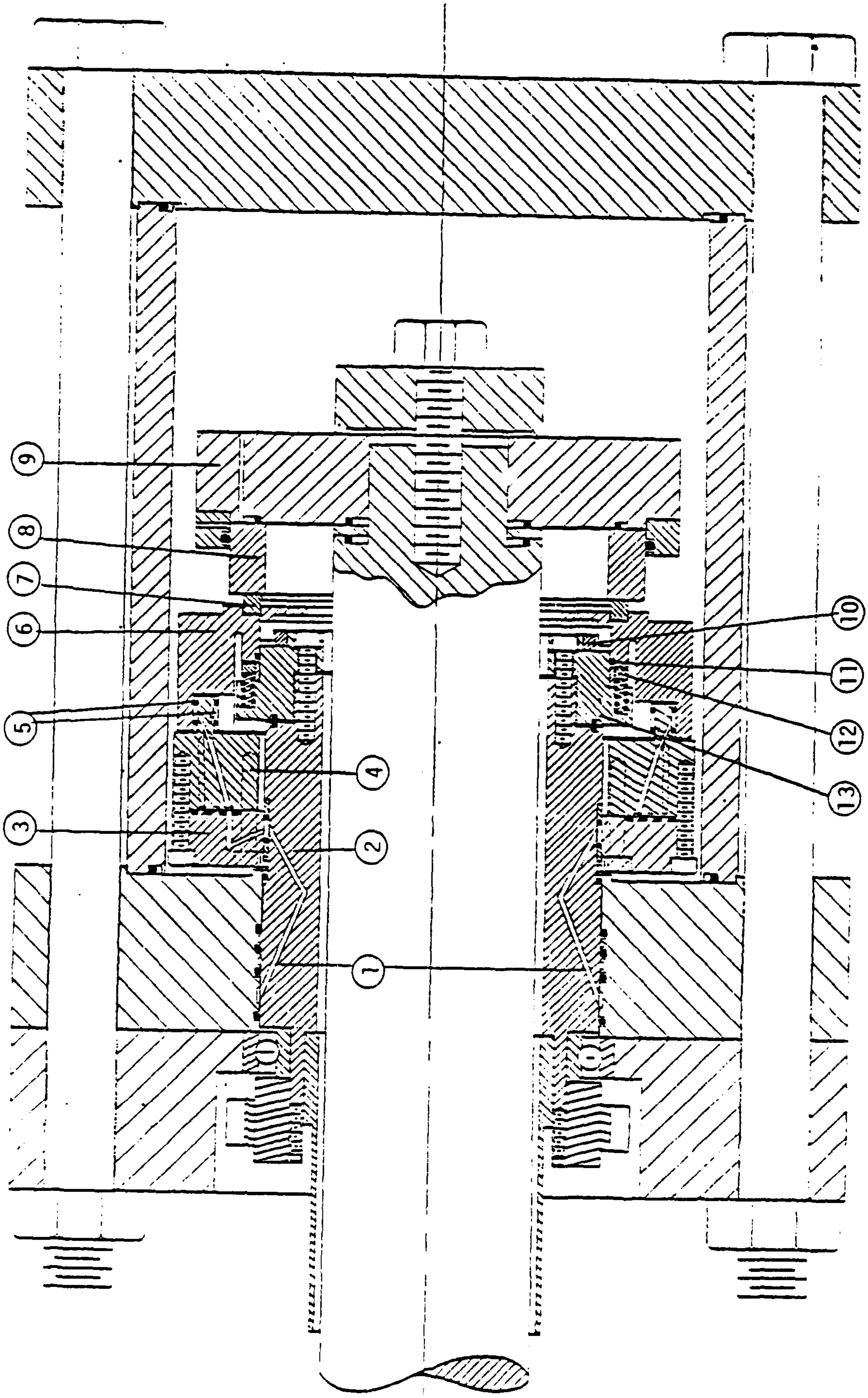

Figure 2-1. Nine-Wave Seal Assembly View.

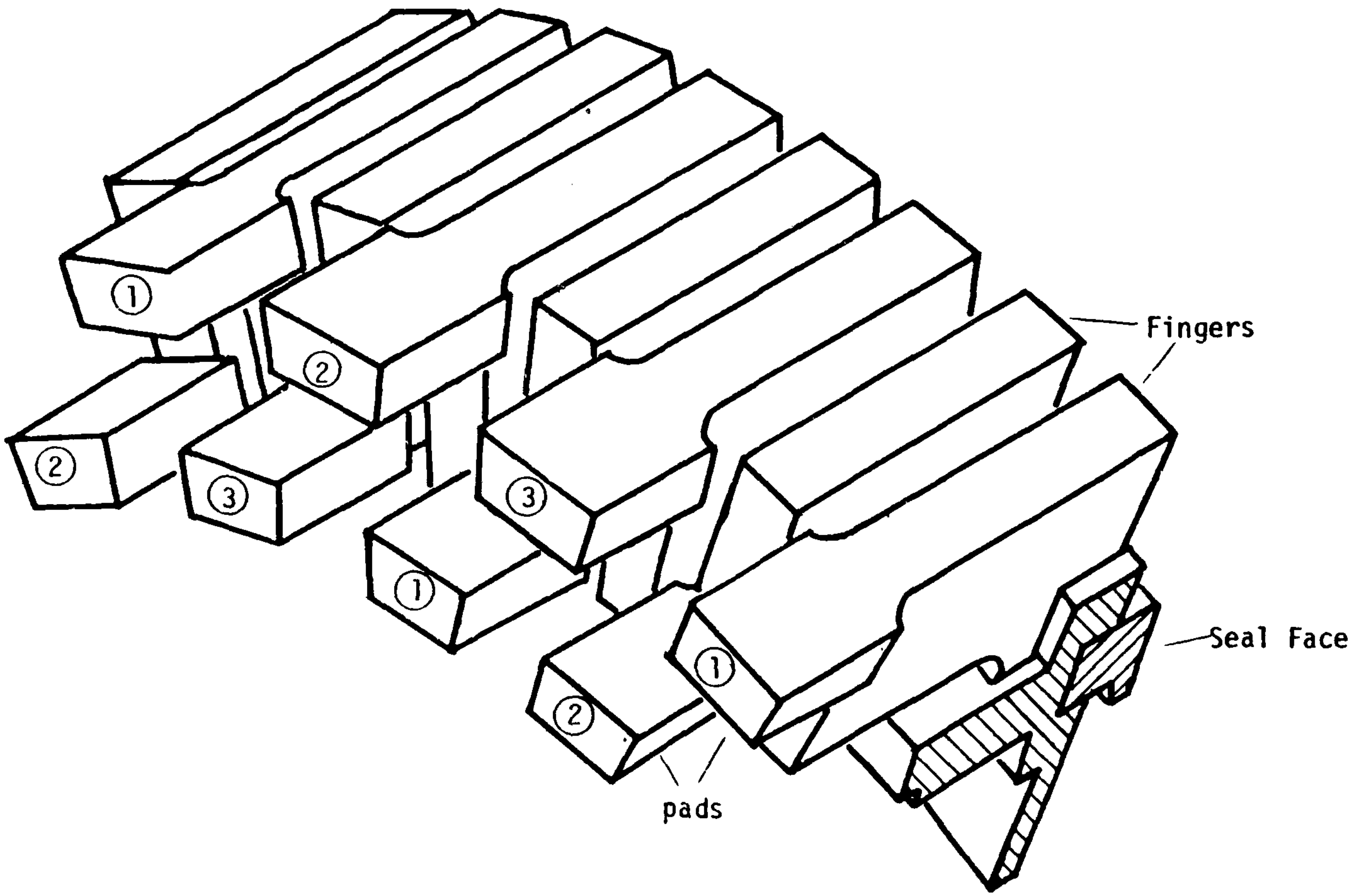

Figure 2-2. Nine-Wave Seal - Modified Isometric Cross Section.

on all inner pads is directed inward on the outside radius of the corresponding pad. With this configuration three sets of nine waves each can be imposed on the face of the carbon insert. As discussed previously [5], by sinusoidally varying the three separate pressures (and waves) with time, the result is one set of nine waves which moves circumferentially around the seal with time.

The irregular shape of the nine-wave seal (cross section) is due in part to the adjustments made on the geometry so as to obtain a zero moment design, i.e., there is no rotation of the seal about a circumferential axis due to pressure variation. Other reasons include the need for a low stiffness, so that the wave could more easily be transmitted to the carbon insert 7, and the need for the centroid to be placed at such a location so that the wave contact point, between the carbon insert 7 and the silicon carbide seat 8, is radially located for optimum seal performance.

The secondary seal 11 is located at the left end of the nine-wave seal on the inside diameter. Springs to the left of the seal, housed in the seal ring spring retainer 13, provide preload through the spring seat 12. The balance ratio for the design shown is unity.

The carbon insert 7 is a Pure Carbon P658RC material which is epoxied into the nine-wave seal using 3M 1838 B/A adhesive. It should be pointed out at this time that the carbon insert, as shown in Figures 2-1 and 2-2, has a small lip on the inside radius. This lip has a slight relief ground into it, approximately 76 μm deep in the axial direction and 500 μm deep in the radial direction, for purposes of wear measurements.

The drive ring 10 is designed so that the primary ring can float and align itself but cannot rotate about the shaft axis. The nine-wave seal therefore takes its alignment from the face of the rotating secondary ring. The secondary ring is a Carborundum KT® silicon carbide material which is also of zero moment design.

Modifications--Modifications to the overall design were made in light of the results obtained from preliminary testing. Figure 2-3 shows the original design cross section of the nine-wave seal. The original cross section shape, as mentioned earlier, was designed to meet specific requirements, and as a result, does not adhere closely to the assumptions used for the ring equations used to predict waviness. Bench tests to measure waviness on the carbon face showed that less than half of the needed waviness was present. Torsional deformation is predominant and for this particular shape and mode of deflection, warping becomes of considerable importance and as a result increases the stiffness. The addition of a warping factor to the design analysis did indeed show that the original cross section was much too stiff. To reduce the stiffness and maintain a zero moment design the cuts as shown in Figure 2-4 were made to the seal.

Another problem encountered was that of the epoxy bond between the carbon insert and the seal. The original design called for a 0.0254 cm (0.01 in.) bond thickness around the carbon insert. Static tests done with 100 percent sealed pressure and with a convergent taper (400 μm/m) lapped into the carbon face showed that the epoxy bond "creeped" in 24 hours. Final traces of the radial profile showed no taper at all. As discussed in detail later, several bonding techniques were experimented with. These included the use of Loctite Speedbonder 319, with and without a primer, Loctite Superbonder 420 with the addition of two stainless steel rings for the inner and outer diameter of the carbon insert to give a near zero clearance fit, and the use of the 3M 1838 B/A epoxy also with the same stainless steel rings. Static and dynamic tests on the seal under water pressure and independent tests on the strength of each adhesive showed that the 3M 1838 B/A epoxy with the stainless steel spacer rings was the best method of bonding.

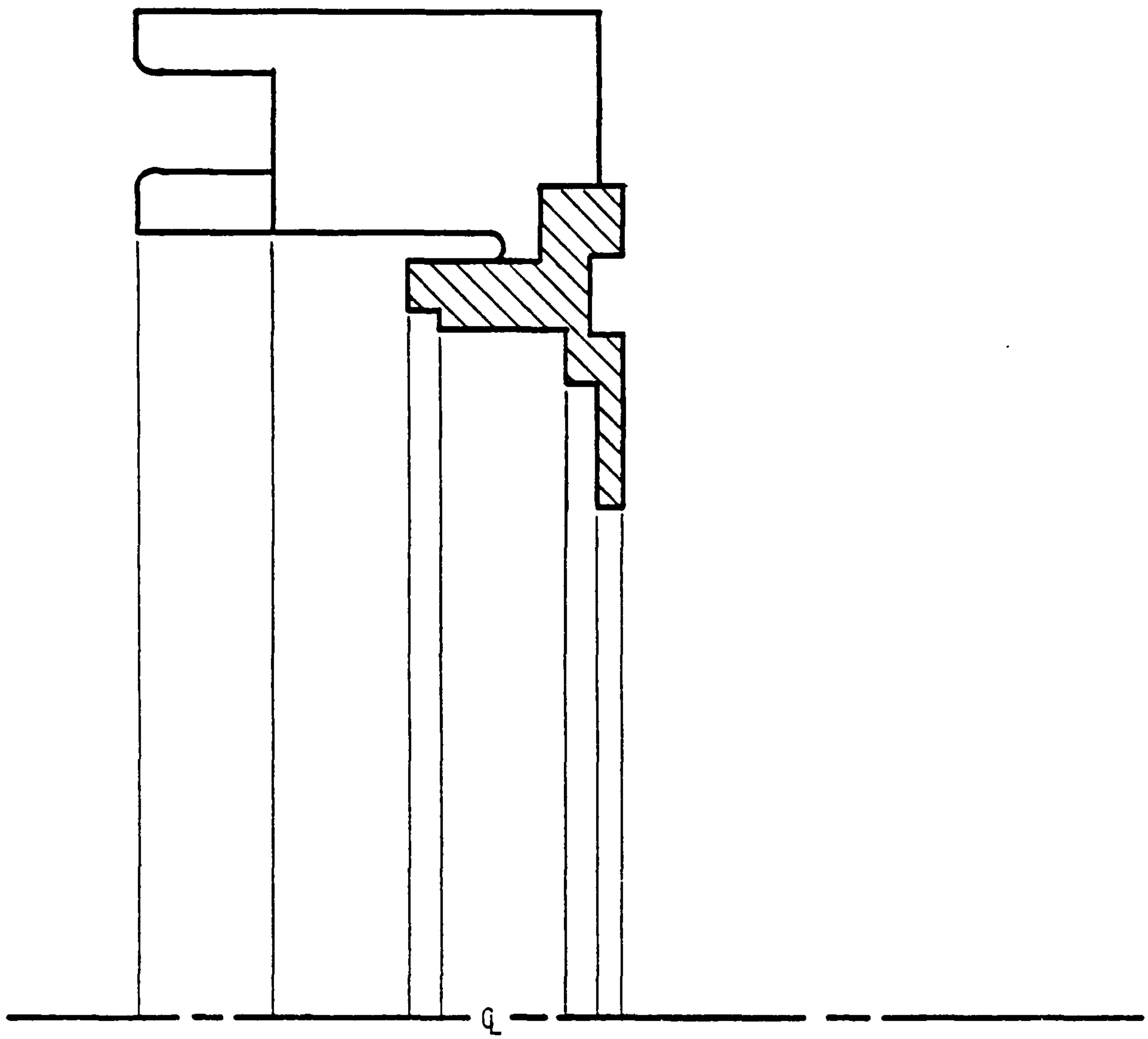

Figure 2-3. Original Design Cross Section.

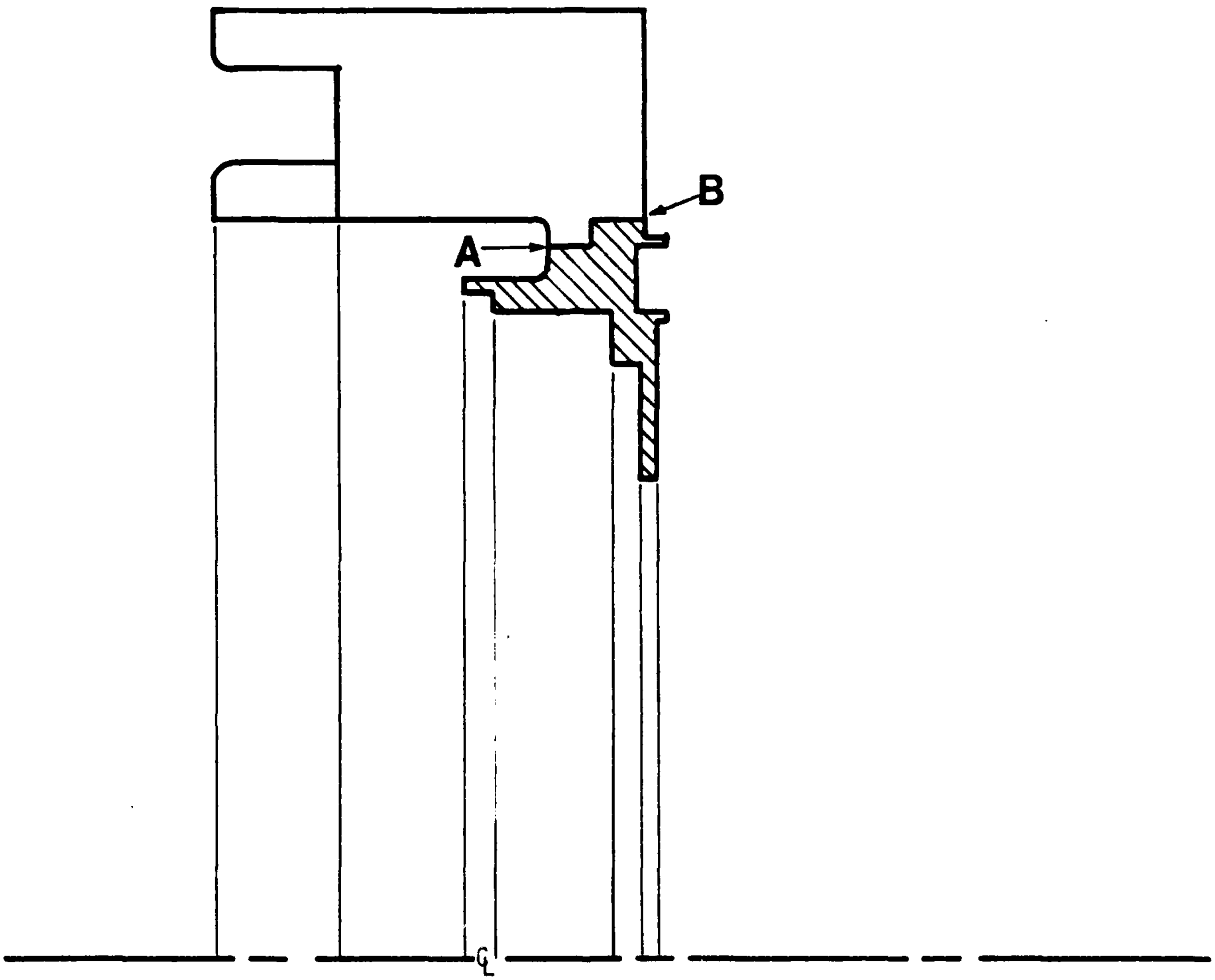

Figure 2-4. Actual Working Cross Section.

By lowering the stiffness another problem developed and hence a design change was needed. Figure 2-5 shows the original O-ring configuration. By lowering the stiffness, the "fingers" were subject to greater deflections which resulted in the O-rings extruding out from under the pad sections. Even with recommended clearance, O-ring extrusion was discovered to be a problem simply because the cyclic motion of the clearance proved to aid extrusion by somewhat of a ratchet mechanism. To remedy this problem, the waviness rings were ground down in thickness to incorporate a spacer, and a piston pad with a smaller O-ring cross section were added (Figure 2-6). This now allowed the "fingers" to flex and the O-rings to be contained without leakage and without extruding.

Waviness Measurements--As an aid to understanding the problem with creating sufficient waviness, a means of measuring waviness outside the seal environment was devised. A fixture was made which can pressurize one set of 18 pockets at one time using gas pressure. With one set of pockets under pressure the seal ring was placed on a precision rotary table. The table rotates and the stylus of the surface analyzer was placed so as to read axial displacement near the O-D of the carbon. The signal was digitized and a Fourier analysis of waviness components was made. Using this techique, the nine-wave component was easily picked out. Table 2-1 shows the results of the many measurements taken to analyze the waviness problem.

Test Results--A series of six seal tests were run with the new nine-wave seal. The tests occurred at different points in the modification process mentioned before. As a result, the tests must be carefully compared to one another. Only the performance of Test No. 117 can be evaluated for comparison to theory as a final design seal.

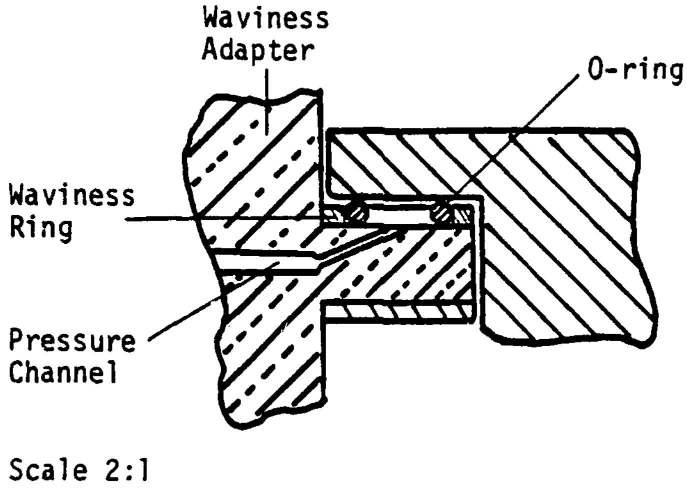

Figure 2-5. Original O-Ring Configuration.

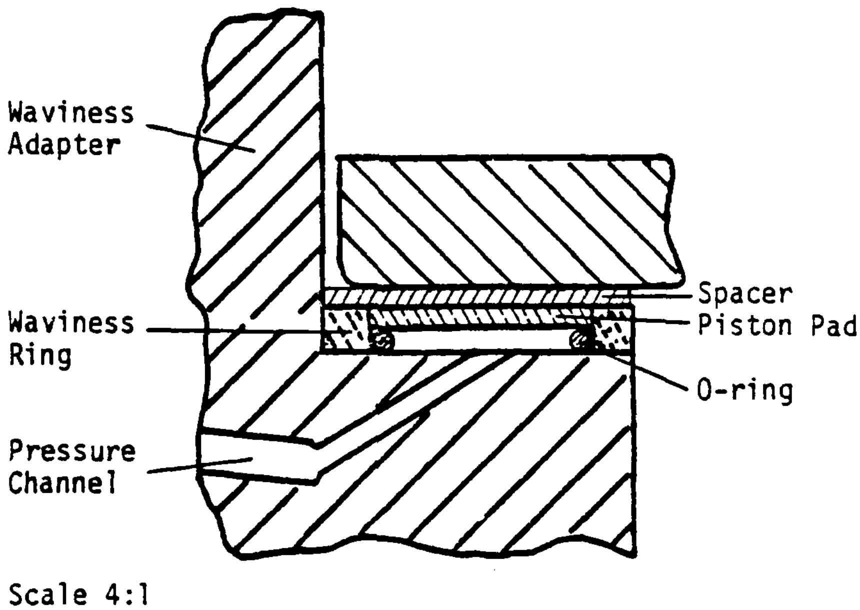

Figure 2-6. Final O-Ring Configuration with Piston Pads.

Table 2-1

Nine-Wave Amplitude Study
Waviness Amplitude Near Seal O.D.

Date	h_9	P_{test}	h_9* @1500 psi	Conditions
6/28	33	750	66	Close gap epoxy bond, 54-0.030 pads
6/28	59	1390	64	Close gap epoxy bond, 54-0.030 pads
6/16	80	1150	104	Close gap epoxy bond, 18 O-rings only
6/16	65	1050	93	Close gap epoxy bond, 18 O-rings only
6/4	123	1175	157	Groove bottom, 18 O-rings
6/4	129	1200	161	Groove bottom, 18 O-rings
6/2	29	1500	29	Super Glue - after test run, 90 Durometer
6/2	23	1500	23	Super Glue - after test 70 Durometer O-rings
4/7	72	1500	72	Carbon-thick bond epoxy after final x-section modification
4/6	73	1500	73	Carbon-thick bond epoxy after final x-section modification
3/27	54	1500	54	Carbon-thick bond epoxy before final x-section change
3/15	16	1500	16	After first test - thick epoxy

*Two times the effective waviness pressure in operation.

Table 2-2 shows the results of the tests performed. Test No. 112 (Figure 2-7), first of the series, was run where the carbon insert had a bond line of 0.0254 cm 3M 1836 B/A adhesive. The initial torque levels were quite high, approximately 14 N•m. There was one shutdown at 16 hours into the test due to excessive torque levels. The performance of this test was not as expected.

It was at this point that the stiffness of the seal ring was re-analyzed and as a result, a warping factor was incorporated into the design computer program. Computer results showed that to obtain the desired waviness, the stiffness would have to be reduced by at least 50 percent. The seal was then modified and Test No. 113 (Figure 2-8) was run. This test had the identical start-up behavior of Test No. 112. The test was stopped after only 4.7 hours.

The seal was removed from the test apparatus, traces made of the face, and then a 300 μm/m convergent taper was lapped into the face. The seal was then replaced in the test apparatus and pressurized to 100 percent pressure for a static test. The seal was left overnight under these conditions. After disassembly, traces showed no convergent taper at all, but rather a flat face condition. This result showed that the epoxy bond creeps and allows the seal face to rotate under pressure. The seal was then re-installed with this flat face condition and run without waviness pressure. The results, Test No. 114 (Figure 2-9), show that the performance was quite similar to the two previous tests. Clearly, any waviness imparted to the seal was not being transmitted to the carbon insert. Other adhesives were investigated and tested to try and remedy this problem.

The carbon insert was machined out and a new one installed using Loctite Speedbonder No. 319 as the adhesive. The bond thickness on the back of the carbon was reduced to zero to stiffen the connection. Test No. 115 (Figure 2-10) was then run. It showed a torque level which was about half of that of

Table 2-2

Waviness Tests
P_{H_2O} = 100% pressure, 1800 rpm

P_{Wave}* (MPa)	Test No.	Test Duration (h)	Average Face Temperature (°C)	Average Torque (N•m)	Average Leakage (cm^3/min
5.2	112	23.5	39.6	11.0	0.00
5.2	113	4.7	39.8	10.2	0.00
0	114	13.2	41.1	11.7	0.00
5.2	115	67.7	39.2	6.4	0.00
5.2	116	47.8	38.8	4.9	0.00
5.2	117	99.8	38.4	2.6	0.19

*Equivalent waviness pressure

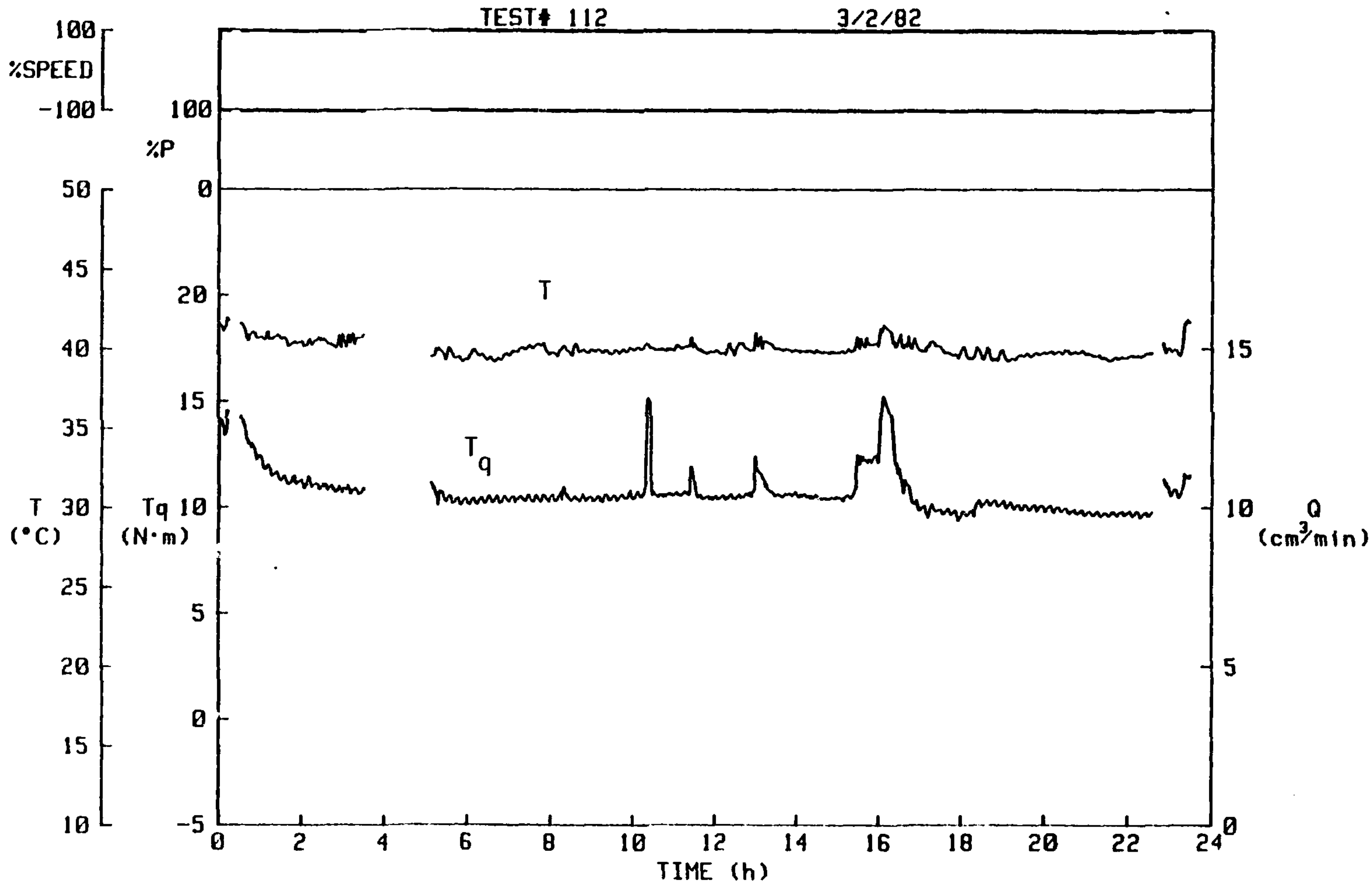

Figure 2-7. Test #112 - Nine-Wave Seal, 100% pressure, 1800 rpm.

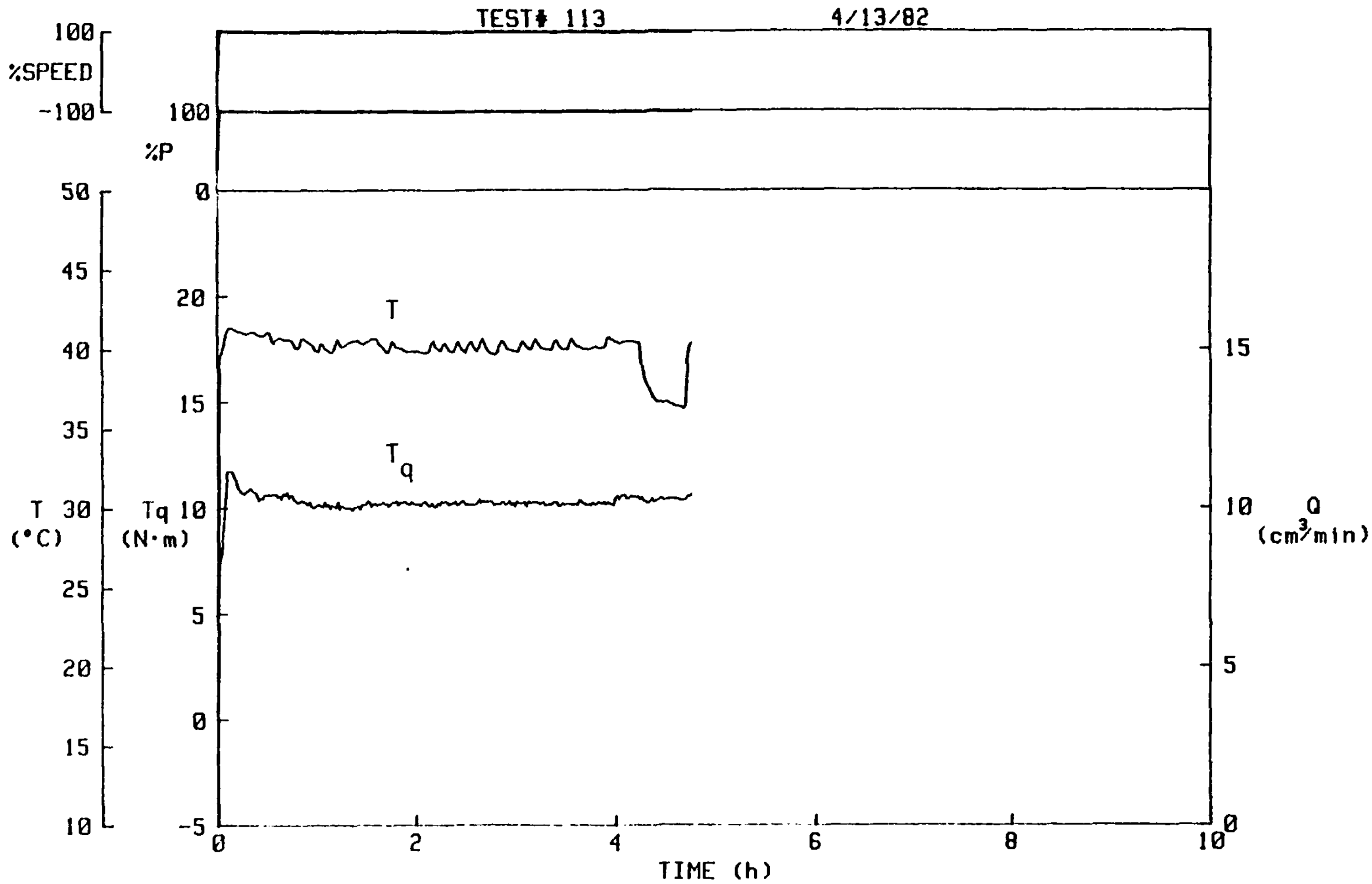

Figure 2-8. Test #113 - Nine-Wave Seal, 100% pressure. 1800 rpm.

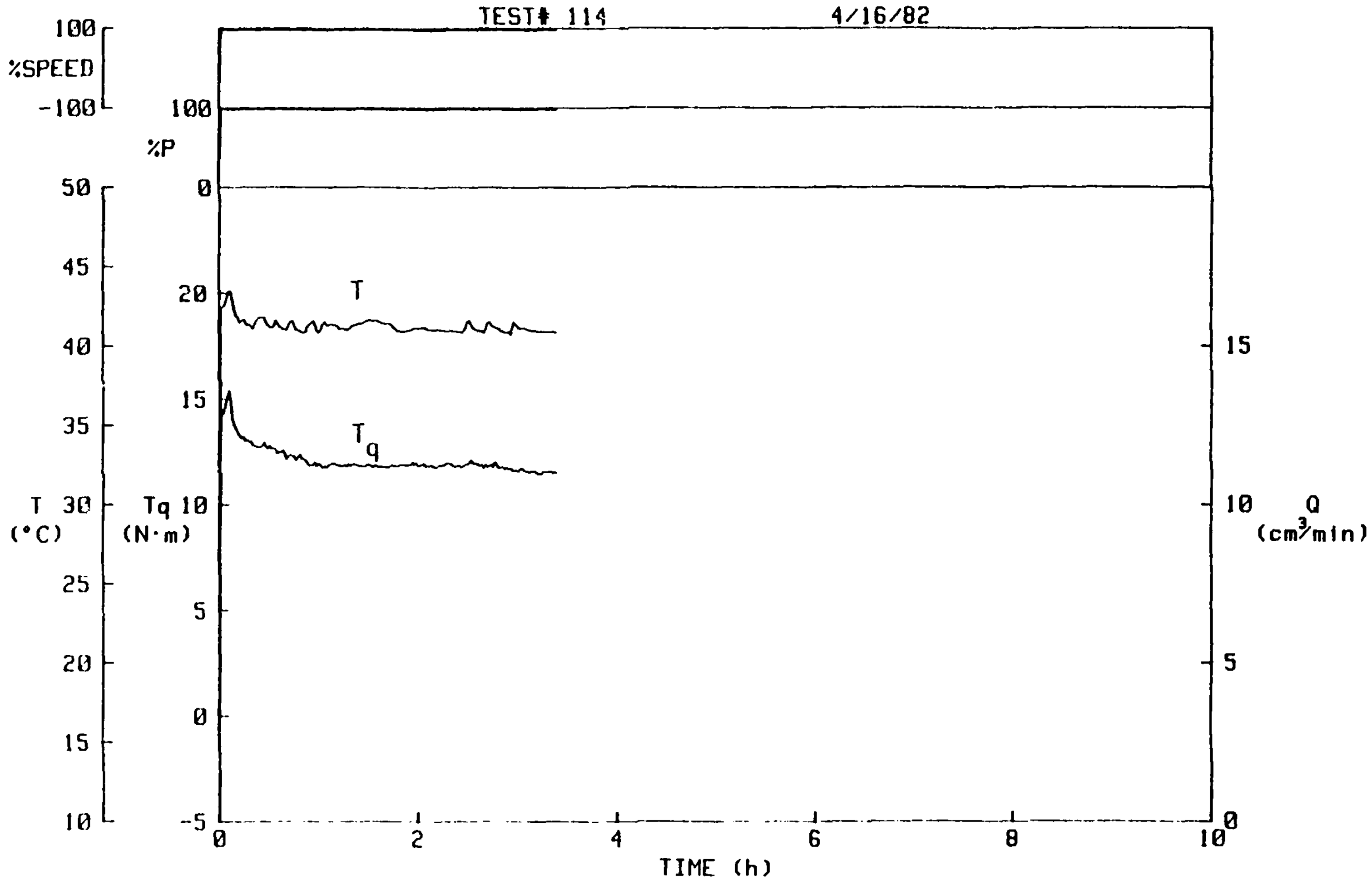

Figure 2-9. Test #114 - Nine-Wave Seal, 100% pressure, 1800 rpm.

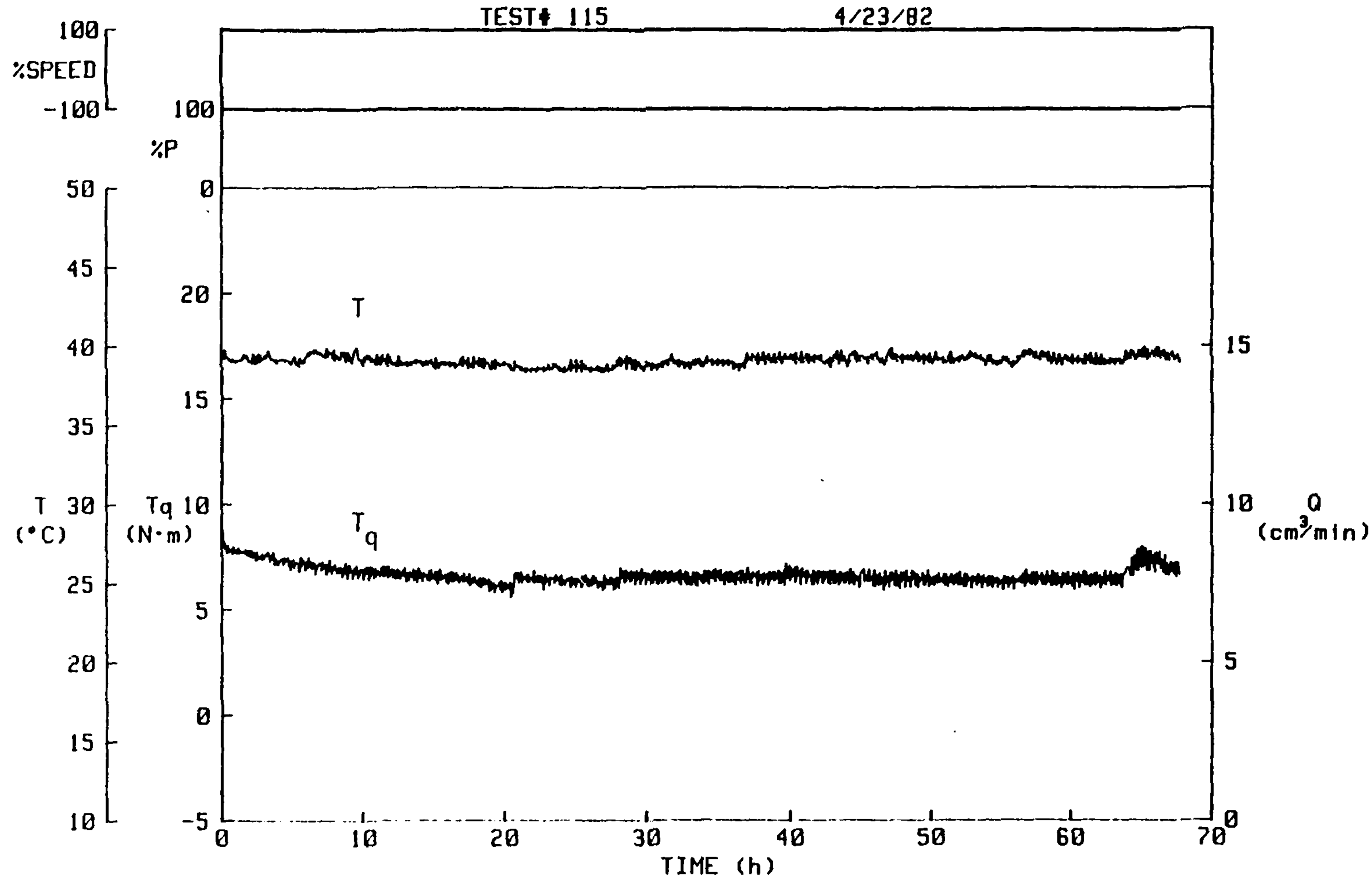

Figure 2-10. Test #115 - Nine-Wave Seal, 100% pressure, 1800 rpm.

previous tests. However, there was no leakage and some was to be expected. The test was ended after 47 hours and the carbon insert was again machined out. There were indications that incomplete bonding had occurred between the seal and insert at certain locations, mainly on the outside diameter.

The next step was to reduce the inner and outer diametrial clearances around the carbon insert. This was accomplished by making two stainless steel spacer rings for the inner and outer diameters. The rings were 0.0254 cm thick and as a result made the carbon insert a slight press fit into the seal. Because of the press fit another type of adhesive was needed. Loctite Superbonder No. 420 was used because of its low viscosity properties and post assembly application ability. The seal was bench tested for waviness and then re-installed in the test apparatus. Test No. 116 (Figure 2-11) was run for more than 47 hours and showed a performance similar to Test No. 115. Some leakage had occurred between 4-1/2 hours and 14-1/2 hours into the test but at no other time.

The test was stopped after the torque readings became erratic, varying as much as 5 N•m. The carbon ring was machined out and again showed indications of incomplete bonding, this possibly being the result of water weakening the adhesive strength. It was decided to test the strengths of the various adhesives used by independent experiment. Table 2-3 shows the results. The results show clearly that the Loctite Superbonder No. 420 is weakened by water contamination and that 3M 1838 B/A was the strongest even after soaking in water.

Based on the previous findings a new carbon insert was cemented into the seal along with the stainless steel spacer rings using the 3M 1838 B/A adhesive. Because of the high viscosity of the epoxy, installation required careful application of the expoxy and pressing in the carbon. The O-rings in the pressure adapter were also modified. Because of the reduced

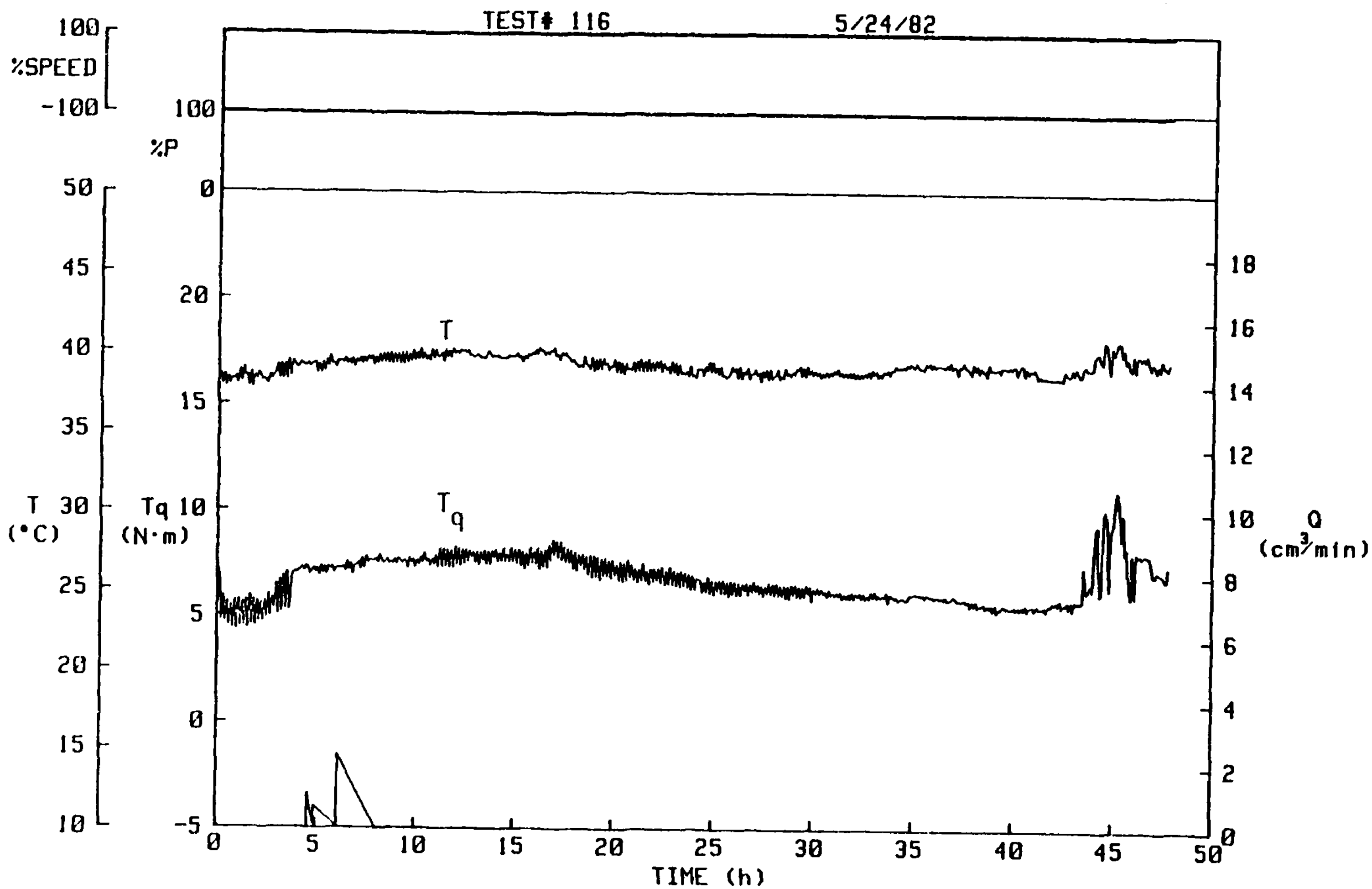

Figure 2-11. Test #116 - Nine-Wave Seal, 100% pressure, 1800 rpm.

Table 2-3

Carbon to Stainless Steel Bond Strength Tests

Test Specimen	Adhesive	Load at Failure (lb)	Comments
1	Loctite 420 (Super bonder)	3.45	Under static line water pressure for 2 days--clean break at glue line (one side)
2	Loctite 420 (Super bonder)	6.85	Under water 0 psi for 2 days--clean break at glue line (one side)
3	Loctite 420 (Super bonder)	10.25	Moisture free--clean break at glue line (both sides)
4	Loctite 420	--	Not tested
5	Loctite 319 (Speed bonder)	--	Carbon too porous for adhesion--no bond
6	Loctite 319 (Speed bonder)	--	Same as above
7	3M 1838 B/A Epoxy	29+	No break
8	3M 1838 B/A Epoxy	29.05	Carbon broke (not at glue line)

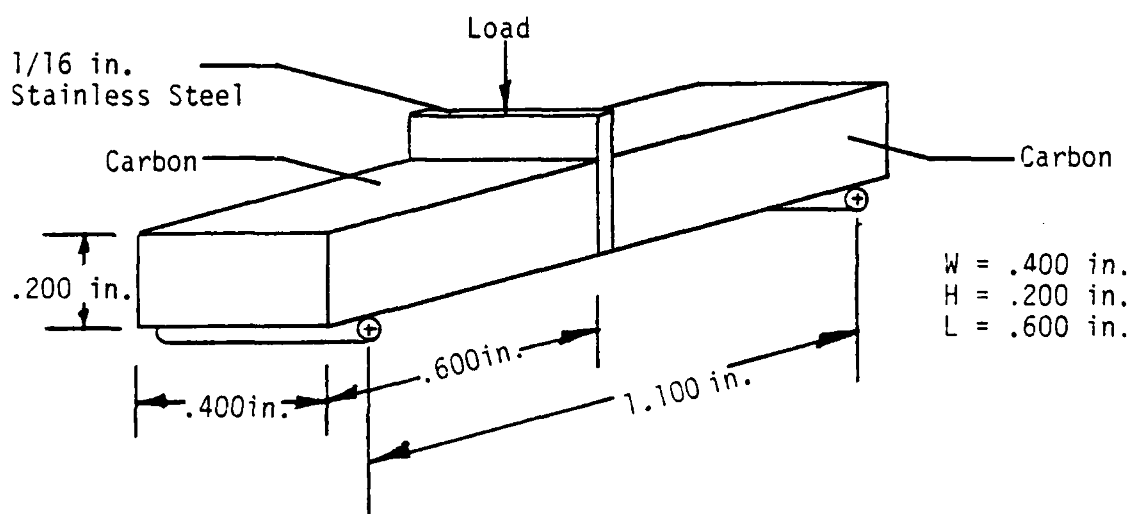

stiffness, O-ring extrusion was becoming a problem, so modifications's were made to use smaller O-rings along with piston pads and Delrin retaining rings. The seal assembly was bench tested for waviness and showed good results.

The seal was re-installed and Test No. 117 (Figure 2-12) started. The test showed a start-up performance similar to Test Nos. 116 and 115. The torque was falling to around 5 N•m when water contamination from the building's air compressor clogged the hydraulic pump to the waviness generator. The test had to be stopped after four hours of operation and the pump cleaned. A temporary separate air compressor to operate all air-assisted devices on the test rig was added. The test was re-started and ran for almost 100 hours. Leakage began about eight hours after start and continued throughout the test at about 0.2 cm^3/min.

Test 117 shows torque and leakage values approaching those expected for the nine-wave seal design and would seem to indicate that the design is successful on a preliminary basis. However, radial taper measurements after the test show that a much greater than expected radial taper is present in the seal. This question is being investigated at this time.

Test Machine Modification

Automatic operation of the test apparatus under variable operating conditions required certain modifications of the test apparatus and control hardware and software. These changes are described here.

Speed Controller--The test apparatus is equipped with a 3700 W (5 Hp) belt type variable speed drive ac motor. Speed change, as equipped from the factory, was accomplished by means of a hand crank which varied belt pulley ratios. By this method, speeds from 380 to 4000 rpm were obtained. However, for the simulated submarine operation test program, it was desired that

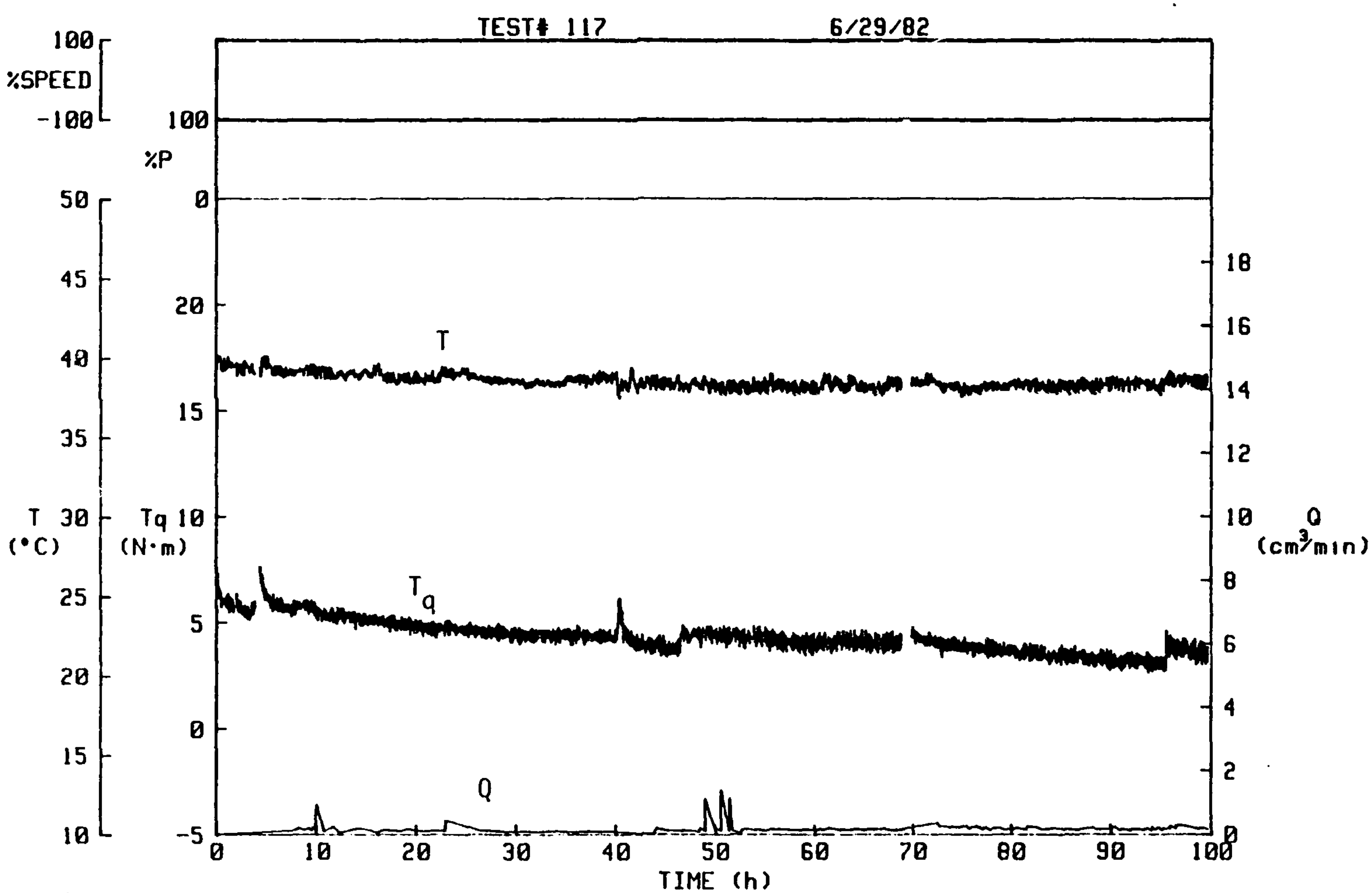

Figure 2-12. Test #117 - Nine-Wave Seal, 100% pressure, 1800 rpm.

the computer system would control the speed, thus providing an automatic operation so the operator could save time and do other things while running a test.

Modification began with the addition of a Superior Electric Co. Slo-Syn stepping motor, Model No. SS 250-1027, and a 2:1 step-down gear ratio in place of the hand crank mechanism. This, coupled with a Slo-Syn ST 1800B stepping motor translator and a H.P. 69335A stepping motor control card for use in the H.P. 6940B multiprogrammer unit, was the basic hardware of the speed control apparatus. Since the stepping motor operates by the input of a pre-programmed pulse train, each pulse of which will rotate the stepping motor shaft by 1.8°, a relationship between stepping motor shaft rotation and the main drive motor rpm was found. Motor speed control was achieved by inputing the desired rpm into the computer which then converts this to the appropriate number of pulses. A data word is sent to the stepping motor control card in the multiprogrammer unit which contains the desired number of pulses. The stepping motor control card in turn outputs the pulse train to the translator wnich then sends the stepping motor the required number of pulses which in turn changes the ratios of the variable speed drive.

Two other factors had to be considered for complete motor control. The first is the capability of forward and reverse control and the second is minimum speed. Forward and reverse control was accomplished by use of two reed relays on the relay card in the multiprogrammer unit, two DPDT relays and two motor starter control units. Figure 2-13 shows the schematic diagram of the directional control circuit. Directional control is achieved by sending a control word from the computer to the relay card to close either Relay Nos. 9 or 10 depending on the desired motor direction. A desirable feature of this circuit is that it is impossible to energize both forward and reverse motor starter units simultaneously by closing both Relay Nos. 9 and 10 on the

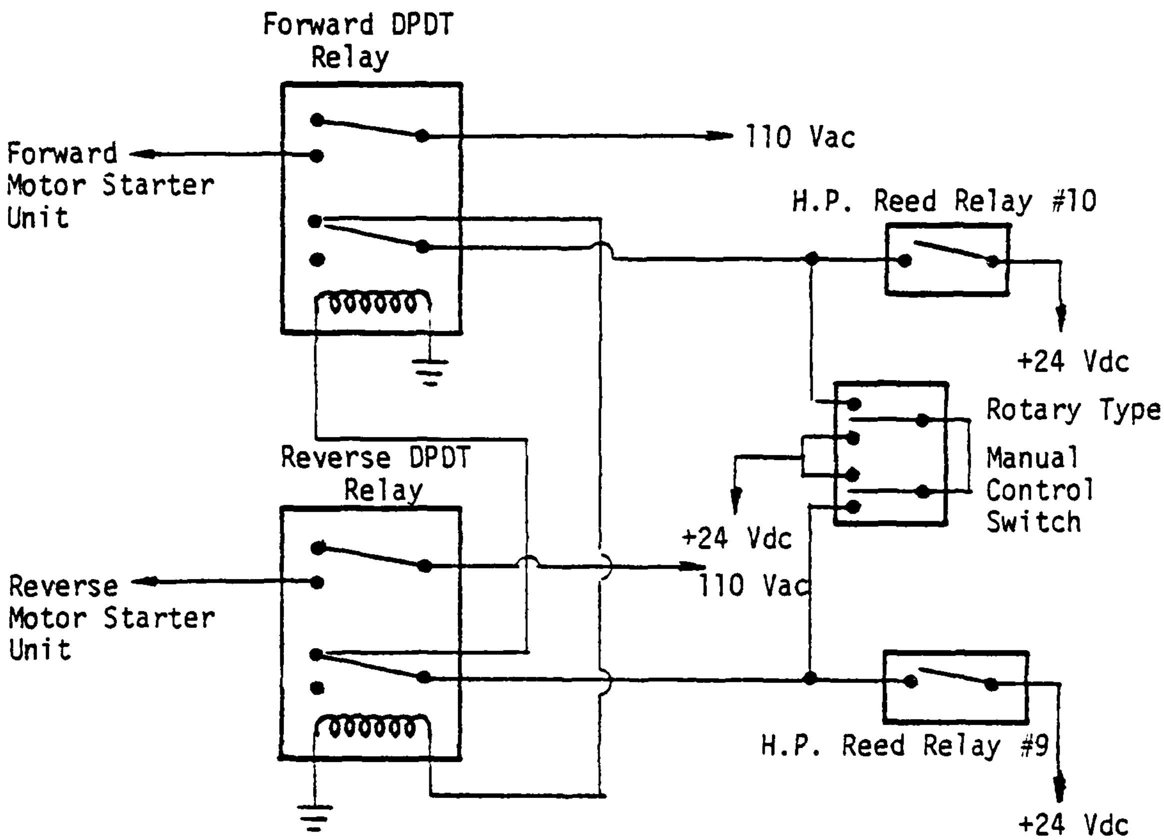

Figure 2-13. Directional Control Circuit.

relay card. A rotary type switch was added so as to obtain manual directional control external to the computer.

A lower minimum speed was obtained by the use of a Reliance Electric variable frequency ac motor speed controller. This unit has the capability of changing the input frequency to the ac motor from 6 to 60 Hz, thereby changing the speed of the motor also. This device used in conjunction with the stepping motor speed controller now gives a range of speed control from approximately 40 to 4000 rpm.

Pressure Controller--Another area of computer control needed for the test program is that of sealed water pressure regulation. The test apparatus is equipped with an accumulator to dampen out pressure surges. The accumulator is shown in Figure 2-14. When the accumulator is charged with nitrogen gas to 75 percent of the water pressure, then proper surge control is obtained in that 75 percent of the original accumulator volume remains as gas when the liquid and gas pressures become equal. But once charged, if the water pressure is changed significantly, up or down, then the diaphragm will also change location and as a result poor performance of the accumulator can be expected. To operate at variable pressure conditions, it therefore becomes necessary to be able to detect the location of the diaphragm and correct its position when needed for optimum performance.

Figure 2-14 shows how this positioning capability is obtained. When the diaphragm is displaced either up or down due to changes in water pressure, the guide rod will move the permanent magnet also. When the permanent magnet is moved so that it is adjacent to one of the magnetic reed switches, the magnetic field induces a contact closure in that reed switch. By correctly positioning the reed switches, an upper and lower bound for diaphragm location can be set along with a sufficient dead zone of operation and an optimum diaphragm position.

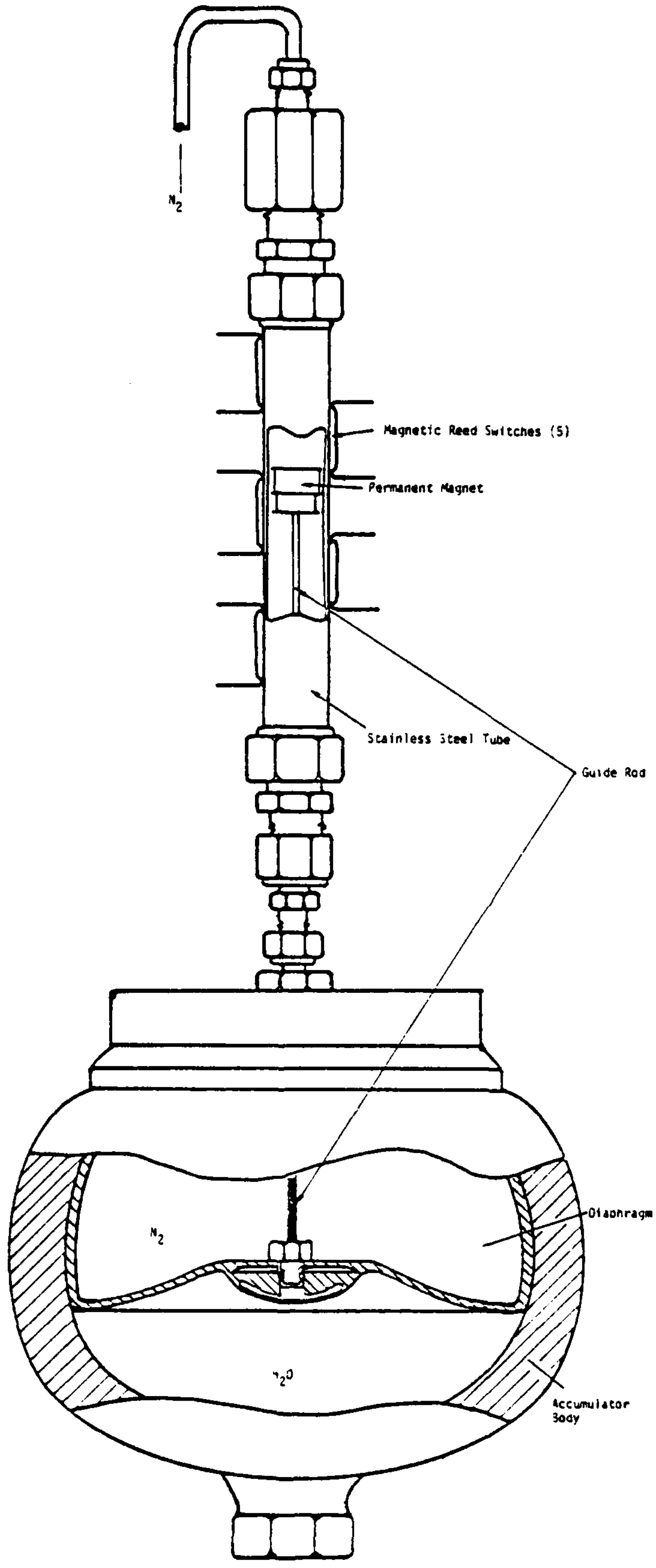

Figure 2-14. Diaphragm Positioning Device.

The accumulator diaphragm positioning circuit is shown in Figure 2-15. When the permanent magnet is adjacent to the No. 3 reed switch then the engaging coil of both Nos. 6 and 7 dual coil relays will be energized, thereby setting the switch in both relays to the engaged position. If the diaphragm rises so that it is next to either the No. 2 or 1 reed switch then the disengaging coil of No. 6 dual coil relay is energized which then registers an interrupt on Channel No. 6 of the interrupt card in the multiprogrammer unit. The computer recognizes that this interrupt indicates a high diaphragm and in turn operates two solenoid valves to let water out of the system and add N_2 to the top side of the accumulator which will result in lowering the diaphragm. Once the disengaging coil is energized, it will remain so sending an interrupt to the multiprogrammer unit. This will continue until the diaphragm moves down so that the magnet again closes the No. 3 reed switch and as a result energizes the engaging coil and discontinues the interrupts. Likewise, a low diaphragm will register an interrupt on Channel No. 5 of the interrupt card. This prompts the computer to cause the pump to pump more water into the system and let some N_2 out by means of another solenoid valve. This set-up therefore allows for preprogrammed pressure changes during testing and ensures that the optimum diaphragm positioning is obtained at any pressure.

Misalignment Control--Another feature required for the simulated submarine operation test program is a variable tilt and offset of the seal. This was accomplished by the set-up shown in Figure 2-16. A Slo-Syn SS 250-1027 stepping motor and gear reduction arrangement is connected to the shaft of the worm which drives the waviness cylinder. This waviness cylinder has a tilt and offset machined into it which begins just right of the end plate. To the left of this point the waviness cylinder is concentric with the shaft. Using the computer to pulse the stepping motor, three different tilts with corresponding offsets, as

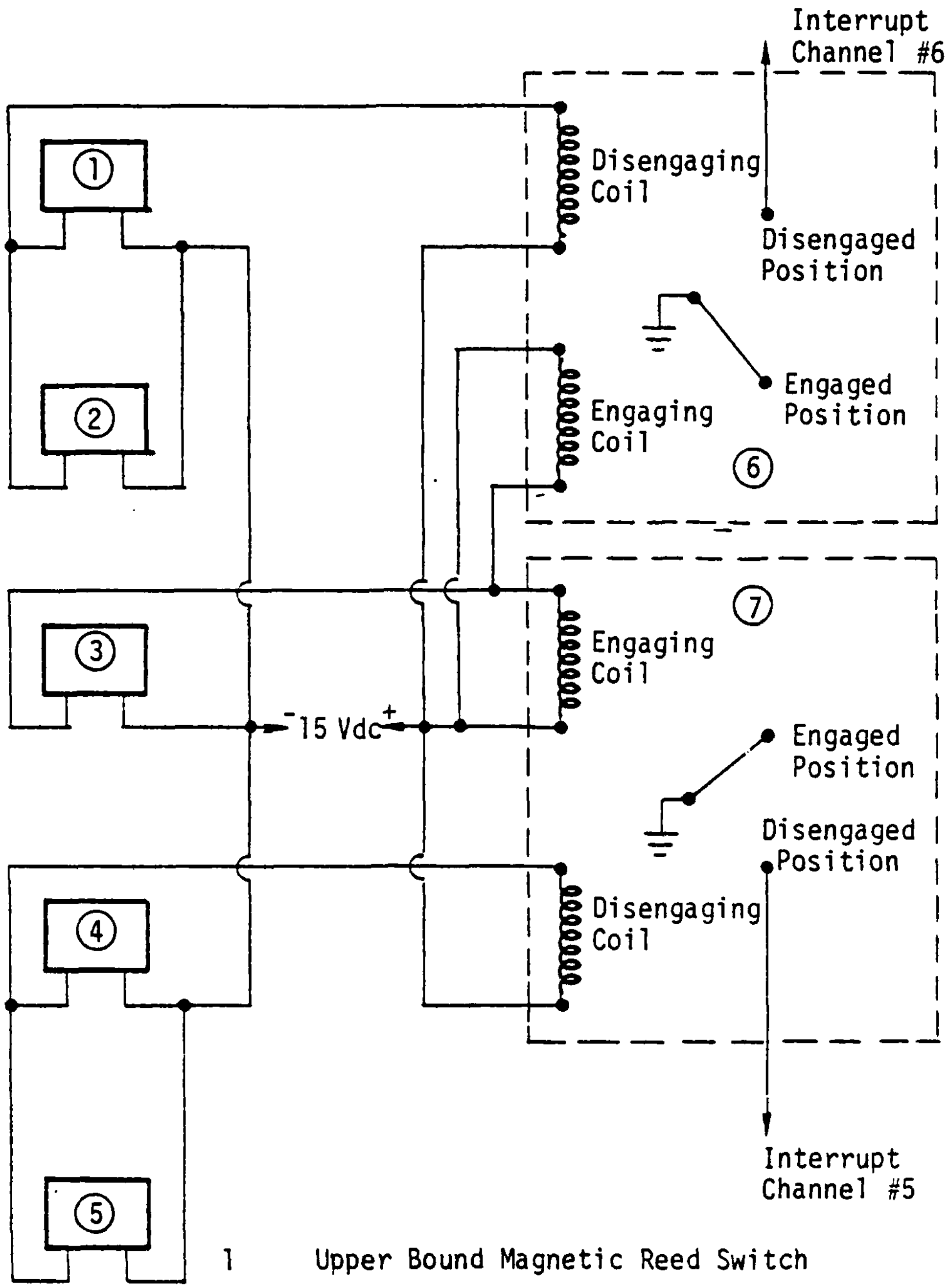

1	Upper Bound Magnetic Reed Switch
2	Upper Dead Zone Magnetic Reed Switch
3	Operating Point Magnetic Reed Switch
4	Lower Dead Zone Magnetic Reed Switch
5	Lower Bound Magnetic Reed Switch
6	Dual Coil Down Relay
7	Dual Coil Up Relay

Figure 2-15. Accumulator Diaphragm Positioning Circuit.

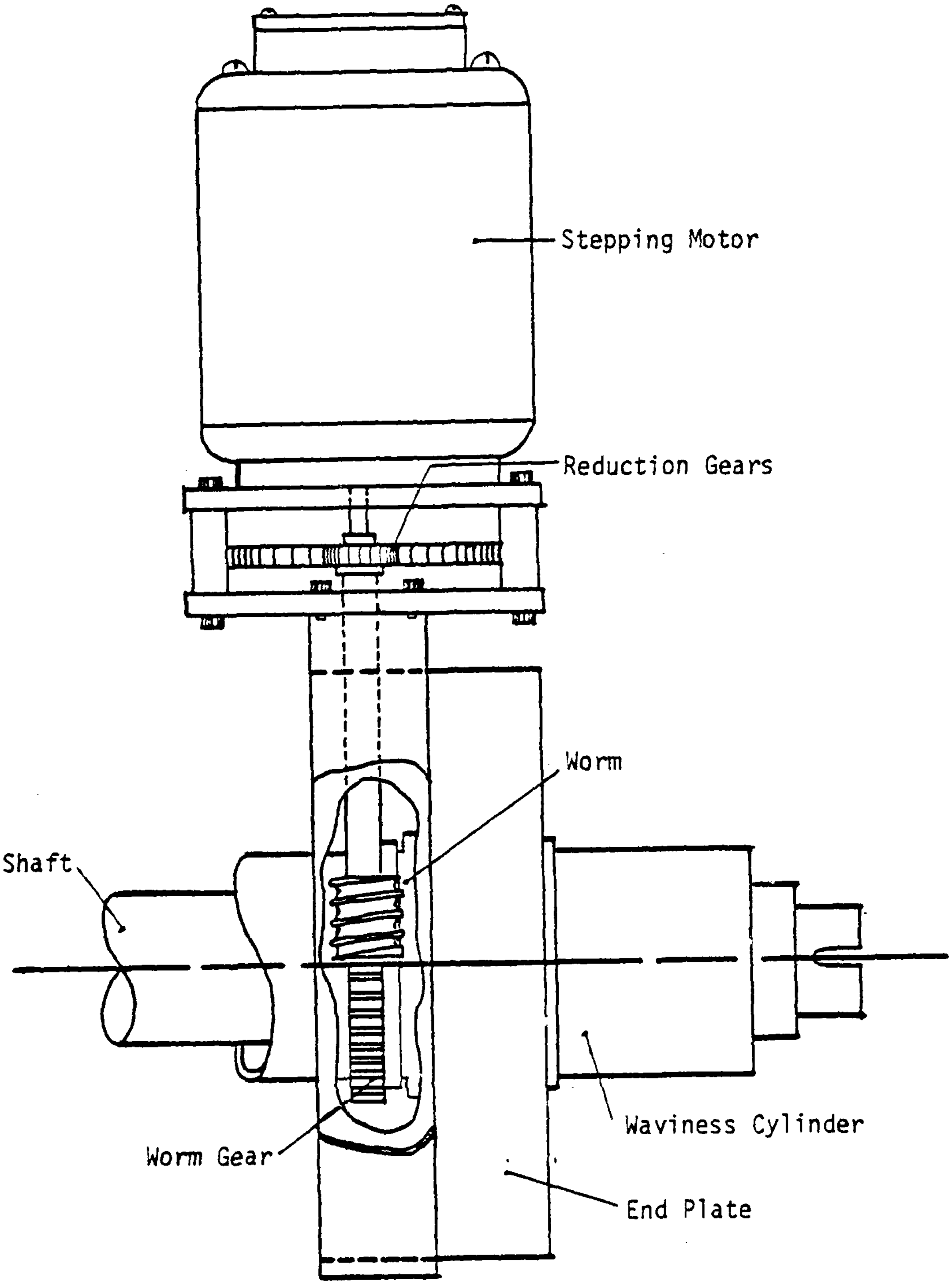

Figure 2-16. Tilt and Offset Drive.

specified by the test program, can be obtained. Details of the geometry related to this procedure are described in Chapter 3.

Seventy-Five Percent Balance Ratio Test

Test No. 111, Appendix A, was run at a balance ratio of 0.75 and zero initial taper so as to obtain additional wear rate data. The operation of this test was somewhat similar to previous tests run under the same conditions. One difference was that leakage did not occur until some 390 hours into the test. Similar tests showed leakage initially. Also, whereas the average torque level was comparable to other tests, there were large fluctuations associated with it in the initial start-up. These became lower as the test proceeded. The test ran much more smoothly after 48 hours of operation and up to approximately 412 hours where the torque levels again began to fluctuate. The test was eventually shut down due to high torque at 494 hours.

This type of operation at the end of the test is comparable with Test Nos. 75 and 76 [5], and final radial traces of the carbon face also showed a taper of about -1000 μm/m. Test No. 75 had a final taper of -710 μm/m and Test No. 76 -982 μm/m. This behavior is to be compared to that for Test 66 which was also for a zero initial taper. Test 66 started up with low torque and some leakage and continued about the same for over 100 hours. Clearly, Test 111, which was outwardly identical, started out in a different mode. Test 66 started out taking advantage of a thermal taper which never wore off during the test. Test 111 never got into this mode. It somehow got started in a mode where it wore rapidly into a nonleaking parallel face condition with a high but worn away thermal taper. The last hours of operation of Test 111 show that this mode is not really stable but can lead to high friction, high wear operation. The intriguing question which requires still more testing to answer is why this test started in the high friction mode and Test 66 started in a low friction mode.

CHAPTER 3
NINE-WAVE SEAL DESIGN

Criteria

In this chapter the design procedure for the nine-wave seal is presented in detail. The criteria set forth for the design are as follows.

1) Very low wear--10 year life,
2) Moderate to low leakage--leakage to be consistent with time,
3) Low friction (to ensure low thermal distortions)
4) Operation in the 500 psi, 1800 rpm at 4 inch mean diameter range,
5) Operation in seawater,
6) Variable speed, pressure, and distortion as functions of time to conform to simulated submarine operation,
7) Seal components themselves must be reliable to be compatible with 1) above,
8) Use of carbon insert in a metal ring to be compatible with large scale design.

To satisfy the above conditions using a wavy seal, certain additional criteria become apparent. Some of these are based on conclusions from the previous report [5] and a paper on this subject [14].

1) The seal rings must be designed so that the pressure caused rotation is zero. This is essential in a seal where operating pressure changes frequently. If pressure caused rotation occurs, then the seal face must wear to a new profile at each operating pressure.

2) Nine waves must be imposed on the seal. References [5] and [14] show that the natural pressure variation on the seal

face produces a tilt angle which is dependent on operating conditions. Such changes will lead to accelerated wear and must be minimized. By increasing the number of waves the relative tilt stiffness of the seal increases such that operating conditions no longer produce a change in tilt which is significant relative to the applied tilt. At nine waves the tilt changes only a few percent with variable operating conditions.

3) The centroid of the cross section must be located so that the sealing radius is near the inside radius r_i. This ensures that both minimum leakage and maximum load support will occur. This imposes a severe geometrical constraint on the cross section.

4) So that the seal may easily comply with the mating ring at the lower harmonics and so that the needed waviness can be reasonably imposed, the cross sectional properties (moments of inertia) must be maintained at low values (no stiff rings). This requirement restricts the size of the cross section.

Assumed Configuration

Figure 3-1 shows the assumed basic configuration for the design. Several other configurations were evaluated, but the one shown appeared to be the best. There are 54 moment arms attached to the seal cross section, 27 on the inside and 27 on the outside. This number represents 3 sets of 18 arms (see details in previous chapter). Eighteen arms (nine inside and nine outside are required to produce one set of nine waves. The force is applied hydraulically as shown. O-rings create a pressurized pocket, and this pressure acts on the pad. The carbon is bonded into a metal ring. The centroid is shown to be located near the inside radius of the ring. Since the forces on the pads alternate in direction, there is no net radial force due to hydraulic pressure acting on the ring. The seal support must drop down after the secondary O-ring so that some significant amount of

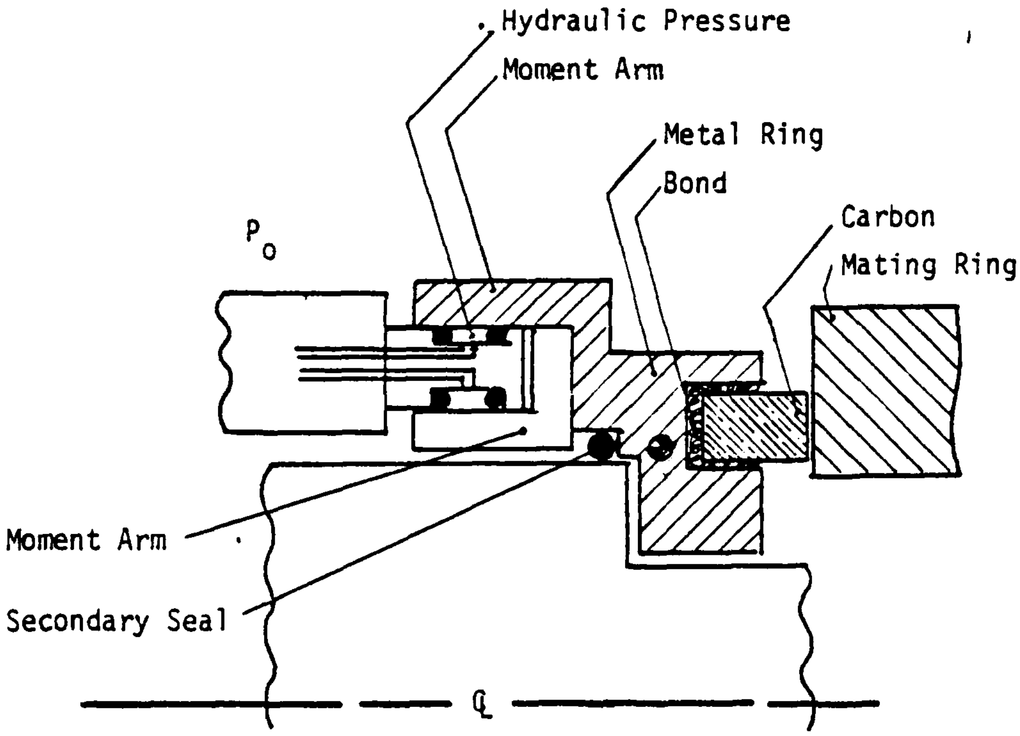

Figure 3-1. Assumed Nine-Wave Seal Configuration.

material can be attached to the cross section below the balance radius in order to lower the centroid.

The diameter of the existing test vessel contains the outside diameter of the seal assembly, and this restricts the size of the moment arms. The fact that the hydraulic pressure is applied on the pressurized side of the seal creates a problem in that the hydraulic pressure must always be above the sealed pressure. If it is not, the O-rings can collapse inward as shown. Even if this problem is overcome by inserts inside the O-rings, it can be shown that a force discontinuity will occur as pressure drops below the sealed pressure. According to theory previously developed [5], the average hydraulic pressure (which is influenced by the sealed pressure) does not affect the amplitude of the wave, so having the hydraulic pads in the sealed pressure environment causes no theoretical problem.

It was immediately recognized that because of all of the O-ring seals operating at high pressure, no significant corrosion of the surfaces could be tolerated. It was learned that Inconel 625 was one of the few alloys that would not pit in seawater, so it was chosen for the metal parts of the seal assembly. Inconel 625 is known to be difficult to machine compared to stainless steel alloys and monel, but it appeared to be the only acceptable alloy from the corrosion standpoint.

Seal Ring Design Solution

Figures 3-2 and 3-3 show the details of the seal ring itself. Many of the dimensions shown had to be selected based on the criteria discussed. The details of this procedure will now be described.

1) Fix certain parameters (see Figures 3-2 and 3-3)

K = 1.005 (explained later)

R_i = 1.9 in. (consistent with test machine)

R_b = 1.9 in. (balance ratio = 1.0)

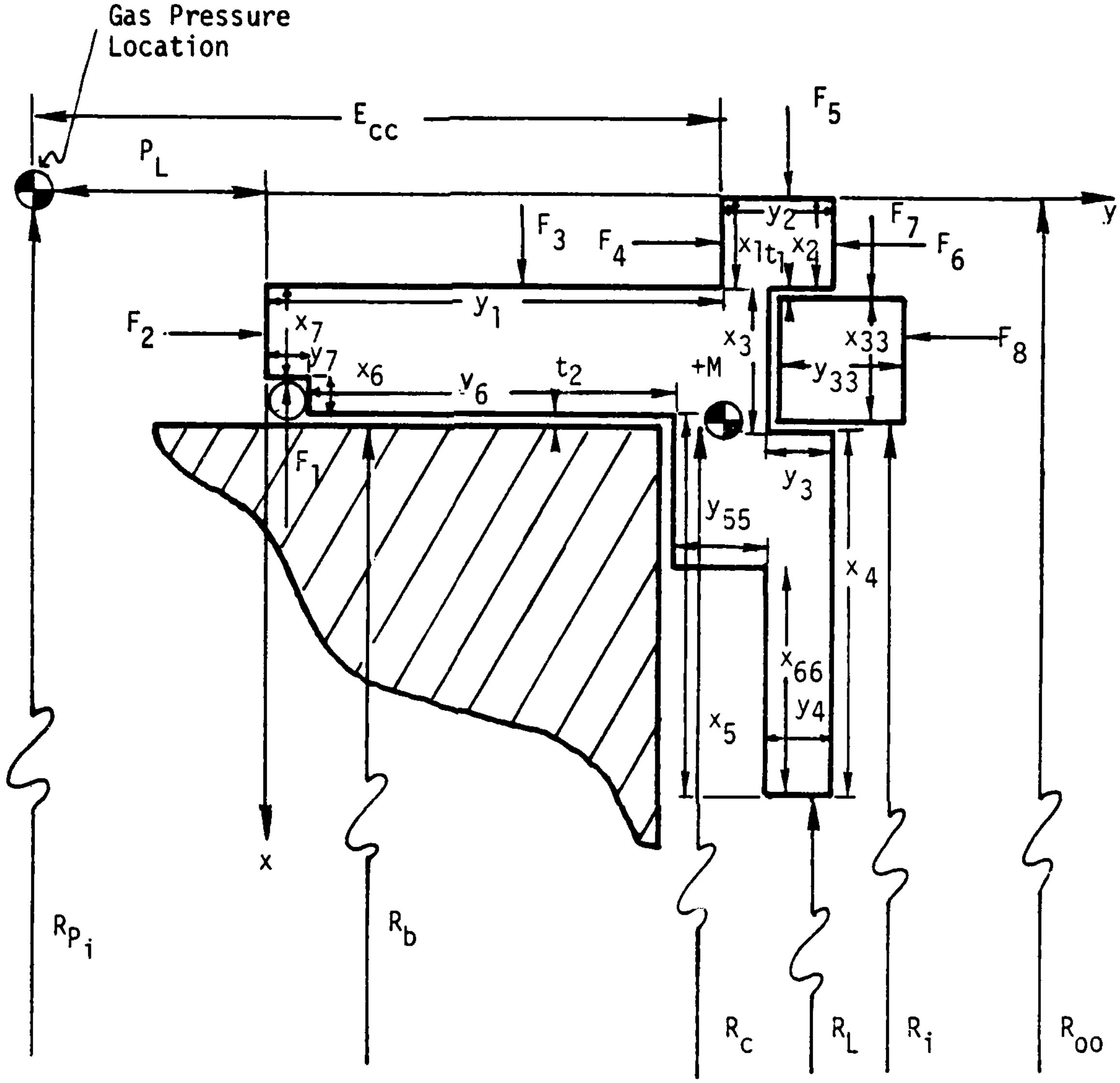

Figure 3-2. Assumed Seal Ring and Moment Arm Geometry.

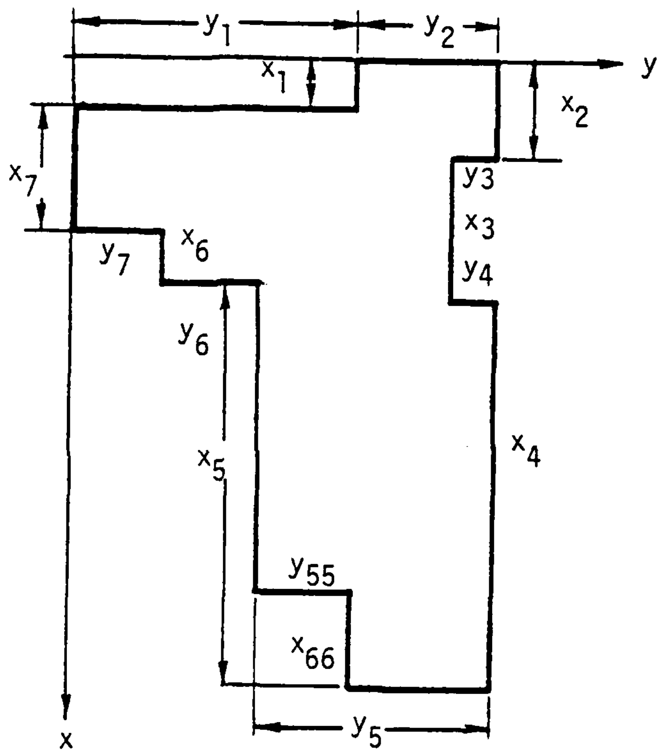

Figure 3-3. Assumed Cross Sectional Geometry.

$xx3$ = 0.1875 in. (face width is equal to existing test seal)

$yy3$ = 0.125 in. (nose height)

t_1 = 0.010 in. (bond thickness)

t_2 = 0.003 in. (clearance)

x_6 = 0.051 in. (required for proper squeeze) (3-1)

y_7 = 0.080 in.

p_0 = 500 psi (seal working pressure for design purposes)

n = 9 (number of waves)

p_g = 1000 psi (equivalent gas pressure for calculation. Using a moving wave produced by three sinusoidal with time waves requires that each of the waves have a pressure amplitude of 667 psi

$E = 31 \times 10^6$ psi (Inconel 625)

$\mu = 0.3$

$$G = \frac{E}{2(1 + \mu)}$$

2) Choose the remaining set of dimensions. These will be varied to obtain the desired design. They are:

x1, x2, x66, y1, y2, y3, y55, y6 - defined as shown in Figure 3-2

d - pressure pad O-ring diameter (3-2)

ϕ - desired seal from tilt amplitude

3) Assuming a value for R_L, calculate section properties $\bar{X}$, $\bar{Y}$, r_c, and I_x. These are calculated by breaking the cross section up into rectangular subparts as shown in Figure 3-3 using the parallel axis theorem.

4) Calculate J_θ (torsional stiffness). Torsional theory requires that the following partial differential equation be solved for the cross section.

$$\frac{\partial^2 \psi}{\partial x^2} + \frac{\partial^2 \psi}{2y^2} = -2 \ , \tag{3-3}$$

$$\psi = 0 \text{ on boundary .} \tag{3-4}$$

Once ψ is found, then

$$J_\theta = 2 \iint_A \psi \, dA \ . \tag{3-5}$$

This problem was solved numerically by dividing up the cross section into a grid as shown in Figure 3-4. Note the grid pattern corresponds to the exact boundaries of the cross section. This causes unequal spacing of the grid points. Equation (3-5) was solved using finite difference formulas which account for unequal spacing. The system of equations was solved quickly by relaxation.

5) Calculate $A = EJ_x/GJ_\theta$. Using this and the previously derived formulas [5],

$$\phi = \frac{m_{\theta_o} \, r_c^2}{EJ_x} \, \frac{1 + An^2}{(n^2 - 1)^2} \ , \tag{3-6}$$

$$m_{\theta_o} = \frac{p_g \, d \, Rp_i \, e}{r_c} \sin\left(\frac{nd}{2 \, Rp_i}\right) , \tag{3-7}$$

calculate the required m_{θ_o}. Given

$$Rp_i = R_L + x5 + x6 + x7/2 \tag{3-8}$$

which places the pressure force near the middle of the back edge of the seal ring, calculate the moment arm e needed to produce the required tilt.

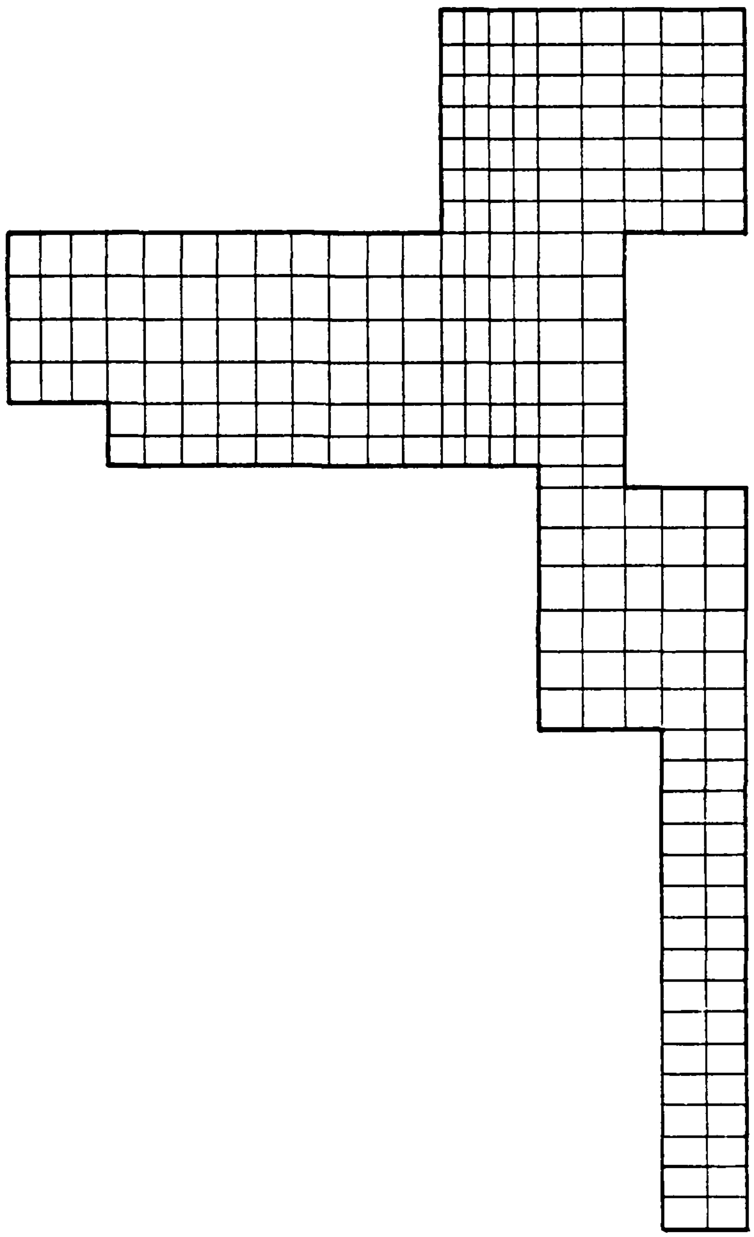

Figure 3-4. Finite Difference Mesh for Calculating Torsional Stiffness.

6) From before [5], calculate

$$v = \frac{m_{\theta_o} r_c^3}{EJ_x} \frac{(1 + A)}{(n^2 - 1)^2} \tag{3-9}$$

and

$$r_{\substack{contact\\actual}} = \frac{v}{\phi} + r_c \; . \tag{3-10}$$

7) To insure proper sealing but also maximizing load support, the contact radius must be just inside the inside radius of the seal or

$$r_{\substack{contact\\desired}} = Kr_i \; . \tag{3-11}$$

K was defined previously as a number greater than one. Now compare:

$$r_{\substack{contact\\actual}} \text{ to } r_{\substack{contact\\desired}} \; . \tag{3-12}$$

If they are significantly different, adjust R_L using a root finding technique. Go back to Step 3 and repeat all of the calculations until Equation (3-12) is satisfied.

8) Calculate I_y. Calculate the moments due to pressure as shown in Figure 3-2. Calculate pressure caused rotation

$$\phi_{pressure} = \frac{m_\theta r_c^2}{EJ_x} \tag{3-13}$$

where m_θ is the moment about the centroid in N•m/m of centroidal circumference.

9) The above program is rerun adjusting the input parameters (3-2) until pressure caused rotation (3-13) is made sufficiently small.

The computer program written to perform the above calculations is included in Appendix B.

Final Design

After many trials and alterations in configuration, the final design selected is described by the output from the program shown as Table 3-1. Figure 3-5 shows the seal cross section which corresponds to these dimensions. Figures in Chapter 2 show other details of the seal.

Predicted Performance

Using programs developed previously [5], performance of the new seal design was predicted. Figures 3-6 and 3-7 were obtained using a program which neglects elastic deflection of the seal rings brought about by face pressure itself. As discussed previously at $n = 9$ this deflection is negligible. Figure 3-6 shows a significant friction torque at the lower speeds with a significant reduction at increased speed. Even at zero speed, predicted torque is about one half of what it would be without any waviness. Some wear is expected at the lower speeds because the fraction of the load supported by fluid pressure drops to 75 percent at 200 rpm. However, because the speed is low where the fluid pressure load support is low, the amount of wear will be minimized. At the higher speeds, the predicted fluid pressure load support becomes 100 percent due to hydrodynamic effects as is suggested by the decreasing torque with increasing speed curve.

Leakage is shown in Figure 3-7. Leakage is predicted to be less than 1.0 cc/min under all test conditions. A large value of ϕ increases leakage considerably but reduces torque very little.

Table 3-1

Seal Design

$\phi = 320 \times 10^6$

$d = 0.254$ in.

$x_1 = 0.2100$ in.	$y_1 = 0.3800$ in.
$x_2 = 0.2100$ in.	$y_2 = 0.2200$ in.
$x_3 = 0.2075$ in.	$y_3 = 0.1000$ in.
$x_4 = 0.5010$ in.	$y_4 = 0.1000$ in.
$x_5 = 0.5140$ in.	$y_5 = 0.1700$ in.
$x_6 = 0.0510$ in.	$y_6 = 0.3500$ in.
$x_7 = 0.1435$ in.	$y_7 = 0.0800$ in.

$R_{pi} = 2.4840$ in.

$R_L = 1.3890$ in.

$\bar{x} = 0.3518$ in.

$\bar{y} = 0.3943$ in.

$I_x = 0.00542$ in.^{4}

$I_y = 0.00916$ in.^{4}

$J_\theta = 0.00176$ in.^{4}

$A = 7.86$

$v = 8.7 \times 10^{-6}$ in.

$e = 0.953$ in.

$r_c = 1.9557$ in.

$\phi_{pressure} = 6.8 \times 10^{-8}$ in./in.

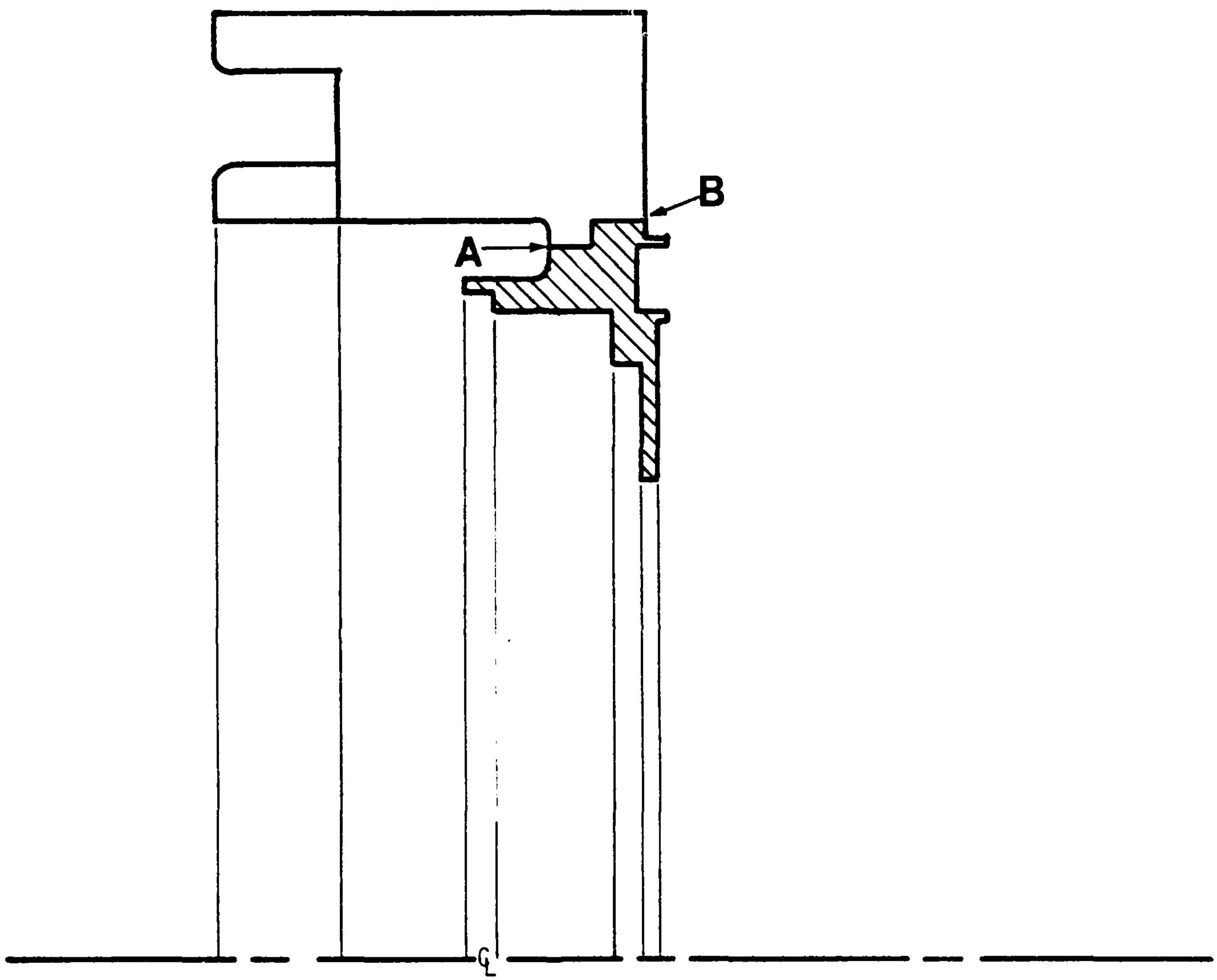

Figure 3-5. Actual Seal Cross Section.

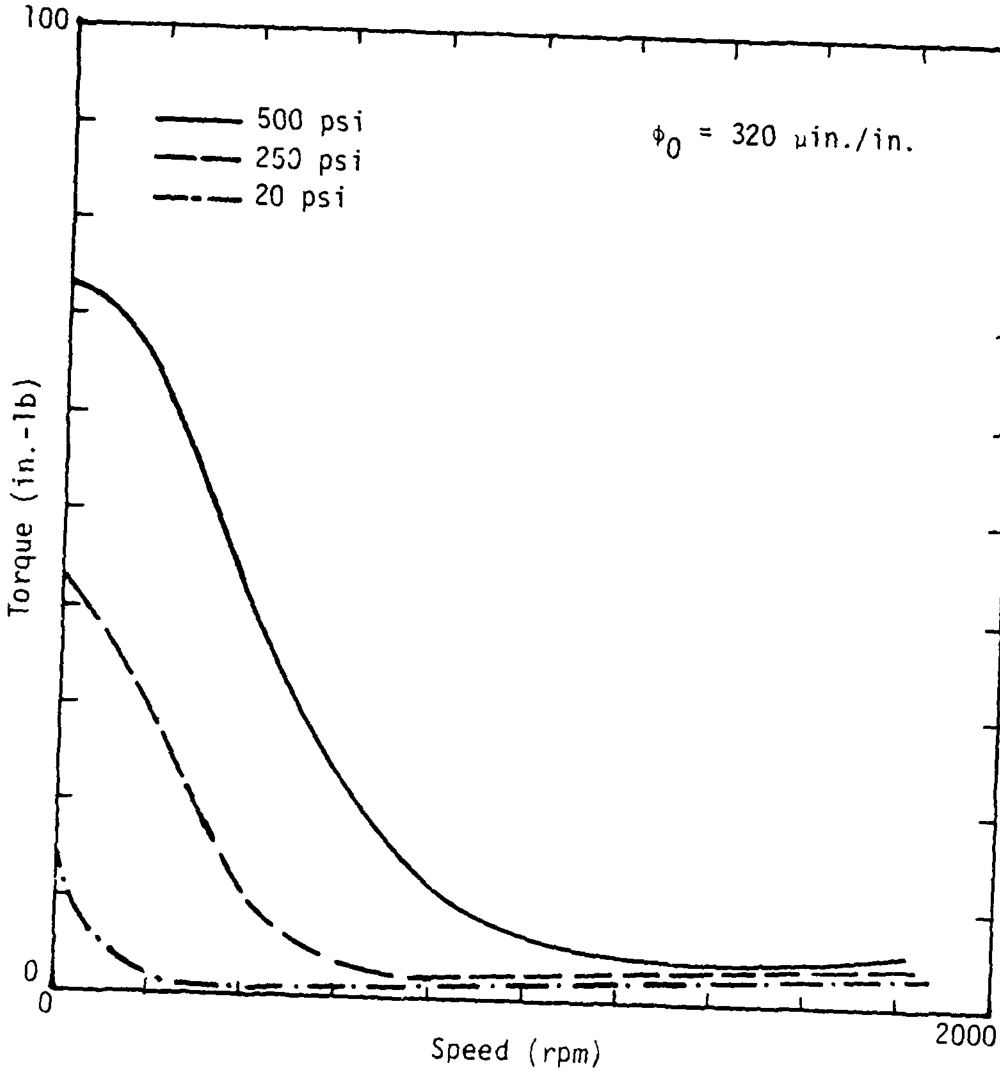

Figure 3-6. Predicted Performance - Torque.

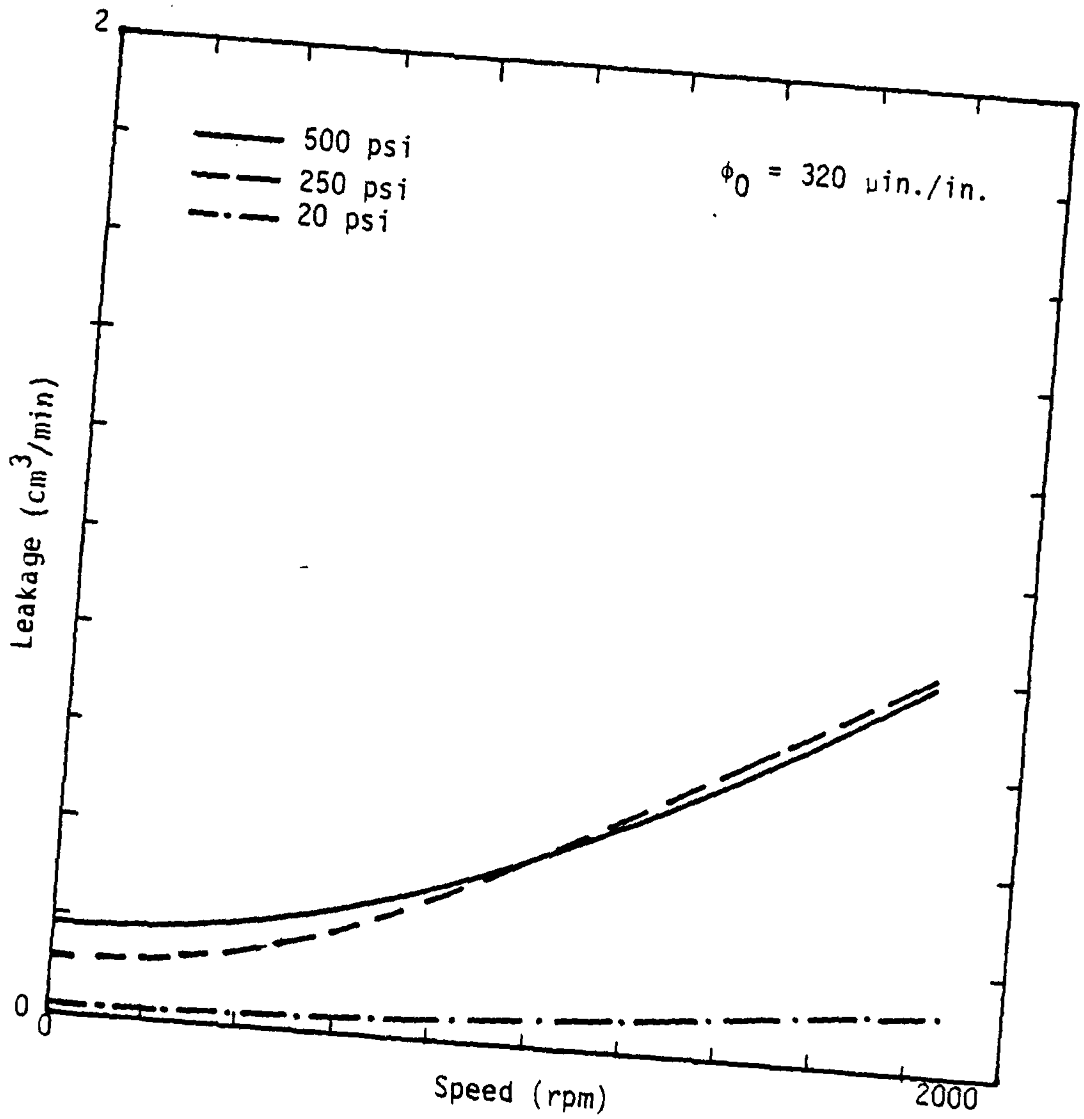

Figure 3-7. Predicted Performance - Leakage.

Thus, the ϕ = 320 was selected as a compromise between reduced friction and increased leakage.

Figure 3-8 shows a comparison between the worn in shape of the seal at two extreme operating conditions. Note the worn in shape is almost the same. These curves were calculated using another computer program which accounts for the deflections of the seal rings. Thus, as expected at nine waves, there is little change in the worn shape of the seal due to a change in operating conditions. Thus, no acceleration in wear would be expected in the design due to variable operating conditions. Furthermore, the additional small deflection component makes virtually no difference on the predicted performance.

Finite Element Calculation

To provide an additional check on the calculation for zero pressure rotation contained in the design program, a completely independent calculation for pressure caused rotation was made. Using SAP IV two-dimensional axisymmetrical elements, the cross section shown in Figure 3-5 was modeled using 161 nodes and 126 rectangular elements. The results showed that a rotation of 19 μin./in. convergent resulted. This is quite small. This result shows that the beam theory used in the design program is adequate for calculating zero pressure moment designs and that the design itself is correct from the pressure rotation standpoint.

Strength and Deflection Calculations

Room temperature properties of annealed Inconel 625 are as follows:

$$S_u = 120 \text{ to } 150{,}000 \text{ psi}$$

$$S_y = 60 \text{ to } 95{,}000 \text{ psi} \qquad (3\text{-}14)$$

$$S_e' = 90{,}000 \text{ psi at } 10^8 \text{ cycles}$$

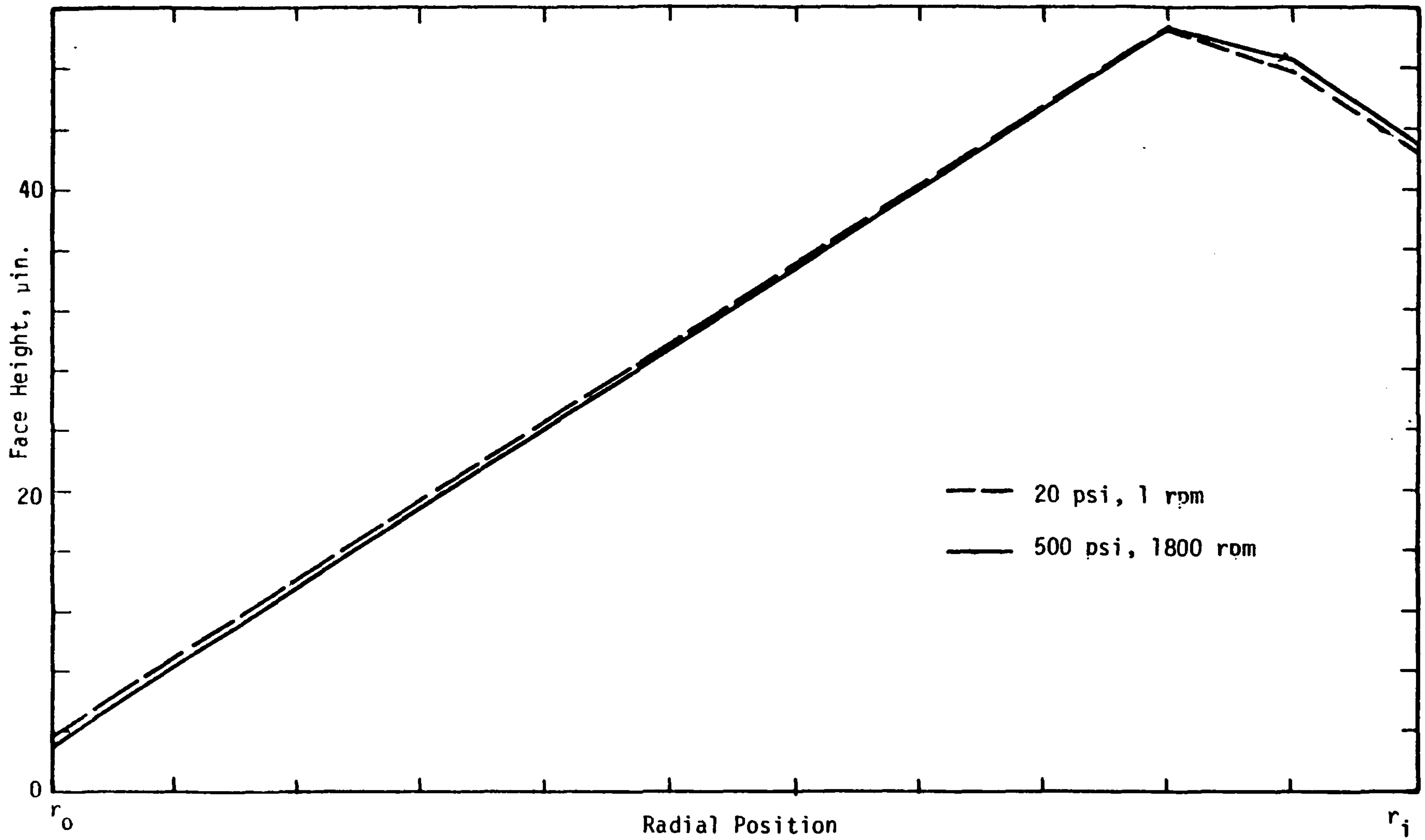

Figure 3-8. Predicted Worn Face Shape.

Several strength calculations were made. Points A and B shown in Figure 3-5 are highly stressed points. σ = 38,000 was allowed at these points. This stress determined the pad thickness and the moment arm connection system, both of which are to be as small as possible from a space point of view. It was assumed that the moment arm itself does not deflect because of the deep cross section of the arm.

Other Calculations

Many other design types of calculations were made. These include:

1) Ninth harmonic radial deflection (effects O-ring seals)
2) Assembly bolts (Monel and Inconel)
3) O-ring assembly
4) Spring pressure--spring design
5) Pressure drop in oil passages
6) Mating ring rotation
7) O-ring friction

Tilt and Offset

One of the test requirements for the simulated submarine operation test is to introduce known and variable tilt and offset misalignments in the seal. The purpose is to simulate the misalignment which results from hull deflection with variable pressure. In the test apparatus the tilt and misalignment are obtained by the rotation of a misaligned mounting cylinder.

Figure 3-9 shows the geometry of the required tilt and offset. Tilt and offset are in the same plane. The tilt and offset are specificed at each simulated test depth. Figure 3-10 shows schematically how the tilt and offset are achieved in the test apparatus. The shaft is tilted and offset relative to the end-plate as shown. The mating ring axis coincides with the shaft

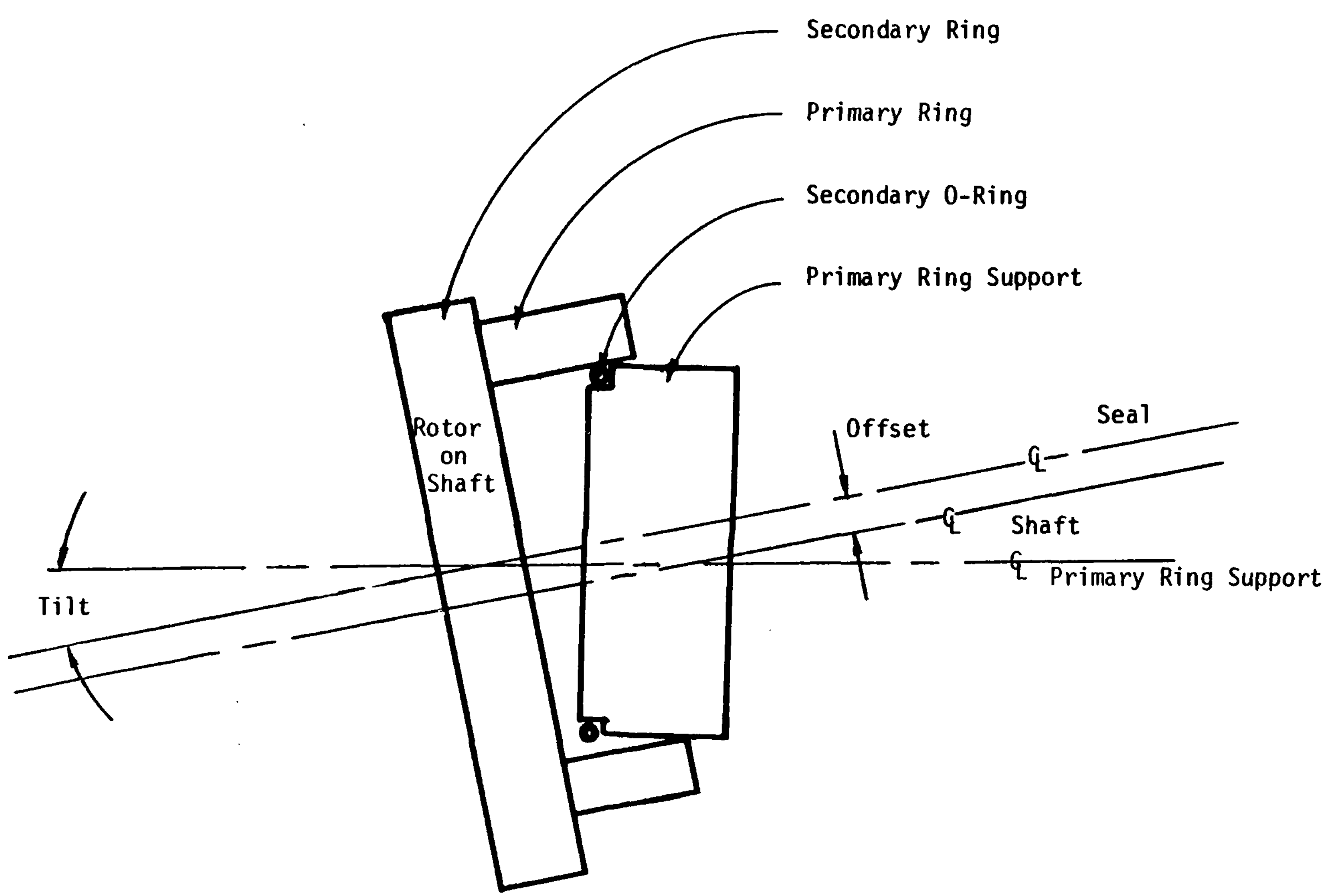

Notes: 1) Tilt and offset are in same plane.
2) Housing (primary ring) is higher than shaft.

Figure 3-9. Required Offset and Tilt.

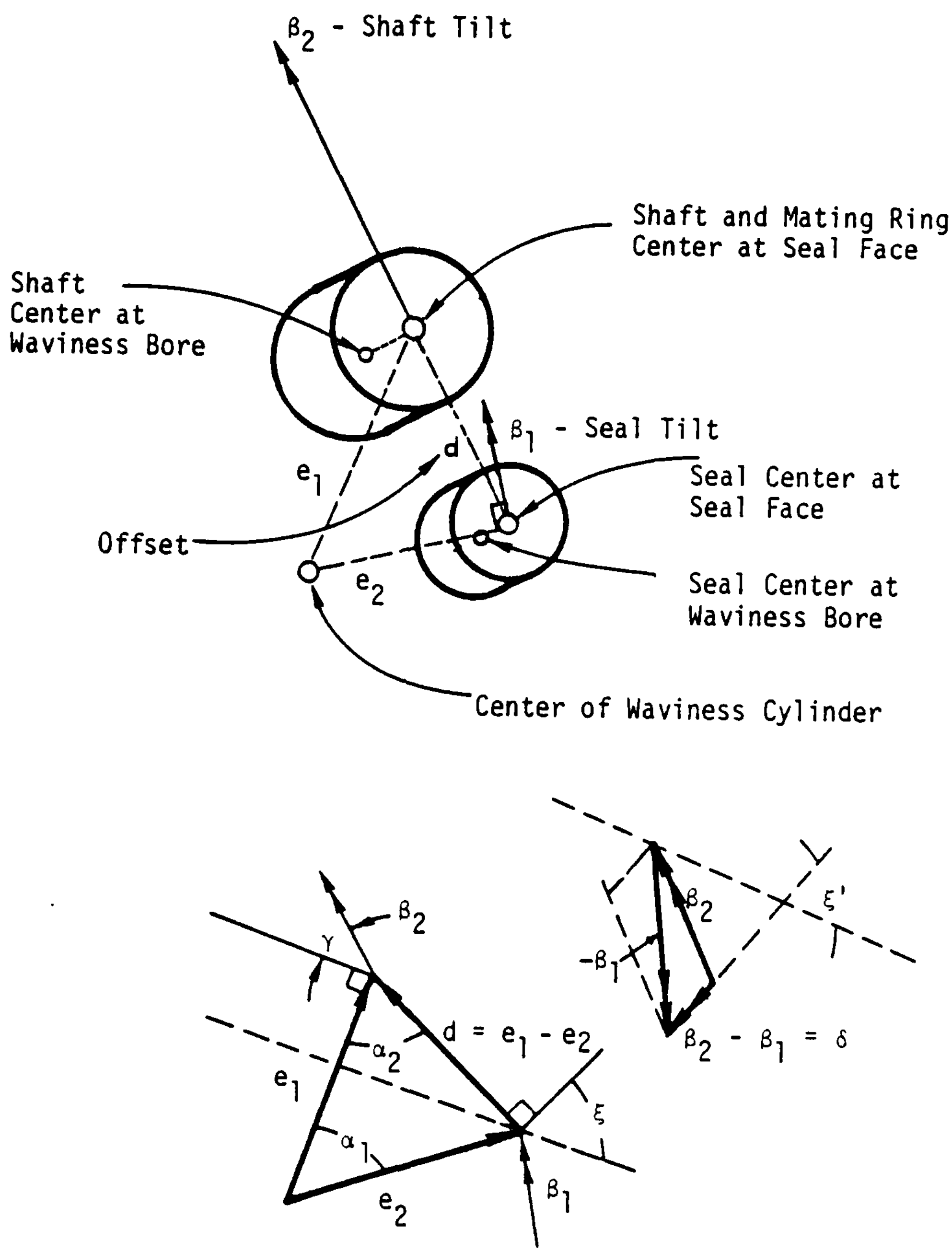

Figure 3-10. Method of Controlling Offset and Tilt.

axis. The seal axis is fixed to the waviness cyclinder axis but it is in turn tilted and offset relative to the endplate. The relative offset between the shaft and the seal are of interest. Thus the relative offset is equal to the shaft offset vectorially minus the seal offset. The tilt is equal to the shift tilt vectorially minus the seal tilt. The angle α_1 represents the positions of the waviness cylinder. If α_1 changes and all tilts and offsets are held fixed, their vector sums change with this rotation. Thus by varying the position of the waviness cylinder, it is possible to cause a variable offset and tilt. The problem of course, is to find all of the various tilt and offset angles which give the desired results.

Before the method of solution is presented, first the mathematics of the problem must be put forth. The parameters over which one has control either by manufacture or adjustment are:

β_1 - seal tilt relative to endplate

β_2 - shaft tilt relative to endplate

γ - angle of β_2 relative to e_1

e_1 - shaft offset relative to endplate

e_2 - seal offset relative to endplate

α_1 - angle of e_2 relative to e_1

Note β_1 is taken as perpendicular to e_2. This is done to simply eliminate a variable. The needed offset and tilt are shown in Figure 3-10 as vector sums of the various components. Note that ξ and ξ' should be approximately equal so that the tilt and offset are in the same plane.

Now given the above values

$$d = \sqrt{e_1^2 + e_2^2 - 2e_1e_2 \cos \alpha_1}\ , \qquad (3\text{-}15)$$

$$\alpha_2 = \cos^{-1}\left[\frac{e_1^2 + d^2 - e_2^2}{2e_1 d}\right], \tag{3-16}$$

$$\xi = \alpha_2 , \tag{3-17}$$

$$\delta = \sqrt{\beta_1^2 + \beta_2^2 - 2\beta_1\beta_2 \cos(\alpha_1 - \gamma)} , \tag{3-18}$$

$$\xi' = \cos^{-1}\left[\frac{\delta^2 + \beta_2^2 - \beta_1^2}{2\delta\beta_2}\right] - \gamma . \tag{3-19}$$

Thus, the required parameter values may be calculated quite readily.

After some considerable trial and error, the following calculational method was devised. (Note from Table 3-2 that d and δ are given as three sets of values which will be given subscripts a, b, and c.)

1) Choose e_1, e_2, β_1 and β_2.

2) Calculate α_2 from (3-16) and α_1 from the law of sines for all d.

3) Find $d\delta/d\alpha_1 \approx (\delta_c - \delta_a)/(\alpha_{1c} - \alpha_{1a})$.

4) Find $\delta_b/(d\delta/d\alpha_1)$ from above.

5) Now, from (3-18)

$$\frac{\delta}{\frac{d\delta}{d\alpha_1}} = \frac{\beta_1^2 + \beta_2^2 - 2\beta_1\beta_2 \cos(\alpha_1 - \gamma)}{\beta_1\beta_2 \sin(\alpha_1 - \gamma)} . \tag{3-20}$$

Solve this for $(\alpha_{1b} - \gamma)$.

6) Find γ since α_{1b} is known.

7) Calculate actual $\delta_a\delta_b\delta_c$ and ξ and ξ'. Compare to desired results.

Table 3-2

Offset and Tilt Results

Position	Desired Offset	Desired Tilt	Computed Offset d	Computed Tilt δ	$\xi' - \xi$	α_1
a	0.058 in.	0.0002	0.058 in.	0.00028	21°	56.2°
b	0.063 in.	0.0005	0.063 in.	0.00050	0°	61.6
c	0.067 in.	0.0007	0.067 in.	0.00070	8°	66.0

Computed results for: $e_1 = 0.063$ $e_2 = 0.060$

$\beta_1 = 0.0029$ $\beta_2 = 0.0027$

$\gamma = 52.1°$

specified by the test program, can be obtained. Details of the geometry related to this procedure are described in Chapter 3. Table 3-2 shows the final results for the selected parameter values shown. The offset values can be matched exactly. It was found that there was no way to exactly match the tilt values; so there is some error in δ_a. It is also not possible to make δ exactly perpendicular to d at all positions. $\xi' - \xi$ shows the error in the first and last positions.

Given the reasons for introducing the tilt, it was judged that the above is sufficiently close to the desired to assess the effects of variable offset and tilt in operation. At the same time, the tilt and offset are readily changed by rotating the waviness cylinder. This can be performed by computer control and thus saves a great amount of repetitive manual adjusting.

Summary

The preceding sections provide brief descriptions for the computational portion of the nine-wave seal design. Details of the hardware itself are given in Chapter 2.

CHAPTER 4

MOVING WAVE GAS SEAL

Background

There are several types of gas seals being used in industry today, but due to the demands of advanced technology, a more reliable gas seal is still needed. Experimental work on the moving wave liquid seal has demonstrated some promising results in minimizing leakage, friction, and wear using this concept. The potential advantages of a moving wave gas seal are that 1) the seal will not foul by dirt or oil because the faces are continuously wiped by the moving wave action, 2) the seal will not be detrimentally affected by liquid contamination since it can be designed to operate in liquid and gas environments, 3) uneven wear caused by hot spots or contact can be smoothed out by the continual wearing in process of the seal, and 4) the seal is stiff and good tracking at high speeds would be expected. In this chapter, this concept has been applied to a gas seal. A moving wave gas seal has been modeled and the results are presented herein.

State-of-Art of the Gas Seals--It was not until the late 50s and early 60s that gas bearings and gas interface gas seals respectively were developed. In order to satisfy different kinds of applications and requirements, various types of gas seals have been tried. There are about four main types of gas seals.

A buffered gas seal is a double seal configuration (Figure 4-1) using oil as a buffer. The purpose of the buffer oil is to guard against the escape of the sealed fluid to the external atmosphere and also to provide lubrication between the seal faces. The buffered seal can seal corrosive gases up to 750 psi (5.17 MPa) with rubbing speeds up to 350 ft/s (106.7 m/s). The

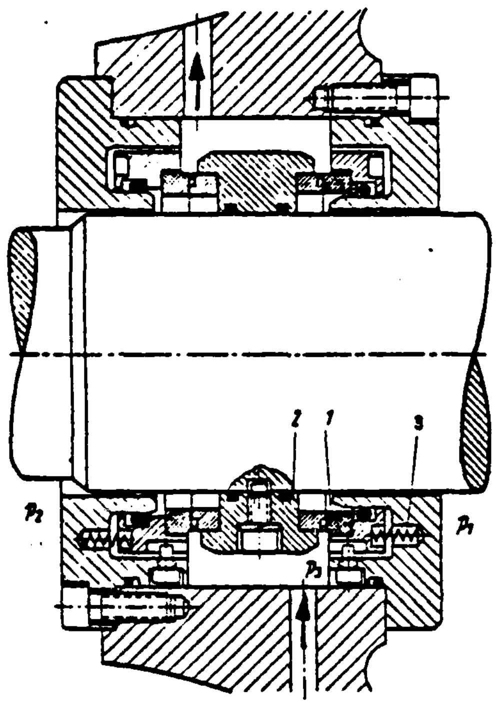

1. Primary Ring

2. Secondary Ring

3. Spring

$\left.\begin{array}{l} P_1 \\ P_2 \end{array}\right\}$ Sealed Gas Pressures

P3 Buffered Oil Pressure

Figure 4-1. Buffered Gas Seal.

oil pressure is about 30 to 50 psi (0.21 to 0.34 MPa) higher than the system gas pressure. The buffer oil also acts as a coolant to the system. The major disadvantages of this gas seal are that a pressure pump, a filter, and a heat exchanger are required to deliver the buffer oil from an external source [25] and that the oil may contaminate the process fluid.

A shrouded Rayleigh step gas seal is shown in Figure 4-2. Basically, it contains a pumping land or dam and a pocket which is surrounded by a sealing area of small gap. There are other configurations as shown in Figure 4-2. When the secondary seal ring rotates, the Rayleigh pockets will scoop up the sealed gas and raise the gas pressure; at the same time the lands around the pocket will restrict the gas outflow. So the performance of this kind of seal depends on the land area to pocket area trade-off. This implies that if the land is wide, less area is available for pressure generation, but sealing is good. According to Cheng, Castelli and Chow [26], the leakage of this seal is largely determined by hydrodynamic action; the stronger the hydrodynamic action is, the more the leakage will be. Quantitatively speaking, the leakage rate is slightly higher than that of the spiral-groove orifice gas seal discussed later. The change of a pressure ratio (P_o/P_i) has little effect upon the stiffness as well as the load support.

According to Zuk, Ludwig and Johnson [27], NASA has sponsored tests of the Rayleigh seal for future supersonic tranport engines. The performance demonstrated the feasibility of operation at gas temperatures up to 1200°F (650°C), pressure differentials across the seal up to 250 psi (1.7 MPa) and relative surface speeds up to 450 ft/sec (140 m/sec). After 338.5 hours of testing, the average wear on the carbon seal was less than 5 μin. (0.13 μm). In the total 500 hours test, the seal had encountered over 50 startups and shutdowns and the leakage rates

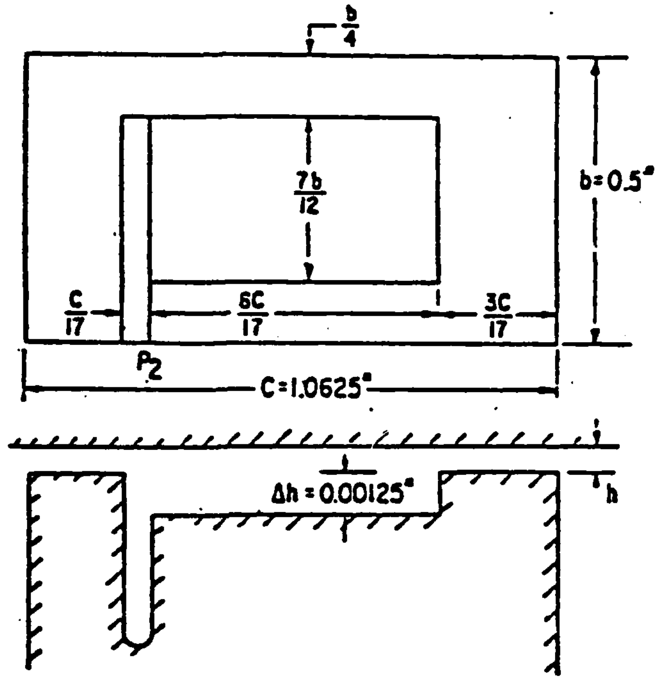

(a) Typical Configuration of a Rayleigh Step Seal

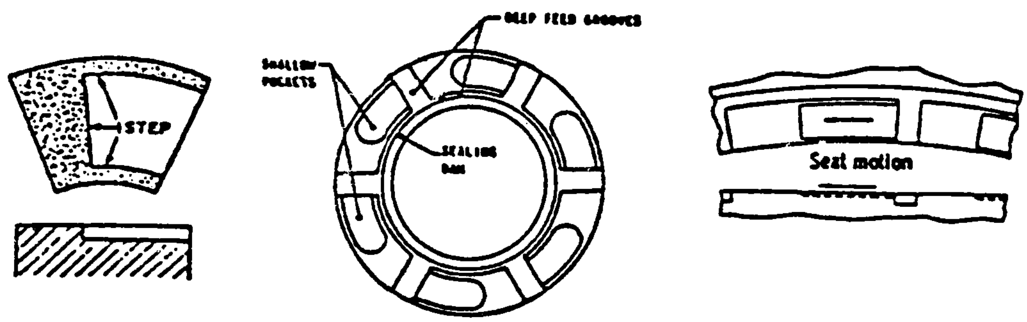

(b) Other Configurations of Step Seals

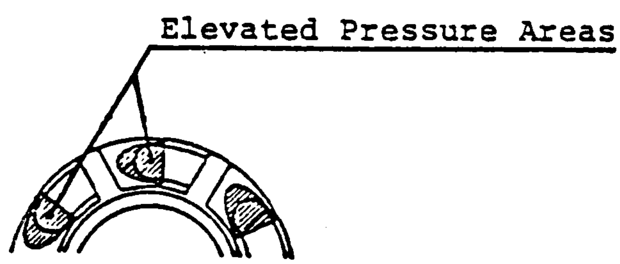

(c) High Pressure Areas

Figure 4-2. Shrouded Rayleigh Step.

varied from 11 to 32 SCFM (0.31 to 0.91 SCMM) with an average leakage about 25 SCFM (0.71 SCMM).

Among the various kind of gas seals, the so-called spiral-groove gas seal is well known. As shown in Figure 4-3, the surface of the secondary seal has been machined or etched in the form of spiral-grooves which are equally spaced. The spiral does not extend across the full width of the seal but terminates in a circumferential sealing dam. The purpose of the spiral is to pump the sealed gas inward while the dam restricts radial leakage. Thus, the gas is pressurized over the whole area of the seal and the seal load is supported by this pressure. According to Sedy [28], leakage rates as low as 0.1 SCFM at 850 psig (5.86 MPa) gas pressure on 4.5 inches (114.3 mm) diameter seal with 10,380 rpm speed have been recorded. Typically the leakage is about 1.9 SCFM (0.05 SCMM) in the same test and seal. The wear which occurred on the seal face during this test was about 4 μin. (0.1 μm) after 1000 hours.

At the present state-of-art, existing gas seals are satisfactory for many applications; leakage is relatively low and shaft speeds up to 20,000 rpm can be used for smaller seals. However, improvements are still needed. For instance, the gas film riding seals above are sensitive to the detrimental effects of dirt or liquid contamination. Dirt or liquid will alter the pressure distribution and abrasive wear may occur. Seal leakage rate and wear may dramatically change. High spots occur on most mechanical seal faces. As a result, hot spots may occur due to highly localized friction, and wear as well as driving torque may ultimately become higher. This behavior can lead to complete seal failure. Most gas film riding gas seals have relatively high leakage rates. With regard to these problems, further improvements in the state-of-art would be most beneficial. In pursuit of such improvements, the wavy gas seal deserves study.

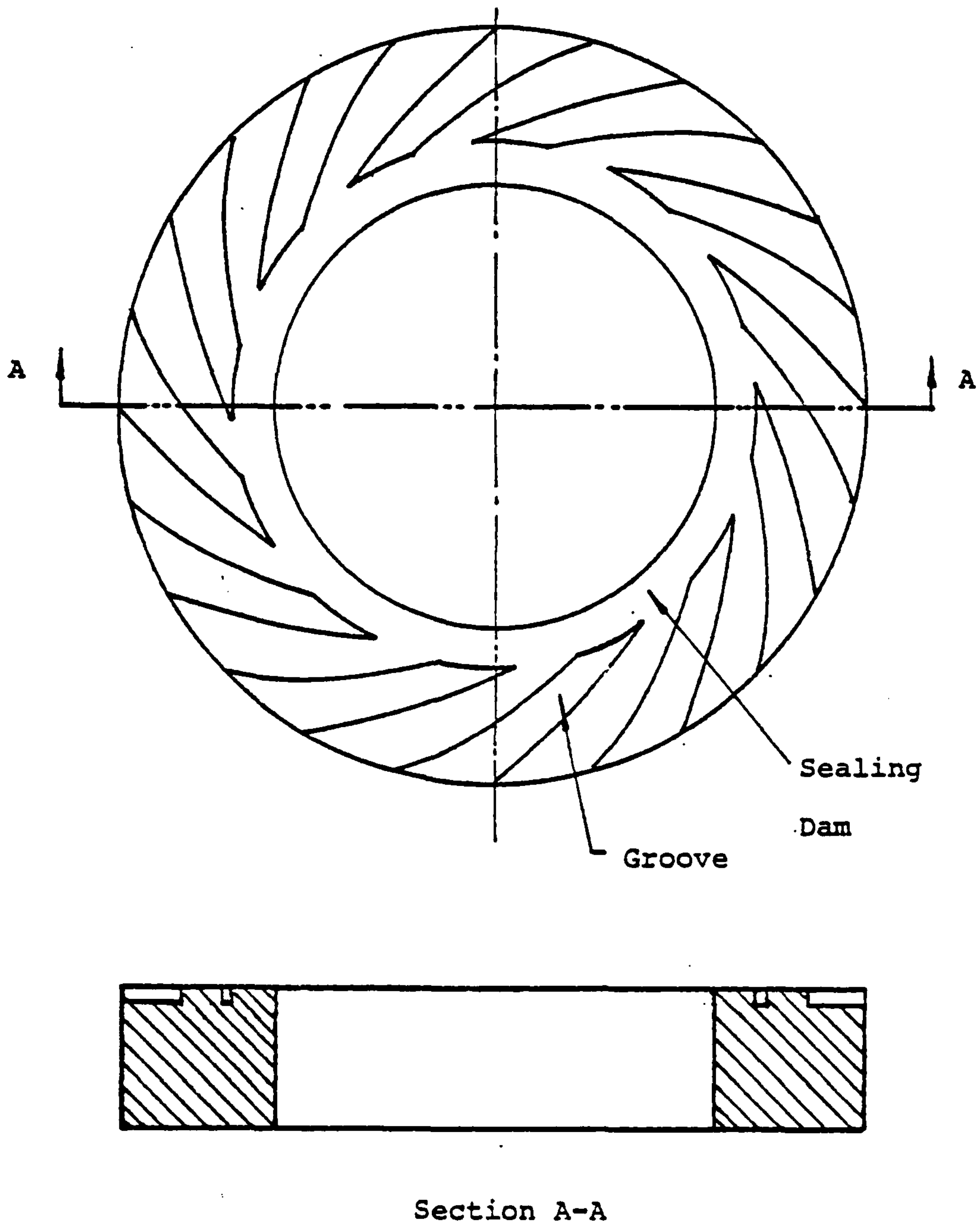

Figure 4-3. Spiral Groove Gas Seal.

In terms of the required analysis the gas seal is somewhat different than the liquid seal studied previously herein. Thus it is useful to review the literature for studies of other types of gas seals to better understand what is important and the computational methods available.

Literature Review--In the late 1960s, many successful and efficient techniques of seal analysis were developed. First, James and Potter [29] solved for the pressure distribution for both spiral-groove thrust bearings and spiral-groove compressors. They derived a "jump" boundary equation between the land and the groove, and then made use of variable transformations to straighten out the groove for easier computation. To facilitate further the analysis, they changed the dependent variable from P to Q where $Q = 1/2\ P^2$. Finally, they used an iterative technique to find the pressure distribution. Given the pressure distribution, the gas flow, load support, friction, static stiffness, power consumption and efficiency can be calculated.

Cheng, Castelli and Chow [26] made detailed analyses of two high speed noncontacting hybird seals, the spiral-groove and Rayleigh step seals. The first part of their paper shows the performance of the spiral-groove seal with orifices and then without orifices. The differences in performance between the cases where the grooves are located at the high pressure and the low pressure or both sides were also studied.

In the Rayleigh step real analysis [26], several assumptions were made: laminar and isothermal flow, Newtonian fluid, and negligible inertia. With the change of variable $P^2 = Q$, the Reynolds equation was expressed in finite difference form. The result is a set of equations with the pressure (Q) at five points operated on by a linear algebraic operator. These equations were solved by the so-called matrix inversion technique developed from Reference [30]. This technique enables one to formulate the m x n unknowns in m x n linear equations with known coefficients. However, because pressure P acts as a variable coefficient (which is assumed to be a constant for each iteration), an iterative procedure was adopted to improve the guess values of P.

The second part of the Cheng, Castelli and Chow paper [26] gives typical performance for a non-parallel film profile spiral-groove-orifice seal as well as for the Rayleigh step seal. Finally, a comparison was made between the two seal geometries on their tolerance to tilt or coning under a constant seal load. The authors concluded that the difference in stiffness and leakage between the two seals is small, but the spiral-groove-orifice seal shows small variations in leakage rate as well as axial stiffness with respect to tilt or coning.

Gardener [31] has summarized and presented a numerical method for solving the design problem of a spiral groove noncontacting seal. Gardener considered pressure to be a function of radius only, so that the analysis was simplified. Some time later, Gardener [32] presented a paper covering additional developments on noncontacting spiral-groove seals. He pointed out several modifications to improve performance.

Zuk, Ludwig and Johnson [27] presented an approximate quasi-one-dimensional model for compressible fluid flow across face seals. Both the flat face and Rayleigh step gas seals were considered and tested. The model includes fluid inertia, viscous friction and entrance losses. It is valid for both laminar and turbulent flows. Both subsonic and choked flow conditions can be predicted by using an approximate integrated model (an iterative technique). Results agree with classical subsonic compressible viscous flow theory for Mach number less than $1/\sqrt{\gamma}$, where γ is the ratio of specific heats. If Mach number is equal to 1, sonic velocity and thus choked flow will occur. Results also show that near critical flow conditions (Mach number = 1), the film stiffness is negative, that is, as film thickness and Mach number increase, the applied load actually increases. For choked flow the analysis predicts a high positive film thickness. The authors also found that as the sealing dam width increases, the critical pressure ratio (ambient pressure over sealed pressure) for choking decreases.

Later, Zuk [33] presented an application of the finite element method to compressible problems using a Galerkin solution technique. The most significant aspect of this paper is the inclusion of a fluid inertia term as well as choked flow conditions which make the compressible flow equations nonlinear. He also compares the advantages and disadvantages between the finite element method and the finite difference method.

In the late 1970s, Sedy [28] found that the performance of a spiral-groove gas seal can be improved through enhancement of hydrodynamic effects. Similar results are also applied to Rayleigh step gas seals. The methods of improving the performance include 1) using a high balance ratio, 2) widening the sealing dam, 3) increasing the overall face width, and 4) modifying the carbon sealing ring cross section.

Later, Sedy [34] presented a new self-aligning mechanism for improving the stability of spiral-groove gas seal. That is, when originally parallel faces of the mating rings deflect, the change in pressure profile tends to return the deflected ring toward its parallel position. It does not matter whether the deflection is convergent or divergent. If the gap is stable, the leakage and radial distortion are also stable. However, to benefit from this effect the pressure between the spiral-groove and the dam must be higher than the sealed pressure and the centroid location must be controlled. This mechanism not only minimizes angular deflection of the primary low-modulus seal ring, but also minimizes fluctuations in the gap width.

Concerning methods of solution for the pressure, from a mathematical point of view, gas seal analysis is more complicated than liquid seal analysis. Although gas seal analysis is not a new branch of research, relevant information and techniques to solve for the pressure distribution are still being developed. In 1968, Castelli and Pirvics [35] reviewed different kinds of numerical methods for the solution of the gas bearing problems. The authors described some of the techniques using explicit, implicit and semi-implicit methods for the time-dependent Reynolds equation. The Alternating Direction Implicit method was also mentioned. Due to the nonlinear nature of the compressible Reynolds equation, solution techniques such as Gaussian Elimination become just a part of a larger iteration solution.

According to Fairweather and Mitchell [36], Alternating Direction Implicit (A.D.I.) methods have proven to be valuable finite difference methods for various types of partial differential equations, such as the parabolic and elliptic equations in two or three space variables. They discussed the computation procedure of the A.D.I. method from a pure numerical point of view. A paper by Evans and Gane [37] is a good example of the application of A.D.I. They were successful in applying this method to transient heat conduction problems. Also, Roache [38] has a concise description on the A.D.I. method. He generalized the experience of some researchers and concluded that A.D.I. methods do allow large time steps and fast overall computation.

One of the more useful references for bearing analysis was written by Shapiro [39]. He gives very detailed discussions of numerical techniques, presents several examples, and makes suggestions for future development. One of his examples is the A.D.I. scheme applied to a gas-lubricated bearing. He used a so-called "cell" approach which operates on the continuity equation rather than on Reynolds equation. This method is said to be more convenient in solving complex goemetries than the direct Reynolds equation analysis.

Finally, according to Gargiulo and Gilmour [40], the A.D.I. method has been shown to be efficient, flexible and free from cummulative round off errors for the design of externally pressurized porous gas bearings. They used a systematic method to replace the Laplace difference operator in the pressure field by a finite difference approximation according to the A.D.I. scheme. They also gave a set of linear algebraic equations first in radial direction and then in the circumferential direction. The two tridiagonal systems were efficiently solved by an elimination algorithm.

Theory

In this section, a model of a moving wave gas seal is presented. The moving wave gas seal can be described as a gas seal that has both moving waviness and tilt imposed upon the seal face of the primary seal ring (see Figure 1-3). This section includes the derivation of the difference equations from the Navier-Stokes equations and techniques for obtaining load support, leakage, and friction. Mesh effect, time step effect and convergence criteria are also investigated. Finally, a flow chart of the computer program and its subroutines and example solutions are presented.

Compressible Flow Equations--Compressible flow equations for a thin film are obtained from a simplification of the Navier-Stokes equations. The simplifying assumptions used are:

1) Gas viscosity is constant
2) Perfect gas
3) Body forces are negligible
4) Flow is laminar, there are no vortices or turbulence anywhere in the lubricant film
5) Inertial forces are negligible compared with the viscous forces
6) No slippagae occurs at the sealing faces

7) The curvature of the fluid film surface is negligible

8) Compared with the two velocity gradients, $\partial V_r/\partial z$ and $\partial V_\theta/\partial z$, all other velocity gradients are negligible.

Since these assumptions are widely accepted for gas seal analysis, further justification will not be given here. However, details are available in Reference [23].

One further assumption made is that the seal surface roughness as shown in Figure 4-4 does not significantly affect the resulting flow equations and that the mean film thickness may be used instead of the actual film thickness for computational purposes. This assumption is discussed in detail in Reference [4].

By applying the above assumptions, the Navier-Stokes equations in polar coordinates can be simplified to the following,

$$\frac{\partial P}{\partial r} = \eta \frac{\partial^2 V_r}{\partial z^2} , \tag{4-1}$$

$$\frac{\partial P}{r\partial \theta} = \eta \frac{\partial^2 V_\theta}{\partial z^2} , \tag{4-2}$$

$$\frac{\partial P}{\partial z} = 0 . \tag{4-3}$$

Figure 4-5 shows the applicable coordinate system. Integrating the above differential equations, the result is

$$V_r = \frac{1}{2\eta} \frac{\partial P}{\partial r} z^2 + C_1 z + C_2 , \tag{4-4}$$

$$V_\theta = \frac{1}{2\eta r} \frac{\partial P}{\partial \theta} z^2 + C_3 z + C_4 . \tag{4-5}$$

Applying the boundary conditions shown in Figure 4-5

$$z = 0 \quad V_{r_1} = 0 \quad V_{\theta_1} = \omega r \quad V_{z_1} = 0 , \tag{4-6}$$

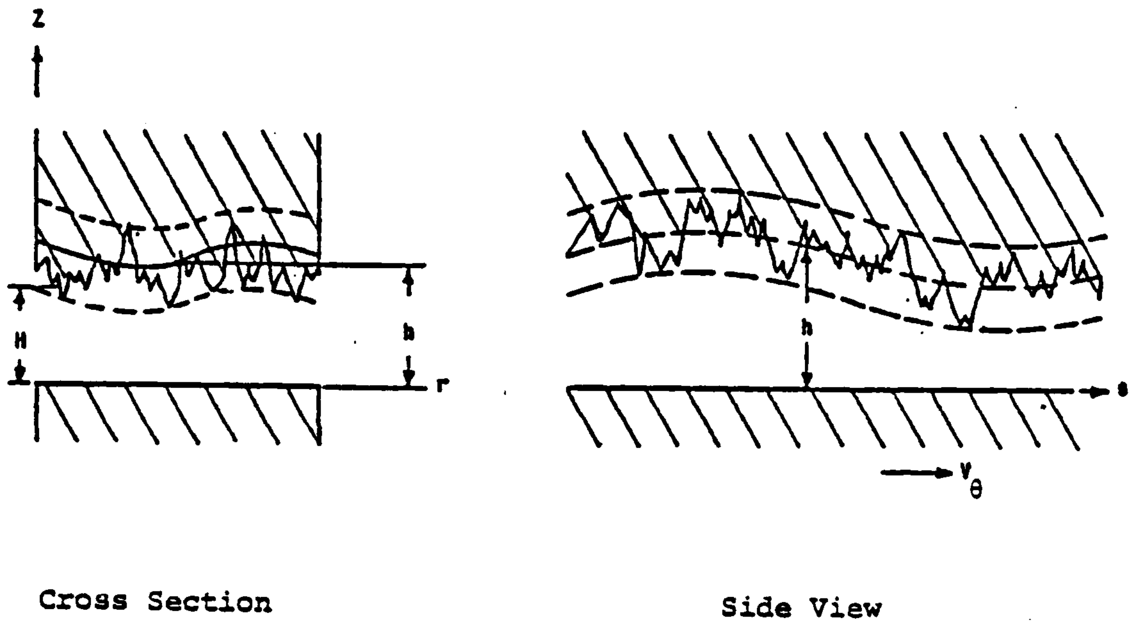

Figure 4-4. Radial and Circumferential Profiles.

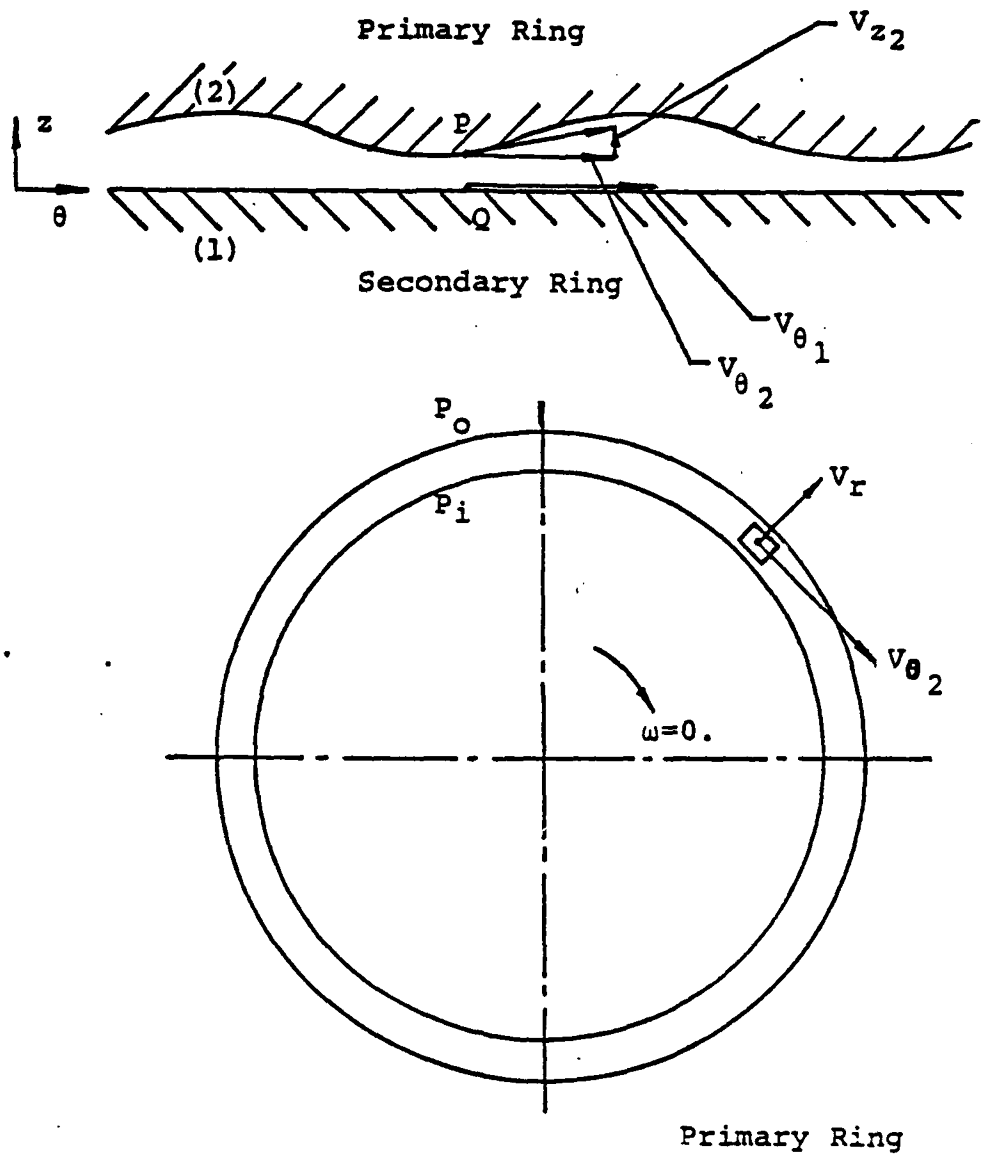

Figure 4-5. Boundary Conditions and Geometry.

$$z = h \quad V_{r_2} = 0 \quad V_{\theta_2} = 0 \quad V_{z_2} = 0 \ , \tag{4-7}$$

we then obtain two component equations of the fluid flow,

$$V_r = \frac{\partial P}{2\eta \partial r} (z^2 - zh) \ , \tag{4-8}$$

$$V_\theta = \frac{\partial P}{2r\eta\partial\theta} (z^2 - zh) + \omega r(1 - \frac{z}{h}) \ . \tag{4-9}$$

The mass flow rate is,

$$m_r = \int_0^h \rho V_r (r d\theta) \, dz \ , \tag{4-10}$$

$$m_r = - \frac{\rho r \Delta\theta}{12\eta} h^3 \frac{\partial P}{\partial r} \ , \tag{4-11}$$

$$m_\theta = - \frac{\rho \Delta r}{2} \left[\frac{h^3}{6\eta r} \frac{\partial P}{\partial \theta} - \omega \, rh \right] . \tag{4-12}$$

The continuity equations for an element of volume is

$$\frac{\partial}{\partial t} \int_V \rho \, dV + \int_s \rho \vec{V} \cdot n \, ds = 0 \ . \tag{4-13}$$

With Reference to Figure (4-6) the continuity equation can be written as,

$$\frac{\partial}{\partial t} \int_0^h \rho \ \Delta a \ dz + m_{j+1/2} + m_{i+1/2} + m_{j-1/2} + m_{i-1/2} = 0 \ , \tag{4-14}$$

where the 1/2 points refer to mass flow halfway between nodes. The mass change inside the control volume can be written in differential form as

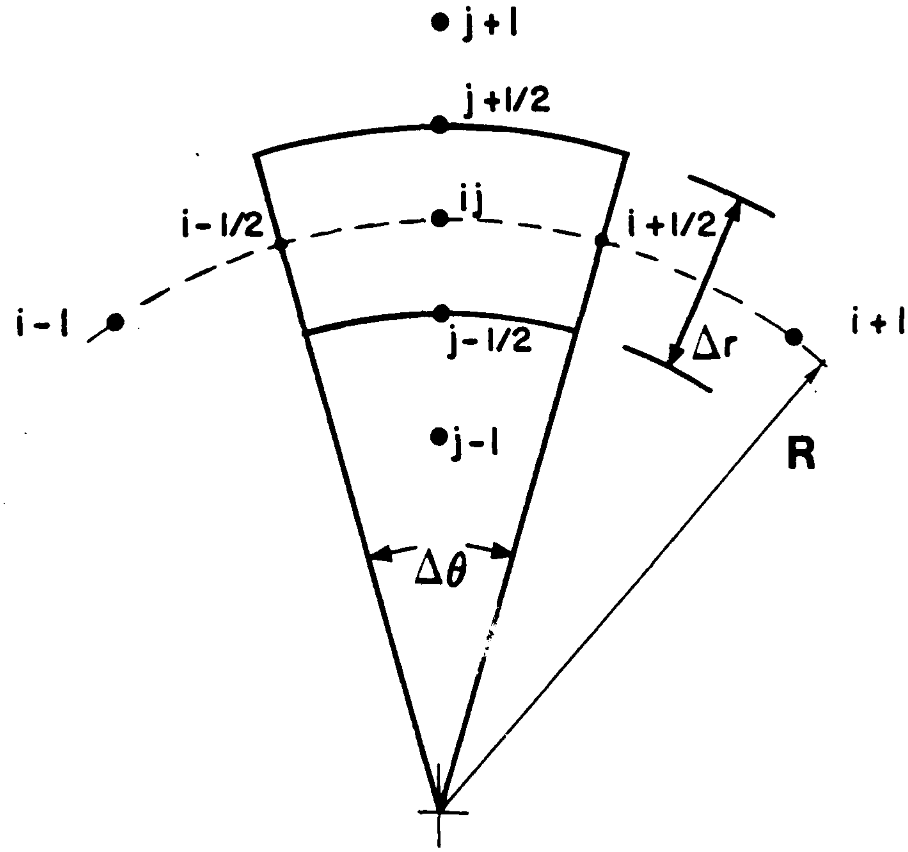

Figure 4-6. Control Volume.

$$m_V = \frac{\partial}{\partial t}\,[\rho h \Delta a] \; , \tag{4-15}$$

where Δa = surface area of top or bottom of the control volume. Using Equations (4[illegible] (4-12) the mass flows are

$$m_{j+1/2} = -\left[\frac{r\Delta\theta\rho h^3}{12\eta}\,\frac{\partial P}{\partial r}\right]_{j+1/2} \; , \tag{4-16}$$

$$m_{j-1/2} = +\left[\frac{r\Delta\theta\rho h^3}{12\eta}\,\frac{\partial P}{\partial r}\right]_{j-1/2} \; , \tag{4-17}$$

$$m_{i+1/2} = -\left[\Delta r\;\frac{\rho h^3}{12\eta r}\,\frac{\partial P}{\partial \theta} - \frac{\rho\omega r h}{2}\right]_{i+1/2} \; , \tag{4-18}$$

$$m_{i-1/2} = +\left[\Delta r\;\frac{\rho h^3}{12\eta r}\,\frac{\partial P}{\partial \theta} - \frac{\rho\omega r h}{2}\right]_{i-1/2} \; . \tag{4-19}$$

Substituting Equations (4-15) through (4-19) into Equation (4-14), assuming a perfect gas, isothermal conditions and $\partial h/\partial t \to 0$ (no squeeze), one gets

$$\left[12\eta h\,\frac{\partial P}{\partial t}\right]_{i,j} - \left[\frac{r\Delta\theta P h^3}{\Delta a}\,\frac{\partial P}{\partial r}\right]_{j+1/2} + \left[\frac{r\Delta\theta P h^3}{\Delta a}\,\frac{\partial P}{\partial r}\right]_{j-1/2}$$

$$+ \left[\frac{\Delta r P h^3}{r\Delta a}\,\frac{\partial P}{\partial \theta}\right]_{i-1/2} - \left[\frac{\Delta r P h^3}{r\Delta a}\,\frac{\partial P}{\partial \theta}\right]_{i+1/2}$$

$$+ \frac{6\eta\Delta r\omega}{\Delta a}\left[(Prh)_{i+1/2} - (Prh)_{i-1/2}\right] = 0 \; . \tag{4-20}$$

AD-A125 810 APPLICATION OF THE WAVY MECHANICAL FACE SEAL TO SUBMARINE SEAL DESIGN(U) NEW MEXICO UNIV ALBUQUERQUE COLL OF ENGINEERING A O LEBECK ET AL. JUL 82 2/3

UNCLASSIFIED ME-117(82)ONR-414-1 N00014-76-C-0071 F/G 11/1 NL

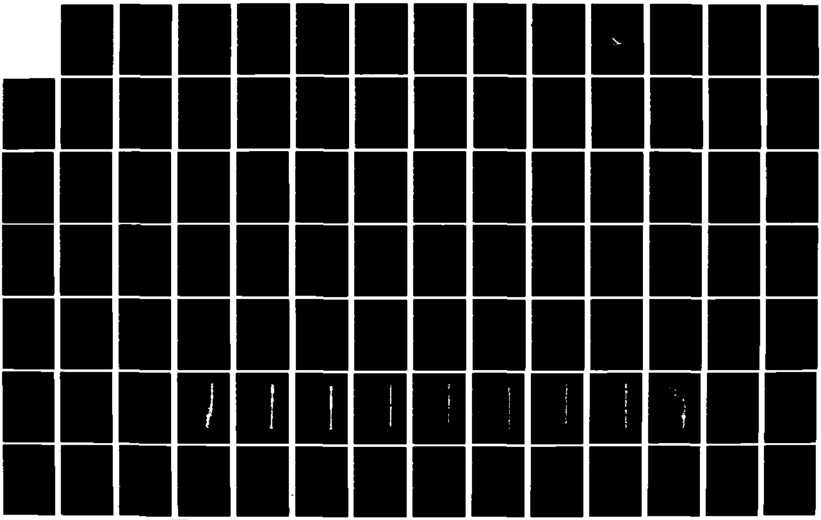

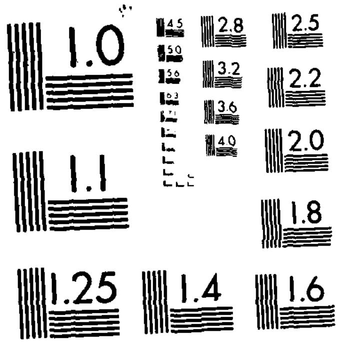

MICROCOPY RESOLUTION TEST CHART
NATIONAL BUREAU OF STANDARDS-1963 A

To linearize the problem a change of variable is made,

$$Q = P^2 \tag{4-21}$$

so that

$$P \frac{\partial P}{\partial \theta} = \frac{1}{2} \frac{\partial Q}{\partial \theta} \text{ , etc .} \tag{4-22}$$

Incorporating this change in Equation (4-20) and using central differences to approximate the derivatives,

$$\frac{12\eta h_{i,j}}{P^*_{i,j}} \frac{(Q_{i,j} - \bar{Q}_{i,j})}{2\Delta t} - \frac{(h^3\ r)_{j+1/2}\ \Delta\theta}{2\Delta a} \frac{(Q_{i,j+1} - Q_{i,j})}{\Delta r}$$

$$+ \frac{(h^3\ r)_{j-1/2}\ \Delta\theta}{2\Delta a} \frac{(Q_{i,j} - Q_{i,j-1})}{\Delta r} + \frac{h^3_{i-1/2}\ \Delta r}{2r_{i,j}} \frac{(Q_{i,j} - Q_{i-1,j})}{\Delta a\Delta\theta}$$

$$- \frac{h^3_{i+1/2}\ \Delta r}{2r_{i,j}} \frac{(Q_{i+1,j} - Q_{i,j})}{\Delta a\Delta\theta} + \frac{6\eta\omega r_{i,j}\Delta r}{2\Delta a}$$

$$\times \left\{ \left[\frac{Q_{i+1,j}}{P^*_{i+1,j}} + \frac{Q_{i,j}}{P^*_{i,j}}\right] h_{i+1/2} - \left[\frac{Q_{i,j}}{P^*_{i,j}} + \frac{Q_{i-1,j}}{P^*_{i-1,j}}\right] h_{i-1/2} \right\}$$

$$= 0 \text{ .} \tag{4-23}$$

where $\tilde{Q}$ is the value of Q at a previous time step and the remaining P^*'s are assumed known from a previous iteration. Since $\tilde{Q}$ and the remaining P's are assumed known, Equations (4-23) become linear equations at any time step with variable Q. Grouping all the like terms as coefficients, the above equation becomes,

$$
\begin{aligned}
Q_{i,j}&\left[\frac{12h_{i,j}\ \Delta a}{P^{*}_{i,j}\ \Delta t\,\Delta r} + \frac{(h_{i,j+1/2})^{3}\ r_{i,j+1/2}\ \Delta\theta}{\Delta r\Delta r} - \frac{(h_{i,j+1/2})^{3}\ r_{i,j-1/2}\ \Delta\theta}{\Delta r\Delta r}\right] \\
&+ Q_{i,j+1}\left[-\frac{(h_{i,j+1/2})^{3}\ r_{i,j+1/2}\ \Delta\theta}{\Delta r\Delta r}\right] \\
&+ Q_{i,j-1}\left[-\frac{(h_{i,j-1/2})^{3}\ r_{i,j-1/2}\ \Delta\theta}{\Delta r\Delta r}\right] \\
= \tilde{Q}_{i,j}&\left[\frac{12\eta\Delta a h_{i,j}}{P^{*}_{i,j}\ \Delta t\,\Delta r} - \frac{(h_{i-1/2,j})^{3}}{r_{i,j}\ \Delta\theta} - \frac{(h_{i+1/2,j})^{3}}{r_{i,j}\ \Delta\theta} - \frac{\Delta r_{i,j}}{P_{i,j}}\left(h_{i+1/2,j} - h_{i-1/2,j}\right)\right] \\
&+ \tilde{Q}_{i+1,j}\left[\frac{(h_{i+1/2,j})^{3}}{r_{i,j}\ \Delta\theta} + \frac{r_{i,j}\ h_{i+1/2,j}}{P^{*}_{i+1,j}}\right] \\
&+ \tilde{Q}_{i-1,j}\left[\frac{(h_{i-1/2,j})^{3}}{r_{i,j}\ \Delta\theta} + \frac{r_{i,j}\ h_{i-1/2,j}}{P^{*}_{i-1,j}}\right]. \qquad (4\text{-}27)
\end{aligned}
$$

A special Gaussian elimination subroutine is used to solve the above tridiagonal equations. It stores the diagonal coefficients in a compact column matrix and takes advantage of the sparseness of the matrix to save computer time.

Boundary Conditions--The boundary conditions for the gas seal are similar to those for a liquid seal. That is,

$$P(r_i) = P_i \ ,$$

$$P(r_o) = P_o \ , \qquad (4\text{-}28)$$

where P_i and P_o are the inside and outside pressures of the seal, respectively. Within the seal region pressures are set initially at time zero to values based on linear interpolations between the inside and outside pressure.

Mesh effect--One measure of solution accuracy is to compare the leakage rates at the inside and outside radii of the seal. Figure 4-7 shows this comparison as a function of tilt for two mesh sizes. A different grid size results in different leakage rates, but the difference is decreased by a finer mesh. The error increases with increasing tilt because a greater change in gap across the seal is produced.

Presumably, the leakages will converge to each other at all tilt angles if one can refine the mesh as small as possible. In practice one cannot refine the mesh too far because of cost. Hence, grid size comparison is terminated at the 19 x 20 mesh. All the results obtained are based on this mesh scheme.

Convergence and Time Step--Using the ADI method, one solves for the pressure field as a function of time. In this steady-state problem, one is actually solving for the transient response from an arbitrary starting pressure field to that which is the steady-state solution keeping the film thickness constant with time. A measure of satisfactory convergence is the total load supported by the pressure. Presumably, when this load stops changing with time, steady state has been reached.

In order to check the stability and convergence of the program, a series of data was computed and is plotted in

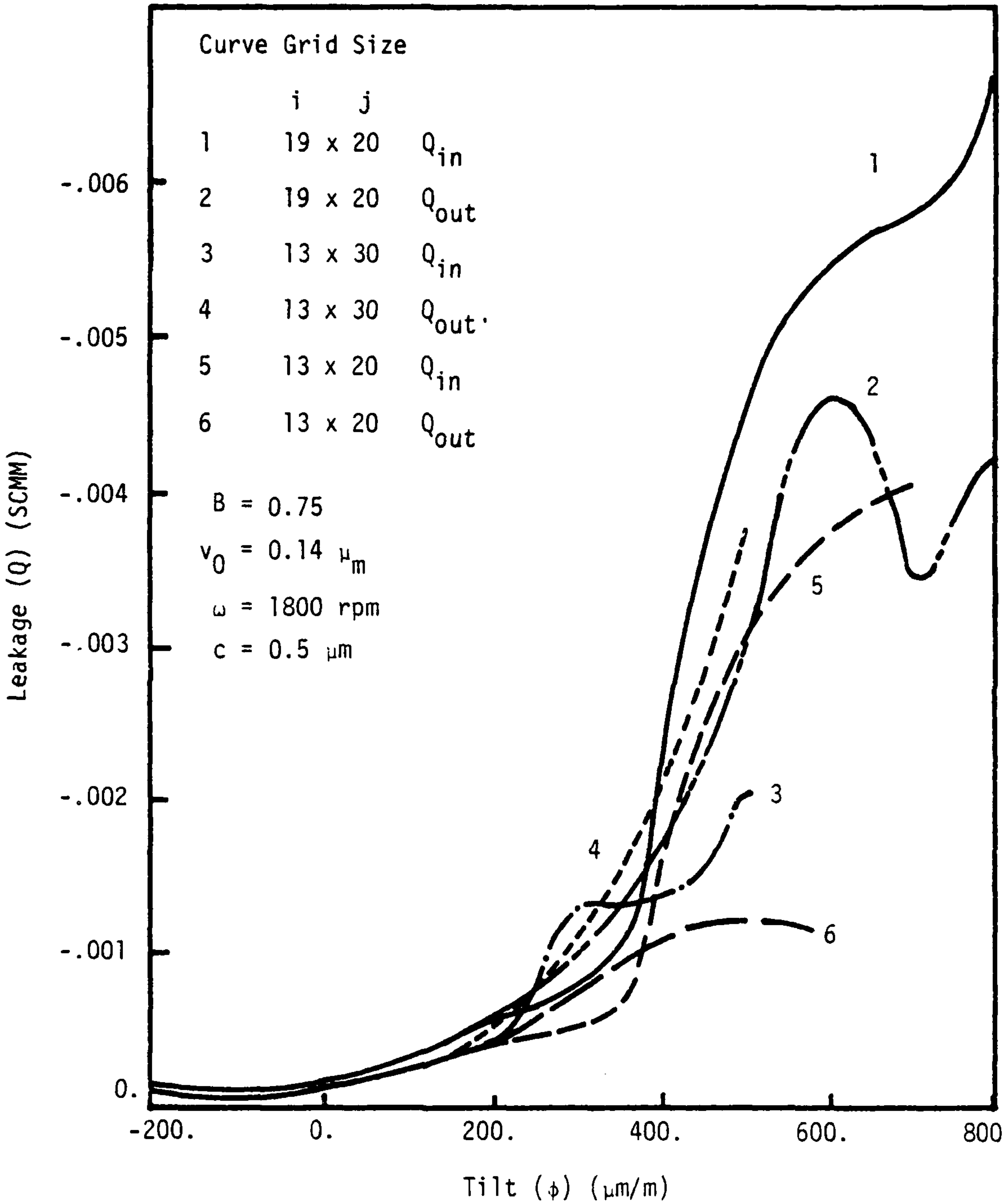

Figure 4-7. Leakage as a Function of Tilt.

Figure 4-8. In this figure, the maximum difference in absolute pressure (ΔP) between the old iteration values and the new values is used as a convergence criterion. The effect of pressure error and the time step on the fluid load support and the total computation time is shown. The figures show clearly that the pressure error can be used to get a satisfactory convergence on load support.

It is shown that a larger pressure error criterion requires a larger time step to obtain proper convergence on load. Less computational time is taken using this approach. If the pressure error remains the same while the time step is decreased as shown in Figure 4-8, a false or premature convergence results. On the other hand, if the pressure error is decreased, very consistent load support is found at various time steps. However, if the pressure error is decreased even more (e.g., $\Delta P < 5.5$ Pa), the execution for the larger time step ($\Delta T = 5 \times 10^{-5}$ S) will be terminated because negative pressures occur. Also, the program loops without stopping for the smallest time step ($\Delta T = 5 \times 10^{-7}$ S) because the pressure error (ΔP) is too small to meet.

As shown, care must be taken in order to pick a suitable pressure error and time step. Otherwise, too much computer time or false convergence will result. In this investigation, the pressure error criterion is taken to be the sum of the absolute changes for all the nodes. This value is taken at 3.5 KPa for 18 x 18 nodes. This corresponds approximately to 11 Pa in Figure 4-8. The time step is chosen to be 5×10^{-6} seconds.

Seal System--the moving wave gas seal can be defined by two sets of parameters, application parameters and design parameters. The former category includes the pressure differential to be sealed ($P_o - P_i$), the angular speed (ω) of the shaft, shaft diameter (D), seal centroid radius (r_c) and fluid viscosity (η). All of these parameters are fixed because of the requirements of a particular seal application.

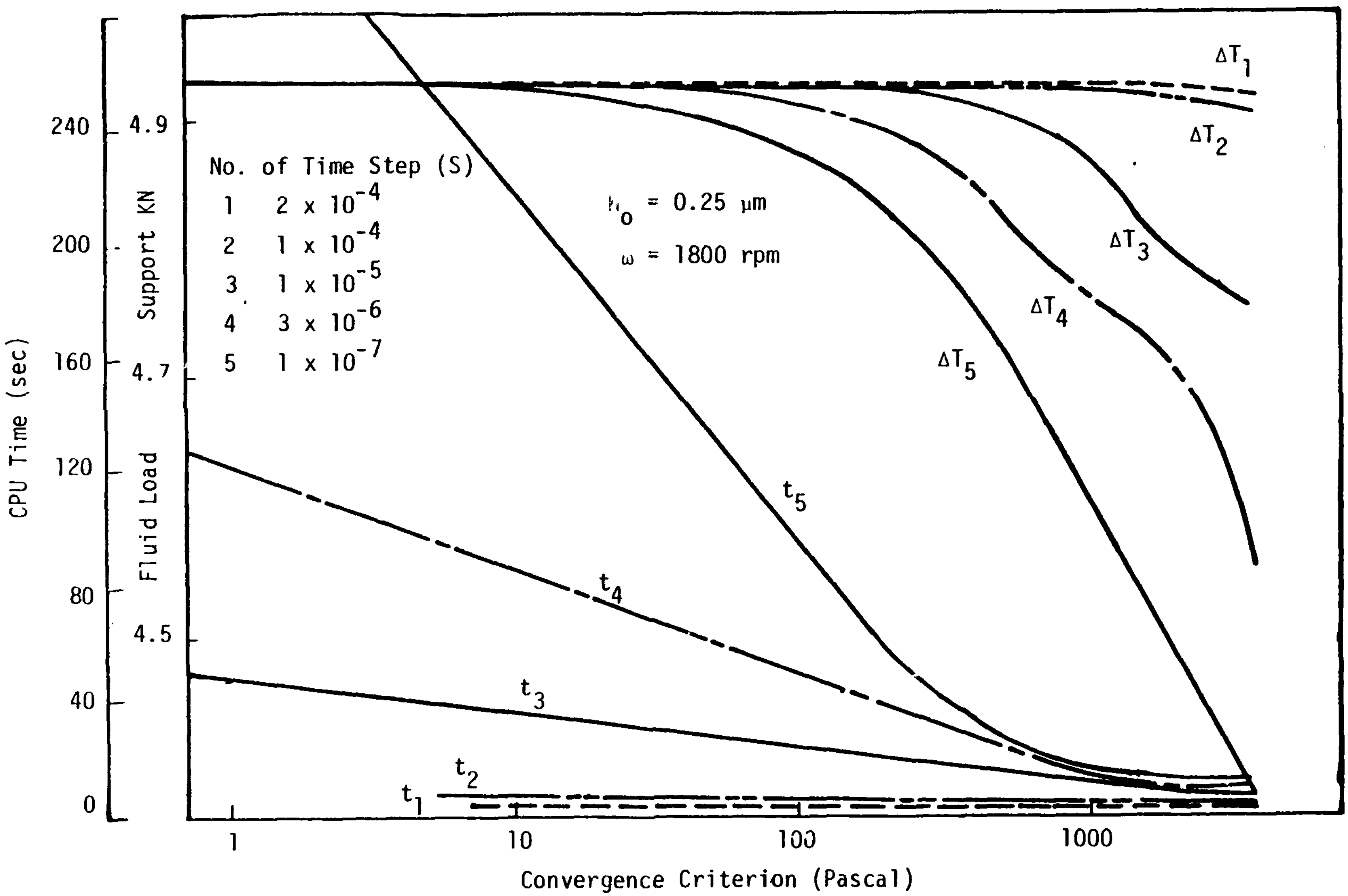

Figure 4-8. Convergence Conditions.

The design parameters consist of balance ratio (B), material properties such as compressive strength (P_m), seal surface roughness (c), seal face width ($r_o - r_i$), number of waves around the seal face (n), tilt angle (ϕ), amplitude of the waves, the ring stiffness ratio (A), spring pressure (P_{sp}) and modulus of elasticity of the primary seal ring (E). The values of the above application parameters, design parameters as well as some constants are given in Table 4-1. Most of the system parameters are shown in the previous figures, such as Figure 1-3, Figure 4-4, and Figure 4-5. The definitions used are the same as those in previous reports.

Film Thickness Shape--the nature of the wavy tilted shape of the gas film in the seal is described in detail in Reference [5]. Film thickness is essentially a function of wear, deflection, and initial shape. For a moving wave or tilted seal, the film thickness function has been shown to be [5]:

$$h = h_o + w(r) + [v_o + (r - r_c)\ \phi_o] \cos(n\theta + \Omega t) \qquad (4\text{-}29)$$

where

$$w(r) = -\min\{[v_o + (r - r_c)\ \phi_o] \cos(n\theta + \Omega t)\} \qquad (4\text{-}30)$$

v_o and ϕ_o can be somewhat arbitrarily chosen, and their choice influences the shape of the film. In this gas seal study, v_o and ϕ_o are chosen just as in the liquid seal work [5] such that there is a circumferential wave, a radial taper, and a distinct sealing dam. Ω represents the wave motion required to maintain the wave in spite of wear and is so small that it can be neglected in the pressure computations. Figure 4-9 shows a three-dimensional plot of the wavy film thickness for a particular ϕ and v.

Table 4-1

Gas Seal Parameters and Constants

Face Seal Application Parameters

Viscosity of nitrogen	η	- 1.74 x 10^{-5} Pa•S (2.52 x 10^{-9} lbf-s/in.^{2})
Outside pressure	p_o	- 3.55 MPa (514.7 psia) (varies)
Inside pressure	p_i	- 0.1 MPa (14.7 psia)
Angular speed of shaft	ω	- 1800 rpm (188 rps) (varies)
Seal centroid radius	r_c	- 49.18 mm (1.9361 in.)
Shaft diameter	D	- 88.90 mm (3.50 in.)

Face Seal Design Parameters

Ring Stiffness Ratio	A	- EJ_x/GJ_θ = 7.44
Compressive strength of carbon ring	p_m	- 262 MPa (38,000 psia)
Balance ratio	B	- 0.75
Surface roughness	c	- 0.51 μm (20.0 μin.) (varies)
Face width: inside radius	r_i	- 48.26 mm (1.9000 in.)
outside radius	r_o	- 53.04 mm (2.0875 in.)
Number of waves	n	- 9
Waviness amplitude	h_o	- 0.14 μm (5.4 μin.)
Spring pressure	Psp	- 0.196 MPa (28.5 psi)
Modulus of elasticy	E	- 20.7 GPa (3.0 x 10^6 psi)
Shear modulus	G	- 9.6 GPa (1.25 x 10^6 psi)
Tilt	ϕ	- 500 μm/m (varies)

Other Constants

Gravity	g	- 9.81 m/s^2 (32.174 ft/s^2)
Density of nitrogen	ρ	- 1.18 Kg/m^3 (0.0023 slug/ft^3)
Spring constant	k	- 3.36 KN/m (19.159 lb/in.)
Temperature	T	- 23.9°C (75.0°F)
Universal constant	U	- 287 J/Kg°K (53.3 ft-lb/lbm/R°)

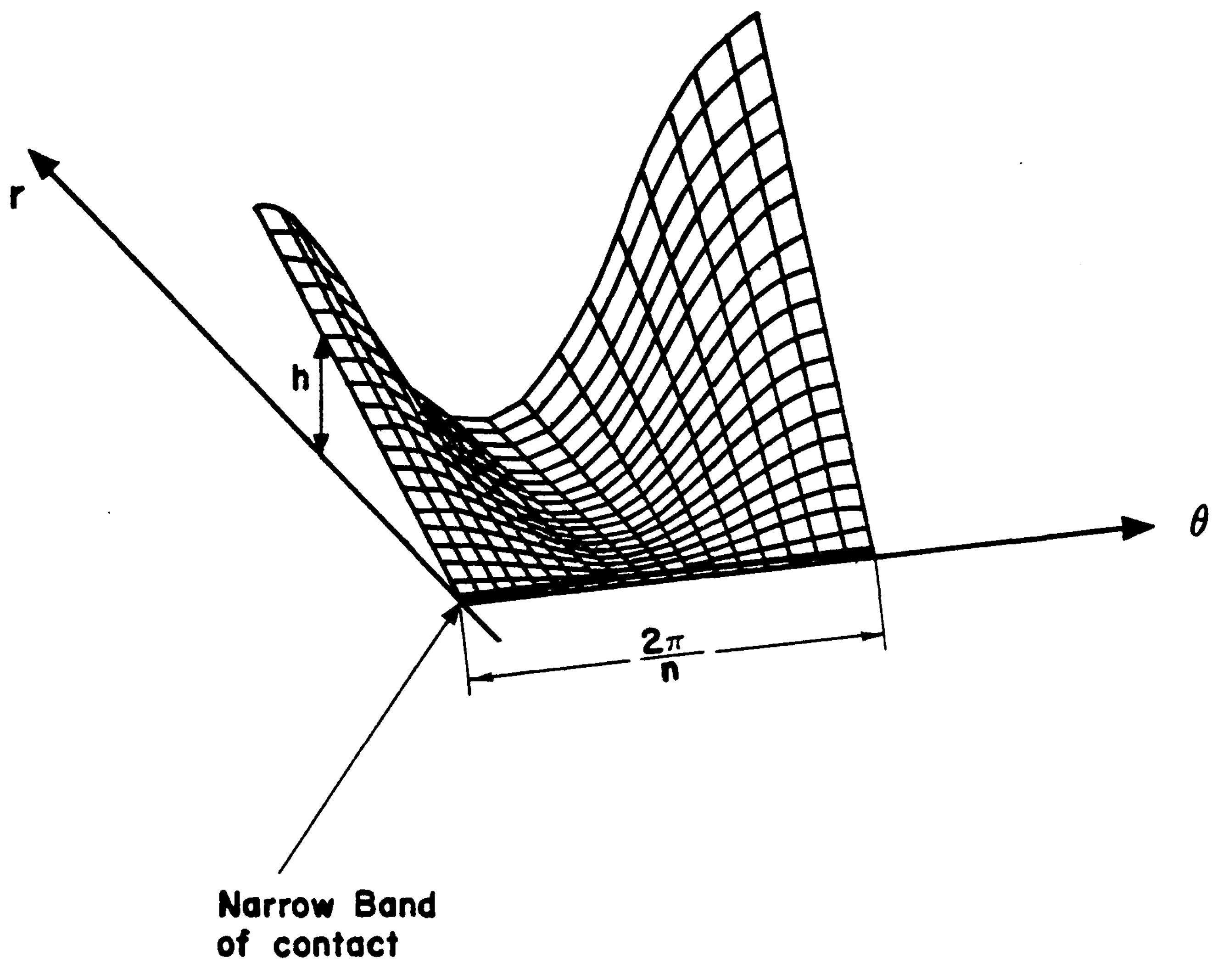

Figure 4-9. 3-D Plot of Film Thickness.

Load Support--Load support consists of the fluid pressure component and the mechnical component. The fluid pressure component is due to the hydrostatic and hydrodynamic effects while the mechanical component is obtained by flattening the peaks of the asperities in contact. As before, it is assumed that asperity pressure is equal to the compressive strength of the softer seal face material, and that this pressure remains constant.

The total load support in the gas seal is calculated by integrating the hydrodynamic, hydrostatic and asperity pressure distributions over the entire seal face area. That is

$$W = n\int_0^{\frac{2\pi}{n}} \int_{r_i}^{r_o} [P + P_m(1 - b)]\, r\, dr\, d\theta \ , \qquad (4\text{-}31)$$

where b is the fraction of the face not in mechanical contact (given in Reference [6]).

The load that must be supported for the seal to be in equilibrium is a function of the seal pressures P_o and P_i, the balance ratio B, and the spring pressures P_{sp}.

$$W^* = \pi(r_o^2 - r_i^2)\ [P_oB + P_i(1 - B) + P_{sp}] \qquad (4\text{-}32)$$

As before [1-5], the total load support W increases with decreasing h_o, thus, this load support may be adjusted to be equal to the applied load W* by selecting a suitable h_o. Such a procedure is used for the solutions presented herein.

For comparison purposes, the ratio of fluid pressure load support to the total load (W_f/W) expressed as a percent is an index to indicate the relative wear rate. If the ratio is equal to one ($W_f/W \rightarrow 1.0$) theoretically, adhesive wear will become zero.

Leakage--Gas seal leakage is computed by the integration of the equations

$$Q_{out} = -\int_0^{2\pi} \frac{h_o^3}{12\eta} \frac{\partial P}{\partial r}\bigg|_{r_o} r_o \, d\theta \qquad (4\text{-}33)$$

and

$$Q_{in} = -\int_0^{2\pi} \frac{h_i^3}{12\eta} \frac{\partial P}{\partial r}\bigg|_{r_i} r_i \, d\theta \, , \qquad (4\text{-}34)$$

Q_{in} and Q_{out} represent the inside and outside leakage, respectively. Both the inside and outside leakages are used as a check to see whether accuracy is acceptable. A numerical average of the inside and outside leakages is used to represent the nominal seal leakage.

Friction--From the previous work [6], considering the fluid film regime, tangential fluid friction shear stress is given by

$$\tau_f = [\eta\omega r \, E(\frac{1}{H}) + \frac{1}{2r} \frac{\partial P}{\partial \theta} E(H)] \times b \qquad (4\text{-}35)$$

where E( ) is the expectancy operator and b is the fraction of the face not in contact and has been given previously [6].

Roughness is taken as being given by a parabolic distribution as before,

$$f(h_S) = \frac{35}{32c^7} (c^2 - h_S^2)^3 \, , \qquad -c < h < c \, . \qquad (4\text{-}36)$$

The expected value functions are given in Reference [6].

The average friction shear stress due to asperity contact is given by,

$$\tau_a = P_S(1 - b) \ . \tag{4-37}$$

The mechanical torque is calculated by the integration of the tangential fluid shear stress plus the average frictional shear stress due to the asperity contact over the whole seal face. Thus,

$$\text{Torq} = n\int_0^{\frac{2\pi}{n}} \int_{r_i}^{r_o} (\tau_f + \tau_a)\, r^2 \, dr \, d\theta \tag{4-38}$$

and the mechanical driving power required is,

$$\text{Power} = \omega \times \text{Torq} \ . \tag{4-39}$$

The coefficient of friction is defined as

$$\mu = \frac{\text{Torq}/r_f}{W} \ , \tag{4-40}$$

where r_f is the mean seal radius.

Stiffness--The stiffness in the gas seal is computed numerically by varying h_o by,

$$S = \frac{dW}{dh_o} \ . \tag{4-41}$$

Example

The solution technique for the pressure has already been discussed in previous sections. Considering the total solution, h_o must be adjusted to satisfy equilibrium. Therefore, h_o becomes a dependent variable in the problem.

Specifically, the method of solution is:

1) Select a system of seal parameters and determine the applied load W*.
2) Calculate the wear term w(r) using Equation (4-30).
3) Assume a value for minimum film thickness h_0.
4) By using the A.D.I. technique as described, the pressure distribution is solved for the given boundary conditions as described. A typical resultant pressure distribution is shown in Figure 4-10.
5) Calculate the total load support W using Equation (4-31).
6) Compare W to W* and adjust h_0 using a secant root finding method. Return to Step 4) and repeat until W = W* within a desired accuracy.
7) Calculate coefficient of friction, leakage, percent load support and torque.

Appendix C contains a computer program listing for the solution to this problem.

Using the parameter values in Table 4-1, an example solution was obtained. The film thickness is similar to that shown in Figure 4-9. The values of pressure are shown in Figure 4-10. Pressure gradient in the outer edge of the seal is low and at the inner edge high. This suggests that accuracy of the leakage at the outer edge (Q_{out}) is good while the accuracy at the inner edge (Q_{in}) is low. It is much more difficult numerically to predict the steep gradient accurately. The load support required for equilibrium is 982.3 lbf (4.4 KN). The total load support determined by the fluid load and asperity load is found to be 982.26 lbf. Thus, equilibrium (W = W*) is attained. The minimum film thickness h_0 is 30.2 μin. (0.76 μm). Since $h_0 > c$ (0.5 μm), no contact occurs. NITA, NITB and NITN are the numbers of iterations in the A.D.I. method required for the two initially guessed minimum film thicknesses and the equilibrium minimum film thickness respectively. The stiffness of the seal is

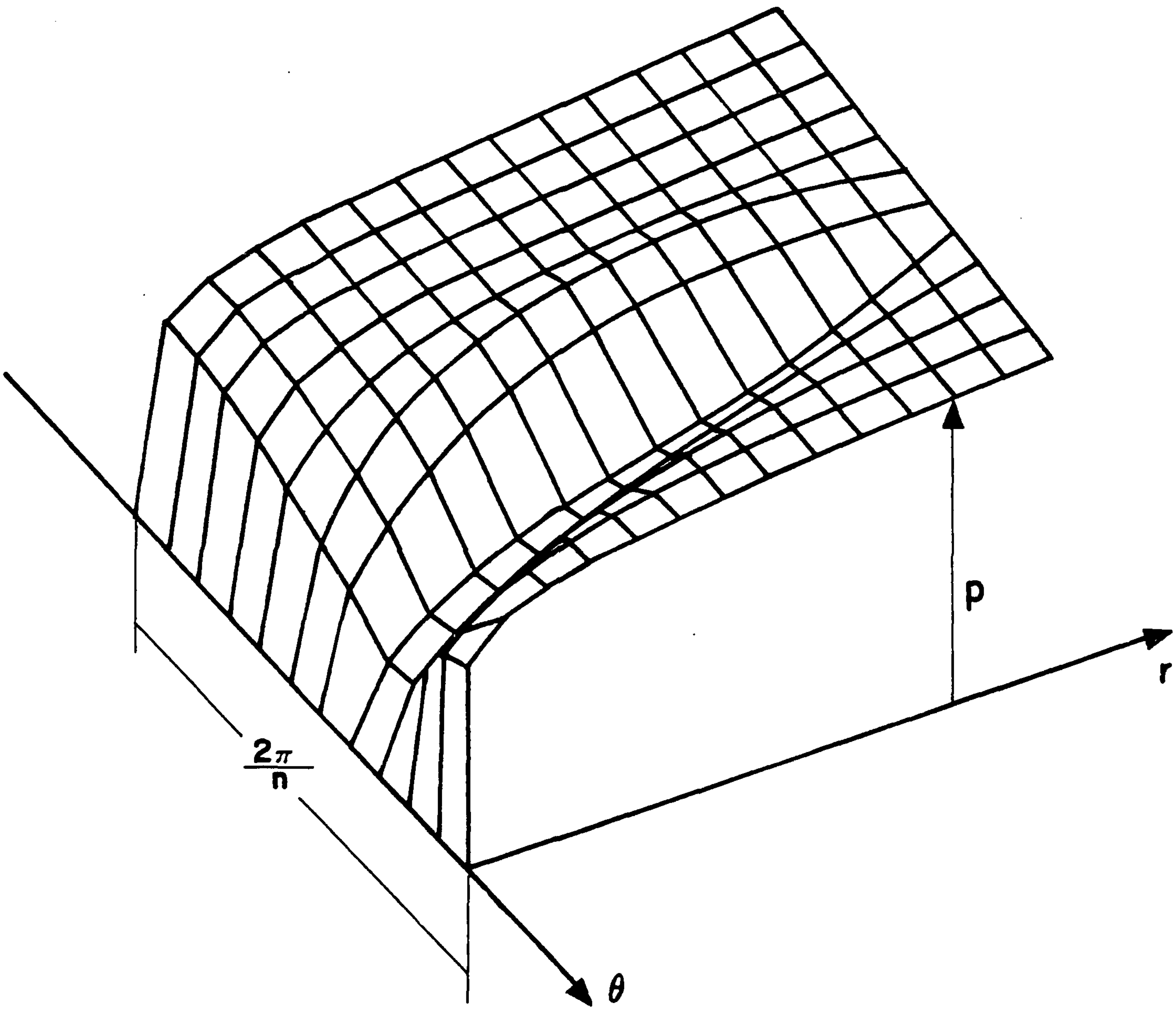

Figure 4-10. 3-D Plot of Pressure.

high (-1.15×10^6 lbf/in.) where the minus sign represents increasing load with decreasing gap. The leakage rate is 0.12 SCFM (3.4×10^{-3} SCMM). Negative Q_{in} and Q_{out} represent leakage flow radially inward as expected for this example. The coefficient of friction is only 0.000045 which implies that the frictional force is small (only 0.043 lbf). One hundred percent fluid load support occurs. Total driving torque is only 0.088 in.-lb. Thus, both the leakage and torque are low. Using such results, the studies below were completed.

Parameter Studies

In this section parameter studies are made using the computational model developed. Four parameters, tilt, outside pressure, surface roughness, and speed have been considered in this initial study.

Tilt--Tilt is a design variable over which nearly complete control is possible. Increased tilt increases both radial taper and waviness. The effects of changing the tilt of a moving wave gas seal from negative 200 to positive 800 μm/m are illustrated in Figure 4-11. The former value denotes a profile having a somewhat divergent radial taper over most of its circumferential period, while the latter value denotes a profile which has a predominantly convergent radial taper. These two extreme conditions are illustrated in Figure 4-12.

For negative and low values of tilt, the gas film stiffness, the coefficient of friction and the driving torque are relatively high, and at the same time the leakage rate is low indicating that mechanical or asperity-to-asperity contact has occurred. This is verified by the minimum film thickness h_0 being less than the one-half maximum roughness height c as well as the percentage of the fluid film load support being less than 100 percent full film load support. However, as the tilt shifts in the

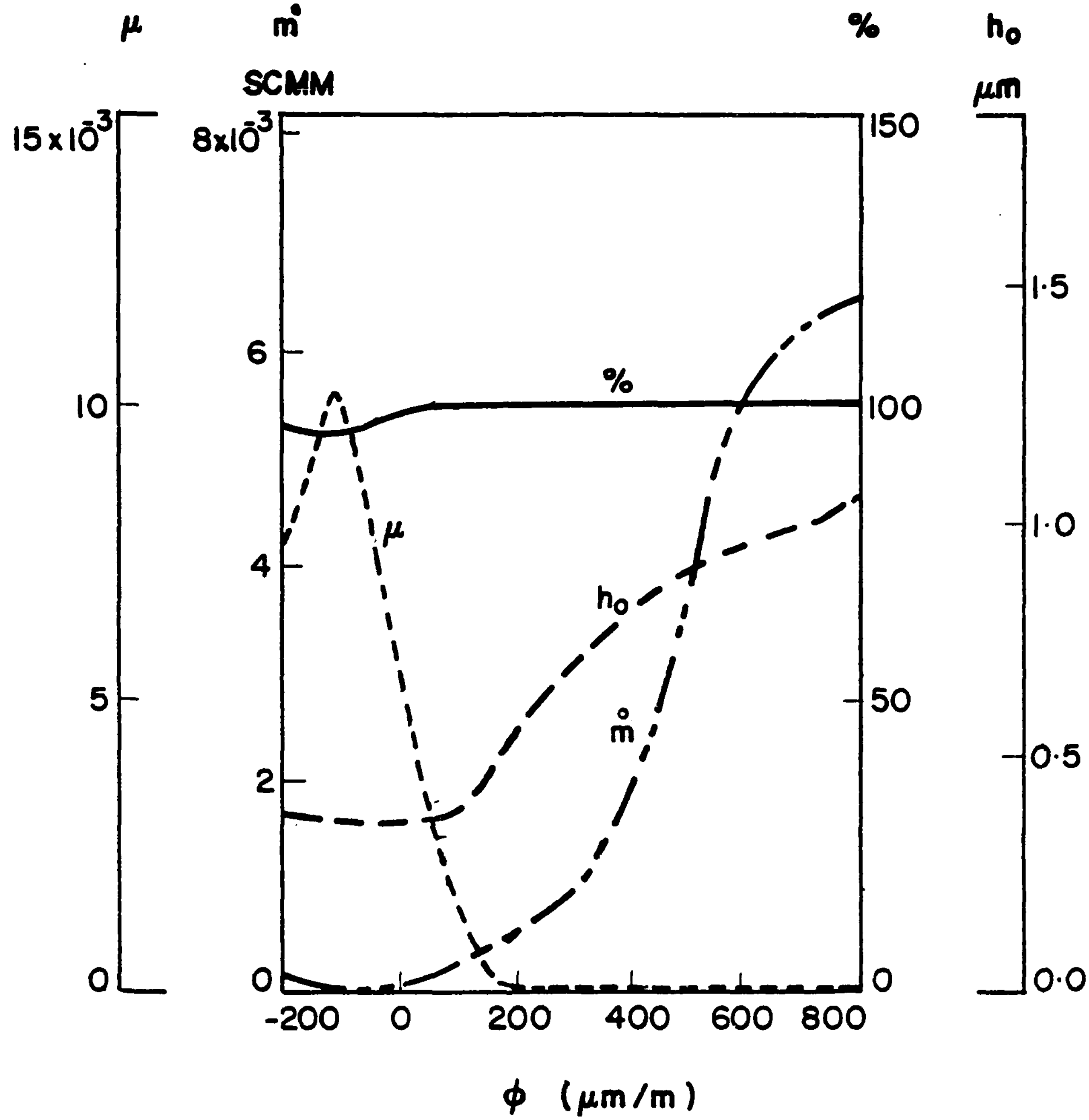

Figure 4-11. Effect of Tilt on Performance.

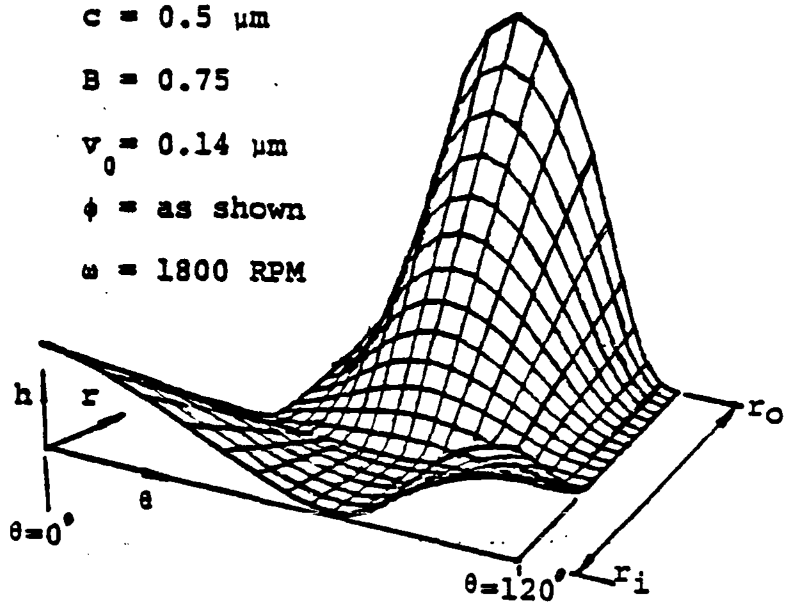

Tilt at -200 μm/m

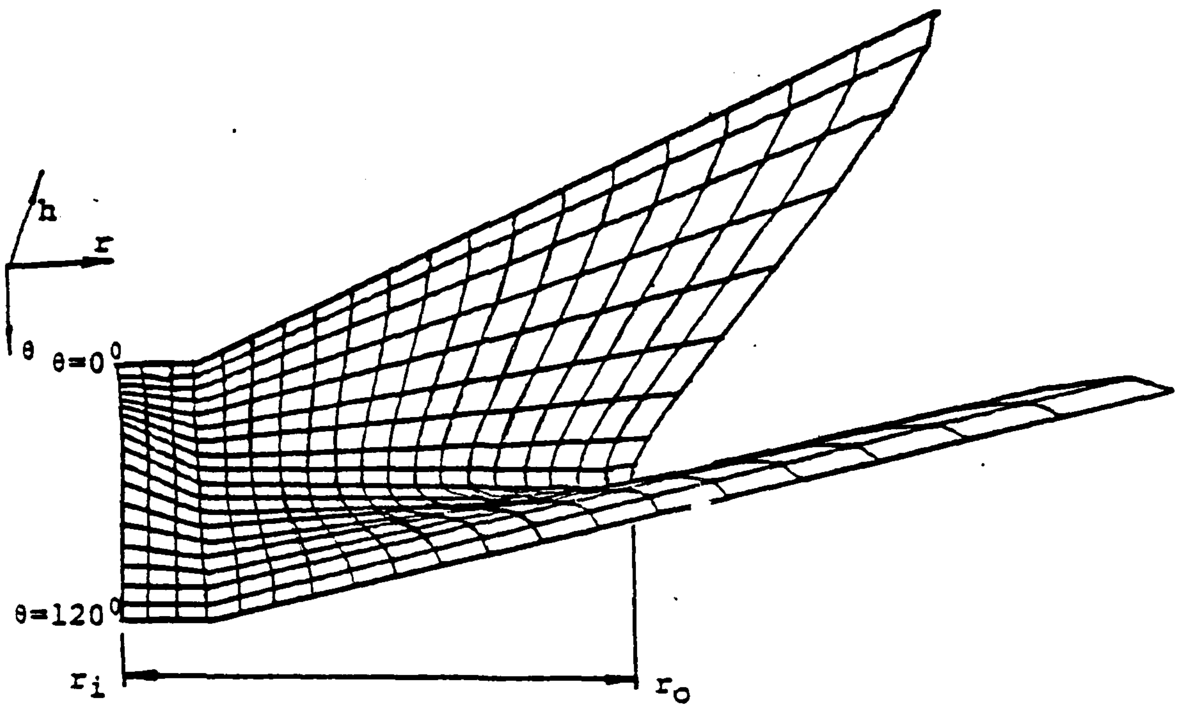

Tilt at 800 μm/m

Figure 4-12. Effect of Tilt on Film Thickness.

convergent direction, higher average fluid pressure results. The pressure distribution across the seal face has already been shown in Figure 4-10. As the tilt is increased the seal faces eventually separate, thus, the mean film thickness increases gradually and the leakage is higher. Thus, there is some minimum value of tilt increase to cause lift off.

Outside Pressure--The results of changing the outside pressure P_o while keeping the inside pressure P_i constant are shown in Figure 4-13. As the outside pressure increases from 0.0 to 1000 psig (0 to 7 MPa), the percentage of fluid load support increases rapidly to 100 percent. At low pressure there exists some mechanical asperity contact because the spring pressure is greater than the total lift force provided by hydrodynamic effects. The hydrostatic effect is zero at zero pressure.

Full film operation occurs when the pressure differential is high. As p_o approaches 200 psia, the minimum film thickness h_o becomes larger than the one-half maximum roughness height (c), and mechanical asperity-to-asperity contact no longer occurs. The hydrodynamic effect is not sufficient to lift off the seal against the spring load at zero sealed pressure.

In the gas seal analyzed the velocity of gas discharge is about 500 ft/sec under 1000 psig pressure differential (the worst case in Figure 4-13 is chosen) which is about 0.5 Mach number. The method of calculating discharge velocity is shown in Reference [23]. Therefore, sonic discharge does not occur. However, if the pressure differential keeps increasing, sonic flow will occur and the method of analysis will become quite complex according to [27].

Finally, the stiffness of the gaseous film is high when the outside pressure is less than 200 psig (1.4 MPa) because of mechanical contact.

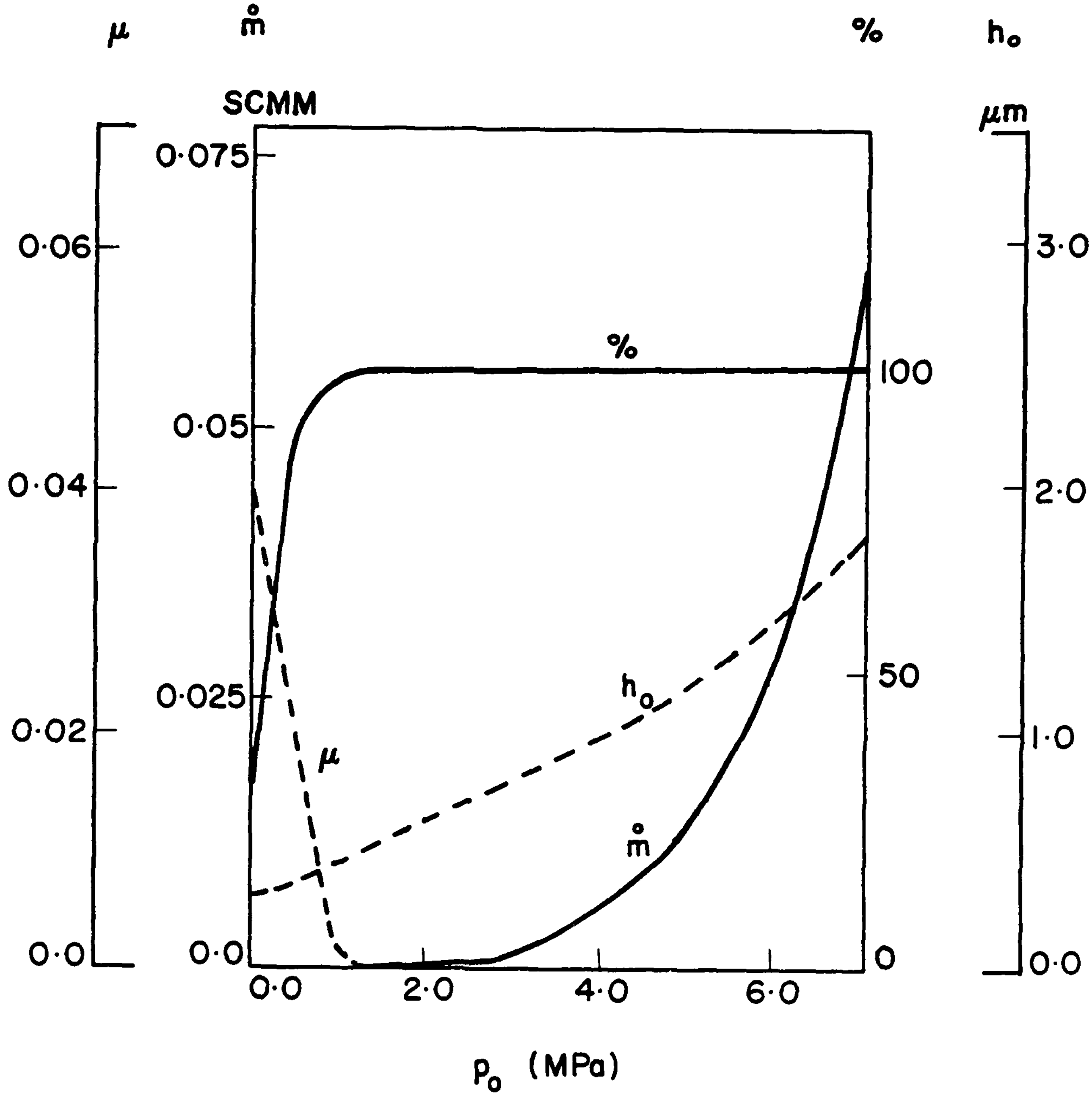

Figure 4-13. Effect of Outside Pressure.

Surface Roughness--The effect of surface roughness is shown in Figure 4-14. The performance parameters are quite constant when c is less than 35 μin. (0.88 μm). But as c increases, the friction begins to rapidly increase. The reason is that surface roughness c is now higher than the mean film thickness and thus asperity-to-asperity mechanical contact occurs.

Figure 4-15 shows the effect of surface roughness when there is no pressure difference between the two sides of the seal. Now, as the surface roughness decreases, the minimum film thickness decreases, the hydrodynamic effect becomes larger and larger until the seal lifts off (full film conditions). This is an important characteristic of the gas seal because if the seal cannot lift off at zero pressure difference, high frictional heat might occur at the contacting surfaces thus destroying the seal. The figure shows at $n = 3$ that the maximum roughness allowable on the seal parts in order to provide the 95 percent lift off at zero pressure differential is in the order of $c = 0.10$ μm or 4 μin. This corresponds to an RMS of about 1.5 μ-in. In practice, this surface roughness is difficult to achieve and maintain. Thus, it remains to be seen whether or not such a seal could survive operation at zero pressure differential. Clearly, $n = 9$ would work better according to the figure. Also, a smaller spring load would help.

Angular Speed--The effect of angular velocity on performance parameters is illustrated in Figure 4-16. With the tilt at 500 μm/m, there is no mechanical asperity contact even at zero speed. This and the fact that h_0 does not significantly drop at low speed means that there is no significant hydrodynamic load support component. The entire load is supported by hydrostatic effects due to the radial taper ϕ.

The coefficient of friction is approximately linearly proportional to the angular rotational speed ω because the viscous drag force is proportional to angular speed.

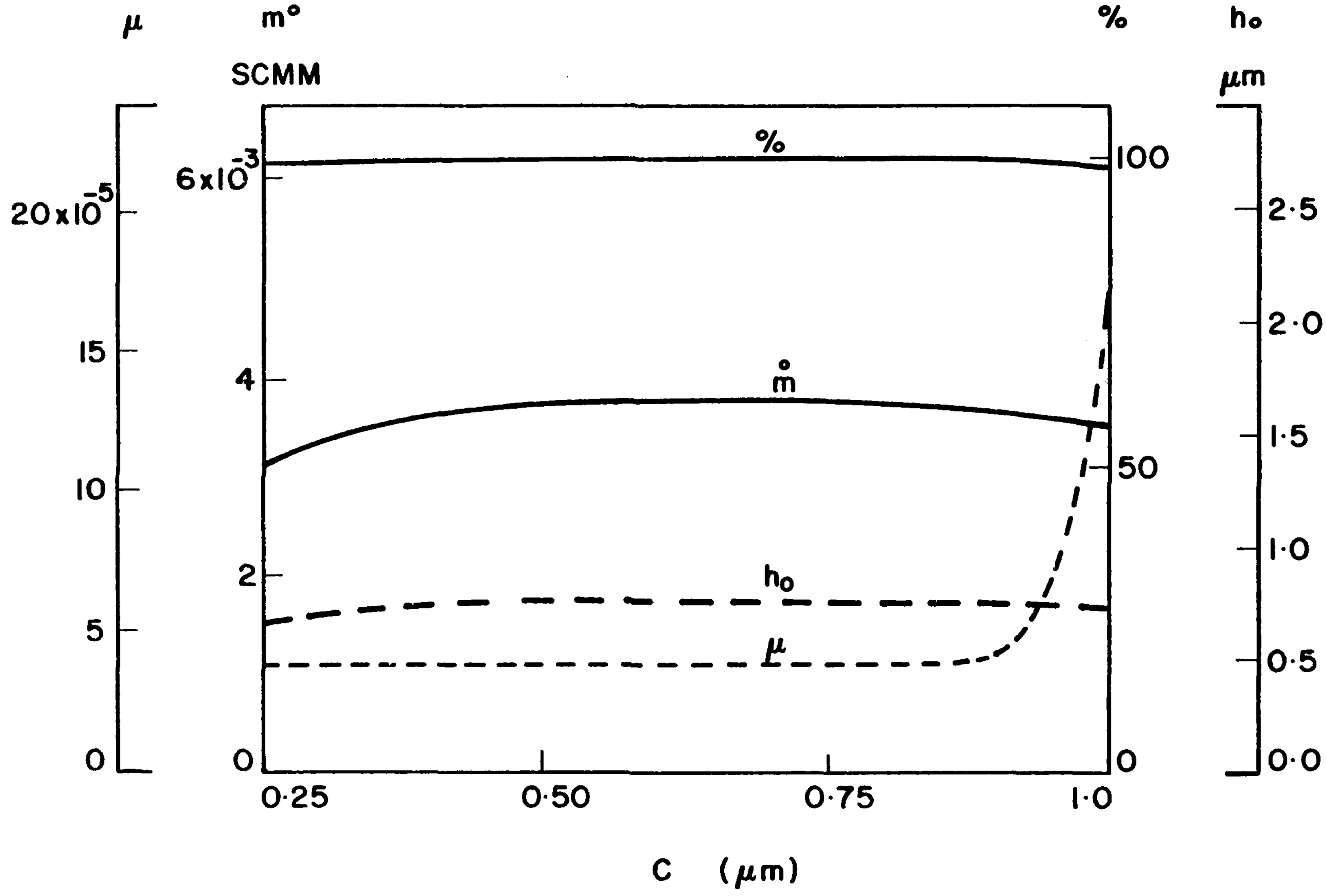

Figure 4-14. Effect of Surface Roughness.

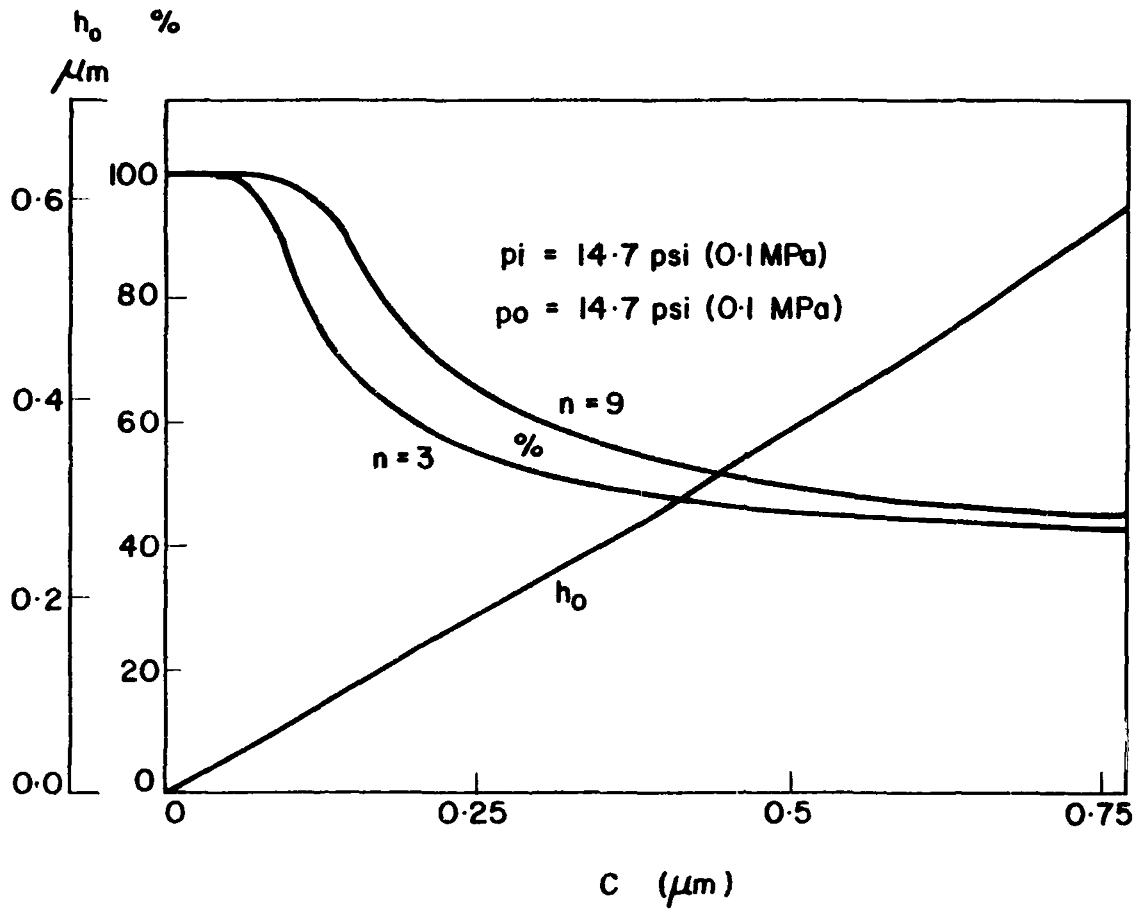

Figure 4-15. Hydrodynamic Effect.

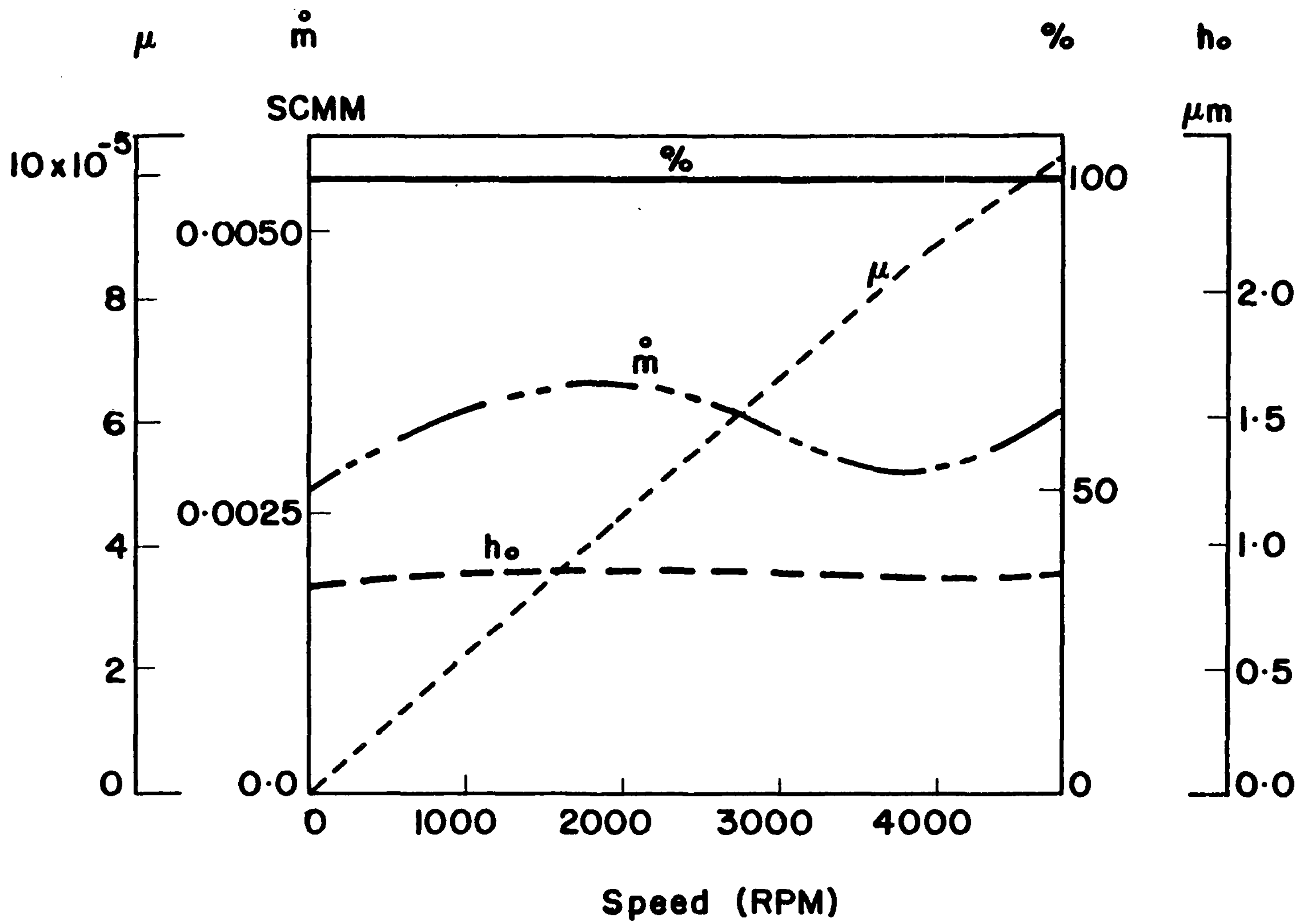

Figure 4-16. Effect of Angular Speed.

Potential Application--The preceding results show that a moving wave gas seal could theoretically operate at extremely low friction and wear with very low gas leakage. Load is supported primarily hydrostatically. The main question to be answered is whether or not sufficient hydrodynamic lift will develop under zero differential pressure conditions so as to avoid serious thermal distortion and/or wear of the seal. Theory shows that a flow surface roughness is essential to develop hydrodynamic load support. It is possible that a carbon surface would polish to the extent needed. Spring load could also be lowered. In any case, the answer to this question must be obtained experimentally.

CHAPTER 5

SEAL RING DEFLECTION

Background

It has long been recognized that seal ring faces may deflect out of their original lapped-in plane under the influence of non-axisymmetric loads, non-axisymmetric section properties, non-axisymmetric swelling of the carbon, or a combination of these factors. If such deflections are greater than those which can be flattened out by the axial load applied to the seal faces, unwanted gaps and leakage will result.

It is thought that one of the possible problems with present submarine seals is that the rings are too stiff to be able to close gaps created by shifting carbon segments. When gaps occur between seal faces, erosion continues to widen the gap until leakage becomes excessive. This potential problem or some variation of it affects the design of all seals including the design proposed and tested herein.

Thus, both for the purpose of analyzing problems with present seals and for designing new seals, some tool is needed to predict non-axisymmetric deflection for seal rings and also to predict potential gaps in seal ring pairs (the distribution of face loading). For simple rings with constant cross sectional properties, no splits, and simple harmonic deflections, the face loading distribution required for continuous contact is relatively easily obtained [41-42]. However, for more realistic conditions relating to the cross section properties and more complex distortions, finding the correct distribution of face loading becomes a very difficult problem.

The state of the art of predicing face loading in complex cases is illustrated by a report by Noell, Rippel, and Niemkiewicz of the Franklin Institute [43]. An evaluation of out-of-plane seal distortion caused by nonuniform joints was made. It is shown how a nonuniform cross section near the joints causes out of flatness. In the report the contact between the seal faces is modeled by springs where tensile stresses across the faces are allowed. Since such stresses cannot occur in reality, the computed results do not predict how much and where the faces separate. Thus, the utility of the work to date is limited.

To serve as a useful tool in seal design a more exacting but general program is needed. Specifically, given two rings of arbitrary and circumferentially varying cross sections and load contacting on a plane and pressed together by axial loads, one must find the resulting face loading pressure distribution which arises as the rings are loaded up and distort. At regions where the faces do not contact, the resulting gap must be found. The same program would be capable of finding the resulting pressure and gap distribution given faces originally distorted out-of-plane as well.

There are two major features in the needed model. In the first place, one needs a very general tool to predict deflections in arbitrarily loaded variable cross section rings. Then, the two rings are brought together to contact and the pressure distribution is predicted. This second feature represents a specific type of contact problem. Suitable models for rings are not available in the literature and are developed herein. Several special ring models are developed and each one is tested against known solutions. The contact problem has been treated previously using finite element methods. A specific example which illustrates the technique is given here. Finally, it is shown how these models will be put together to find the needed solutions. All of the work is based on the finite elements techniques. Such a technique is essential for the contact problem.

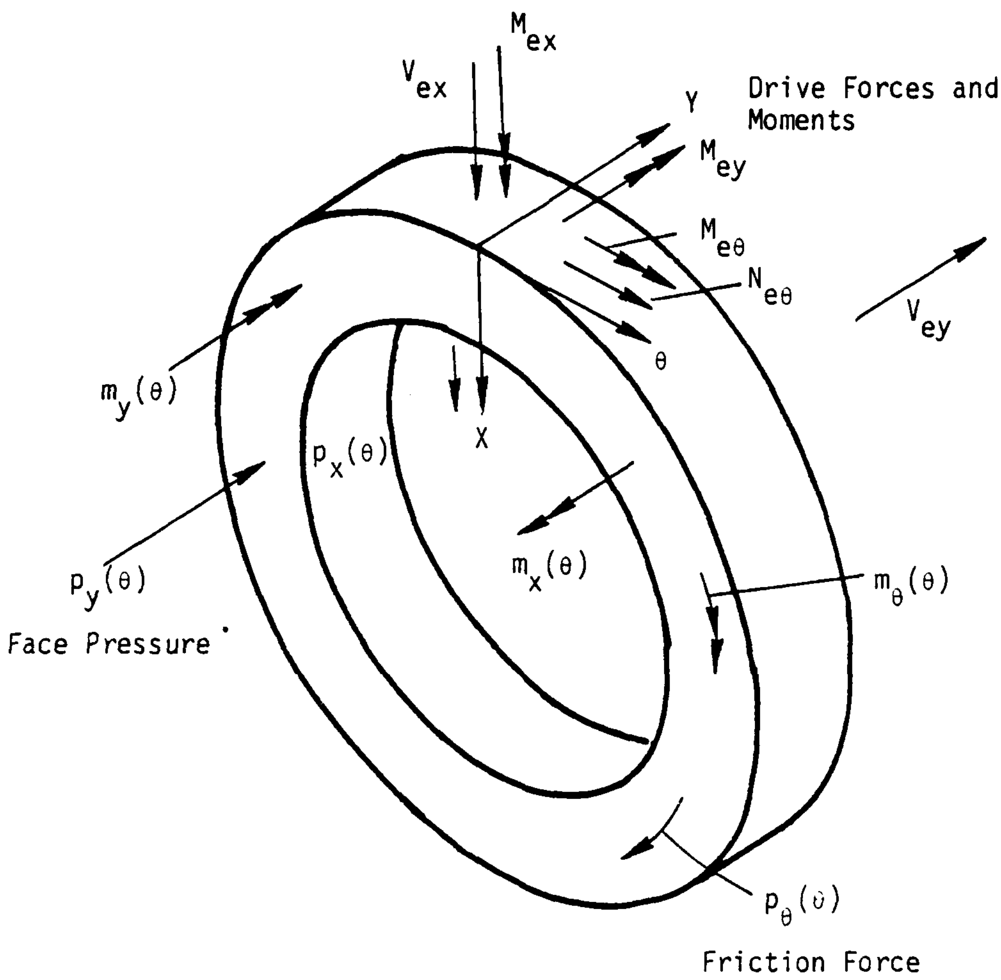

Figure 5-1. Mechanical Loading on a Seal Ring.

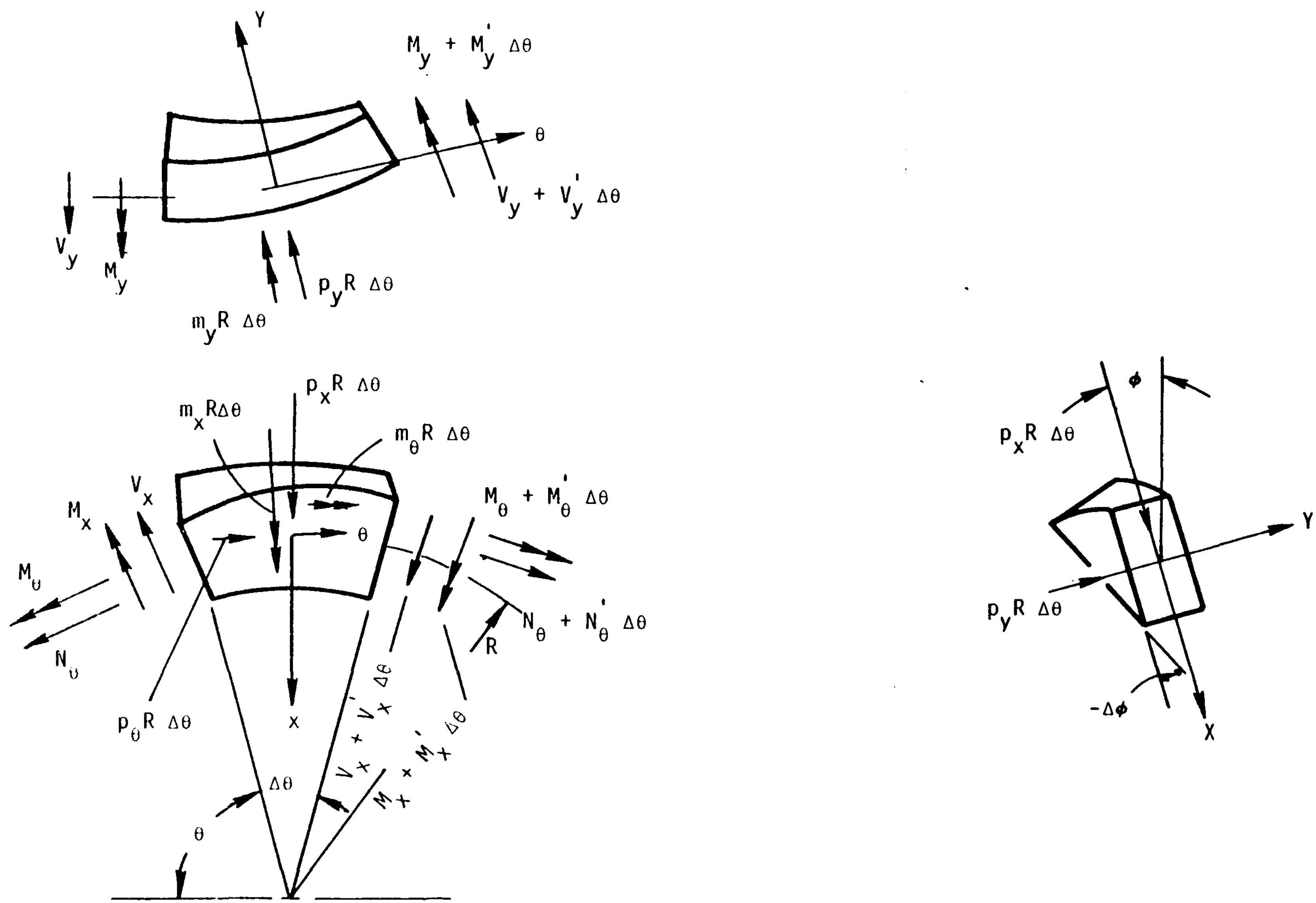

Figure 5-2. Segment of a Ring.

deflections. Based on the previous work [41-42] and neglecting all distributed loads (these will be added later at the nodes), the equations of equilibrium are:

$$V_x' + N_\theta = 0^* \tag{5-1}$$

$$V_y' = 0 \tag{5-2}$$

$$N_\theta' - V_x = 0 \tag{5-3}$$

$$M_x' + M_\theta - V_y R = 0 \tag{5-4}$$

$$M_y' + RV_x = 0 \tag{5-5}$$

$$M_\theta' - M_x = 0 \tag{5-6}$$

The above equations assume the distance between the shear center and the centroid is negligibly small. Combining the above, the equilibrium equations become

$$N''_\theta = N_\theta = 0 \tag{5-7}$$

$$M_x'' + M_\theta' = 0 \tag{5-8}$$

$$M_y''' + M_y' = 0 \tag{5-9}$$

$$M_\theta' - M_x = 0 \tag{5-10}$$

Stress resultant-displacement equations are given by

$$N_\theta + \frac{M_y}{R} = \frac{Ea}{R}\left[w' - u\right] \tag{5-11}$$

$$M_x = \frac{E}{R^2}\left[(\phi R - v'')\, J_x - (u'' + u)\, J_{xy}\right] \tag{5-12}$$

---

*Primes denote derivatives with respect to θ.

$$M_y = \frac{E}{R^2} [(u + u'') J_y - (\phi R - v'') J_{xy}] \tag{5-13}$$

$$M_\theta = \frac{G}{R^2} J_\theta [\phi' R + v'] \tag{5-14}$$

where

$$J_x = \int_a \frac{y^2}{1 - x/R} da \tag{5-15}$$

$$J_y = \int_a \frac{x^2}{1 - x/R} da \tag{5-16}$$

$$J_{xy} = \int_a \frac{xy}{1 - x/R} da \tag{5-17}$$

J_θ = torsional stiffness constant such as in Oden [45] (5-18)

$$a = \int_a da \tag{5-19}$$

Substituting Equations (5-11) through (5-14) into Equations (5-7) through (5-10) results in the following differential equations describing deflections:

$$w' + w''' - (u + u'') \left(1 + \frac{J_y}{aR^2}\right) - (u'' + u'''') \frac{J_y}{aR^2} + (\phi R + \phi'' R - v'' - v'''') \frac{J_{xy}}{aR^2} = 0 \tag{5-20}$$

$$\phi'' R \left(1 + \frac{GJ_\theta}{EJ_x}\right) - v'''' + v'' \frac{GJ_\theta}{EJ_x} - (u'''' + u'') \frac{J_{xy}}{J_x} = 0 \tag{5-21}$$

$$(u' + 2u''' + u''''') J_y - (\phi'R + \phi'''R - v''' - v''''') J_{xy} = 0 \tag{5-22}$$

$$(\phi''R + v'') \frac{GJ_\theta}{EJ_x} - (\phi R - v'') + (u'' + u) \frac{J_{xy}}{J_x} = 0 \tag{5-23}$$

It can be seen if $J_{xy} = 0$, then the out-of-plane displacements v, ϕ are decoupled from the in-plane displacements u, w. The above equations consist of four differential equations in the unknowns u, v, w, ϕ.

Finite Element

Given the governing deflection equations, one can now derive a finite element stiffness matrix for a general ring element. The stiffness matrix is defined by

$$[F] = [K]\,[\delta] \,. \tag{5-24}$$

That is, given an arbitrary set of displacmeents at the end of the element δ, what are the forces and moments necessary. [K], the stiffness matrix, defines this characteristic and is all that is required to define a finite element.

There are various coordinate systems in which the stiffness matrix can be defined. In this work, a polar coordinate system was chosen. This makes the stiffness matrix invariant around the ring assuming constant section properties. Thus the stiffness matrix only needs to be computed one time for a given element size. It can then be used at any location around the ring without using a coordinate transformation as is required for other stiffness matrices such as those presented by Morris [49].

Three different stiffness matrices will now be derived, one for in-plane bending, one for out-of-plane bending, and one for the coupled problem. The two simpler cases are used to provide a check on the limiting cases of the coupled problem of interest. The solution of the two simple cases also helps in understanding the solution to the coupled problem.

In-Plane Stiffness--Figure 5-3 shows an element defined for in-plane stiffness. For the in-plane case, Equations (5-20) and (5-22) for $J_{xy} = 0$ reduce to the following

$$w' + w''' - (u + u'')\left(1 + \frac{J_y}{aR^2}\right) - (u'' + u'''')\frac{J_y}{aR^2} = 0 , \quad (5\text{-}25)$$

$$u' + 2\,u''' + u''''' = 0 . \quad (5\text{-}26)$$

The objective is to solve the above two equations subject to the displacement boundary conditions shown in Figure 5-3.

The general solution to Equation (5-26) is

$$u = C_1 + C_2 \sin\theta + C_3 \cos\theta + C_4\,\theta \sin\theta + C_5\,\theta \cos\theta . \quad (5\text{-}27)$$

Substitution of (5-27) into (5-25) and solving for w gives

$$w = C_6 + C_7 \sin\theta + C_8 \cos\theta + C_1\left(\frac{J_y}{aR^2} + 1\right)\theta$$

$$- C_4\,\theta \cos\theta + C_5\,\theta \sin\theta . \quad (5\text{-}28)$$

There are six displacement boundary conditions shown in Figure 5-3 and eight arbitrary constants above. It follows that there are too many constants and that substitution back into the original differential equation will eliminate two of the constants.

Using Equations (5-11), (5-12), (5-27), and (5-28), one may show that

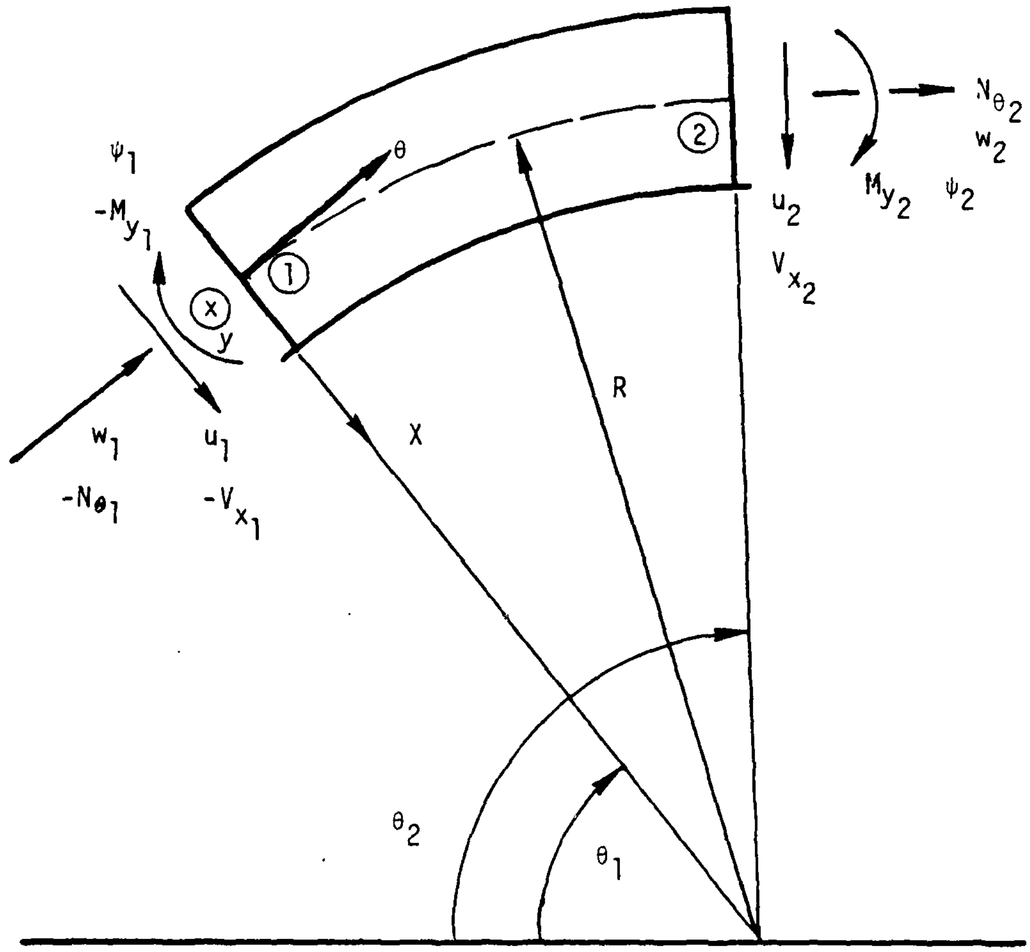

Figure 5-3. Finite Element for In-plane Loading

$$N_\theta = \frac{Ea}{R}[C_7 \cos\theta - C_8 \sin\theta - C_4 \cos\theta + C_5 \sin\theta - C_2 \sin\theta - C_3 \cos\theta]$$

$$- \frac{EJ_y}{R^3}(2C_4 \cos\theta - 2C_5 \sin\theta) \qquad (5\text{-}29)$$

Similarly,

$$M_y = \frac{EJ_y}{R^2}(C_1 + 2C_4 \cos\theta - 2C_5 \sin\theta) \ . \qquad (5\text{-}30)$$

Going back to the original equilibrium equations, Equations (5-3) and (5-5) show that

$$M_y' = -RN_\theta' \ . \qquad (5\text{-}31)$$

Substituting (5-29) and (5-30) into (5-31) shows that

$$C_8 = C_5 - C_2 \qquad (5\text{-}32)$$

$$C_7 = C_4 + C_3 \qquad (5\text{-}33)$$

so that two of the constants are eliminated.

The boundary conditions are shown in Figure 5-3. Rotation ψ represents the total in-plane rotation which is compatible with M_y.

$$\psi = \frac{1}{R}\frac{du}{d\theta} + \frac{w}{R} \ . \qquad (5\text{-}34)$$

The negative forces and moments shown at end 1 of the beam elements are in the same direction as the displacements as required for the stiffness matrix.

Using Equations (5-27), (5-28), (5-32) and (5-33) and summarizing

$$u = C_1 + C_2 \sin\theta + C_3 \cos\theta + C_4\,\theta \sin\theta + C_5\,\theta\cos\theta\ , \qquad (5\text{-}35)$$

$$\psi = \frac{1}{R}\left[C_1\left(\frac{J_y}{aR^2} + 1\right)\theta + 2C_4 \sin\theta + 2C_5 \cos\theta + C_6\right], \qquad (5\text{-}36)$$

$$w = C_1\left(\frac{J_y}{aR^2} + 1\right)\theta - C_2\cos\theta + C_3\sin\theta + C_4(\sin\theta - \theta\cos\theta)$$

$$+ C_5(\cos\theta + \theta\sin\theta) + C_6\ . \qquad (5\text{-}37)$$

Thus, to solve for the constants C_i boundary conditions as shown are applied to Equations (5-35), (5-36) and (5-37) as follows.

$$\begin{bmatrix} 1 & \sin\theta_1 & \cos\theta_1 & \theta_1\sin\theta_1 & \theta_1\cos\theta_1 & 0 \\ \left(\frac{J_y}{aR^2}+1\right)\frac{\theta_1}{R} & 0 & 0 & \frac{2\sin\theta_1}{R} & \frac{2\cos\theta_1}{R} & \frac{1}{R} \\ \left(\frac{J_y}{aR^2}+1\right)\theta_1 & -\cos\theta_1 & \sin\theta_1 & \sin\theta_1 - \theta_1\cos\theta_1 & \cos\theta_1 + \theta_1\sin\theta_1 & 1 \\ 1 & \sin\theta_2 & \cos\theta_2 & \theta_2\sin\theta_2 & \theta_2\cos\theta_2 & 0 \\ \left(\frac{J_y}{aR^2}+1\right)\frac{\theta_2}{R} & 0 & 0 & \frac{2\sin\theta_2}{R} & \frac{2\cos\theta_2}{R} & \frac{1}{R} \\ \left(\frac{J_y}{aR^2}+1\right)\theta_2 & -\cos\theta_2 & \sin\theta_2 & \sin\theta_2 - \theta_2\cos\theta_2 & \cos\theta_2 + \theta_2\sin\theta_2 & 1 \end{bmatrix} \begin{bmatrix} C_1 \\ C_2 \\ C_3 \\ C_4 \\ C_5 \\ C_6 \end{bmatrix} = \begin{bmatrix} u_1 \\ \psi_1 \\ w_1 \\ u_2 \\ \psi_2 \\ w_2 \end{bmatrix}$$

(5-38)

or

$$[A_{in}]\,[C] = [\delta_{in}]\ . \qquad (5\text{-}39)$$

Now, using Equations (5-5), (5-29), and (5-30) one may summarize the forces as follows.

$$V_x = \frac{EJ_y}{R^3}\,(2C_4 \sin\theta + 2C_5 \cos\theta)\ , \tag{5-40}$$

$$M_y = \frac{EJ_y}{R^2}\,(C_1 + 2C_4 \cos\theta - 2C_5 \sin\theta)\ , \tag{5-41}$$

$$N_\theta = \frac{EJ_y}{R^3}\,(-2C_4 \cos\theta + 2C_5 \sin\theta)\ . \tag{5-42}$$

The generalized force vector is given by

$$\frac{EJ_y}{R^2}\begin{bmatrix} 0 & 0 & 0 & -\frac{2}{R}\sin\theta_1 & -\frac{2}{R}\cos\theta_1 & 0 \\ -1 & 0 & 0 & -2\cos\theta_1 & 2\sin\theta_1 & 0 \\ 0 & 0 & 0 & \frac{2}{R}\cos\theta_1 & -\frac{2}{R}\sin\theta_1 & 0 \\ 0 & 0 & 0 & \frac{2}{R}\sin\theta_2 & \frac{2}{R}\cos\theta_2 & 0 \\ 1 & 0 & 0 & 2\cos\theta_2 & -2\sin\theta_2 & 0 \\ 0 & 0 & 0 & -\frac{2}{R}\cos\theta_2 & \frac{2}{R}\sin\theta_2 & 0 \end{bmatrix}\begin{bmatrix} C_1 \\ C_2 \\ C_3 \\ C_4 \\ C_5 \\ C_6 \end{bmatrix} = \begin{bmatrix} -V_{x_1} \\ -M_{y_1} \\ -N_{\theta_1} \\ V_{x_2} \\ M_{y_2} \\ N_{\theta_2} \end{bmatrix} \tag{5-43}$$

or

$$\frac{EJ_y}{R^2}\,[D_{in}]\,[C] = [F_{in}]\ . \tag{5-44}$$

From (5-39) and (5-44)

$$[F_{in}] = \frac{EJ_y}{R^2} [D_{in}] [A_{in}]^{-1} [\delta_{in}] \tag{5-45}$$

so

$$[K_{in}] = \frac{EJ_y}{R^2} [D_{in}] [A_{in}]^{-1} . \tag{5-46}$$

To provide an example for future reference, the following parameter values are selected

$$\begin{aligned} R &= 3.0 \text{ in} \\ \frac{J_y}{aR^2} &= 0.01 \\ \theta_2 &= 0 \\ \theta_2 &= \pi/6 \end{aligned} \tag{5-47}$$

For this example the stiffness matrix [K] is:

$$[K_{in}] = \frac{EJ_y}{R^2} \begin{bmatrix} 30.72 & 21.84 & 9.21 & 22.00 & 20.54 & 23.34 \\ 21.89 & 22.80 & -3.24 & -20.54 & 11.26 & -8.11 \\ 9.21 & -3.24 & 62.62 & 23.34 & -8.11 & -58.84 \\ -22.00 & -20.54 & 23.34 & 30.72 & -21.84 & -9.21 \\ 20.54 & 11.26 & -8.11 & -21.84 & 22.80 & -3.24 \\ -23.34 & -8.11 & -58.84 & -9.21 & -3.24 & 62.62 \end{bmatrix}$$

(5-48)

The above equations have been checked against those given by Morris [49]. The stiffness matrix is invariant with orientation θ_1 given a constant $\theta_2 - \theta_1$ as it should be.

Out-of-Plane Stiffness--Figure 5-4 shows an element defined for out-of-plane stiffness. The moments and forces are shown which are compatible with the displacements. The stiffness for this element is determined in a manner similar to that for the in-plane case. Letting $J_{xy} \to 0$, the out-of-plane equations are taken from Equation (5-21) and (5-23).

$$\phi''R(1 + A) - v''''A + v'' = 0 , \tag{5-49}$$

$$(\phi''R + v'') - A(\phi R - v'') = 0 , \tag{5-50}$$

where

$$A = \frac{EJ_x}{GJ_\theta} . \tag{5-51}$$

Elimination of ϕ between (5-49) and (5-50) gives

$$v'''''' + 2v'''' + v'' = 0 \tag{5-52}$$

to which the general solution is

$$v = B_1 + B_2 \theta + B_3 \sin \theta + B_4 \cos \theta + B_5 \theta \sin \theta + B_6 \theta \cos \theta . \tag{5-53}$$

Using (5-49) to solve for ϕ gives

$$\phi R = -B_3 \sin \theta - B_4 \cos \theta - B_5 \theta \sin \theta - B_6 \theta \cos \theta$$
$$+ 2B_5 \frac{A}{1 + A} \cos \theta - 2B_6 \frac{A}{1 + A} \sin \theta + B_7\theta + B_8 . \tag{5-54}$$

Substitution into (5-50) shows that

$$B_7 = 0 , \quad B_8 = 0 . \tag{5-55}$$

Thus, the solutions for ϕ and v are now given.

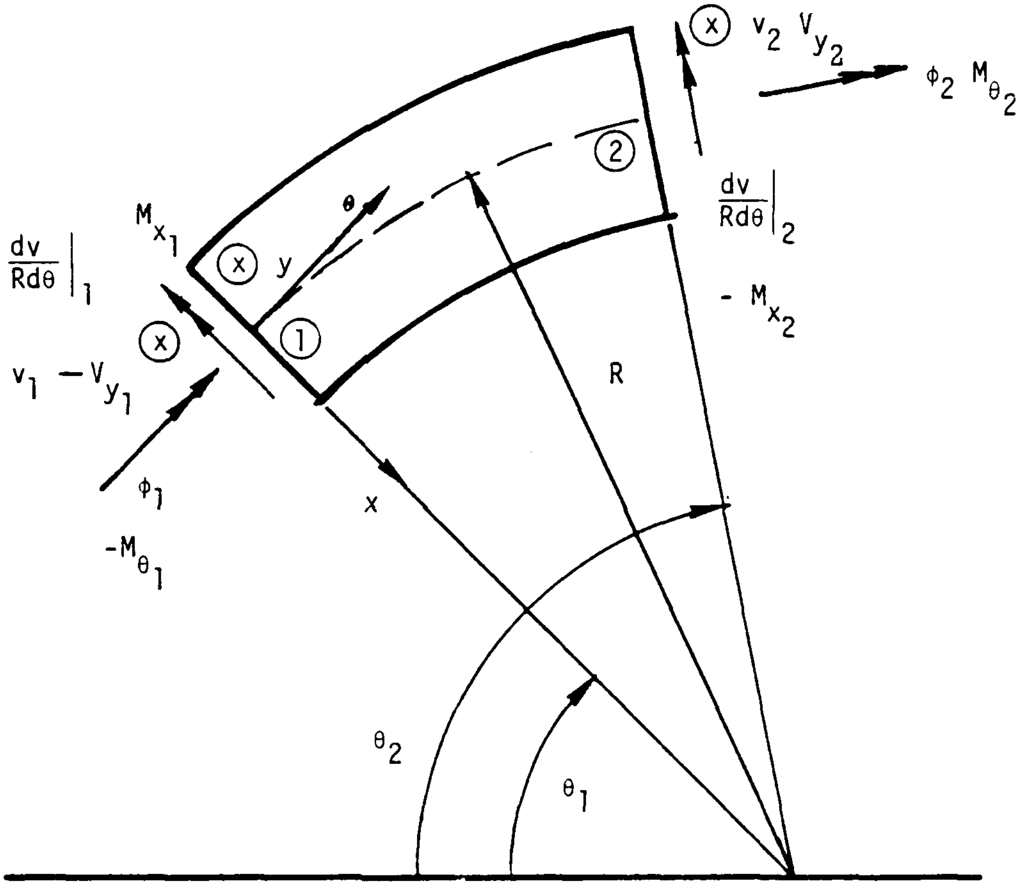

Figure 5-4. Finite Element for Out-of-Plane Loading.

Applying the boundary conditions of Figure 5-4 to Equations (5-53) and (5-54) gives the following matrix equations

$$\begin{bmatrix} 1 & \theta_1 & \sin\theta_1 & \cos\theta_1 & \theta_1 \sin\theta_1 & \theta_1 \cos\theta_1 \\ 0 & \frac{1}{R} & \frac{1}{R}\cos\theta_1 & -\frac{1}{R}\sin\theta_1 & \frac{1}{R}\sin\theta_1 + \frac{1}{R}\theta_1 \cos\theta_1 & \frac{1}{R}\cos\theta_1 - \frac{1}{R}\theta_1 \sin\theta_1 \\ 0 & 0 & -\frac{1}{R}\sin\theta_1 & -\frac{1}{R}\cos\theta_1 & -\frac{\theta_1}{R}\sin\theta_1 + \frac{2}{R}\frac{A}{1+A}\cos\theta & -\frac{\theta_1}{R}\cos\theta_1 - \frac{2}{R}\frac{A}{1+A}\sin\theta_1 \\ 1 & \theta_2 & \sin\theta_2 & \cos\theta_2 & \theta_2 \sin\theta_2 & \theta_2 \cos\theta_2 \\ 0 & \frac{1}{R} & \frac{1}{R}\cos\theta_2 & -\frac{1}{R}\sin\theta_2 & \frac{1}{R}\sin\theta_2 + \frac{1}{R}\theta_2 \cos\theta_2 & \frac{1}{R}\cos\theta_2 - \frac{1}{R}\theta_2 \sin\theta_2 \\ 0 & 0 & -\frac{1}{R}\sin\theta_2 & -\frac{1}{R}\cos\theta_2 & -\frac{\theta_2}{R}\sin\theta_2 + \frac{2}{R}\frac{A}{1+A}\cos\theta_2 & -\frac{\theta_2}{R}\cos\theta_2 - \frac{2}{R}\frac{A}{1+A}\sin\theta_2 \end{bmatrix} \begin{bmatrix} B_1 \\ B_2 \\ B_3 \\ B_4 \\ B_5 \\ B_6 \end{bmatrix} = \begin{bmatrix} v_1 \\ \frac{1}{R}\frac{dv}{d\theta}\Big|_1 \\ \phi_1 \\ v_2 \\ \frac{1}{R}\frac{dv}{d\theta}\Big|_2 \\ \phi_2 \end{bmatrix}$$

(5-56)

or

$$[A_{out}]\,[B] = [\delta_{out}] \; . \qquad (5\text{-}57)$$

Using Equations (5-4), (5-13), and (5-14) and substituting for v and ϕ, one can show that

$$V_y = \frac{EJ_x}{R^3}\,\frac{B_2}{A} \; , \qquad (5\text{-}58)$$

$$M_x = \frac{EJ_x}{R^2}\left(\frac{2}{1+A}\right)(-B_5 \cos\theta + B_6 \sin\theta) \qquad (5\text{-}59)$$

$$M_\theta = \frac{EJ_x}{R^2}\left(\frac{B_2}{A} - \frac{2B_5}{1+A}\sin\theta - \frac{2B_6}{1+A}\cos\theta\right) . \qquad (5\text{-}60)$$

Thus the generalized force vector is given by

$$\frac{EJ_x}{R^2}\begin{bmatrix} 0 & -\frac{1}{RA} & 0 & 0 & 0 & 0 \\ 0 & 0 & 0 & 0 & -\frac{2}{1+A}\cos\theta_1 & \frac{2}{1+A}\sin\theta_1 \\ 0 & -\frac{1}{A} & 0 & 0 & \frac{2}{1+A}\sin\theta_1 & \frac{2}{1+A}\cos\theta_1 \\ 0 & \frac{1}{RA} & 0 & 0 & 0 & 0 \\ 0 & 0 & 0 & 0 & \frac{2}{1+A}\cos\theta_2 & -\frac{2}{1+A}\sin\theta_2 \\ 0 & \frac{1}{A} & 0 & 0 & -\frac{2}{1+A}\sin\theta_2 & -\frac{2}{1+A}\cos\theta_2 \end{bmatrix}\begin{bmatrix} B_1 \\ B_2 \\ B_3 \\ B_4 \\ B_5 \\ B_6 \end{bmatrix} = \begin{bmatrix} -V_{y_1} \\ M_{x_1} \\ -M_{\theta_1} \\ V_{y_2} \\ -M_{x_2} \\ M_{\theta_2} \end{bmatrix} \tag{5-61}$$

or

$$\frac{EJ_x}{R^2}[D_{out}][B] = [F_{out}] \ . \tag{5-62}$$

From Equations (5-57) and (5-62)

$$[F_{out}] = \frac{EJ_x}{R^2}[D_{out}][A_{out}]^{-1}[\delta_{out}] \tag{5-63}$$

so

$$[K_{out}] = \frac{EJ_x}{R^2}[D_{out}][A_{out}]^{-1} \ . \tag{5-64}$$

Using as an example

$R = 3.0$ in.

$A = 5.0$

$$\theta_1 = 0 \tag{5-65}$$

$\theta_2 = \pi/6$,

The stiffness matrix for the out-of-plane case is:

$$[K_{out}] = \frac{EJ_x}{R^2} \begin{bmatrix} 27.12 & -21.20 & 2.24 & -27.12 & 21.20 & -2.24 \\ 21.20 & 21.55 & 2.77 & -21.20 & 11.75 & -0.15 \\ 2.24 & 2.77 & 1.63 & -2.24 & 0.15 & -0.92 \\ -27.12 & -21.20 & -2.24 & 27.12 & -21.20 & 2.24 \\ 21.20 & 11.75 & 0.15 & -21.20 & 21.55 & -2.77 \\ -2.24 & -0.15 & -0.92 & 2.24 & -2.77 & 1.63 \end{bmatrix} \tag{5-66}$$

Coupled Stiffness--Figure 5-5 shows an element defined for both in- and out-of-plane stiffness. The forces and displacements defined for the two previous cases are shown together in Figure 5-5.

To find the stiffness for this element, the set of coupled Equations (5-20) through (5-23) must be solved subject to the general displacement boundary conditions shown on Figure 5-5. Eliminating u and ϕ between Equations (5-21), (5-22), and (5-23) an equation in v only is found.

$$v'''''' + 2v'''' + v'' = 0 \; . \tag{5-67}$$

As before, the general solution is

$$v = G_1 + G_2\,\theta + G_3 \sin\theta + G_4 \cos\theta + G_5\,\theta \sin\theta + G_6\,\theta \cos\theta \; . \tag{5-68}$$

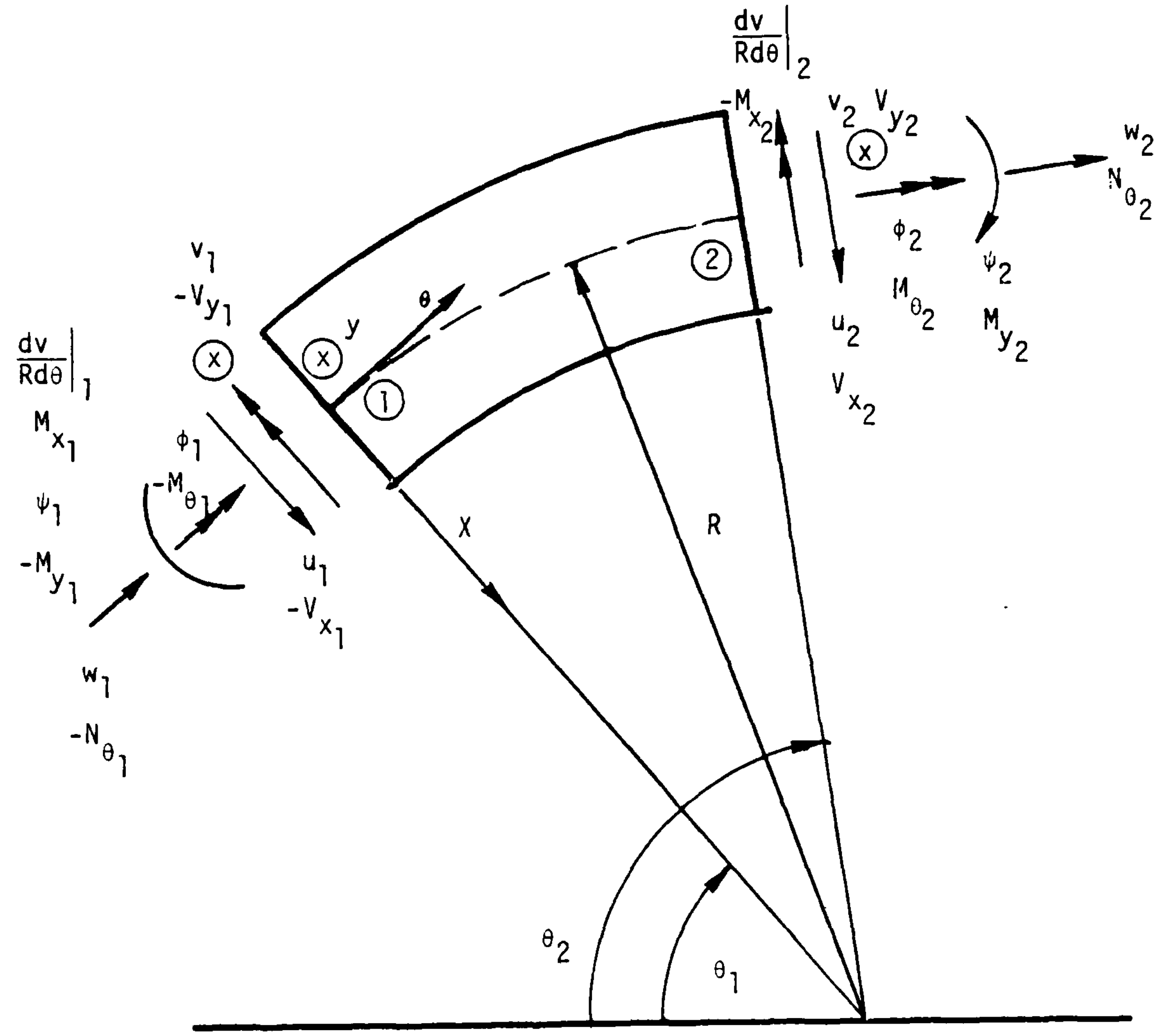

Figure 5-5. Finite Element for Coupled Problem.

Eliminating u between Equations (5-21) and (5-23)

$$\phi'' + \phi'''' = -v'' - v'''' . \tag{5-69}$$

Substituting for v,

$$\phi'' + \phi'''' = -2G_6 \sin\theta + 2G_5 \cos\theta . \tag{5-70}$$

The homogeneous and particular solutions to this equation give

$$\phi R = G_7 + G_{15}\,\theta + G_8 \sin\theta + G_9 \cos\theta$$

$$- G_5\,\theta \sin\theta - G_6\,\theta \cos\theta . \tag{5-71}$$

Rewriting Equation (5-23),

$$(u + u'')\,\frac{J_{xy}}{J_x} = \phi R - v'' - (\phi'' R + v'')\,\frac{1}{A} , \tag{5-72}$$

where

$$A = \frac{EJ_x}{GJ_\theta} \tag{5-73}$$

Substituting for ϕ and v, the equation becomes

$$(u + u'')\,\frac{J_{xy}}{J_x} = G_7 + G_{15}\,\theta + [(G_8 + G_3)\,(1 + \frac{1}{A}) + 2G_6] \sin\theta$$

$$+ [(G_9 + G_4)\,(1 + \frac{1}{A}) - 2G_5] \cos\theta . \tag{5-74}$$

The homogeneous and particular solutions for u give

$$\frac{J_{xy}}{J_x} u = G_7 + G_{15}\,\theta + G_{10} \sin\theta + G_{11} \cos\theta$$

$$+ [\tfrac{1}{2} (G_9 + G_4) (1 + \tfrac{1}{A}) - G_5]\,\theta \sin\theta$$

$$- [\tfrac{1}{2} (G_8 + G_3) (1 + \tfrac{1}{A}) + G_6]\,\theta \cos\theta\ . \tag{5-75}$$

Substitution for v, ϕ, and u into Equation (5-22) shows that

$$G_{15}\left(1 - \frac{J_{xy}^2}{J_x J_y}\right) = 0\ . \tag{5-76}$$

So G_{15} is an extra constant and

$$G_{15} = 0\ . \tag{5-77}$$

Now substituting for u, v, and ϕ into Equation (5-20),

$$w' + w''' = \left[\left(1 + \frac{J_y}{aR^2}\right) \frac{J_x}{J_{xy}} - \frac{J_{xy}}{aR^2}\right] G_7$$

$$+ 2\,\frac{J_x}{J_{xy}} [\tfrac{1}{2} (G_8 + G_3) (1 + \tfrac{1}{A}) + G_6] \sin\theta$$

$$+ 2\,\frac{J_x}{J_{xy}} [\tfrac{1}{2} (G_9 + G_4) (1 + \tfrac{1}{A}) - G_5] \cos\theta\ . \tag{5-78}$$

The particular and homogeneous solutions for w give

$$w = G_{12} + \left[\left(1 + \frac{J_y}{aR^2}\right) \frac{J_x}{J_{xy}} \right] - \frac{J_{xy}}{aR^2} \, G_7 + G_{13} \sin\theta + G_{14} \cos\theta$$

$$- \frac{J_x}{J_{xy}} \left[\frac{1}{2} (G_8 + G_3)\left(1 + \frac{1}{A}\right) + G_6\right] \theta \sin\theta$$

$$- \frac{J_x}{J_{xy}} \left[\frac{1}{2} (G_9 + G_4)\left(1 + \frac{1}{A}\right) - G_5\right] \theta \cos\theta \, . \tag{5-79}$$

We now have the solution for u, v, w, and ϕ in terms of 14 arbitrary constants, two more than dictated by the boundary conditions of the problem. To find the extra constants, one must check to see that the original differential equations of equilibrium (5-1) through (5-6) are satisfied. A combination of (5-3) and (5-5) give

$$M_y' + RN_\theta' = 0 \, . \tag{5-80}$$

But from (5-11)

$$M_y' + RN_\theta' = Ea[w'' - u'] \tag{5-81}$$

so

$$w'' - u' = 0 \, . \tag{5-82}$$

Substituting for w and u from Equations (5-79) and (5-75) into the above shows that G_{13} and G_{14} are extra constants and can be expressed in terms of the other constants.

$$G_{13} = \frac{J_x}{J_{xy}} \left[G_{11} + \frac{1}{2} (G_9 + G_4)\left(1 + \frac{1}{A}\right) - G_5\right] , \tag{5-83}$$

$$G_{14} = \frac{J_x}{J_{xy}} \left[-G_{10} - \frac{1}{2} (G_8 + G_3)\left(1 + \frac{1}{A}\right) - G_6\right] . \tag{5-84}$$

Thus, in summary, in terms of the 12 remaining constants,

$$v = G_1 + G_2\,\theta + G_3 \sin\theta + G_4 \cos\theta + G_5\,\theta \sin\theta + G_6\,\theta\cos\theta \tag{5-85}$$

$$\phi = \frac{1}{R}\{G_7 + G_8 \sin\theta + G_9 \cos\theta - G_5\,\theta\sin\theta - G_6\,\theta\cos\theta\} \tag{5-86}$$

$$u = \frac{J_x}{J_{xy}}\{G_7 + G_{10}\sin\theta + G_{11}\cos\theta + [\tfrac{1}{2}(G_9 + G_4)(1 + \tfrac{1}{A})$$

$$- G_5]\,\theta\sin\theta - [\tfrac{1}{2}(G_8 + G_3)(1 + \tfrac{1}{A}) + G_6]\,\theta\cos\theta\} \tag{5-87}$$

$$w = G_{12} + \left[\left(1 + \frac{J_y}{aR^2}\right)\frac{J_x}{J_{xy}} - \frac{J_{xy}}{aR^2}\right]G_7\,\theta$$

$$+ \frac{J_x}{J_{xy}}\Big\{[G_{11} + \tfrac{1}{2}(G_9 + G_4)(1 + \tfrac{1}{A}) - G_5]\sin\theta$$

$$+ [-G_{10} - \tfrac{1}{2}(G_8 + G_3)(1 + \tfrac{1}{A}) - G_6]\cos\theta$$

$$- [\tfrac{1}{2}(G_8 + G_3)(1 + \tfrac{1}{A}) + G_6]\,G\sin\theta$$

$$- [\tfrac{1}{2}(G_9 + G_4)(1 + \tfrac{1}{A}) - G_5]\,\theta\cos\theta\Big\}\,. \tag{5-88}$$

To satisfy the boundary conditions one needs in addition

$$\psi = \frac{u'}{R} + \frac{w}{R} = \frac{1}{R}\left\{G_{12} + \left[\left(1 + \frac{J_y}{aR^2}\right)\frac{J_x}{J_{xy}} - \frac{J_{xy}}{aR^2}\right]G_7\,\theta\right\}$$

$$+ \frac{1}{R}\frac{J_x}{J_{xy}}\left\{2\left[\frac{1}{2}(G_9 + G_4)\left(1 + \frac{1}{A}\right) - G_5\right]\sin\theta\right.$$

$$\left. - 2\left[\frac{1}{2}(G_8 + G_3)\left(1 + \frac{1}{A}\right) + G_6\right]\cos\theta\right\}, \quad (5\text{-}89)$$

$$\frac{v'}{R} = \frac{1}{R}\left\{G_2 + G_3\cos\theta - G_4\sin\theta + G_5(\theta\cos\theta + \sin\theta)\right.$$

$$\left. + G_6(-\theta\sin\theta + \cos\theta)\right\}, \quad (5\text{-}90)$$

Applying the boundary conditions shown in Figure 5-4 gives the matrix Equation (5-91) (next page) which is equivalent to

$$[A_{coupled}]\,[G] = [\delta_{coupled}] \quad (5\text{-}92)$$

To get the corresponding forces, substituting for u, v, ϕ, and w into-Equations (5-11) through (5-14) and (5-3) and (5-4) gives

$$V_x = -\frac{EJ_x}{R^3}\left\{\left(\frac{J_y}{J_{xy}} - \frac{J_{xy}}{J_x}\right)(2G_6\cos\theta + 2G_5\sin\theta)\right.$$

$$\left. + \left[\frac{J_y}{J_{xy}}\left(1 + \frac{1}{A}\right) - \frac{J_{xy}}{J_x}\right]\left[-(G_9 + G_4)\sin\theta + (G_8 + G_3)\cos\theta\right]\right\},$$

$$(5\text{-}93)$$

$$V_y = \frac{EJ_x}{R^3}\frac{G_2}{A}, \quad (5\text{-}94)$$

$$
\begin{bmatrix}
0 & 0 & -Q\,\theta_1 \cos\theta_1 & Q\,\theta_1 \sin\theta_1 & -P\,\theta_1 \sin\theta_1 & -P\,\theta_1 \cos\theta_1 & P & -Q\,\theta_1 \cos\theta_1 & Q\,\theta_1 \sin\theta_1 & P \sin\theta_1 & P\cos\theta_1 & 0 \\
1 & \theta_1 & \sin\theta_1 & \cos\theta_1 & \theta_1 \sin\theta_1 & \theta_1 \cos\theta_1 & 0 & 0 & 0 & 0 & 0 & 0 \\
0 & 0 & -Q(\cos\theta_1 + \theta_1 \sin\theta_1) & Q(\sin\theta_1 - \theta_1\cos\theta_1) & -P(\sin\theta_1 - \theta_1\cos\theta_1) & -P(\cos\theta_1 + \theta_1\sin\theta_1) & S\theta_1 & -Q(\cos\theta_1 + \theta_1\sin\theta_1) & Q(\sin\theta_1 - \theta_1\cos\theta_1) & -P\cos\theta_1 & P\sin\theta_1 & 1 \\
0 & \frac{1}{R} & \frac{1}{R}\cos\theta_1 & -\frac{1}{R}\sin\theta_1 & \frac{1}{R}(\theta_1\cos\theta_1 + \sin\theta_1) & \frac{1}{R}(-\theta_1\sin\theta_1 + \cos\theta_1) & 0 & 0 & 0 & 0 & 0 & 0 \\
0 & 0 & -\frac{2}{R}Q\cos\theta_1 & \frac{2}{R}Q\sin\theta_1 & -\frac{2}{R}P\sin\theta_1 & -\frac{2}{R}P\cos\theta_1 & \frac{S}{R}\theta_1 & -\frac{2}{R}Q\cos\theta_1 & \frac{2}{R}Q\sin\theta_1 & 0 & 0 & \frac{1}{R} \\
0 & 0 & 0 & 0 & -\frac{1}{R}\theta_1\sin\theta_1 & -\frac{1}{R}\theta_1\cos\theta_1 & \frac{1}{R} & \frac{1}{R}\sin\theta_1 & \frac{1}{R}\cos\theta_1 & 0 & 0 & 0 \\
0 & 0 & -Q\,\theta_2\cos\theta_2 & Q\,\theta_2\sin\theta_2 & -P\,\theta_2\sin\theta_2 & -P\,\theta_2\cos\theta_2 & P & -Q\,\theta_2\cos\theta_2 & Q\,\theta_2\sin\theta_2 & P\sin\theta_2 & P\cos\theta_2 & 0 \\
1 & \theta_2 & \sin\theta_2 & \cos\theta_2 & \theta_2\sin\theta_2 & \theta_2\cos\theta_2 & 0 & 0 & 0 & 0 & 0 & 0 \\
0 & 0 & -Q(\cos\theta_2 + \theta_2\sin\theta_2) & Q(\sin\theta_2 - \theta_2\cos\theta_2) & -P(\sin\theta_2 - \theta_2\cos\theta_2) & -P(\cos\theta_2 + \theta_2\sin\theta_2) & S\theta_2 & -Q(\cos\theta_2 + \theta_2\sin\theta_2) & Q(\sin\theta_2 - \theta_2\cos\theta_2) & -P\cos\theta_2 & P\sin\theta_2 & 1 \\
0 & \frac{1}{R} & \frac{1}{R}\cos\theta_2 & -\frac{1}{R}\sin\theta_2 & \frac{1}{R}(\theta_2\cos\theta_2 + \sin\theta_2) & \frac{1}{R}(-\theta_2\sin\theta_2 + \cos\theta_2) & 0 & 0 & 0 & 0 & 0 & 0 \\
0 & 0 & -\frac{2}{R}Q\cos\theta_2 & \frac{2}{R}Q\sin\theta_2 & -\frac{2}{R}P\sin\theta_2 & -\frac{2}{R}P\cos\theta_2 & \frac{S}{R}\theta_2 & -\frac{2}{R}Q\cos\theta_2 & \frac{2}{R}Q\sin\theta_2 & 0 & 0 & \frac{1}{R} \\
0 & 0 & 0 & 0 & -\frac{1}{R}\theta_2\sin\theta_2 & -\frac{1}{R}\theta_2\cos\theta_2 & \frac{1}{R} & \frac{1}{R}\sin\theta_2 & \frac{1}{R}\cos\theta_2 & 0 & 0 & 0
\end{bmatrix}
\begin{bmatrix} G_1 \\ G_2 \\ G_3 \\ G_4 \\ G_5 \\ G_6 \\ G_7 \\ G_8 \\ G_9 \\ G_{10} \\ G_{11} \\ G_{12} \end{bmatrix}
=
\begin{bmatrix} u_1 \\ v_1 \\ w_1 \\ \frac{1}{R}\frac{dv}{d\theta}\Big|_1 \\ \psi_1 \\ \phi_1 \\ u_2 \\ v_2 \\ w_2 \\ \frac{1}{R}\frac{dv}{d\theta}\Big|_2 \\ \psi_2 \\ \phi_2 \end{bmatrix}
$$

$P = \frac{J_x}{J_{xy}}$, $Q = \frac{1}{2}\frac{J_x}{J_{xy}}(1 + \frac{1}{A})$, $S = (1 + \frac{J_y}{aR^2})\frac{J_x}{J_{xy}} - \frac{J_{xy}}{aR^2}$

Equation (5-91)

$$N_\theta = -\frac{EJ_x}{R^3}\left\{\left(\frac{J_y}{J_{xy}} - \frac{J_{xy}}{J_x}\right)(2G_6 \sin\theta - 2G_5 \cos\theta)\right.$$

$$\left. + \left[\frac{J_y}{J_{xy}}\left(1 + \frac{1}{A}\right) - \frac{J_{xy}}{J_x}\right][(G_9 + G_4)\cos\theta + (G_8 + G_3)\sin\theta]\right\} , \tag{5-95}$$

$$M_x = -\frac{EJ_x}{R^2}\frac{1}{A}[(G_3 + G_8)\sin\theta + (G_4 + G_9)\cos\theta] , \tag{5-96}$$

$$M_y = \frac{EJ_x}{R^2}\left\{\left(\frac{J_y}{J_{xy}} - \frac{J_{xy}}{J_x}\right)(G_7 - 2G_5 \cos\theta + 2G_6 \sin\theta)\right.$$

$$\left. + \left[\frac{J_y}{J_{xy}}\left(1 + \frac{1}{A}\right) - \frac{J_{xy}}{J_x}\right][(G_9 + G_4)\cos\theta + (G_8 + G_3)\sin\theta]\right\} . \tag{5-97}$$

$$M_\theta = \frac{EJ_x}{R^2}\frac{1}{A}[G_2 + (G_3 + G_8)\cos\theta - (G_4 + G_9)\sin\theta] . \tag{5-98}$$

Using the above, the generalized force vector is given by Equation (5-99) (next page). This equation has the form

$$\frac{EJ_x}{R^2}[D_{coupled}]\,[G] = [F_{coupled}] . \tag{5-100}$$

Using Equations (5-92) and (5-100)

$$[F_{coupled}] = \frac{EJ_x}{R^2}[D_{coupled}]\,[A_{coupled}]^{-1}\,[\delta_{coupled}] . \tag{5-101}$$

Thus,

$$
\frac{EJ_x}{R^2}
\begin{bmatrix}
0 & 0 & \frac{V}{R}\cos\theta_1 & -\frac{V}{R}\sin\theta_1 & \frac{2U}{R}\sin\theta_1 & \frac{2U}{R}\cos\theta_1 & 0 & \frac{V}{R}\cos\theta_1 & -\frac{V}{R}\sin\theta_1 & 0 & 0 & 0 \\
0 & -\frac{1}{RA} & 0 & 0 & 0 & 0 & 0 & 0 & 0 & 0 & 0 & 0 \\
0 & 0 & \frac{V}{R}\sin\theta_1 & \frac{V}{R}\cos\theta_1 & -\frac{2U}{R}\cos\theta_1 & \frac{2U}{R}\sin\theta_1 & 0 & \frac{V}{R}\sin\theta_1 & \frac{V}{R}\cos\theta_1 & 0 & 0 & 0 \\
0 & 0 & -\frac{1}{A}\sin\theta_1 & -\frac{1}{A}\cos\theta_1 & 0 & 0 & 0 & -\frac{1}{A}\sin\theta_1 & -\frac{1}{A}\cos\theta_1 & 0 & 0 & 0 \\
0 & 0 & -V\sin\theta_1 & -V\cos\theta_1 & 2U\cos\theta_1 & -2U\sin\theta_1 & -U & -V\sin\theta_1 & -V\cos\theta_1 & 0 & 0 & 0 \\
0 & -\frac{1}{A} & -\frac{1}{A}\cos\theta_1 & \frac{1}{A}\sin\theta_1 & 0 & 0 & 0 & -\frac{1}{A}\cos\theta_1 & \frac{1}{A}\sin\theta_1 & 0 & 0 & 0 \\
0 & 0 & -\frac{V}{R}\cos\theta_2 & \frac{V}{R}\sin\theta_2 & -\frac{2U}{R}\cos\theta_2 & -\frac{2U}{R}\cos\theta_2 & 0 & -\frac{V}{R}\cos\theta_2 & \frac{V}{R}\sin\theta_2 & 0 & 0 & 0 \\
0 & \frac{1}{RA} & 0 & 0 & 0 & 0 & 0 & 0 & 0 & 0 & 0 & 0 \\
0 & 0 & -\frac{V}{R}\sin\theta_2 & -\frac{V}{R}\cos\theta_2 & \frac{2U}{R}\cos\theta_2 & -\frac{2U}{R}\sin\theta_2 & 0 & -\frac{V}{R}\sin\theta_2 & -\frac{V}{R}\cos\theta_2 & 0 & 0 & 0 \\
0 & 0 & \frac{1}{A}\sin\theta_2 & \frac{1}{A}\cos\theta_2 & 0 & 0 & 0 & \frac{1}{A}\sin\theta_2 & \frac{1}{A}\cos\theta_2 & 0 & 0 & 0 \\
0 & 0 & V\sin\theta_2 & V\cos\theta_2 & -2U\cos\theta_2 & 2U\sin\theta_2 & U & V\sin\theta_2 & V\cos\theta_2 & 0 & 0 & 0 \\
0 & \frac{1}{A} & \frac{1}{A}\cos\theta_2 & -\frac{1}{A}\sin\theta_2 & 0 & 0 & 0 & \frac{1}{A}\cos\theta_2 & -\frac{1}{A}\sin\theta_2 & 0 & 0 & 0
\end{bmatrix}
\begin{bmatrix} G_1 \\ G_2 \\ G_3 \\ G_4 \\ G_5 \\ G_6 \\ G_7 \\ G_8 \\ G_9 \\ G_{10} \\ G_{11} \\ G_{12} \end{bmatrix}
=
\begin{bmatrix} -V_{x1} \\ -V_{y1} \\ -N_{\theta 1} \\ M_{x1} \\ -M_{y1} \\ -M_{\theta 1} \\ V_{x2} \\ V_{y2} \\ N_{\theta 2} \\ -M_{x2} \\ M_{y2} \\ M_{\theta 2} \end{bmatrix}
$$

$$U = \frac{J_y}{J_{xy}} - \frac{J_{xy}}{J_x}, \qquad V = \frac{J_y}{J_{xy}}\left(1 + \frac{1}{A}\right) - \frac{J_{xy}}{J_x}$$

Equation (5-99)

$$[K_{coupled}] = \frac{EJ_x}{R^2} [D_{coupled}] [A_{coupled}]^{-1} . \quad (5\text{-}102)$$

As an example, let

$$\begin{aligned} R &= 3.0 \\ \theta_1 &= 0 \\ \theta_2 &= \pi/6 \\ A &= 5 \\ \frac{J_y}{aR^2} &= 0.01 \\ \frac{J_{xy}}{J_x} &= 0.1 \\ \frac{J_{xy}}{J_y} &= 0.1 \end{aligned} \quad (5\text{-}103)$$

For this case the stiffness matrix $[K_{coupled}]$ is calculated as

$$[K_{coupled}] = \frac{EJ_x}{R^2} \begin{bmatrix} 30.71 & 2.64 & 9.21 & 2.03 & 21.84 & 0.17 & -21.99 & -2.64 & -23.33 & 2.12 & 20.53 & -0.19 \\ 2.64 & 27.12 & -0.71 & 21.20 & 2.12 & 2.24 & -2.64 & -27.12 & -0.71 & 21.20 & 2.12 & -2.24 \\ 9.21 & -0.71 & 62.62 & -0.72 & -3.24 & -0.09 & 23.33 & 0.71 & -58.83 & -0.39 & -8.11 & 0.00 \\ 2.03 & 21.20 & -0.72 & 21.55 & 2.16 & 2.77 & -2.12 & -21.20 & -0.39 & 11.75 & 1.17 & -0.15 \\ 21.84 & 2.12 & -3.24 & 2.16 & 22.79 & 0.28 & -20.53 & -2.12 & -8.11 & 1.17 & 11.26 & -0.01 \\ 0.17 & 2.24 & -0.09 & 2.77 & 0.28 & 1.63 & -0.19 & -2.24 & -0.00 & 0.15 & 0.01 & -0.92 \\ -21.99 & -2.64 & 23.33 & -2.12 & -20.53 & -0.19 & 30.71 & 2.64 & -9.21 & -2.03 & -21.84 & 0.17 \\ -2.64 & -27.12 & 0.71 & -21.20 & -2.12 & -2.24 & 2.64 & 27.12 & 0.71 & -21.20 & -2.12 & 2.24 \\ -23.33 & -0.71 & -58.83 & -0.39 & -8.11 & -0.00 & -9.21 & 0.71 & 62.62 & -0.72 & -3.24 & 0.09 \\ 2.12 & 21.20 & -0.39 & 11.75 & 1.17 & 0.15 & -2.03 & -21.20 & -0.72 & 21.55 & 2.16 & -2.77 \\ 20.53 & 2.12 & -8.11 & 1.17 & 11.26 & 0.01 & -21.84 & -2.12 & -3.24 & 2.16 & 22.79 & -0.28 \\ -0.19 & -2.24 & 0.00 & -0.15 & -0.01 & -0.92 & 0.17 & 2.24 & 0.09 & -2.77 & -0.28 & 1.63 \end{bmatrix}$$

(5-104)

Verification of Stiffness Matrices--The correctness of the preceding stiffness matrices has been verified in detail by Knowlton [24]. He assembled the elements into rings, performed solutions and compared to known results. The in-plane results were compared to those of Morris [49] and straight beam theory. There is some slight difference when compared to Morris because he uses straight beam theory. Comparison is perfect of course as $R \to \infty$.

The out-of-plane case was verified by comparing to a problem solution for out-of-plane deflection presented by Roark [44]. Agreement was perfect.

Finally for the coupled problem, the only completely independent solutions formed are those by Meck [47]. Comparison was made to a cantilever curved beam section loaded in two planes and with $J_{xy} \neq 0$. Again, agreement was perfect. Coupled numerical solutions were also compared to those analytical solutions presented by Lebeck [41]. Again agreement was perfect.

Thus, based on these limited checks the preceding results appear to be correct. The reader is again cautioned that warping is not included here and this is valid for compact sections. However, warping does play a major role in many practical problems and must be included where necessary.

General Contact Problem

Given the stiffness matrix results for a ring, the next step in the solution of the general seal ring contact problem is to create a model of contact and incorporate it into problem solutions. Before illustrating how this is to be done for the actual seal assembly, a simple example will be used to show how such a contact problem can be solved.

The example problem will start with a beam on an elastic foundation (Figure 5-6). This problem can be modeled using beam finite elements (Figure 5-7). The stiffness matrix for a beam element as given by Irons [51] is

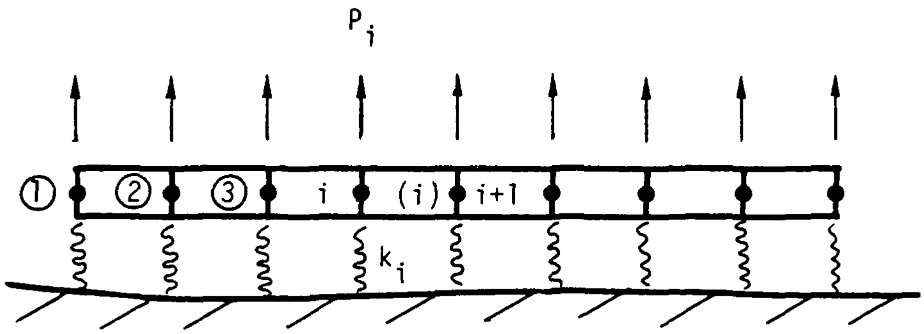

Figure 5-6. Beam on Elastic Foundation.

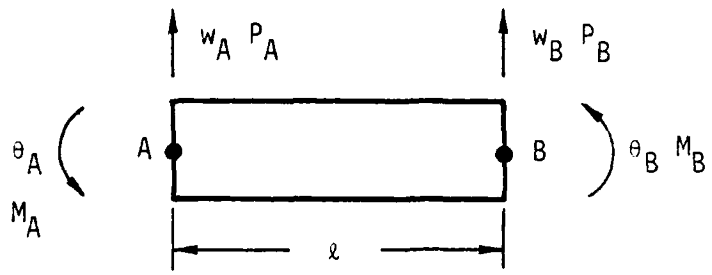

Figure 5-7. Beam Element.

$$K_e = \frac{EI}{\ell^3}\begin{bmatrix} 12 & 6\ell & -12 & 6\ell \\ 6\ell & 4\ell^2 & -6\ell & 2\ell^2 \\ -12 & -6\ell & 12 & -6\ell \\ 6\ell & 2\ell & -6\ell & 4\ell \end{bmatrix} \tag{5-105}$$

where the displacement and force vectors are

$$[\delta] = \begin{bmatrix} w_A \\ \theta_A \\ w_B \\ \theta_B \end{bmatrix} \quad (5\text{-}106) \qquad [F] = \begin{bmatrix} P_A \\ M_A \\ P_B \\ M_B \end{bmatrix} \quad (5\text{-}107)$$

For a solution by the finite element method, one requires an expression for the total strain energy of the system. The strain energy for one beam element and the springs under the element is

$$U^{(e)} = \frac{1}{2}[\delta]^T [K_e][\delta] + \frac{1}{2}\frac{k_A}{2}(w_A - \Delta_{0A})^2 + \frac{1}{2}\frac{k_B}{2}(w_B - \Delta_{0B})^2 . \tag{5-108}$$

The terms $k_A/2$ and $k_B/2$ assume the spring under each node is divided into two equal parts, one part associated with each adjacent element.

Total potential energy is the strain energy over all of the elements plus that due to the potential of applied loads or

$$U = \sum_e U^{(e)} - [F]^T [\delta] . \tag{5-109}$$

According to the principle of minimum potential energy

$$\delta U = 0 . \tag{5-110}$$

Applying this principle to Equations (5-108) and (5-109) combined gives

$$\left\{\sum_e [K_e] + \sum_e \left[\frac{k_A}{2}(w_A - \Delta_{OA}) + \frac{k_B}{2}(w_B - \Delta_{OA})\right]_e\right\}[\delta] = \sum_e [F_e] \; .$$

(5-111)

In matrix form, using the numbering system shown in Figure (5-6), the system of equations to be solved is:

$$\frac{EI}{\ell^3}\begin{bmatrix} 12 + \frac{k_1}{2}\frac{\ell^3}{EI} & 6\ell & -12 & 6\ell & & & & \\ 6\ell & 4\ell^2 & -6\ell & 2\ell^2 & & & & \\ -12 & -6\ell & 24 + k_2\frac{\ell^3}{EI} & 0 & -12 & 6\ell & & \\ 6\ell & 2\ell^2 & 0 & 8\ell^2 & -6\ell & 2\ell^2 & & \\ & & -12 & -6\ell & 24 + k_3\frac{\ell^3}{EI} & 0 & -12 & 6\ell \\ & & 6\ell & 2\ell^2 & 0 & 8\ell^2 & -6\ell & 2\ell^2 \\ & & & & -12 & -6\ell & 24 + k_4\frac{\ell^3}{EI} & 0 \\ & & & & 6\ell & 2\ell^2 & 0 & 8\ell^2 \\ & & & & & & \cdots & \cdots \\ & & & & & & \cdots & \cdots \\ & & & & & & & \end{bmatrix}\begin{bmatrix} w_1 \\ \theta_1 \\ w_2 \\ \theta_2 \\ w_3 \\ \theta_3 \\ w_4 \\ \theta_4 \\ \cdot \\ \cdot \\ \cdot \end{bmatrix} = \begin{bmatrix} P_1 - \frac{k_1\Delta_1}{2} \\ \\ P_2 - k_2\Delta_2 \\ \\ P_3 - k_3\Delta_3 \\ \\ P_4 - k_4\Delta_4 \\ \\ \cdots \\ \cdots \\ \\ \end{bmatrix}$$

(5-112)

System of Equations (5-112) can be readily solved for the equilibrium displacements w_i for arbitrary k_i and P_i. The Δ_i allow for any preload of the springs. An algorithm solving Equation (5-112) was written and solutions to various beam on elastic foundation problems were carried out. For the case of a semi-infinite beam on elastic foundation loaded at the end only, the displacement at the end was found to be within 9.2 percent with 20 elements, 2.5 percent with 40 elements, and 0.4 percent with 80 elements of the exact solution results. Thus the method was verified.

Now to solve a contact problem one need only make the springs stiff enough to approximate contact stiffness, allow for preload by adjusting the Δ_i, and allow for noncontact by causing the $k_i \to 0$ where appropriate. The example problem to be solved is shown in Figure 5-8. Here a beam is brought into contact with two circularly curved surfaces of high rigidity. Loads P_1 and P_2 act to deflect the beam making it contact the two surfaces with some knowable contact pressure distribution. The problem to be solved is to find this pressure distribution, or more precisely to find which points in the discretized problem make contact and at what load.

The procedure used to solve the stated problem is as follows:

1) Pick initial contact points A and B and set k_A and k_B equal to contact stiffness. Set all other $k_i \to 0$.
2) Set $P_1' = nF \times P_1$ and $P_2' = nF \times P_2$ where F is some fraction of 1.0 and n = 1 (F = 0.1 appears to work). Solve for the deflection using this reduced load.
3) Compare the deflection to the known gap. If deflection is greater than gap at i, set k_i equal to contact stiffness and set Δ_i also.
4) If deflection is less than Δ at i, the set $k_i \to 0$.
5) Repeat steps 2), 3), and 4) with n = 2,3 ··· 1/F.
6) If assumed contact pattern agrees with solved for contact pattern at nF = 1, the solution is consistent and in hand. If it does not, then set F equal to a finer increment at least near full load.

The above procedure was found to give a unique solution to the example problem. It was found that only by slowly increasing the load was it possible to arrive at a consistent solution (see 6) above). Applying full load resulted in continual changes in contact pattern with each iteration--some of the time.

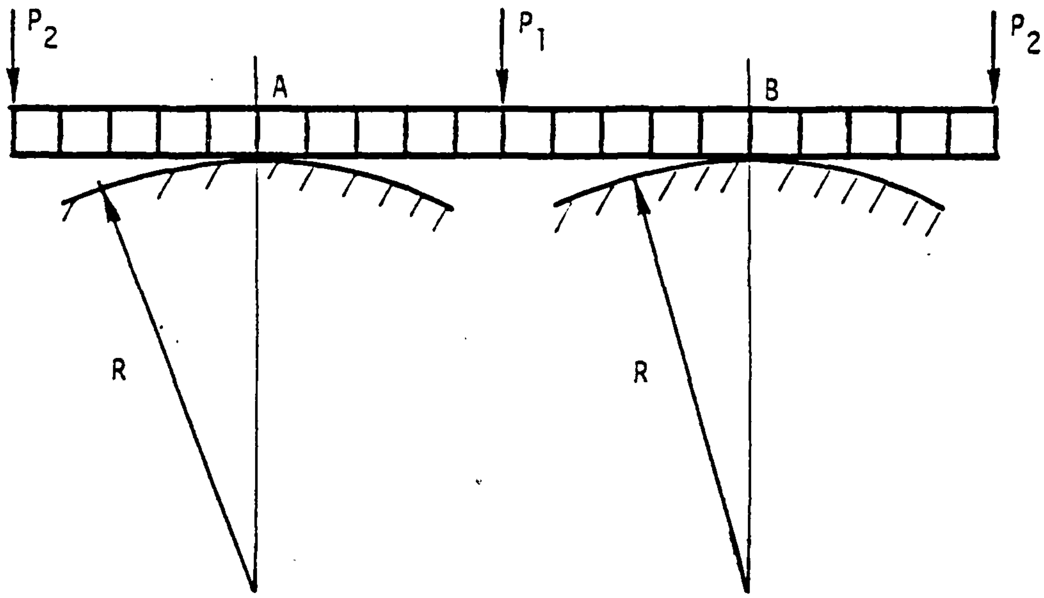

Figure 5-8. Beam Contact Problem.

For the example problem,

$$
\begin{aligned}
\ell &= 1 \text{ in. (total length 20 in.)} \\
E &= 30 \times 10^6 \text{ lb/in.}^2 \\
k_i &= 100 \times 10^6 \text{ lb/in.} \\
P_1 &= 20000 \text{ lb} \\
P_2 &= 10000 \text{ lb} \\
R &= 100 \text{ in.} \\
I &= 0.085 \text{ in.}^4 \\
\Delta_i &- \text{based on circular support}
\end{aligned}
\tag{5-113}
$$

The computed result is shown in Table 5-1.

Ring Contact Problem

The contact problem for two rings is considerably more difficult than that for the beam. Figure 5-9 shows how the problem can be set up. The two seal rings are pushed together by arbitrary loads. k_s represents the stiffness of the support and k_f is the stiffness of the contact at the face. The contact is represented only by one set of springs at the mean contact radius. Additional sets could be included to better model face contact, but it is thought that for initial analysis at least, one set is sufficient.

The solution to the problem represented in Figure 5-9 is accomplished in much the same way as that for the beam. First, using the stiffness matrices derived for the ring elements, the strain energy of the entire assembly including the springs is found. Then, derivatives are taken and the set of resulting equations solved.

These final steps remain to be completed.

Table 5-1

Computed Results - Beam Contact Problem

Node	w_i	Δ_i	Contact Force
1	-0.1141	-0.1251	0
2	-0.07761	-0.08003	0
3	-0.04505	-0.04501	3459
4	-0.02007	-0.02000	7014
5	-0.005011	-0.005005	602
6	-0.00008922	-0.0	8922
7	-0.004347	-0.005005	0
8	-0.01446	-0.02000	0
9	-0.02652	-0.04501	0
10	-0.03662	-0.08003	0
11	-0.04085	-0.1251	0
12	-0.03662	-0.08003	0
13	-0.02652	-0.04501	0
14	-0.01446	-0.02000	0
15	-0.004347	-0.005005	0
16	-0.00008922	-0.0	8922
17	-0.005011	-0.005005	602
18	-0.02007	-0.02000	7014
19	-0.04505	-0.04501	3459
20	-0.07761	-0.08003	0
21	-0.1141	-0.1251	0

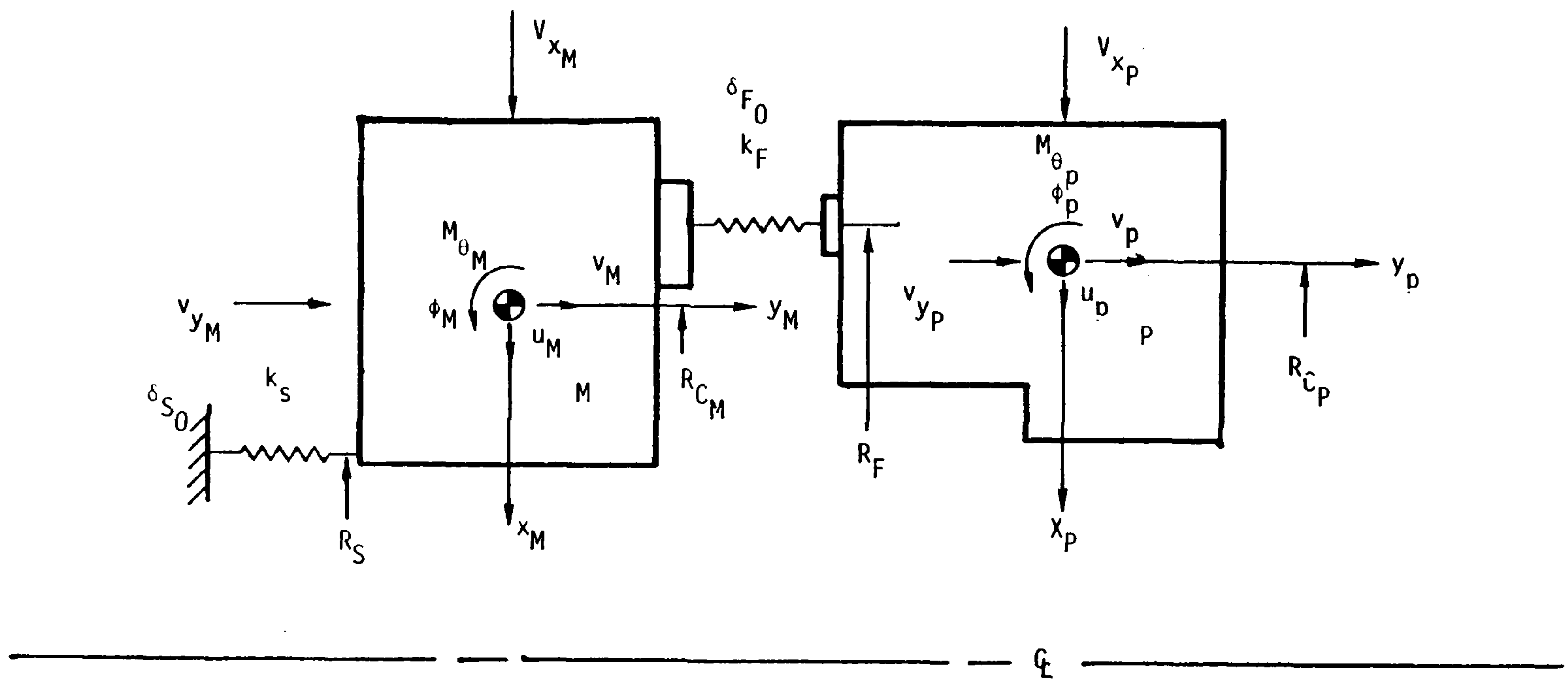

Figure 5-9. Two Ring Contact Problem.

CHAPTER 6

SUMMARY, CONCLUSIONS, AND RECOMMENDATIONS

Nine-Wave Seal Design

As of Test 117, nine-wave seal performance began to approach expected performance and the various design problems appear to have been solved. Conclusions concerning the long-term performance must await the completion of the scheduled 2000 hour test. However, several conclusions can be reached concerning the design itself.

1) As designed, 54 thin arms must be machined out of a solid Inconel 625 piece. While there was success in accomplishing this difficult machining task, a great amount of NC machine time was required. A simpler design or a more easily worked material must be found for practical application of the concept.

2) As designed, many 1/32-in. holes were needed in the Inconel 625. Again, while there was ultimately success in drilling these holes, a great amount of machine time was required. Special techniques had to be developed to remove broken drills. This problem could probably be overcome by using an EDM machine to make these holes. Alternatively, more easily worked material or a design which does not require so many small holes in a hard to work metal is to be preferred.

3) Larger than expected arm deflections led to hydraulic leakage problems. A 3-D stress analysis of the configuration would have shown this problem or a simpler more readily analyzed configuration should be used.

4) Ring stiffness with regard to waviness turned out to be larger than expected because significant torsional warping stresses developed. Again, a 3-D stress analysis would have shown this problem earlier and should have been used. This problem was overcome by reducing the cross section.

5) A method was developed to retain all O-rings on assembly. This should have been incorporated in the original design.

6) A large thickness epoxy bond of the carbon into the Inconel allows the carbon to creep such that it need not conform to the desired waviness. This problem was eliminated by reducing the bond thickness to 0.001 in. or less.

7) To eliminate hydraulic leakage in spite of the large arm deflection, a piston arrangement was used which gives the O-ring a zero gap through which it can extrude. After trying several other approaches it was concluded that if there exists any seal ring gap which must be sealed by the O-ring, the periodic motion of the arms will encourage the O-ring to extrude through the gap--even though the gap size is perfectly acceptable for a static O-ring application.

Test Machine Modification

The test machine was modified so that it can automatically run a seal test consisting of variable speed, pressure, and misalignment. The test becomes completely computer controlled. These changes required considerable modification of the test apparatus and its associated electronics. While existing software was modified to run the 2000 hour test, it became clear that a new software package incorporating greater flexibility and refined logic should be written. The computer controlled test cycle works as planned.

Seventy-Five Percent Balance Ratio Test

A 500 hour 75 percent balance ratio flat face test was run to try to duplicate and explain some previous data. It was concluded that the seal can start up in one of at least two modes of operation and that the second mode of high friction zero leakage is not stable.

Nine-Wave Seal Design Methodology

Chapter 3 points out the design criteria for the nine-wave seal. Many factors were considered including zero moment design, location of the centroid, low stiffness, and corrosion resistance. A good part of the design was accomplished using a computer program which relates the various geometrical variables to the design criteria. Alternative configurations were evaluated. Finite element and finite difference stress and deflection calculations were made. Performance was predicted using previously developed models. A clear design methodology has been set forth which should be generally applicable to wavy seal design for other purposes.

Misalignment

Since submarine seals undergo misalignment as a submarine decends, a condition for the simulated submarine operation test is to create a similar variable misalignment. This was achieved in a unique way for the wavy seal tests. Using the worm gear drive seal support originally used to move waviness and machining angles into the parts, the amount of misalignment can be adjusted as needed. This saves a lot of time in not having to remisalign the machine by hand for each test condition. The misalignment is computer controlled.

Moving Wave Gas Seal

The complete analysis of a moving wave gas seal is included in Chapter 4. Certain advantages of a moving wave gas seal compared to other types are pointed out. The analysis uses the alternating direction implicit method to solve the compressible flow equation. Other aspects of the analysis are similar to those already used for liquid seals. Parameter studies are made which show that at low speed operation the fluid pressure left is predominately due to hydrostatic effects. At zero pressure differential, a very smooth surface is required to allow the seal to hydrodynamically lift off. The design theoretically appears to work and offers a gas seal with very low friction and leakage. Experiments are needed to confirm these predictions.

Predicting Seal Ring Gap

To address the difficult problem of predicting seal ring gap (or zero gap as is desired) when rings are not axisymmetric or when seals have complex out of flatness, two significant developments were made which will lead to the development of a generalized computer program for predicting seal gap.

1) A new ring finite element was developed for the case of coupled in-plane and out-of-plane loading and deflection. The element has been checked. It provides a relatively simple method to solve the contact problem compared to 3-D solid elements.

2) Contact problems for beams otherwise similar to the one of interest have been solved using an iteration method.

After 1) and 2) are combined, the analysis of actual seal rings can be initiated.

References

1. Lebeck, A. O., Teale, J. L., and Pierce, R. E., "Elastohydrodynamic Lubrication with Wear and Asperity Contact in Mechanical Face Seals," Annual Report ME-76(77)ONR-414-1, ONR Contract N-00014-76-C-0071, Bureau of Engineering Research, The University of New Mexico, Albuquerque, New Mexico, January 1977.

2. Lebeck, A. O., Teale, J. L., and Pierce, R. E., "Hydrodynamic Lubrication with Wear and Asperity Contact in Mechanical Face Seals," Annual Report ME-86(78)ONR-414-1, prepared for the Office of Naval Research under Contract No. ONRN-00014-76-C-0071, Bureau of Engineering Research, The University of New Mexico, Albuquerque, New Mexico, January 1978.

3. Lebeck, A. O., Teale, J. L. and Pierce, R. E., "Hydrodynamic Lubrication with Wear and Asperity Contact in Mechanical Face Seals," Annual Report ME-95(79)ONR-414-1, prepared for the Office of Naval Research under Contract No. ONR-N-00014-76-C-0071, Bureau of Engineering Research, The University of New Mexico, Albuquerque, New Mexico, January 1979.

4. Lebeck, A. O. and Young, L. A., "The Wavy Mechanical Face Seal--Theoretical and Experimental Results," Annual Report ME-105(80)ONR-414-1, prepared for the Office of Naval Research under Contract ONR-N-00014-76-C-0071, Bureau of Engineering Research, The University of New Mexico, Albuquerque, New Mexico, January 1980.

5. Lebeck, A. O. and Young, L. A., "The Wavy Mechanical Face Seal--Theoretical and Experimental Results," Annual Report ME-111(81)ONR-414-1, prepared for the Office of Naval Research under Contract ONR-N-00014-76-C-0071, Bureau of Engineering Research, the University of New Mexico, Albuquerque, New Mexico, January 1981.

6. Lebeck, A. O., Teale, J. L., and Pierce, R. E., "Hydrodynamic Lubrication and Wear in Wavy Contacting Face Seals," Journal of Lubrication Technology, Vol. 100, January 1978, pp. 81-91.

7. Lebeck, A. O., "A Study of Mixed Lubrication in Contacting Mechanical Face Seals," presented at the 4th Leeds-Lyon Symposium on Lubrication, Lyon, France, September 13-16, 1977, published in "Surface Roughness Effects in Lubrication," proceedings of the 4th Leeds-Lyon Symposium on Tribology. Published by Mechanical Engineering Publications Limited for the Institute of Tribology, Leeds University and the Institut National Des Sciences Appliquées de Lyon, 1978.

8. Lebeck, A. O., "A Mixed Friction Hydrostatic Face Seal Model with Thermal Rotation and Wear," ASLE Transactions, Vol. 23, No. 4, October 1980, pp. 375-387.

9. Lebeck, A. O., "The Effect of Ring Deflection and Heat Transfer on the Thermoelastic Instability of Rotating Face Seals," presented at the ONR Thermal Deformation Workshop, June 1979, published in Thermal Deformation in Frictionally Heated Systems, R. A. Burton, Editor, Elsevier, The Netherlands, 1980.

10. Lebeck, A. O., "A Mixed Friction Hydrostatic Face Seal Model with Phase Change," Journal of Lubrication Technology, Vol. 102, No. 2, April 1980, pp. 133-138.

11. Teale, J. L. and Lebeck, A. O., "An Evaluation of the Average Flow Model [i] for Surface Roughness Effects in Lubrication," Journal of Lubrication Technology, Vol. 102, No. 3, July 1980, pp. 360-367.

12. Lebeck, A. O., "Hydrodynamic Lubrication in Wavy Contacting Face Seals--A Two-dimensional Model," Journal of Lubrication Technology, Vol. 103, No. 4, October 1981, pp. 578-586.

13. Lebeck, A. O., "A Test Apparatus for Measuring the Effects of Waviness in Mechanical Face Seals," ASLE Transactions, Vol. 24, No. 3, July 1981, pp. 371-378.

14. Lebeck, A. O. and Young, L. A., "Design of an Optimum Moving Wave and Tilt Mechanical Face Seal for Liquid Applications," 9th International Conference on Fluid Sealing, sponsored by the BHRA, The Netherlands, April 1-3, 1981.

15. Young, L. A. and Lebeck, A. O., "Experimental Evaluation of a Mixed Friction Hydrostatic Mechanical Face Seal Model Considering Radial Taper, Thermal Taper, and Wear," ASME paper 81-Lub-38, presented at the 1981 ASLE-ASME Meeting, New Orleans, October 1981, to be published in the Journal of Lubrication Technology.

16. Lebeck, A. O. and Chiou, B. C., "Two Phase Mechanical Face Seal Operation: Experimental and Theoretical Observations," Proceedings, 11th Annual Turbomachinery Symposium, Turbomachinery Laboratories, Department of Mechanical Engineering, Texas A&M University, December 1982.

17. Lebeck, A. O. and Wong, K. L., "Moving Wave Gas Seal," submitted to the ASLE Transactions for review, November 1982.

18. Lebeck, A. O. and Knowlton, J. S., "A Finite Element for the Three-Dimensional Deformation of a Circular Ring of Arbitrary Cross Section," submitted for International Journal of Numerical Methods in Engineering, November 1982.

19. Teale, J. L., "Surface Roughness Effects in Hydrodynamic Lubrication," M.S. Thesis, Mechanical Engineering Department, University of New Mexico, August 1978.

20. Pierce, R. E., "A Design Study for a Wavy Hydrodynamic Mechanical Face Seal," M.S. Thesis, Mechanical Engineering Department, University of New Mexico, May 1978.

21. Young, L. A., "Experimental Evaluation of a Mixed Friction Hydrostatic Mechanical Face Seal Model," M.S. Thesis, Mechanical Engineering Department, University of New Mexico, December 1980.

22. Chiou, B. C., "The Effect of Two-Phase Operation on Seal Performance," M.S. Thesis, Mechanical Engineering Department, University of New Mexico, December 1980.

23. Wong, K. L., "Moving Wave Gas Seal," M.S. Thesis, Mechanical Engineering Department, University of New Mexico, January 1982.

24. Knowlton, J. S., "A Finite Element for the Three-Dimensional Deformation of a Circular Ring of Arbitrary Cross Section," M. S. Thesis, Mechanical Engineering Department, University of New Mexico, December 1982.

25. Buchter, H. H., Industrial Sealing Technology, John Wiley and Sons, Inc., 1979.

26. Cheng, C. H., Castelli, V. and Chow, C. Y., "Performance Characteristics of Spiral-groove and Shrouded Rayleigh Step Profiles for High-speed Noncontacting Gas Seals," presented at the Lubrication Symposium of the ASME, Las Vegas, Nevada, June 17-20, 1968.

27. Zuk, J., Ludwig, L. P. and Johnson, R. L., "Compressible Flow Across Shaft Face Seals," presented at the Fifth International Conference on Fluid Sealing, 1971, Paper H6, March 30 to April 2, 1971.

28. Sedy, J., "Improved Performance of Film-Riding Gas Seals through Enhancement of Hydrodynamic Effects," presented at the ASLE/ASME Lubrication Conference in Minneapolis, Minnesota, October 24-26, 1978.

29. James, D. D. and Potter, A. F., "Numerical Analysis of the Gas Lubricated Spiral Groove Thrust Bearing-compressor," Journal of Lubricating Technology, pp. 439-444, October 1967.

30. Castelli, V. and Pirvics, J., "Equilibrium Characteristics of Axial-Groove Gas-Lubricated Bearings," Trans. ASME, Series F, Vol. 89, No. 2, pp. 177-196, April 1967.

31. Gardener, J. F., "Computer Analysis of Seal Design Problems Using Numerical Methods," Crane Packing Co., Morton Grove, IL., May 1970.

32. Gardener, J. F., "Recent Developments on Noncontacting Face Seals," presented at the 28th ASLE Annual Meeting in Chicago, Illinois, April 30 to May 3, 1973.

33. Zuk, J., "Compressible Seal Flow Analysis Using Finite Element Method with Galerkin Solution Technique," presented at the ASLE/ASME Lubrication Conference held at Montreal, Canada, October 8-10, 1974, ASLE Transactions, Vol. 19, No. 1, pp. 61-71, 1974.

34. Sedy, J., "A New Self-Aligning Mechanism for the Spiral-Groove Gas Seal Stability," presented at the ASLE/ASME Lubrication Conference in Dayton, Ohio, October 16-18, 1979.

35. Castelli, V. and Pirvics, J., "Review of Numerical Methods in Gas Bearing Film Analysis," presented at the Lubrication Symposium of the ASME, Las Vegas, Nevada, June 18-20, 1968.

36. Fairweather, G. and Mitchell, A. R., "A New Computational Procedure for A.D.I. Methods," SIAM Journal of Numerical Analysis, Vol. 4, No. 2, 1967.

37. Evans, D. J. and Gane, C. R., "A.D.I. Methods for the Solution of Transient Heat Conduction Problems in r-Geometry," International Journal for Numerical Methods in Engineering, Vol. 12, pp. 1799-1807, 1978.

38. Roache, P. J., Computational Fluid Dynamics, Hermosa Publishers, P.O. Box 8172, Albuquerque, New Mexico, 1972.

39. Shapiro, W., Fluid Film Bearing Response to Dynamic Loading, Mechanical Technology Incorporation, Latham, New York, 1973.

40. Gargiulo, E. P. and Gilmour, P. W., "A Numerical Solution for the Design of Externally Pressurized Porous Gas Bearing: Thrust Bearings," presented at the Lubrication Symposium of the ASME, Las Vegas, Nevada, June 17-20, 1968.

41. Lebeck, A. O., "Mechanical Loading--A Primary Source of Waviness in Mechanical Face Seals," presented at the 31st Annual ASLE Meeting, Philadelphia, PA, May 1976, ASLE Trans., 20(3), pp. 195-208.

42. Lebeck, A. O., "Causes and Effects of Waviness in Contacting Mechanical Face Seals," Final Report for NSF Grant GK37384, The University of New Mexico, Bureau of Engineering Research, Albuquerque, New Mexico, January 1976.

43. Noell, P., Rippel, H., and Hiemkiewicz, J., "Evaluation of Split Design for High-Pressure Seals--Phase II," prepared for Department of the Navy, Naval Sea Systems Command, Naval Ship Engineering Center, Final Report F-C4953-08, March 31, 1979, Franklin Research Center.

44. Roark, Raymond J. and Young, Warren C., Formulas for Stress and Strain (New York: McGraw-Hill, 1975), pp. 283-284.

45. Oden, J. T., Mechanics of Elastic Structures, McGraw-Hill, 1967.

46. Vlasov, V. Z., "Thin Walled Elastic Beams," translated from Russian, NTIS TT-61-11400, 1961.

47. Meck, H. R., "Three-Dimensional Deformation and Buckling of a Circular Ring of Arbitrary Section," Transactions of the ASME Journal of Engineering for Industry, February 1969, pp. 266-272.

48. Williams, H. E., "The Stability of Circular Rings Under a Uniformly Distributed Radial Load," California Institute of Technology, Pasadena, California, January 1970, NTIS N70-17318.

49. Morris, Dale L., "Curved Beam Stiffness Coefficients," Journal of the Proceedings of the American Society of Civil Engineers, Structural Division, May 1968, pp. 1165-1174.

50. Irons, B. and Sohrab, A., Techniques of Finite Elements, Ellis Horwood, Ltd., Chichester, 1980.

APPENDIX A

TEST RESULTS

APPENDIX A

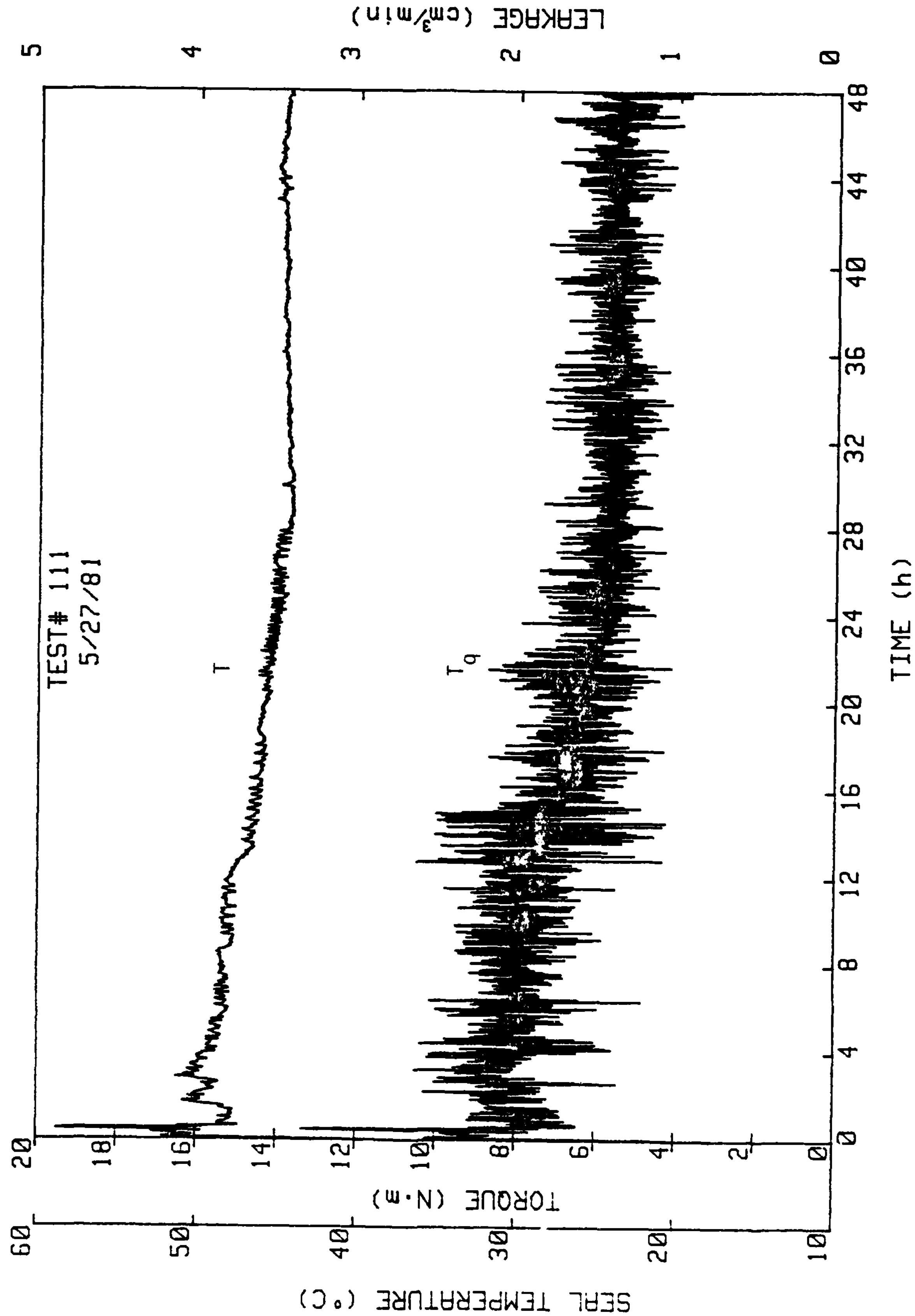

Figure A-1. Test #111, 75% Balance, Parallel Faces, 500 psi, 1800 rpm.

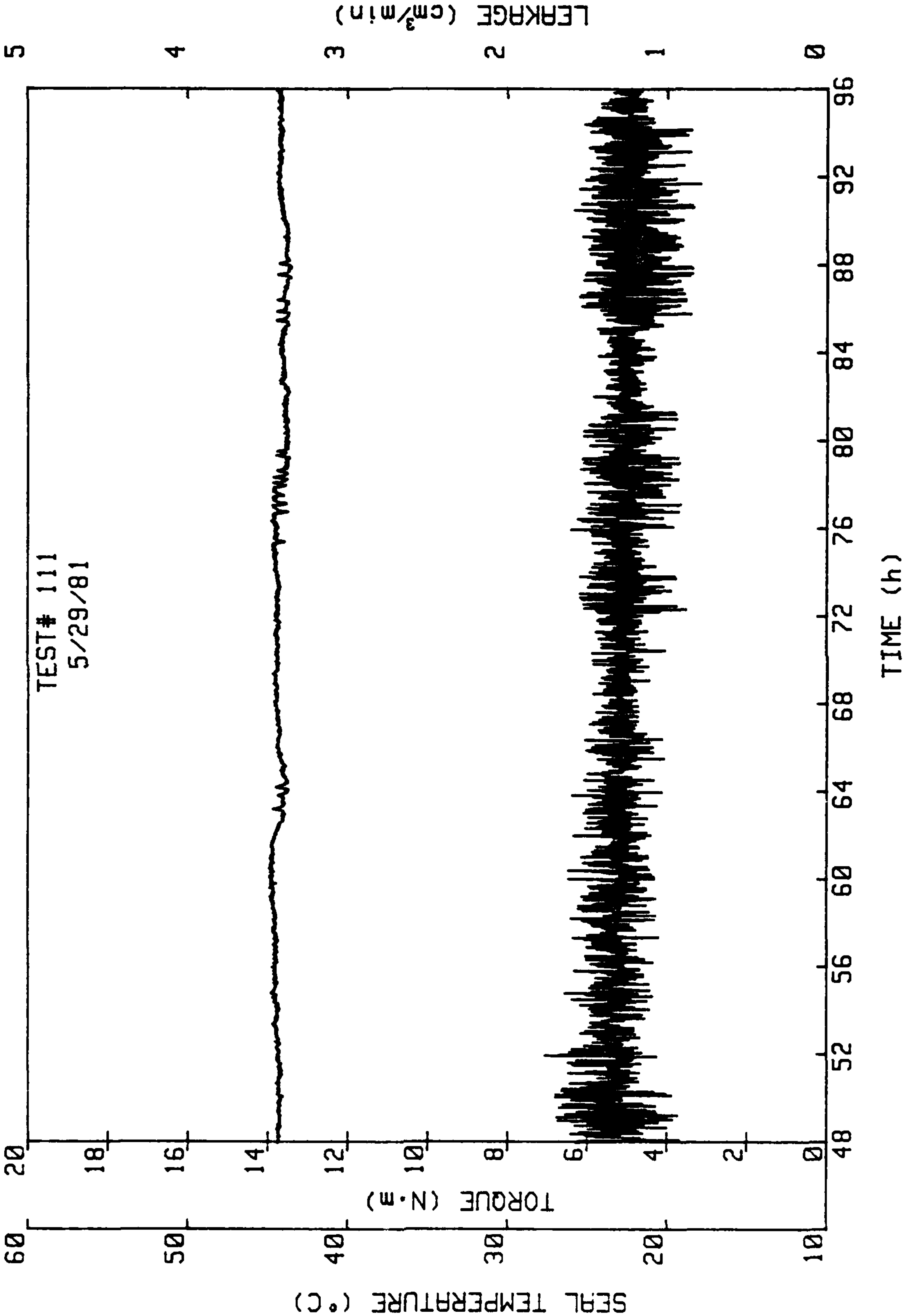

TEST# 111
5/29/81
TIME (h)
48 52 56 60 64 68 72 76 80 84 88 92 96
TORQUE (N·m)
0 2 4 6 8 10 12 14 16 18 20
SEAL TEMPERATURE (°C)
10 20 30 40 50 60
LEAKAGE (cm³/min)
0 1 2 3 4 5

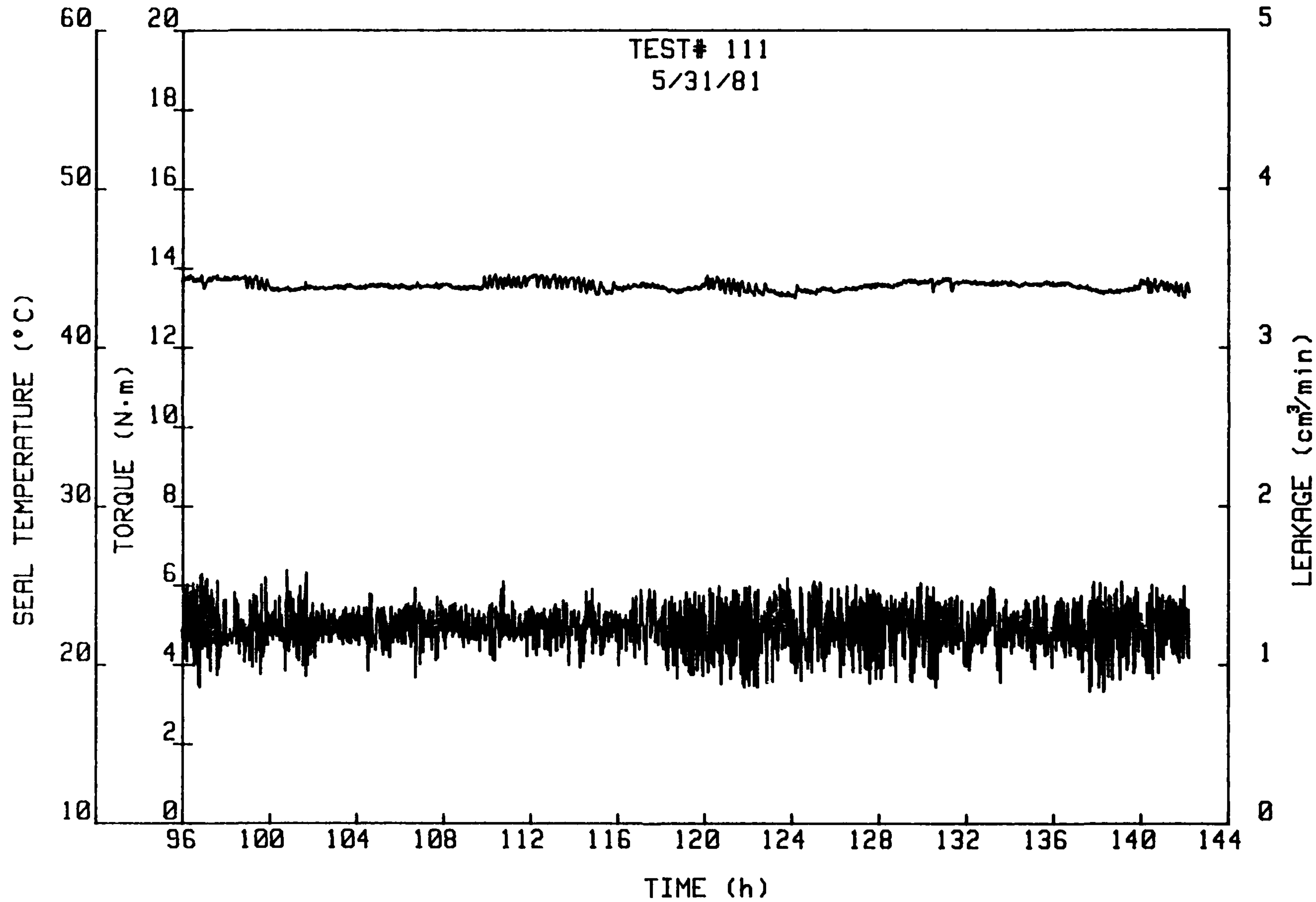

TEST# 111
5/31/81
SEAL TEMPERATURE (°C)
TORQUE (N·m)
LEAKAGE (cm³/min)
TIME (h)
60
50
40
30
20
10
20
18
16
14
12
10
8
6
4
2
0
5
4
3
2
1
0
96
100
104
108
112
116
120
124
128
132
136
140
144

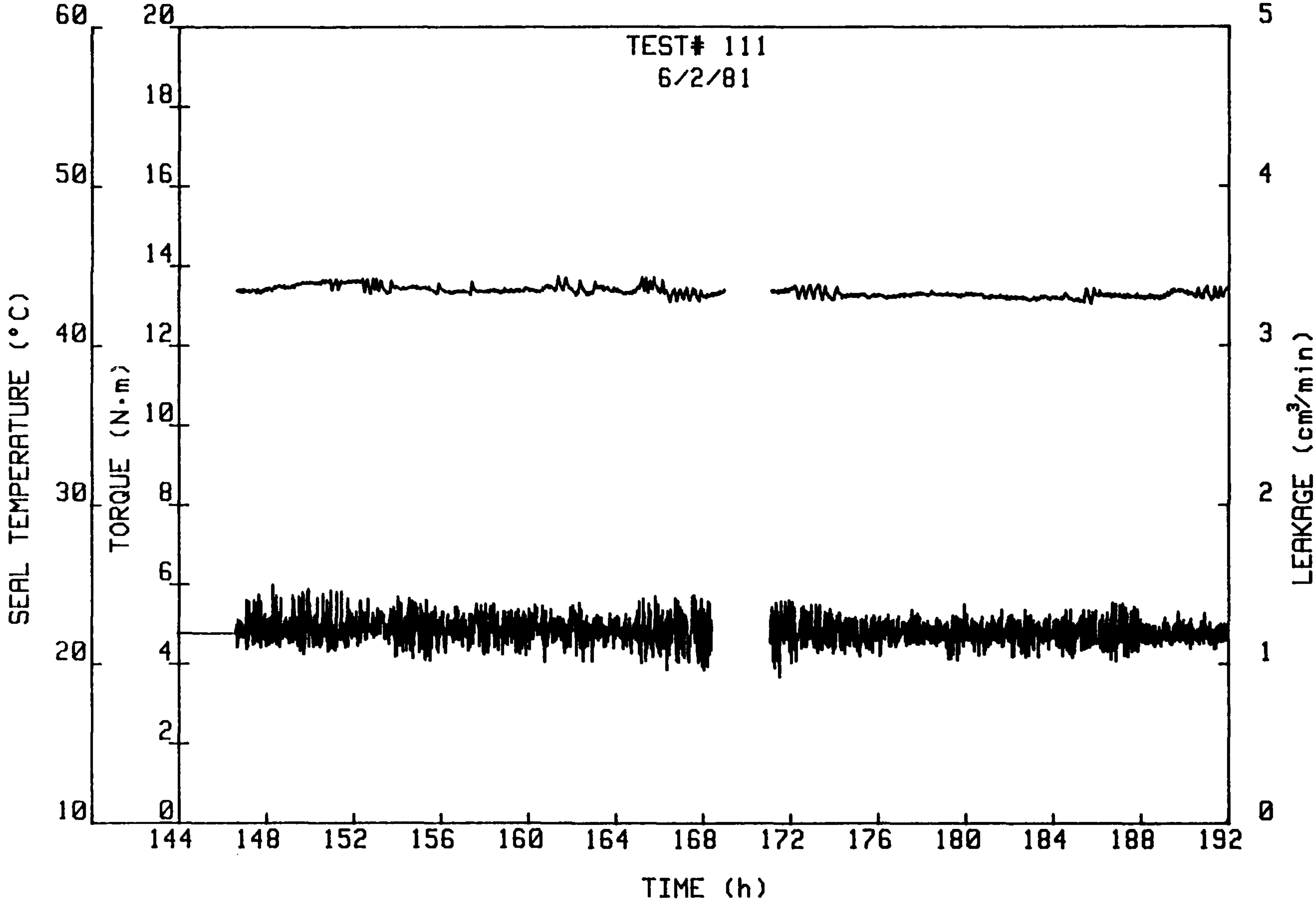
TEST# 111
6/2/81
SEAL TEMPERATURE (°C)
60
50
40
30
20
10
TORQUE (N·m)
20
18
16
14
12
10
8
6
4
2
0
LEAKAGE (cm³/min)
5
4
3
2
1
0
144
148
152
156
160
164
168
172
176
180
184
188
192
TIME (h)

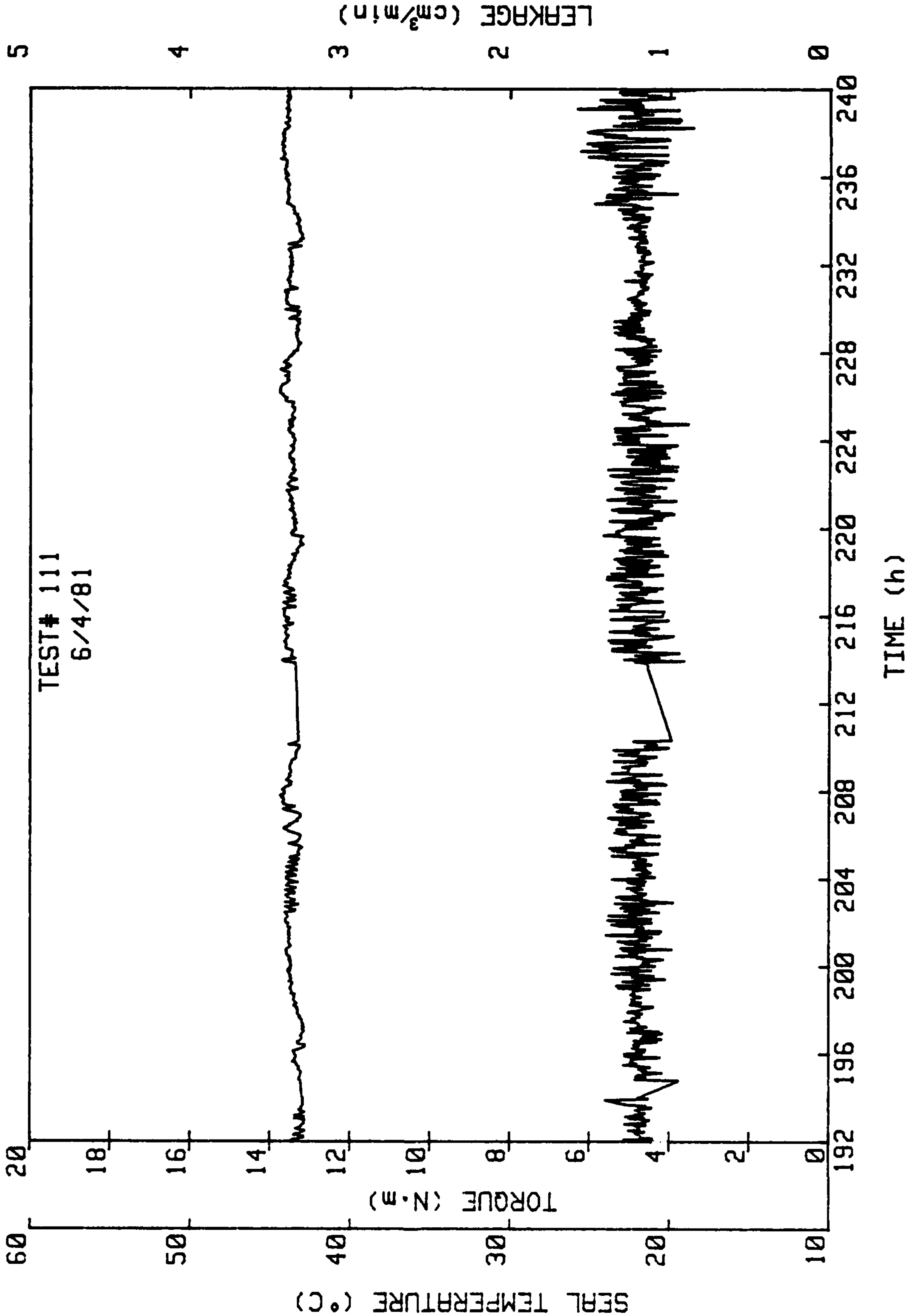
TEST# 111
6/4/81
TIME (h)
TORQUE (N·m)
LEAKAGE (cm³/min)
SEAL TEMPERATURE (°C)

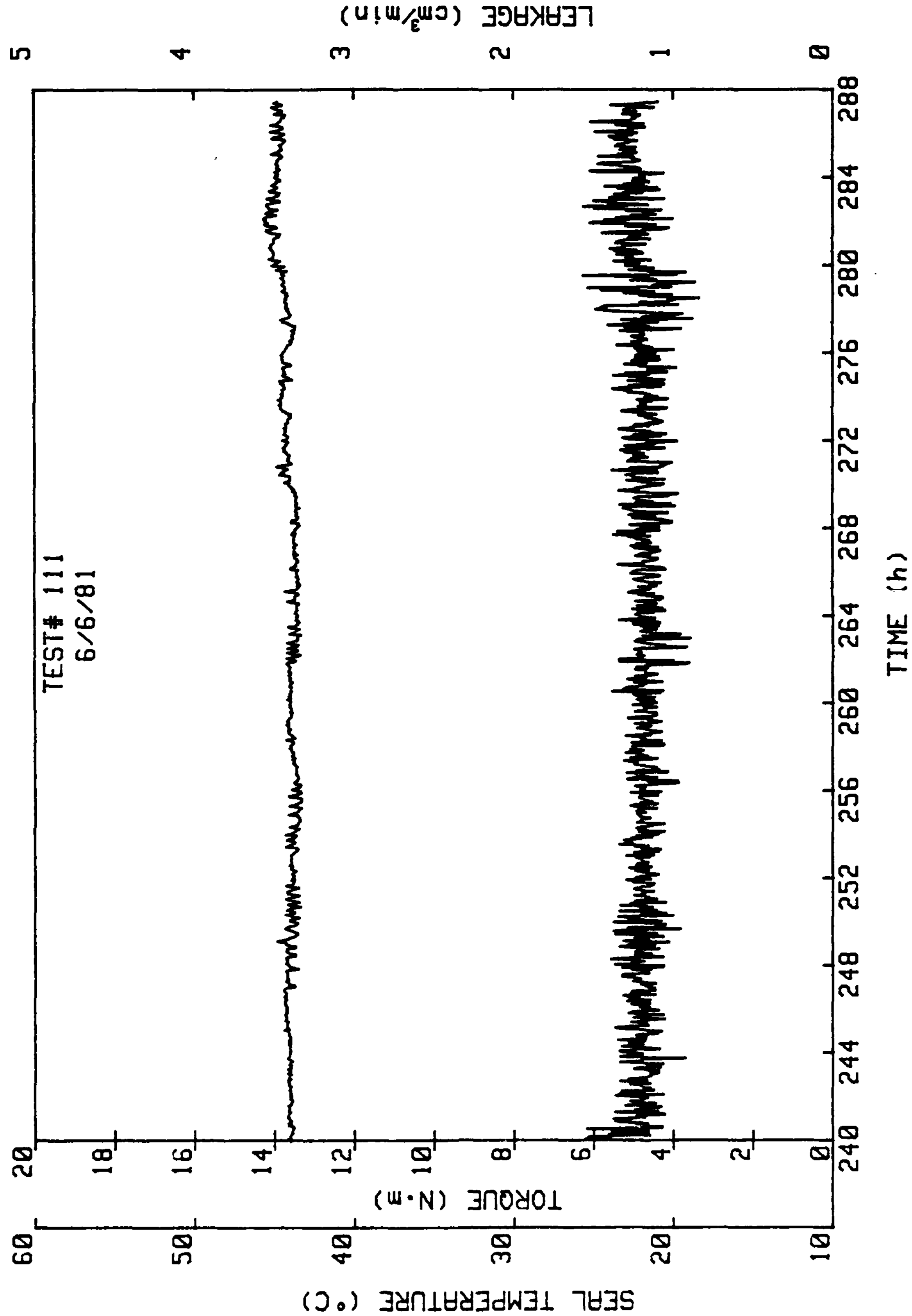
TEST# 111
6/6/81
TIME (h)
TORQUE (N·m)
SEAL TEMPERATURE (°C)
LEAKAGE (cm³/min)

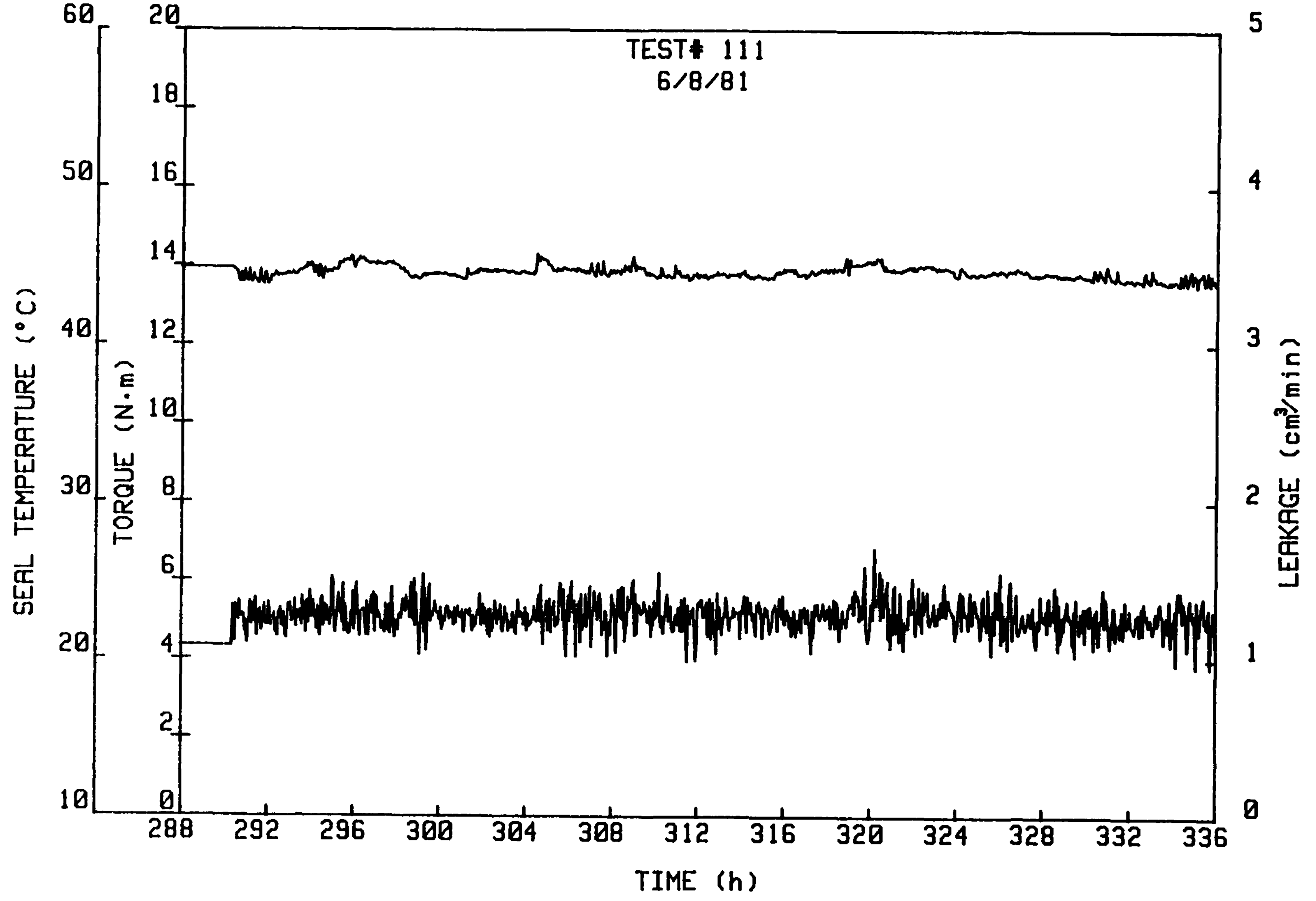
TEST# 111
6/8/81
SEAL TEMPERATURE (°C)
TORQUE (N·m)
LEAKAGE (cm³/min)
TIME (h)
60
50
40
30
20
10
20
18
16
14
12
10
8
6
4
2
0
5
4
3
2
1
0
288
292
296
300
304
308
312
316
320
324
328
332
336

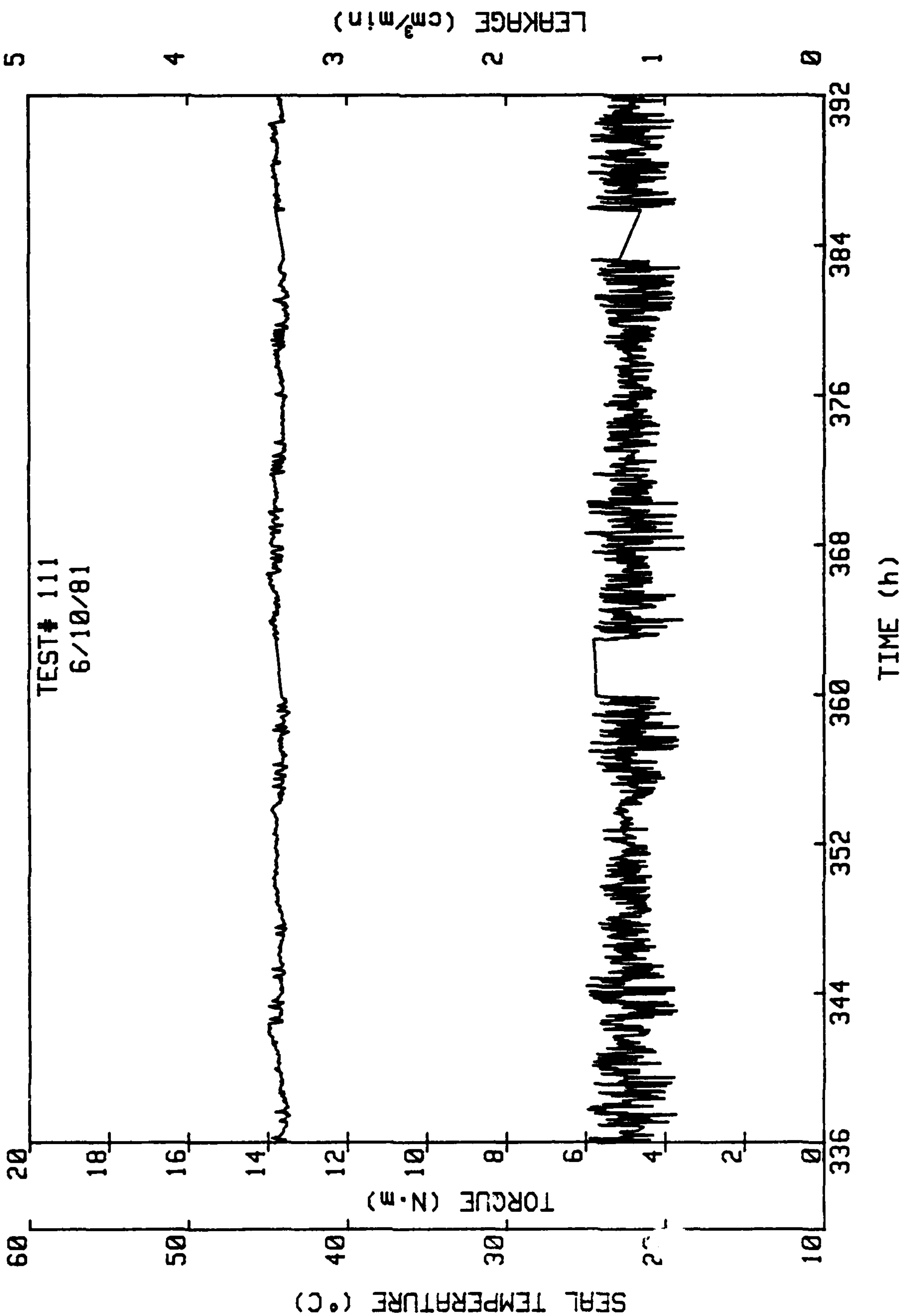
TEST# 111
6/10/81
TIME (h)
336
344
352
360
368
376
384
392
TORQUE (N·m)
0
2
4
6
8
10
12
14
16
18
20
SEAL TEMPERATURE (°C)
10
30
40
50
60
LEAKAGE (cm³/min)
0
1
2
3
4
5

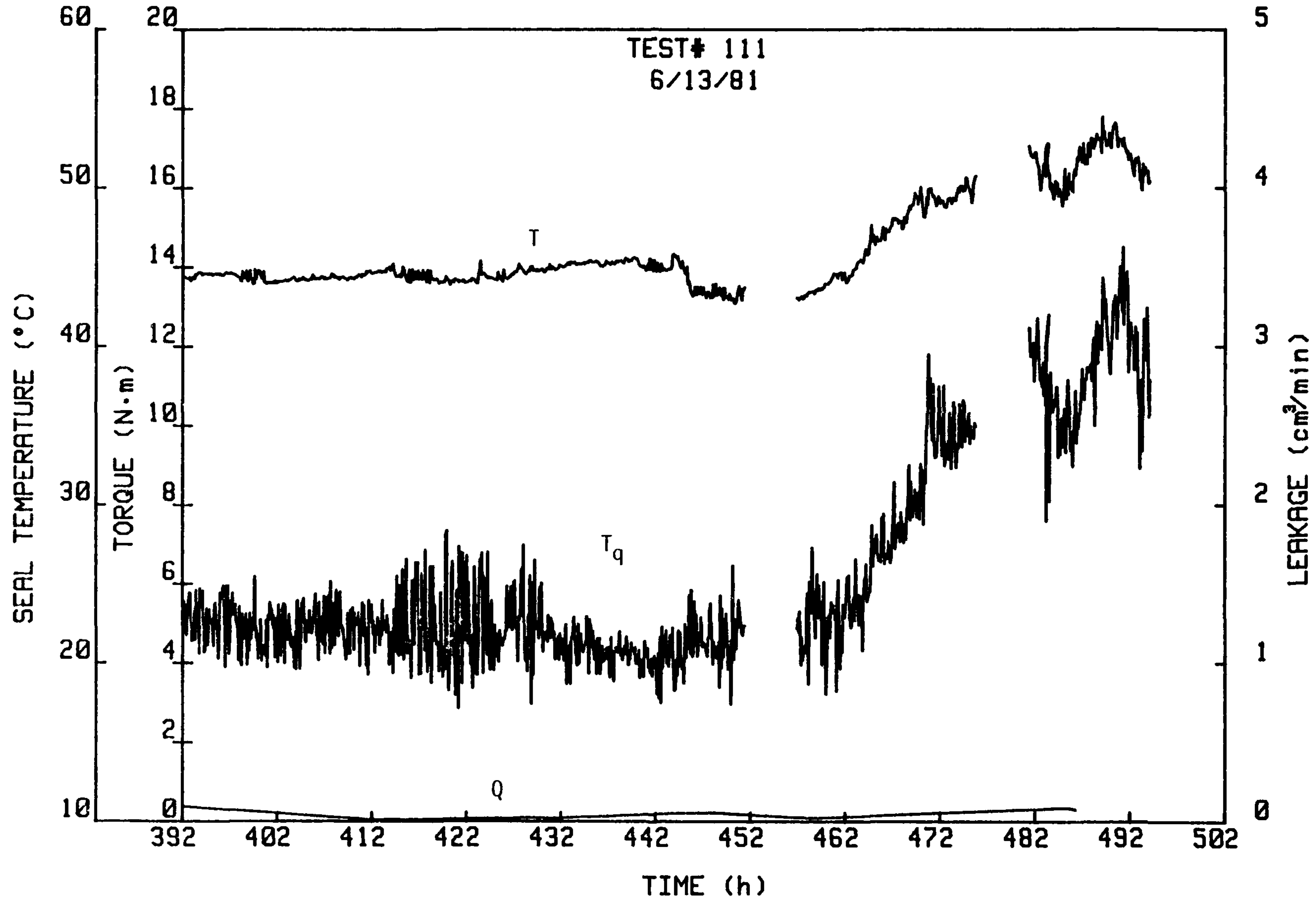
TEST# 111
6/13/81
T
Tq
Q
SEAL TEMPERATURE (°C)
60
50
40
30
20
10
TORQUE (N·m)
20
18
16
14
12
10
8
6
4
2
0
LEAKAGE (cm³/min)
5
4
3
2
1
0
392
402
412
422
432
442
452
462
472
482
492
502
TIME (h)

APPENDIX B

DESIGN PROGRAM

```
C       THIS PROGRAM SOLVES FOR ALL DIMENSIONAL PARAMETERS FOR THE
C       NEW SEAL DESIGN. IT INCORPORATES THE USE OF A FINITE
C       DIFFERENCE METHOD TO SOLVE FOR THE TORSIONAL CONSTANT
C       (JTHETA) AND ALSO UTILLIZES A ROOT FINDING TECHNIQUE TO
C       FIND THE ZERO OF (V/PHI)INITIAL AND (V/PHI)DESIRED.
C       IT WAS FINISHED 12/10/80, A CHECK IS STILL NEEDED.
C       THE PROGRAM WAS WRITTEN BY L.A. YOUNG.
C
C
        EXTERNAL F11
        COMMON RC,X4,X5,X7,Y5,X1,X2,X3,X6,X66,Y1,Y2,Y3,Y4,Y55
        COMMON Y6,Y7,D,PHI,AK,RI,RB,XX3,YY3,T1,T2,AJR
        COMMON A1,A2,A3,A4,A5,A6,A7,XBAR,YBAR,ROO,RPI,PG
        COMMON PI,AMU,PW,E,G,VOPHIG,VOPHI,ECC,A,AMO,AJO,V,EIX,AIX,N
        DOUBLE PRECISION X4,X5,X7,Y5,RL,RC,A11,B11,TOL1
 1000   WRITE(6,1)
    1   FORMAT(/,5X,'INPUT X1,X2,X66')
        READ(5,*) X1,X2,X66
        WRITE(6,2)
    2   FORMAT(/,5X,'INPUT Y1,Y2,Y3,Y55,Y6')
        READ(5,*)Y1,Y2,Y3,Y55,Y6
        WRITE(6,3)
    3   FORMAT(/,5X,'INPUT D,PHI')
        READ(5,*)D,PHI
        Y4=Y3
        AK=1.005
        RI=1.9
        RB=1.9
        XX3=.1875
        YY3=.125
        T1=.010
        T2=.003
        X3=XX3+2.*T1
        X6=.051
        Y7=.08
        PI=3.141592654
        AMU=.3
        PW=500.
        N=9
        E=31.E+06
        G=E/2./(1.+AMU)
        PG=1000.0
        A11=1.200
        B11=1.500
        TOL1=1.0D-6
        RL=ZEROIN(A11,B11,F11,TOL1)
        IF(A1.LT.0.0) GO TO 120
        IF(A2.LT.0.0) GO TO 120
        IF(A3.LT.0.0) GO TO 120
        IF(A4.LT.0.0) GO TO 120
        IF(A5.LT.0.0) GO TO 120
        IF(A6.LT.0.0) GO TO 120
        IF(A7.LT.0.0) GO TO 120
        GO TO 135
  120   WRITE(6,130)A1,A2,A3,A4,A5,A6,A7
  130   FORMAT(5X,'NEGATIVE AREAS ARE PRODUCED BY THOSE DIMENSIONS',/,5X
     * ,'A1=',F8.6,2X,'A2=',F8.6,2X,'A3=',F8.6,2X,'A4=',F8.6,/,5X,'A5=',
     * F8.6,2X,'A6=',F8.6,2X,'A7=',F8.6,///)
        GO TO 1000
  135   AIY=1./12.*X1**3*Y2+A1*(X1/2.-XBAR)**2
        AIY=AIY+1./12.*(X2-X1)**3*(Y1+Y2)+A2*(X1+(X2-X1)/2.-XBAR)**2
        AIY=AIY+1./12.*(X7+X1-X2)**3*(Y1+Y2-Y3)
        AIY=AIY+A3*(X2+(X7+X1-X2)/2.-XBAR)**2
        AIY=AIY+1./12.*X6**3*(Y5+Y5-Y4)+A4*(X1+X7+X5/2.-XBAR)**2
        AIY=AIY+1./12.*(X5-X4)**3*(Y5-Y4)
```


PREVIOUS PAGE IS BLANK

```
      AIY=AIY+A5*(X1+X6+X7+(X5-X4)/2.-XBAR)**2
      AIY=AIY+1./12.*(X4-X66)**3*Y5+A6*(X2+X3+(X4-X66)/2.-XBAR)**2
      AIY=AIY+1./12.*X66**3*(Y5-Y55)+A7*(X2+X3+X4-X66/2.-XBAR)**2
  110 PL=ECC-YBAR
      AJR=AIX+AIY
      F1=2.*PI*(RL+X5+X6)*Y7
      F2=PI*(R00**2-R3**2)
      F3=2.*PI*(R00-X1)*Y1
      F5=2.*PI*(R00)*Y2
      F6=PI*((R00)**2-(RI+XX3)**2)
      F7=2.*PI*(RI+XX3)*YY3
      F8=F2-F4-F6
      AM1=-F1*(YBAR-Y7/2.)
      R2=2./3.*(R00**3-R8**3)/(R00**2-R8**2)
      AM2=-F2*(R2-RC)
      AM3=F3*(YBAR-Y1/2.)
      AM5=-F5*(Y1+Y2/2.-YBAR)
      R6=2./3.*((R00)**3-(RI+XX3)**3)/((R00)**2-(RI+XX3)**2)
      AM6=F6*(R6-RC)
      AM7=-F7*(Y1+Y2+YY3/2.-YBAR)
      R8=2./3.*XX3+RI
      AM8=F8*(R8-RC)
      TM=(AM1+AM2+AM3+AM4+AM5+AM6+AM7+AM8)/(2.*PI*RC)
      ROTATE=TM*RC**2/E/AIX*PW
  140 WRITE(6,150) XBAR,YBAR,AIX,AIY,AJR,AJ0,A,AM0,V,ECC,RC,EIX,ROTATE
  150 FORMAT(/,5X,'XBAR=',F7.4,/,5X,'YBAR=',F7.4,/,5X,'IX=',E12.5,/,5X,
     * 'IY=',E12.5,/,5X,'JR=',E12.5,/,5X,'JTHETA=',E12.5,/,5X,'A=',E12.5
     * ,/,5X,'MTHETA=',E12.5,/,5X,'V=',E12.5,/,5X,'ECC=',E12.5,/,5X,
     * 'RC=',F7.4,/,5X,'EIX=',E12.5,/,5X,'ROTATION=',E12.5)
      WRITE(6,160) VOPHIG,VOPHI,AIXY,X1,X2,X3,X4,X5,X6,X7
      WRITE(6,170) Y1,Y2,Y3,Y4,Y5,Y6,Y7,R00,RPI,PL,RI,RL
  160  FORMAT(5X,'V/PHIG=',E12.5,5X,'V/PHI=',E12.5,/,5X,'IXY=',E12.5,
     * /,5X,'X1=',F6.4,2X,'X2=',F6.4,2X,'X3=',F6.4,2X,'X4=',F6.4,2X,
     * 'X5=',F6.4,2X,'X6=',F5.4,2X,'X7=',F5.4)
  170  FORMAT(5X,'Y1=',F6.4,2X,'Y2=',F6.4,2X,'Y3=',F6.4,2X,'Y4=',F6.4
     * ,2X,'Y5=',F6.4,2X,'Y6=',F5.4,2X,'Y7=',F6.4,/,5X,'R00=',F6.4,2X,
     * 'RPI=',F6.4,2X,'PL=',F5.4,2X,'RI=',F5.4,2X,'RL=',F6.4,///)
      GO TO 1000
      END
      DOUBLE PRECISION FUNCTION F11(RL)
C
      COMMON RC,X4,X5,X7,Y5,X1,X2,X3,X6,X66,Y1,Y2,Y3,Y4,Y55
      COMMON Y6,Y7,D,PHI,AK,RI,R8,XX3,YY3,T1,T2,AJR
      COMMON A1,A2,A3,A4,A5,A6,A7,XBAR,YBAR,R00,RPI,PS
      COMMON PI,AMU,PW,E,G,VOPHIG,VOPHI,ECC,A,AM0,AJ0,V,EIX,AIX,N
      DOUBLE PRECISION X4,X5,X7,Y5,RC
      DIMENSION X(50),Y(50),P(50,50),AIM1(50,50),AIP1(50,50)
      DIMENSION AJP1(50,50),AJM1(50,50),BRHS(50,50)
      X4=RI-T1-RL
      X5=R8+T2-RL
      X7=-X1+X2+X3+X4-X5-X6
      Y5=Y1+Y2-Y3+Y4-Y6-Y7
      A1=X1*Y2
      A2=(X2-X1)*(Y1+Y2)
      A3=(X7+X1-X2)*(Y1+Y2-Y3)
      A4=X6*(Y5+Y6-Y4)
      A5=(X5-X4)*(Y5-Y4)
      A6=(X4-X66)*Y5
      A7=X66*(Y5-Y55)
      XBAR=A1*X1/2.+A2*(X1+(X2-X1)/2.)+A3*(X2+(X7+X1-X2)/2.)
      XBAR=XBAR+A4*(X1+X7+X6/2.)+A5*(X1+X6+X7+(X5-X4)/2.)
      XBAR=XBAR+A6*(X2+X3+(X4-X66)/2.)+A7*(X2+X3+X4-X66/2.)
      XBAR=XBAR/(A1+A2+A3+A4+A5+A6+A7)
C
      YBAR=A1*(Y1+Y2/2.)+A2*(Y1+Y2)/2.+A3*(Y1+Y2-Y3)/2.
      YBAR=YBAR+A4*(Y7+(Y6+Y5-Y4)/2.)+A5*(Y6+Y7+(Y5-Y4)/2.)
```

```
      YBAR=YBAR+A6*(Y6+Y7+Y5/2.)+A7*(Y55+Y6+Y7+(Y5-Y55)/2.)
      YBAR=YBAR/(A1+A2+A3+A4+A5+A6+A7)
C
      AIX=1./12.*X1*Y2**3+A1*(Y1+Y2/2.-YBAR)**2
      AIX=AIX+1./12.*(X2-X1)*(Y1+Y2)**3+A2*((Y1+Y2)/2.-YBAR)**2
      AIX=AIX+1./12.*(X7+X1-X2)*(Y1+Y2-Y3)**3+A3*((Y1+Y2-Y3)/2.-YBAR)**
     *2
      AIX=AIX+1./12.*X6*(Y5+Y6-Y4)**3+A4*(Y7+(Y5+Y5-Y4)/2.-YBAR)**2
      AIX=AIX+1./12.*(X5-X4)*(Y5-Y4)**3+A5*(Y6+Y7+(Y5-Y4)/2.-YBAR)**2
      AIX=AIX+1./12.*(X4-X66)*Y5**3+A6*(Y6+Y7+Y5/2.-YBAR)**2
      AIX=AIX+1./12.*X65*(Y5-Y55)**3+A7*(Y55+Y6+Y7+(Y5-Y55)/2.-YBAR)**2
C
      R00=X2+X3+X4+RL
      RPI=RL+X5+X6+X7/2.
      RC=R00-XBAR
C
C
      EIX=E*AIX
      ERR=0.000001
      AA1=X66
      AA2=X4
      AA3=X5
      AA4=X5+X6
      AA5=X5+X6+X7
      AA6=X1+X5+X6+X7
      B1=Y7
      B2=Y1
      B3=Y6+Y7
      B4=Y1+Y2-Y3
      B5=Y55+Y6+Y7
      B6=Y1+Y2
      I1=4
      I2=13
      I3=17
      I4=19
      I5=20
      I6=22
      J1=17
      J2=23
      J3=24
      J4=26
      J5=30
      J6=37
      XX=0.0
      X(1)=0.0
      DX=B1/(I1-1)
      DO 10 I=2,I6
      IF(I.GT.I1) DX=(B2-B1)/(I2-I1)
      IF(I.GT.I2) DX=(B3-B2)/(I3-I2)
      IF(I.GT.I3) DX=(B4-B3)/(I4-I3)
      IF(I.GT.I4) DX=(B5-B4)/(I5-I4)
      IF(I.GT.I5) DX=(B6-B5)/(I6-I5)
      XX=XX+DX
      X(I)=XX
   10 CONTINUE
      YY=0.0
      Y(1)=0.0
      DY=AA1/(J1-1)
      DO 20 J=2,J6
      IF(J.GT.J1) DY=(AA2-AA1)/(J2-J1)
      IF(J.GT.J2) DY=(AA3-AA2)/(J3-J2)
      IF(J.GT.J3) DY=(AA4-AA3)/(J4-J3)
      IF(J.GT.J4) DY=(AA5-AA4)/(J5-J4)
      IF(J.GT.J5) DY=(AA6-AA5)/(J6-J5)
      YY=YY+DY
      Y(J)=YY
```

```
   20 CØNTINUE
      IMAX=I6-1
      JMAX=J6-1
      DØ 30 I=2,IMAX
      DØ 30 J=2,JMAX
      AIJ=-2./(X(I-1)-X(I))/(X(I+1)-X(I))-2./(Y(J-1)-Y(J))/(Y(J+1)-Y(J)
     *)
      AIM1(I,J)=2./(X(I-1)-X(I))/(X(I-1)-X(I+1))/AIJ
      AIP1(I,J)=-2./(X(I+1)-X(I))/(X(I-1)-X(I+1))/AIJ
      AJM1(I,J)=2./(Y(J-1)-Y(J))/(Y(J-1)-Y(J+1))/AIJ
      AJP1(I,J)=-2./(Y(J+1)-Y(J))/(Y(J-1)-Y(J+1))/AIJ
      BRHS(I,J)=2./AIJ
   30 CØNTINUE
      DØ 40 I=1,I6
      DØ 40 J=1,J6
   40 P(I,J)=0.000000000001
      ØMEG=1.5
      ØMØ=1.-ØMEG
      DØ 60 IT=1,200
      AMAX=0.0
      DØ 50 J=2,JMAX
      IMAX=I6-1
      IMIN=I5+1
      IF(J.GT.J1) IMIN=I3+1
      IF(J.GT.J2) IMAX=I4-1
      IF(J.GT.J3) IMIN=I1+1
      IF(J.GT.J4) IMIN=2
      IF(J.GT.J5) IMIN=I2+1
      IF(J.GT.J5) IMAX=I6-1
      DØ 50 I=IMIN,IMAX
      PØLD=P(I,J)
      PNEW=AIM1(I,J)*P(I-1,J)+AIP1(I,J)*P(I+1,J)+AJM1(I,J)*P(I,J-1)
      PNEW=PNEW+AJP1(I,J)*P(I,J+1)+BRHS(I,J)
      P(I,J)=PNEW*ØMEG+ØMØ*PØLD
      VAL=ABS((P(I,J)-PØLD)/PØLD)
      IF(VAL.GT.AMAX) AMAX=VAL
   50 CØNTINUE
      IF(VAL.LT.ERR) GØ TØ 70
   60 CØNTINUE
      WRITE(6,65)
   65 FØRMAT(2X,'EXCEEDS ITERATIØNS')
   70 JMAX=J6-1
      IMAX=I6-1
      AJ=0.0
      DØ 80 I=1,IMAX
      DØ 80 J=1,JMAX
      Z=P(I,J)+P(I+1,J)+P(I+1,J+1)+P(I,J+1)
   80 AJ=AJ+.25*Z*(X(I+1)-X(I))*(Y(J+1)-Y(J))
      J=J6+1
      AJ=2.*AJ
      AJØ=AJ
      A=E*AIX/G/AJØ
C
      AMØ=(PHI*E*AIX)/RC**2*(N**2-1.)**2/(A*N**2+1.)
      ECC=AMØ/D*RC/RPI/PG/SIN(N*D/2./RPI)
      V=RC**3*AMØ/E/AIX*(1.+A)/(N**2-1.)**2
      VØPHIG=V/PHI
      VØPHI=RC-AK*RI
      F11=VØPHIG-VØPHI
      RETURN
      END
      DØUBLE PRECISIØN FUNCTIØN ZERØIN(AX,BX,F,TØL)
      DØUBLE PRECISIØN AX,BX,F,TØL
      DØUBLE PRECISIØN  A,B,C,D,E,EPS,FA,FB,FC,TØL1,XM,P,Q,R,S
      DØUBLE PRECISIØN  DABS
C
```

```
C  COMPUTE EPS, THE RELATIVE MACHINE PRECISION
C
      EPS = 1.0D0
   10 EPS = EPS/2.0D0
      TOL1 = 1.0D0 + EPS
      IF (TOL1 .GT. 1.0D0) GO TO 10
C
C INITIALIZATION
C
      A = AX
      B = BX
      FA = F(A)
      FB = F(B)
C
C BEGIN STEP
C
   20 C = A
      FC = FA
      D = B - A
      E = D
   30 IF (DABS(FC) .GE. DABS(FB)) GO TO 40
      A = B
      B = C
      C = A
      FA = FB
      FB = FC
      FC = FA
C
C CONVERGENCE TEST
C
   40 TOL1 = 2.0D0*EPS*DABS(B) + 0.5D0*TOL
      XM = .5*(C - B)
      IF (DABS(XM) .LE. TOL1) GO TO 90
      IF (FB .EQ. 0.0D0) GO TO 90
C
C IS BISECTION NECESSARY
C
      IF (DABS(E) .LT. TOL1) GO TO 70
      IF (DABS(FA) .LE. DABS(FB)) GO TO 70
C
C IS QUADRATIC INTERPOLATION POSSIBLE
C
      IF (A .NE. C) GO TO 50
C
C LINEAR INTERPOLATION
C
      S = FB/FA
      P = 2.0D0*XM*S
      Q = 1.0D0 - S
      GO TO 60
C
C INVERSE QUADRATIC INTERPOLATION
C
   50 Q = FA/FC
      R = FB/FC
      S = FB/FA
      P = S*(2.0D0*XM*Q*(Q - R) - (B - A)*(R - 1.0D0))
      Q = (Q - 1.0D0)*(R - 1.0D0)*(S - 1.0D0)
C
C ADJUST SIGNS
C
   60 IF (P .GT. 0.0D0) Q = -Q
      P = DABS(P)
C
C IS INTERPOLATION ACCEPTABLE
C
```

```
      IF ((2.0D0*P) .GE. (3.0D0*XM*Q - DABS(TØL1*Q))) GØ TØ 70
      IF (P .GE. DABS(0.5D0*E*Q)) GØ TØ 70
      E = D
      D = P/Q
      GØ TØ 80
C
C BISECTIØN
C
   70 D = XM
      E = D
C
C CØMPLETE STEP
C
   80 A = B
      FA = FB
      IF (DABS(D) .GT. TØL1) B = B + D
      IF (DABS(D) .LE. TØL1) B = B + DSIGN(TØL1, XM)
      FB = F(B)
      IF ((FB*(FC/DABS(FC))) .GT. 0.0D0) GØ TØ 20
      GØ TØ 30
C
C DØNE
C
   90 ZERØIN = B
      RETURN
      END
```

```
C PROGRAM NAVSEAL1
C DESIGN MODIFICATION PROGRAM TO LOWER THE TORSIONAL STIFFNESS OF
C THE EXISTING SEAL RING.
C
      DIMENSION X(50),Y(50),P(50,50),AIM1(50,50),AIP1(50,50)
      DIMENSION AJP1(50,50),AJM1(50,50),BRHS(50,50)
      REAL K
    5 WRITE(6,10)
   10 FORMAT(/,5X,'INPUT X1,Y1')
      READ(5,*) X1,Y1
      WRITE(6,20)
   20 FORMAT(/,5X,'INPUT X2,X3,Y4')
      READ(5,*)X2,X3,Y4
      WRITE(6,30)
   30 FORMAT(/,5X,'INPUT D,Y6')
      READ(5,*)D,Y6
      K=1.015
      RI=1.9
      RO=1.9
      RL=1.389
      XX3=.1875
      YY3=.125
      T1=.010
      T2=.003
      X7=.36
      X8=.154
      X9=.051
      X10=.1435-X1
      X4=X2-X3
      X5=XX3+2.*T1
   31 X6=RI-T1-RL
      Y2=.38-Y1
      Y3=.22-Y4
      Y5=.1
      Y7=.09-(.1-Y6)
      Y8=.08
      Y9=.35
      Y10=.08
      PI=3.141592654
      AMU=.278
      PW=500.
      PL=.5602
      N=9
      E=31.E+06
      G=E/2./(1.+AMU)
      PG=750.0
  100 A1=X3*Y3
      A2=(Y3+Y4)*X4
      A3=X1*(Y2+Y3+Y4-Y5)
      A4=X10*(Y1+Y2+Y3+Y4-Y5)
      A5=X9*(Y1+Y2+Y3+Y4-Y5-Y10)
      A6=(X7+X8-X6)*(Y7+Y8-Y6)
      A7=(X6-X7)*(Y7+Y8)
      A8=X7*Y7
      IF(A1.LT.0.0) GO TO 36
      IF(A2.LT.0.0) GO TO 36
```

```
      IF(A3.LT.0.0) GO TO 36
      IF(A4.LT.0.0) GO TO 36
      IF(A5.LT.0.0) GO TO 36
      IF(A6.LT.0.0) GO TO 36
      IF(A7.LT.0.0) GO TO 36
      IF(A8.LT.0.0) GO TO 36
      FXA1=X3/2.
      FXA2=X3+X4/2.
      FXA3=X2+X1/2.
      FXA4=X1+X2+X10/2.
      FXA5=X1+X2+X10+X9/2.
      FXA6=X1+X2+X10+X9+(X3+X4+X5-X2-X1-X10-X9)/2.
      FXA7=X3+X4+X5+(X6-X7)/2.
      FXA8=X3+X4+X5+X6-X7/2.
C
      FYA1=Y1+Y2+Y3/2.
      FYA2=Y1+Y2+(Y3+Y4)/2.
      FYA3=Y1+(Y2+Y3+Y4-Y5)/2.
      FYA4=(Y1+Y2+Y3+Y4-Y5)/2.
      FYA5=Y10+(Y1+Y2+Y3+Y4-Y5-Y10)/2.
      FYA6=Y10+Y9+(Y8+Y7-Y6)/2.
      FYA7=Y10+Y9+(Y8+Y7)/2.
      FYA8=Y10+Y9+Y8+Y7/2.
C
      XBAR=A1*FXA1+A2*FXA2+A3*FXA3+A4*FXA4
      XBAR=XBAR+A5*FXA5+A6*FXA6+A7*FXA7+A8*FXA8
      XBAR=XBAR/(A1+A2+A3+A4+A5+A6+A7+A8)
C
      YBAR=A1*FYA1+A2*FYA2+A3*FYA3+A4*FYA4
      YBAR=YBAR+A5*FYA5+A6*FYA6+A7*FYA7+A8*FYA8
      YBAR=YBAR/(A1+A2+A3+A4+A5+A6+A7+A8)
C
      AIX=1./12.*X3*Y3**3+A1*(FYA1-YBAR)**2
      AIX=AIX+1./12.*X4*(Y3+Y4)**3+A2*(FYA2-YBAR)**2
      AIX=AIX+1./12.*X1*(Y2+Y3+Y4-Y5)**3+A3*(FYA3-YBAR)**2
      AIX=AIX+1./12.*X10*(Y1+Y2+Y3+Y4-Y5)**3+A4*(FYA4-YBAR)**2
      AIX=AIX+1./12.*X9*(Y1+Y2+Y3+Y4-Y5-Y10)**3+A5*(FYA5-YBAR)**2
      AIX=AIX+1./12.*(X8-(X6-X7))*(Y7+Y8-Y6)**3+A6*(FYA6-YBAR)**2
      AIX=AIX+1./12.*(X8)*(Y7+Y8)**3+A7*(FYA7-YBAR)**2
      AIX=AIX+1./12.*X7*(Y7)**3+A8*(FYA8-YBAR)**2
C
      AIY=1./12.*X3**3*Y3+A1*(FXA1-XBAR)**2
      AIY=AIY+1./12.*X4**3*(Y3+Y4)+A2*(FXA2-XBAR)**2
      AIY=AIY+1./12.*X1**3*(Y2+Y3+Y4-Y5)+A3*(FXA3-XBAR)**2
      AIY=AIY+1./12.*X10**3*(Y1+Y2+Y3+Y4-Y5)+A4*(FXA4-XBAR)**2
      AIY=AIY+1./12.*X9**3*(Y1+Y2+Y3+Y4-Y5-Y10)+A5*(FXA5-XBAR)**2
      AIY=AIY+1./12.*(X8-(X6-X7))**3*(Y7+Y8-Y6)+A6*(FXA6-XBAR)**2
      AIY=AIY+1./12.*X8**3*(Y7+Y8)+A7*(FXA7-XBAR)**2
      AIY=AIY+1./12.*X7**3*Y7+A8*(FXA8-XBAR)**2
C
      ROO=RL+X6+X5+X4+X3
      RC=ROO-XBAR
      RPI=2.484
C
C
      AJR=AIX+AIY
      EIX=E*AIX
      AJO=(.025*(A1+A2+A3+A4+A5+A6+A7+A8)**4)/AJR
C TORSIONAL CONSTANT CALCULATION USING FINITE DIFFERENCE
      ERR=0.0000001
      AA1=X7
      AA2=X6
      AA3=X7+X8
      AA4=X7+X8+X9
      AA5=X7+X8+X9+X10
      AA6=X5+X6
```

```
      AA7=X4+X5+X6
      AA8=X3+X4+X5+X6
      BB1=Y10
      BB2=Y1
      BB3=Y1+Y2
      BB4=Y9+Y10
      BB5=Y1+Y2+Y3+Y4-Y5
      BB6=Y8+Y9+Y10
      BB7=Y1+Y2+Y3
      BB8=Y7+Y8+Y9+Y10
      BB9=Y1+Y2+Y3+Y4
      I1=4
      I2=5
      I3=13
      I4=17
      I5=19
      I6=20
      I7=21
      I8=22
      I9=23
      J1=17
      J2=23
      J3=24
      J4=26
      J5=29
      J6=30
      J7=36
      J8=37
C MESH GENERATION ROUTINE
      XX=0.0
      X(1)=0.0
      DX=BB1/(I1-1)
      DO 60 I=2,I9
         IF(I.GT.I1) DX=(BB2-BB1)/(I2-I1)
         IF(I.GT.I2) DX=(BB3-BB2)/(I3-I2)
         IF(I.GT.I3) DX=(BB4-BB3)/(I4-I3)
         IF(I GT I4) DX=(BB5-BB4)/(I5-I4)
         IF(I.GT.I5) DX=(BB6-BB5)/(I6-I5)
         IF(I.GT.I6) DX=(BB7-BB6)/(I7-I6)
         IF(I.GT.I7) DX=(BB8-BB7)/(I8-I7)
         IF(I.GT.I8) DX=(BB9-BB8)/(I9-I8)
         XX=XX+DX
         X(I)=XX
   60 CONTINUE
      YY=0.0
      Y(1)=0.0
      DY=AA1/(J1-1)
      DO 70 J=2,J8
         IF(J.GT.J1) DY=(AA2-AA1)/(J2-J1)
         IF(J.GT.J2) DY=(AA3-AA2)/(J3-J2)
         IF(J.GT.J3) DY=(AA4-AA3)/(J4-J3)
         IF(J GT.J4) DY=(AA5-AA4)/(J5-J4)
         IF(J GT.J5) DY=(AA6-AA5)/(J6-J5)
         IF(J.GT.J6) DY=(AA7-AA6)/(J7-J6)
         IF(J.GT.J7) DY=(AA8-AA7)/(J8-J7)
         YY=YY+DY
         Y(J)=YY
   70 CONTINUE
      IMAX=I9-1
      JMAX=J8-1
      DO 80 I=2,IMAX
      DO 80 J=2,JMAX
         AIJ=-2./(X(I-1)-X(I))/(X(I+1)-X(I))-2./(Y(J-1)-Y(J))/
     *   (Y(J+1)-Y(J))
         AIM1(I,J)=2./(X(I-1)-X(I))/(X(I-1)-X(I+1))/AIJ
         AIP1(I,J)=-2./(X(I+1)-X(I))/(X(I-1)-X(I+1))/AIJ
```

```
          AJM1(I,J)=2./(Y(J-1)-Y(J))/(Y(J-1)-Y(J+1))/AIJ
          AJP1(I,J)=-2./(Y(J+1)-Y(J))/(Y(J-1)-Y(J+1))/AIJ
          BRHS(I,J)=2./AIJ
   80  CONTINUE
       DO 90 I=1,I9
       DO 90 J=1,J8
          P(I,J)=0.000000000001
   90  CONTINUE
       OMEG=1.5
       OMO=1.-OMEG
       DO 95 IT=1,800
          AMAX=0.0
       DO 94 J=2,JMAX
          IMAX=I8-1
       IMIN=I6+1
          IF(J.GT.J1) IMIN=I4+1
          IF(J.GT.J2) IMAX=I5-1
          IF(J.GT.J3) IMIN=I1+1
          IF(J.GT.J4) IMIN=2
          IF(J.GT.J5) IMIN=I2+1
          IF(J.GT.J6) IMIN=I3+1
          IF(J.GT.J6) IMAX=I9-1
          IF(J.GT.J7) IMAX=I7-1
       DO 94 I=IMIN,IMAX
          POLD=P(I,J)
          PNEW=AIM1(I,J)*P(I-1,J)+AIP1(I,J)*P(I+1,J)
          PNEW=PNEW+AJM1(I,J)*P(I,J-1)+AJP1(I,J)*P(I,J+1)+BRHS(I,J)
          P(I,J)=PNEW*OMEG+OMO*POLD
          VAL=ABS((P(I,J)-POLD)/POLD)
          IF(VAL.GT.AMAX) AMAX=VAL
   94  CONTINUE
       IF(VAL.LT.ERR) GO TO 110
   95  CONTINUE
       WRITE(6,96)
   96  FORMAT(2X,'EXCEEDS ITERATIONS')
  110  JMAX=J8-1
       IMAX=I8-1
       AJ=0.0
C INTEGRATION ROUTINE
       DO 115 I=1,IMAX
       DO 115 J=1,JMAX
          Z=P(I,J)+P(I+1,J)+P(I+1,J+1)+P(I,J+1)
          AJ=AJ+.25*Z*(X(I+1)-X(I))*(Y(J+1)-Y(J))
  115  CONTINUE
       J=J8+1
       AJ=2.*AJ
       AJO=AJ
  116 CONTINUE
       A=E*AIX/G/AJO
       ECC=PL+YBAR
C WARPING FACTOR CALCULATION (AJMEGA).
       XTOT=X3+X4+X5+X6
       T1AV=Y7*(X7/XTOT)+(Y7+Y8)*((X6-X7)/XTOT)+(Y8+Y7-Y6)*(X5/XTOT)
     * +(Y3+Y4)*(X4/XTOT)+Y3*(X3/XTOT)
       YTOT=Y9+Y10
       T2AV=X10*(Y10/YTOT)+(X9+X10)*((Y1-Y10)/YTOT)+(X1+X9+X10)
     * *((Y2+Y3+Y4)-(Y7+Y8))/YTOT
       H=Y10+Y9+T1AV/2.
       BDIM=XTOT
       AJMEGA=T1AV**3*BDIM**3/144+T2AV**3*H**3/36
       B=AIX*RC**2/AJMEGA
       FAC1=N**2/A+N**4/B+N**2
       FAC2=N**2+1./A+N**2/B
       FAC3=1.+1./A+N**2/B
       FAC4=N**2/A+N**4/B-1.
       AMO=ECC*D*RPI*PG*SIN(N*D/(2.*PPI))/RC
```

```
      PHI=AMO*RC**2/E/AIX*(1./((N**2/A+N**4/B+1.)-(1.+1./A+N**2/B)
     * /(N**2+1./A+N**2/B)*(N**2/A+N**4/B+N**2)))
      V=AMO*RC**2/E/AIX*(1./(FAC1-FAC2/FAC3*FAC4))
      RSEAL=RC-V/PHI
C PRESSURE MOMENT CALCULATION
      F1=2.*PI*(RL+X7+X8+X9)*Y10
      F2=PI*(ROO**2-RB**2)
      F3=2.*PI*(RL+X7+X8+X9+X10)*Y1
      F4=2.*PI*(RL+X7+X8+X9+X10+X1)*Y2
      F5=2.*PI*(ROO)*Y3
      F6=PI*(ROO**2-(ROO-X3)**2)
      F7=2.*PI*(ROO-X3)*Y4
      F8=PI*((ROO-X3)**2-(ROO-(X4+X3+T1))**2)
      F9=2.*PI*(RI+XX3)*YY3
      F10=F2-F6-F8
      AM1=-F1*(YBAR-Y10/2.)
      R2=2./3.*(ROO**3-RB**3)/(ROO**2-RB**2)
      AM2=-F2*(R2-RC)
      AM3=F3*(YBAR-Y1/2.)
      AM4=F4*(YBAR-(Y1+Y2/2.))
      AM5=-F5*(Y1+Y2+Y3/2.-YBAR)
      R6=2./3.*(ROO**3-(ROO-X3)**3)/(ROO**2-(ROO-X3)**2)
      AM6=F6*(R6-RC)
      AM7=-F7*(Y1+Y2+Y3+Y4/2.-YBAR)
      R8=2./3.*((ROO-X3)**3-(ROO-X3-X4-T1)**3)/((ROO-X3)**2-(ROO-X3-
     * X4-T1)**2)
      AM8=F8*(R8-RC)
      AM9=-F9*(Y2+Y1+Y3+Y4+YY3/2.-YBAR)
      R10=2./3.*XX3+RI
      AM10=F10*(R10-RC)
      TM=(AM1+AM2+AM3+AM4+AM5+AM6+AM7+AM8+AM9+AM10)/(2.*PI*RC)
      WRITE(6,*) B
      ROTATE=TM*RC**2/E/AIX*PW
      GO TO 39
   36 WRITE(6,37)A1,A2,A3,A4,A5,A6
   37 FORMAT(5X,'NEGATIVE AREAS ARE PRODUCED BY THOSE DIMENSIONS',/,5X
     *,'A1=',F6.4,2X,'A2=',F6.4,2X,'A3=',F6.4,2X,'A4=',F6.4,2X,'A5=',
     * F6.4,2X,'A6=',F6.4,///)
      GO TO 5
   39 WRITE(6,40) XBAR,YBAR,AIX,AIY,AJR,AJO,A,AMO,V,ECC,RC,EIX,ROTATE
   40 FORMAT(/,5X,'XBAR=',F7.4,/,5X,'YBAR=',F7.4,/,5X,'IX=',E12.5,/,5X,
     * 'IY=',E12.5,/,5X,'JR=',E12.5,/,5X,'JTHETA=',E12.5,/,5X,'A=',E12.5
     * ,/,5X,'MTHETA=',E12.5,/,5X,'V=',E12.5,/,5X,'ECC=',E12.5,/,5X,
     * 'RC=',F7.4,/,5X,'EIX=',E12.5,/,5X,'ROTATION=',E12.5)
      WRITE(6,45) RSEAL,AIXY,X1,X2,X3,X4,X5,X6,X7,X8,X9,X10,PHI
      WRITE(6,50) Y1,Y2,Y3,Y4,Y5,Y6,Y7,Y8,Y9,Y10,ROO,RPI,PL,RI,RL
   45 FORMAT(5X,'RSEAL=',E12.5,/,5X,'IXY=',E12.5,
     * /,5X,'X1=',F6.4,2X,'X2=',F6.4,2X,'X3=',F6.4,2X,'X4=',F6.4,2X,
     * 'X5=',F6.4,2X,'X6=',F6.4,2X,'X7=',F6.4,/,5X,'X8=',F6.4,2X,'X9=',
     * F6.4,2X,'X10=',F6.4,/,5X,'PHI=',E12.5)
   50 FORMAT(5X,'Y1=',F6.4,2X,'Y2=',F6.4,2X,'Y3=',F6.4,2X,'Y4=',F6.4
     *,2X,'Y5=',F6.4,2X,'Y6=',F6.4,2X,'Y7=',F6.4,/,5X,'Y8=',F6.4
     *,2X,'Y9=',F6.4,2X,'Y10=',F6.4,/,5X,'ROO=',F6.4,2X,
     * 'RPI=',F6.4,2X,'PL=',F6.4,2X,'RI=',F6.4,2X,'RL=',F6.4,///)
      GO TO 5
      END
```

APPENDIX C

GAS SEAL PROGRAM

**** Program Listing ****

The fluid used is the nitrogen gas.
Alternating Direction Implicit technique is used to analyze a moving wave gas seal.
A set of simultaneous equations at each time step are solved by a special Gaussian Elimination Subroutine, in which a tridiagonal coefficient matrix is rearranged in a form of three columns matrix. The advantage is to save a lot of computer space, i.e. n x n storages decreases to n x 3 storages.
Implicit real*8 is used to convert all real single precision numbers to double precision numbers.
The seal is divided into three identical parts (3 waves), each part is subdivided into 19x20 nodes, where 19 nodes are in circumferential directions and 20 nodes are in radial directions.
The values used in this program have the following units:

```
C  B      : Balanced ratio
C  c      : One-half maximum roughness height   :in
C  DT     : Time step                           :sec
C  ETA    : Viscosity of nitrogen               :lbf-sec/in/in
C  EM     : Young's Modulus                     :psi
C  GM     : Shear Modulus                       :psi
C  G      : Gravity                             :ft/sec/sec
C  HA     : Ring centroid amplitude             :in
C  PC     : Cavity pressure                     :psi
C  PM     : Pressure at asperity contact        :psi
            (equals compressive strength)
C  PI     : Seal inside pressure                :psi
C  PO     : Seal outside pressure               :psi
C  PSP    : Spring pressure on face             :psi
C  PSBAR  : Shear strength of pressure          :psi
C  PHI    : Tilt                                :in/in
C  RB     : Seal balance radius                 :in
C  RC     : Seal centroid radius                :in
C  RI     : Inside radius                       :in
C  RO     : Outside radius                      :in
C  RF     : Friction radius                     :in
C  RHO    : Density                             :in
C  RPM    : Shaft angular speed                 :rpm
C  TEMP   : temperature                         :°R
C  UCON   : Universal constant                  :ft-lbf/lbm-R°
```

```
C
C
C The main program
C
C
      IMPLICIT REAL*8 (A-H,O-Z)
      DIMENSION NO(18)
      COMMON /BLOCKA/C,DA,DEM,DR,ETA,OMEG,PI,PO,RO,WE,IMAX,JMAX
      COMMON /BLOCKB/AN,DT,HA,PHI,RC,WW,NIT
      COMMON /BLOCKC/H(18,20),P(18,20),Q(18,20),RR(18,20)
      COMMON /BLOCKD/AMAXER,RI,NN,IM1,JM1
      COMMON /BLOCKE/PFAC,PHLS,PM,TOTLD,WMECH
      COMMON /BLOCKF/FCONV,WSTAR,ROOC,NWAVE
      IMAX=19
      JMAX=20
      JM1=JMAX-1
      IM1=IMAX-1
      NWAVE=3
      NN=NWAVE
      RC=1.9361D0
      HA=5.4D-6
      PIE=3.141592654D0
      EM=3.D+6
      GM=EM/2.4D0
      AN=2.D0*PIE/NN
      DA=AN/IM1
      AMAXER=6.0D0
      B=0.75D0
      C=20.D-6
      DT=0.5D-6
      PSP=28.5D0
      PC=0.0D0
      G=32.174D0
      RI=1.900D0
      RO=2.0875D0
      WLIMIT=3.0D0
      DR=(RO-RI)/JM1
      PI=14.7D0
      PO=514.7D0
      RB=DSQRT(RO**2-B*(RO**2-RI**2))
      PHI=500.D-6
      RHO=.0023D0
      RPM=1800.0D0
      OMEG=2.D0*PIE*RPM/60.D0
      SSTIFF=23.D0*.833D0
      DISP=.29125D0
      SPNO=12.D0
      SPLOA=SSTIFF*DISP*SPNO
      ETA=2.5236D-9
      TEMP=598.67D0
      UCON=53.3D0*12.D0
      DEM=-PIE/12.D0/ETA/UCON/TEMP
```

```
      FPLOA=PIE*(PO*(RO**2-RB**2)+PI*(RB**2-RI**2))
      ROOC=RO/C
      PM=38000.DO
      PSBAR=0.1DO*PM
      RF=2.DO*(RO**3-RI**3)/3.DO/(RO**2-RI**2)
      WSTAR=SPLOA+FPLOA
      WRITE(6,1)
    1 FORMAT(1H1,/,15X,'*************************************
     *********************',//21X,'TYPICAL INPUT PARAMETERS
     *AND OUTPUT RESULTS",//,15X,'______________________________
     *_________________________',/)
      WRITE(6,2) WSTAR,HA,PHI,AMAXER,WLIMIT
    2 FORMAT(1X,//15X,'REQUIRED LOAD SUPPORT =',D12.5,4X,
     *'LBS',//15X,'WAVINESS AMPLITUDE HA =',D12.5,4X,'INCH'
     *,//15X,'TILT PHI =',D12.5,17X,'IN/IN',//15X,'PRESSURE
     *CONV. CRIT. AMAXER=',F6.3,5X,'PSI',//15X,
     *'LOAD CONV. CRITER. WLIMIT =',F4.2,8X,'LBS',//)
      WRITE(6,3) B,C,RPM,DT,PI,PO
    3 FORMAT(15X,'BAL RATIO =',F6.3,//15X,'HALF MAX ROUGH HEIGHT
     *C =',D12.5,2X,'INCH' //15X,'RPM =',F8.1,//15X,'HALF
     *TIME STEP DT =',D12.5,8X,'SECONDS',//15X,'PI  ='
     *,F8.2,7X,'PSI',//,15X,'PO  =',F9.2,6X,'PSI',//)
      RWW=RC-HA/PHI
      RNO=(RWW-RI)/(RO-RI)
      WRITE(6,4) RWW,RNO,RB
    4 FORMAT(15X,'RADIUS OF CONTACT POINT =',D12.5,2X,'INCH'
     *,//15X,'DIMENSIONLESS OF CONTACT RADIUS =',F5.2,//15X,
     *'BALANCED RADIUS  =',F12.5,9X,'INCH',//)
      HOB=29.5D-6
      CALL WLOAD(HOB)
      WOB=WE
      NITB=NIT
      HOA=33.0D-6
      CALL WLOAD(HOA)
      WOA=WE
      NITA=NIT
      WRITE(6,5) HOA,HOB,WOA,WOB
    5 FORMAT(15X,'HOA =',D12.5,2X,'INCH',16X,'HOB =',D12.5
     *,2X,'INCH',//,15X,'WOA =',D12.5,2X,'LBS',17X,'WOB ='
     *,D12.5,2x,'LBS',//)
  100 HNEW=HOA+(HOB-HOA)*(WOA-WSTAR)/(WOA-WOB)
      CALL WLOAD(HNEW)
      WNEW=WE
      NITN=NIT
      IF(DABS(WNEW-WSTAR).LT.WLIMIT) GO TO 200
      HOB=HNEW
      WOB=WNEW
      GO TO 100
  200 WRITE(6,6) HNEW,WNEW
    6 FORMAT(15X,'MINIMUM FILM THICKNESS HO=',D12.5,2X,'INCH'
     *,//15X,'FLUID LOAD SUPPORT WNEW =',D12.5,2X,'LBS',//)
      WRITE(6,7) NITA,NITB,NITN
    7 FORMAT(15X,'NITA =',I4,//15X,'NITB =',I4,//15X
```

AD-A125 810 APPLICATION OF THE WAVY MECHANICAL FACE SEAL TO SUBMARINE SEAL DESIGN(U) NEW MEXICO UNIV ALBUQUERQUE COLL OF ENGINEERING A O LEBECK ET AL. JUL 82

UNCLASSIFIED ME-117(82)ONR-414-1 N00014-76-C-0071 F/G 11/1 NL

END

FILMED

DTIC

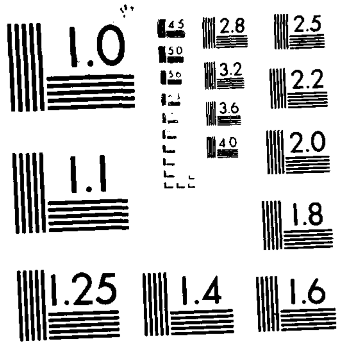

MICROCOPY RESOLUTION TEST CHART
NATIONAL BUREAU OF STANDARDS 1963 A

```
     *,'NITN =',I4,//)
      HST=HNEW+0.5D-6
      CALL WLOAD(HST)
      WOST=WE
      STIFF=(WOST-WNEW)/(HST-HNEW)
      WRITE(6,8) STIFF
    8 FORMAT(15X,'STIFFNESS OF FLUID =',D12.5,7X,'LBS/IN',//)
      FMI=0.D0
      DO 600 I=1,IM1
      J=2
      JMM=J-1
      JP1=J+1
      JP2=J+2
      JP3=J+3
      JP4=J+4
  600 FMI=FMI+DEM*RI*H(I,1)**3*((Q(I,J)-Q(I,JMM))-(Q(I,JP1)
     *-2.D0*Q(I,J)+Q(I,JMM))/2.D0+(Q(I,JP2)-3.D0*Q(I,JP1)
     *+3.D0*Q(I,J)-Q(I,JMM))/3.D0-(Q(I,JP3)
     *-4.D0*Q(I,JP2)+6.D0*Q(I,JP1)-4.D0*Q(I,J)+Q(I,JMM))/4.D0
     *+(Q(I,JP4)-5.D0*Q(I,JP3)+10.D0*Q(I,JP2)-10.D0*Q(I,JP1)
     *+5.D0*Q(I,J)-Q(I,JMM))/5.D0)/DR
      FMI=FMI*NN/G/RHO
      WRITE(6,10) FMI
      FMO=0.D0
      DO 700 I=1,IM1
      J=JMAX
      JMM=J-1
      JM2=J-2
      JM3=J-3
      JM4=J-4
      JM5=J-5
  700 FMO=FMO+DEM*RO*(H(I,JMAX)**3)*((Q(I,JMM)-Q(I,J))-(Q(I,JM2)
     *-2.D0*Q(I,JMM)+Q(I,J))/2.D0+(Q(I,JM3)-3.D0*Q(I,JM2)
     *+3.d)*Q(I,JMM)-Q(I,J))/3.D0-(Q(I,JM4)-4.D0
     **Q(I,JM3)+6.D0*Q(I,JM2)-4.D0*Q(I,JMM)+Q(I,J))/4.D0
     *+(Q(I,JM5)-5.D0*Q(I,JM4)+10.D0*Q(I,JM3)-10.D0*Q(I,JM2)+
     *5.D0*Q(I,JMM)-Q(I,J))/5.D0)/DR
      FMO=-FMO*NN/G/RHO
      FMN=FMI-FMO
      WRITE(6,9) FMO,FMN
    9 FORMAT(15X,'OUTER LEAKAGE QOUT =',D12.4,7X,'SCFM',//,
     *15X,'MASS FL ERROR=',D12.4,13X,'SCFM',//)
   10 FORMAT(//15X,'INNER LEAKAGE QIN =',D12.4,8X,'SCFM',//)
      CALL FRICT(PSBAR,RF,AMU,FFORC,FFA,TORQ)
      WRITE(6,11) AMU,FFORC,PHLS,WMECH,FFA,TORQ
   11 FORMAT(15X,'COEF OF FRICT=',F12.8,//15X,'FRICT  FORCE=',
     *D12.5,26X,'LBS'//,15X,'PERCENT OF FLUID LOAD =',F10.5//,
     *15X,'TOTAL MECH CONTACT SHEAR FORCE =',F10.5,9X,'LBS',//,
     *15X,'TOT FRICTION DUE TO ASPERITY CONTACT =',F13.6,'LBS'//,
     *15X,'TOTAL TORQUE =',F13.6,24X,'IN-LB',///)
      DO 800 I=1,IM1
      NO(I)=I
  800 CONTINUE
```

```
      WRITE(6,12)
   12 FORMAT(1H1,48X,'****** FLUID FILM THICKNESS ******',/60X,
     *'( INCH )',////)
      WRITE(6,13) ((NO(IR),H(IR,JC),IR=1,IM1),JC=1,JMAX)
   13 FORMAT(9(1X,I2,1X,D10.4),/)
      WRITE(6,14)
   14 FORMAT(1H1,48X,'****** PRESSURE DISTRIBUTION ******'
     *,/62X,'( PSI )',////)
      WRITE(6,13) ((NO(IR),P(IR,JC),IR=1,IM1),JC=1,JMAX)
      WRITE(6,15)
   15 FORMAT(////,40X,'**************************************
     ********',//)
      STOP
      END
```

```
C
C
C This subroutine is used to find the pressure distribution
C   all over the seal surface.
C A transformation of tridiagonal coefficient into three
C   column matrix is also shown.
C
C
      SUBROUTINE WLOAD(HMA)
      IMPLICIT REAL*8 (A-H,O-Z)
      DIMENSION NO(18),POLD(18,19)
      DIMENSION RIMH(18,19),RIPH(18,19),RJMH(18,19),RJPH(18,19)
      DIMENSION HIMH(18,19),HIPH(18,19),HJMH(18,19),HJPH(18,19)
      DIMENSION A2(18,19),A2JM1(18,19),A2JP1(18,19)
      DIMENSION A1IP1(18,19),A1(18,19),A1IM1(18,19)
      DIMENSION RJM1(18,19),RJP1(18,19) ,QA(18,19),PA(18,19)
      DIMENSION QIM1(18,19),QIP1(18,19),QJM1(18,19),QJP1(18,19)
      DIMENSION Z(18,5),R(18)
      DIMENSION ZZ(18,3),ZR(18)
      COMMON /BLOCKA/C,DA,DEM,DR,ETA,OMEG,PI,PO,RO,W,IMAX,JMAX
      COMMON /BLOCKB/AN,DT,HA,PHI,RC,WW,NIT
      COMMON /BLOCKC/H(18,20),P(18,20),Q(18,20),RR(18,20)
      COMMON /BLOCKD/AMAXER,RI,NN,IM1,JM1
      COMMON /BLOCKE/PFAC,PHLS,PM,TOTLD,WMECH
      IM2=IMAX-2
      JM2=JMAX-2
      IM=(IMAX+1)/2
      IMM=IM-1
      IMP=IM+1
      CON=6.DO*ETA*OMEG
      VALUE=12.DO*ETA/DT/DR
      RD=RO-RI
      PD=(PO-PI)/RD
      DO 100 J=2,JM1
      DO 100 I=1,IM1
      RJM1(I,J)=RI+(J-2)*DR
      RR(I,J)=RI+(J-1)*DR
      RIMH(I,J)=RR(I,J)
      RIPH(I,J)=RR(I,J)
      RJP1(I,J)=RI+J*DR
      RJMH(I,J)=RI+(J-1.5DO)*DR
      RJPH(I,J)=RI+(J-0.5DO)*DR
  100 CONTINUE
      DO 105 J=1,JMAX
      DO 105 I=1,IM1
      RR(I,1)=RI
      RR(I,JMAX)=RO
  105 CONTINUE
      DO 107 J=1,JMAX
      DO 107 I=1,IM1
      CALL WEAR(RR(I,J))
      H(I,J)=HMA+WW+(HA+ (RR(I,J)-RC)*PHI)*DCOS(NN*(I-1)*DA)
  107 CONTINUE
```

```
      DO 109 J=2,JM1
      DO 109 I=1,IM1
      CALL WEAR (RR(I,J))
      HIMH(I,J)=HMA+WW+(HA+(RR(I,J)-RC)*PHI)*DCOS(NN*(I-1.5D0)*DA)
      HIPH(I,J)=HMA+WW+(HA+(RR(I,J)-RC)*PHI)*DCOS(NN*(I-.5D0)*DA)
      CALL WEAR(RJMH(I,J))
      HJMH(I,J)=HMA+WW+(HA+(RJMH(I,J)-RC)*PHI)*DCOS(NN*(I-1)*DA)
      CALL WEAR(RJPH(I,J))
      HJPH(I,J)=HMA+WW+(HA+(RJPH(I,J)-RC)*PHI)*DCOS(NN*(I-1)*DA)
  109 CONTINUE
      DO 111 KM=1,1000
      ERR=0.D0
      IF(KM.NE.1) GO TO 22
      DO 125 J=2,JM1
      DO 125 I=1,IM1
      P(I,J)=PI+PD*(J-1)*DR
      POLD(I,J)=P(I,J)
      Q(I,J)=P(I,J)**2
      QIP1(I,J)=Q(I,J)
      QIM1(I,J)=Q(I,J)
      QJM1(I,J)=(PI+PD*(J-2)*DR)**2
      QJP1(I,J)=(PI+PD*J*DR)**2
  125 CONTINUE
      DO 135 J=1,JMAX
      DO 135 I=1,IM1
      P(I,1)=PI
      P(I,JMAX)=PO
      Q(I,1)=PI**2
      Q(I,JMAX)=PO**2
  135 CONTINUE
   22 CONTINUE
      DO 150 J=2,JM1
      NEQ=IM1
      M=2
      LMAX=2*M+1
      DO 200 I=1,IM1
      IF(I.GE.IM) GO TO 23
      K=1-(1-I)*M
      GO TO 21
   23 IF(I.GT.IM) GO TO 24
      K=IM1
      GO TO 21
   24 K=(IMAX-I)*M
   21 AREA=RR(I,J)*DA*DR
      A1(I,J)=-(HIPH(I,J)**3/RIPH(I,J)+HIMH(I,J)**3/RIMH(I,J))/DA
     *-CON*(HIPH(I,J)*RIPH(I,J)-HIMH(I,J)*RIMH(I,J))/DSQRT(
     *Q(I,J))-VALUE*H(I,J)*AREA/DSQRT(Q(I,J))
      A1IP1(I,J)=HIPH(I,J)**3/RIPH(I,J)/DA-RIPH(I,J)*CON*HIPH
     *(I,J)/DSQRT(QIP1(I,J))
      A1IM1(I,J)=HIMH(I,J)**3/RIMH(I,J)/DA+CON*HIMH(I,J)*RIMH
     *(I,J)/DSQRT(QIM1(I,J))
      R(K)=DA /DR/DR*(((RJPH(I,J)*HJPH(I,J)**3+RJMH(I,J)*
     *HJMH(I,J)**3)*Q(I,J))-QJP1(I,J)*RJPH(I,J)*HJPH(I,J)**3
```

```
     *-QJM1(I,J)*RJMH(I,J)*HJMH(I,J)**3)
     *-VALUE*H(I,J)*AREA*DSQRT(Q(I,J))
      DO 210 L=1,LMAX
  210 Z(K,L)=0.D0
      Z(K,M+1)=A1(I,J)
      IF(I.NE.1) GO TO 27
      Z(K,M+2)=A1IM1(I,J)
      Z(K,LMAX)=A1IP1(I,J)
      GO TO 200
   27 IF(I.NE.IM1) GO TO 28
      Z(K,M)=A1IP1(I,J)
      Z(K,LMAX)=A1IM1(I,J)
      GO TO 200
   28 IF(I.NE.IMM) GO TO 29
      Z(K,1)=A1IM1(I,J)
      Z(K,M+2)=A1IP1(I,J)
      GO TO 200
   29 IF(I.NE.IM) GO TO 31
      Z(K,1)=A1IP1(I,J)
      Z(K,M)=A1IM1(I,J)
      GO TO 200
   31 IF(I.LT.IM) GO TO 32
      Z(K,LMAX)=A1IM1(I,J)
      Z(K,1)=A1IP1(I,J)
      GO TO 200
   32 Z(K,1)=A1IM1(I,J)
      Z(K,LMAX)=A1IP1(I,J)
  200 CONTINUE
      CALL GAUSS(Z,R,M,NEQ)
      DO 250 I=1,IM1
      IF(I.GE.IM) GO TO 25
      K=1-(1-I)*M
      GO TO 19
   25 IF(I.GT.IM) GO TO 26
      K=IM1
      GO TO 19
   26 K=(IMAX-I)*M
   19 Q(I,J)=R(K)
      P(I,J)=DSQRT(Q(I,J))
      IF(I.NE.1) GO TO 33
      QIP1(I,J)=R(K+M)
      QIM1(I,J)=R(K+1)
      GO TO 250
   33 IF(I.LE.IM) GO TO 34
      QIM1(I,J)=R(K+M)
      IF(I.NE.IM1) GO TO 18
      QIP1(I,J)=R(K-1)
      GO TO 250
   18 QIP1(I,J)=R(K-M)
      GO TO 250
   34 IF(I.LT.IMM) GO TO 35
      IF(I.NE.IMM) GO TO 36
      QIP1(I,J)=R(K+1)
```

```
      QIM1(I,J)=R(K-M)
      GO TO 250
   36 QIP1(I,J)=R(K-M)
      QIM1(I,J)=R(K-1)
      GO TO 250
   35 QIP1(I,J)=R(K+M)
      QIM1(I,J)=R(K-M)
  250 CONTINUE
  150 CONTINUE
      DO 300 I=1,IM1
      M=1
      LMAX=2*M+1
      NEQ=JM2
      DO 350 J=2,JM1
      K=J-1
      AREA=RR(I,J)*DA*DR
      A2(I,J)=-DA /DR/DR*(RJPH(I,J)*HJPH(I,J)**3+RJMH(I,J)*
     *HJMH(I,J)**3)-VALUE*H(I,J)*AREA/DSQRT(Q(I,J))
      A2JP1(I,J)=DA*RJPH(I,J)*HJPH(I,J)**3 /DR/DR
      A2JM1(I,J)=DA*RJMH(I,J)*HJMH(I,J)**3 /DR/DR
      ZR(K)=Q(I,J)*((HIPH(I,J)**3/RIPH(I,J)+HIMH(I,J)**3/RIMH(
     *I,J))/DA-(HIMH(I,J)*RIMH(I,J)-HIPH(I,J)*RIPH(I,J))*CON/
     *DSQRT(Q(I,J)))-QIP1(I,J)*(HIPH(I,J)**3/RIPH(I,J)/DA-CON*
     *HIPH(I,J)*RIPH(I,J)/DSQRT(QIP1(I,J)))-QIM1(I,J)*(HIMH(I,
     *J)**3/RIMH(I,J)/DA+CON*HIMH(I,J)*RIMH(I,J)/DSQRT(QIM1(I,J)
     *))-VALUE*H(I,J)*AREA*DSQRT(Q(I,J))
      DO 310 L=1,LMAX
  310 ZZ(K,L)=0.D0
      ZZ(K,M+1)=A2(I,J)
      IF(J.NE.2) GO TO 40
      ZZ(K,1)=0.D0
      ZZ(K,LMAX)=A2JP1(I,J)
      ZR(K)=ZR(K)-A2JM1(I,J)*PI*PI
      GO TO 350
   40 IF(J.NE.JM1) GO TO 42
      ZZ(K,1)=A2JM1(I,J)
      ZZ(K,LMAX)=0.D0
      ZR(K)=ZR(K)-A2JP1(I,J)*PO*PO
      GO TO 350
   42 ZZ(K,1)=A2JM1(I,J)
      ZZ(K,LMAX)=A2JP1(I,J)
  350 CONTINUE
      CALL ZGAUSS(ZZ,ZR,M,NEQ)
      DO 400 J=2,JM1
      K=J-1
      QA(I,J)=ZR(K)
      PA(I,J)=DSQRT(QA(I,J))
      IF(J.NE.2) GO TO 43
      QJP1(I,J)=ZR(K+M)
      QJM1(I,J)=PI*PI
      GO TO 50
   43 IF(J.NE.JM1) GO TO 45
      QJP1(I,J)=PO*PO
```

```
      QJM1(I,J)=ZR(K-M)
      GO TO 50
   45 QJP1(I,J)=ZR(K+M)
      QJM1(I,J)=ZR(K-M)
   50 DEV=DABS(PA(I,J)-POLD(I,J))
      Q(I,J)=QA(I,J)
      POLD(I,J)=PA(I,J)
      P(I,J)=PA(I,J)
      ERR=ERR+DEV
  400 CONTINUE
  300 CONTINUE
      IF(ERR.LT.AMAXER) GO TO 70
  111 CONTINUE
   70 CALL LDTOT
      W=TOTLD
      NIT=KM
      RETURN
      END
```

```
C
C
C To find the minimum wear with respect to the same radius
C
C
      SUBROUTINE WEAR(XR )
      IMPLICIT REAL*8 (A-H,O-Z)
      DIMENSION W(18)
      COMMON /BLOCKA/C,DA,DEM,DR,ETA,OMEG,PI,PO,RO,WE,IMAX,JMAX
      COMMON /BLOCKD/AMAXER,RI,NN,IM1,JM1
      COMMON /BLOCKB/AN,DT,HA,PHI,RC,WW,NIT
      DA=AN/IM1
      DO 100 I=1,IM1
      W(I)=(HA+(XR-RC)*PHI)*DCOS(NN*(I-1)*DA)
  100 CONTINUE
      SMALL=W(1)
      DO 200 I=1,IM1
      IF(SMALL.LE.W(I)) GO TO 200
      SMALL=W(I)
  200 CONTINUE
      WW=-(SMALL)
      RETURN
      END
```

```
C
C
C To solve simultaneous equations by Gaussian Elimination
C   with tri-column matrix coefficients.
C
C
      SUBROUTINE GAUSS(A,B,MBAND,NEQ)
      IMPLICIT REAL*8 (A-H,O-Z)
      DIMENSION A(90),B(18)
      CALL FSPIE
      NQ1=NEQ-1
      DO 10 I=1,NQ1
      I1=I+1
      I2=I+MBAND
      DO 20 II=I1,I2
      J=I
      K=(J-II+MBAND)*NEQ+II
      IF(A(K).EQ.0.D0) GO TO 20
      KK=(J-I+MBAND)*NEQ+I
      C=A(K)/A(KK)
      J1=J
      J2=J+MBAND
      IF(J2.GT.NEQ) J2=NEQ
      DO 40 JJ=J1,J2
      KKK=(JJ-II+MBAND)*NEQ+II
      KKKK=(JJ-I+MBAND)*NEQ+I
      A(KKK)=A(KKK)-C*A(KKKK)
   40 CONTINUE
      B(II)=B(II)-C*B(I)
   20 CONTINUE
   10 CONTINUE
      K=MBAND*NEQ+NEQ
      B(NEQ)=B(NEQ)/A(K)
      DO 50 II=1,NQ1
      I=NEQ-II
      J1=I+1
      J2=I+MBAND
      S=0.0
      IF(J2.GT.NEQ) J2=NEQ
      DO 60 J=J1,J2
      K=(J-I+MBAND)*NEQ+I
   60 S=S+A(K)*B(J)
      KK=MBAND*NEQ+I
   50 B(I)=(B(I)-S)/A(KK)
      RETURN
      END
```

```
C
C
C To solve simultaneous equations by Gaussian Elimination
C   with tri-diagonal matrix coefficients.
C
C
      SUBROUTINE ZGAUSS(A,B,MBAND,NEQ)
      IMPLICIT REAL*8 (A-H,O-Z)
      DIMENSION A(54),B(18)
      CALL FSPIE
      NQ1=NEQ-1
      DO 10 I=1,NQ1
      I1=I+1
      I2=I+MBAND
      DO 20 II=I1,I2
      J=I
      K=(J-II+MBAND)*NEQ+II
      IF(A(K).EQ.0.D0) GO TO 20
      KK=(J-I+MBAND)*NEQ+I
      C=A(K)/A(KK)
      J1=J
      J2=J+MBAND
      IF(J2.GT.NEQ) J2=NEQ
      DO 40 JJ=J1,J2
      KKK=(JJ-II+MBAND)*NEQ+II
      KKKK=(JJ-I+MBAND)*NEQ+I
   40 A(KKK)=A(KKK)-C*A(KKKK)
      B(II)=B(II)-C*B(I)
   20 CONTINUE
   10 CONTINUE
      K=MBAND*NEQ+NEQ
      B(NEQ)=B(NEQ)/A(K)
      DO 50 II=1,NQ1
      I=NEQ-II
      J1=I+1
      J2=I+MBAND
      S=0.D0
      IF(J2.GT.NEQ) J2=NEQ
      DO 60 J=J1,J2
      K=(J-I+MBAND)*NEQ+I
   60 S=S+A(K)*B(J)
      KK=MBAND*NEQ+I
   50 B(I)=(B(I)-S)/A(KK)
      RETURN
      END
```

```
C
C
C To find the total load support including hydrodynamic,
C   mechanical and shear supports, where,
C   WMECH is the total mechanical load support
C   TOTLD is the total load support
C   PHLS  is the percentage of fluid load
C   W     is the total fluid load support
C
C
      SUBROUTINE LDTOT
      IMPLICIT REAL*8 (A-H,O-Z)
      COMMON /BLOCKA/C,DA,DEM,DR,ETA,OMEG,PI,PO,RO,WE,IMAX,JMAX
      COMMON /BLOCKC/H(18,20),P(18,20),Q(18,20),RR(18,20)
      COMMON /BLOCKD/AMAXER,RI,NWAVE,IM1,JM1
      COMMON /BLOCKE/PFAC,PHLS,PM,TOTLD,WMECH
      W=0.D0
      WMEC=0.D0
      DO 100 J=2,JMAX
      DO 100 I=1,IM1
      JM=J-1
      HT=H(I,J)/C
      CALL ASPRAT(HT,BI)
      IF(I.EQ.1) GO TO 10
      IF(I.EQ.IM1) GO TO 20
      IIM=I-1
      IIP=I+1
      GO TO 30
   10 IIM=IM1
      IIP=I+1
      GO TO 30
   20 IIM=I-1
      IIP=1
   30 W=W+(P(IIP,J)+P(IIP,JM)+P(IIM,J)+P(IIM,JM))/4.D0*(RR(I,J)
     *-DR/2.D0)*DA*DR*BI
      WMEC=WMEC+PM*(1.D0-BI)*DA*DR*(RR(I,J)-DR/2.D0)
  100 CONTINUE
      TOTLD=(W+WMEC)*NWAVE
      WMECH=WMEC*NWAVE
      PHLS=W*NWAVE/TOTLD*100.D0
      RETURN
      END
```

```
C
C
C To find the frictional force and the coefficient of
C   friction, where,
C   FF is the total viscous force
C   FA is the mechanical friction force
C   AMU is the total coefficient of friction
C   TORQ is the torque of the driving shaft
C   FFORC is the total combined friction force
C
      SUBROUTINE FRICT(PSBAR,RF,AMU,FFORC,FFA,TORQ)
      IMPLICIT REAL*8 (A-H,O-Z)
      COMMON /BLOCKA/C,DA,DEM,DR,ETA,OMEG,PI,PO,RO,WE,IMAX,JMAX
      COMMON /BLOCKC/H(18,20),P(18,20),Q(18,20),RR(18,20)
      COMMON /BLOCKF/FCONV,WSTAR,ROOC,NWAVE
      COMMON /BLOCKG/DEL,EH,E1OH,EH3
      FF=0.D0
      FA=0.D0
      DEL=RO*OMEG*ETA/C/PSBAR
      IM1=IMAX-1
      DO 100 J=2,JMAX
      DO 100 I=1,IM1
      R=RR(I,J)-DR/2.D0
      HT=H(I,J)/C
      CALL EXPT(HT)
      CALL ASPRAT(HT,BI)
      JM=J-1
      IF(I.EQ.1) GO TO 10
      IF(I.EQ.IM1) GO TO 20
      IIM=I-1
      IIP=I+1
      GO TO 30
   10 IIM=IM1
      IIP=I+1
      GO TO 30
   20 IIM=I-1
      IIP=1
   30 DP=(P(IIP,J)-P(IIM,J)+P(IIP,JM)-P(IIM,JM))/4.D0/DA
      FF=FF+R*R*(R*ETA*OMEG*E1OH+.5D0/R*DP*EH)*BI/RF*DA*DR
      FA=FA+(1.D0-BI)*PSBAR*R*R*DA*DR/RF
  100 CONTINUE
      FSUM=FF+FA
      AMU=FSUM/WSTAR*NWAVE
      FFA=FA*NWAVE
      FFORC=FSUM*NWAVE
      TORQ=FSUM*RF*NWAVE
      RETURN
      END
```

```
C
C
C To find the expected values of film thickness
C   where E1OH is the expected value of E(1/H)
C
      SUBROUTINE EXPT(HT)
      IMPLICIT REAL*8 (A-H,O-Z)
      COMMON /BLOCKA/C,DA,DEM,DR,ETA,OMEG,PI,PO,RO,WE,IMAX,JMAX
      COMMON /BLOCKG/DEL,EH,E1OH,EH3
      EH=HT*C
      IF(EH.LT.0.D0) EH=0.D0
      EH3=HT**3*C**3
      IF(EH3.LT.0.D0) EH3=0.D0
      IF(HT.LE.1.D0) GO TO 25
      E1OH=1.D0/HT/C
      IF(HT.GT.4.D0) GO TO 50
      E1OH=(1.D0-HT*HT)**3*DLOG((HT+1.D0)/(HT-1.D0))
      E1OH=(E1OH+2.D0*HT*(33.D0+HT*HT*(15.D0*HT*HT-40.D0))
     */15.D0)*35.D0/32.D0/C
      GO TO 50
   25 CONTINUE
      E1OH=-405.D0+HT*(60.D0+147.D0*HT)
      E1OH=-55.D0+HT*(132.D0+HT*(345.D0+HT*(-160.D0+HT*E1OH)))
      E1OH=(E1OH/60.D0+(1.D0-HT*HT)**3*DLOG((1.D0+HT)/DEL))*
     *35.D0/32.D0/C
   50 RETURN
      END
```

```
C
C
C To find the asperity ratio of the surface where
C   BI is the fraction of seal subject to fluid pressure
C
C
      SUBROUTINE ASPRAT(HT,BI)
      IMPLICIT REAL*8 (A-H,O-Z)
      H=HT
      BI=1.DO
      IF(H.GE.1.DO) GO TO 10
      BI=(16.DO+H*(35.DO+H*H*(-35.DO+H*H*(21.DO-5.DO*H*H))))
     */32.DO
   10 RETURN
      END
```

******** The end of the whole programs ********

```
TYPICAL INPUT PARAMETERS AND OUTPUT RESULTS

REQUIRED LOAD SUPPORT = 0.98230D 03     LBS
WAVINESS AMPLITUDE HA = 0.54000D-05     INCH
TILT PHI = 0.50000D-03                  IN/IN
PRESSURE CONV. CRIT. AMAXER= 6.000      PSI
LOAD CONV. CRITER. WLIMIT =3.00         LBS

BAL RATIO = 0.750
HALF MAX ROUGH HEIGHT C = 0.20000D-04   INCH
RPM =  1600.0
HALF TIME STEP DT = 0.50000D-06         SECONDS
PI  =    14.70        PSI
PO  =    514.70       PSI

RADIUS OF CONTACT POINT = 0.19253D 01   INCH
DIMENSIONLESS OF CONTACT RADIUS = 0.13
BALANCED RADIUS  =      1.94857         INCH

HOA = 0.33000D-04   INCH                HOB = 0.29500D-04   INCH
WOA = 0.97921D 03   LBS                 WOB = 0.98304D 03   LBS

MINIMUM FILM THICKNESS HO= 0.30176D-04 INCH
FLUID LOAD SUPPORT WNEW = 0.98233D 03  LBS

NITA = 419
NITB = 462
NITN = 454

STIFFNESS OF FLUID =-0.11464D 07        LBS/IN


INNER LEAKAGE QIN = -0.12090 00         SCFM

OUTER LEAKAGE QOUT = -0.56600-01        SCFM
MASS FL ERROR= -0.64350-01              SCFM

COEF OF FRICT=  0.00004473
FRICT  FORCE= 0.43941D-01                                  LBS
PERCENT OF FLUID LOAD = 100.00000
TOTAL MECH CONTACT SHEAR FORCE =    0.0                    LBS
TOT FRICTION DUE TO ASPERITY CONTACT =      0.0            LBS
TOTAL TORQUE =      0.087673                               IN-LB
```

****** PRESSURE DISTRIBUTION ******
(PSI)

θ →, R ↓

R	1	2	3	4	5	6	7	8	9	10	11	12	13	14	15	16	17	18
1	0.1470D 02	0.1470D 02	0.1470D 02	0.1470D 02	0.1470D 02	0.1470D 02	0.1470D 02	0.1470D 02	0.1470D 02	0.1470D 02	0.1470D 02	0.1470D 02	0.1470D 02	0.1470D 02	0.1470D 02	0.1470D 02	0.1470D 02	0.1470D 02
2	0.2597D 03	0.2491D 03	0.2340D 03	0.2078D 03	0.1782D 03	0.1470D 03	0.1165D 03	0.8761D 02	0.6470D 02	0.5415D 02	0.5710D 02	0.7649D 02	0.1073D 03	0.1410D 03	0.1742D 03	0.2052D 03	0.2310D 03	0.2494D 03
3	0.3595D 03	0.3541D 03	0.3372D 03	0.3099D 03	0.2745D 03	0.2336D 03	0.1899D 03	0.1454D 03	0.1084D 03	0.9400D 02	0.9534D 02	0.1269D 03	0.1753D 03	0.2242D 03	0.2686D 03	0.3065D 03	0.3350D 03	0.3531D 03
4	0.4397D 03	0.4361D 03	0.4241D 03	0.4026D 03	0.3715D 03	0.3303D 03	0.2800D 03	0.2222D 03	0.1695D 03	0.1425D 03	0.1497D 03	0.1950D 03	0.2595D 03	0.3179D 03	0.3642D 03	0.3984D 03	0.4216D 03	0.4350D 03
5	0.4714D 03	0.4691D 03	0.4600D 03	0.4435D 03	0.4209D 03	0.3854D 03	0.3372D 03	0.2760D 03	0.2151D 03	0.1631D 03	0.1913D 03	0.2457D 03	0.3139D 03	0.3718D 03	0.4131D 03	0.4410D 03	0.4565D 03	0.4661D 03
6	0.4869D 03	0.4854D 03	0.4791D 03	0.4684D 03	0.4494D 03	0.4200D 03	0.3767D 03	0.3161D 03	0.2532D 03	0.2169D 03	0.2256D 03	0.2814D 03	0.3521D 03	0.4040D 03	0.4441D 03	0.4649D 03	0.4773D 03	0.4844D 03
7	0.4956D 03	0.4947D 03	0.4905D 03	0.4821D 03	0.4615D 03	0.4435D 03	0.4057D 03	0.3493D 03	0.2659D 03	0.2470D 03	0.2556D 03	0.3125D 03	0.3608D 03	0.4298D 03	0.4601D 03	0.4781D 03	0.4884D 03	0.4937D 03
8	0.5011D 03	0.5004D 03	0.4974D 03	0.4911D 03	0.4797D 03	0.4603D 03	0.4200D 03	0.3762D 03	0.3139D 03	0.2744D 03	0.2628D 03	0.3391D 03	0.4035D 03	0.4572D 03	0.4720D 03	0.4873D 03	0.4954D 03	0.4996D 03
9	0.5047D 03	0.5042D 03	0.5020D 03	0.4972D 03	0.4806D 03	0.4727D 03	0.4454D 03	0.3989D 03	0.3395D 03	0.3000D 03	0.3079D 03	0.3624D 03	0.4220D 03	0.4604D 03	0.4819D 03	0.4930D 03	0.5002D 03	0.5035D 03
10	0.5072D 03	0.5069D 03	0.5052D 03	0.5014D 03	0.4947D 03	0.4822D 03	0.4594D 03	0.4184D 03	0.3629D 03	0.3240D 03	0.3314D 03	0.3830D 03	0.4373D 03	0.4700D 03	0.4880D 03	0.4985D 03	0.5036D 03	0.5062D 03
11	0.5090D 03	0.5088D 03	0.5076D 03	0.5046D 03	0.4994D 03	0.4895D 03	0.4710D 03	0.4351D 03	0.3845D 03	0.3467D 03	0.3535D 03	0.4015D 03	0.4502D 03	0.4791D 03	0.4942D 03	0.5020D 03	0.5061D 03	0.5082D 03
12	0.5103D 03	0.5102D 03	0.5093D 03	0.5072D 03	0.5030D 03	0.4952D 03	0.4799D 03	0.4490D 03	0.4041D 03	0.3667D 03	0.3745D 03	0.4184D 03	0.4613D 03	0.4859D 03	0.4984D 03	0.5040D 03	0.5080D 03	0.5097D 03
13	0.5114D 03	0.5113D 03	0.5106D 03	0.5090D 03	0.5059D 03	0.4997D 03	0.4875D 03	0.4622D 03	0.4222D 03	0.3695D 03	0.3944D 03	0.4330D 03	0.4709D 03	0.4916D 03	0.5018D 03	0.5069D 03	0.5096D 03	0.5109D 03
14	0.5122D 03	0.5122D 03	0.5117D 03	0.5105D 03	0.5081D 03	0.5034D 03	0.4938D 03	0.4732D 03	0.4390D 03	0.4095D 03	0.4136D 03	0.4479D 03	0.4794D 03	0.4964D 03	0.5046D 03	0.5087D 03	0.5108D 03	0.5118D 03
15	0.5128D 03	0.5126D 03	0.5125D 03	0.5116D 03	0.5098D 03	0.5064D 03	0.4990D 03	0.4826D 03	0.4545D 03	0.4287D 03	0.4319D 03	0.4610D 03	0.4869D 03	0.5005D 03	0.5070D 03	0.5101D 03	0.5117D 03	0.5125D 03
16	0.5134D 03	0.5134D 03	0.5131D 03	0.5125D 03	0.5113D 03	0.5088D 03	0.5034D 03	0.4911D 03	0.4687D 03	0.4472D 03	0.4496D 03	0.4732D 03	0.4936D 03	0.5041D 03	0.5090D 03	0.5114D 03	0.5125D 03	0.5131D 03
17	0.5138D 03	0.5138D 03	0.5136D 03	0.5132D 03	0.5124D 03	0.5107D 03	0.5071D 03	0.4984D 03	0.4818D 03	0.4650D 03	0.4667D 03	0.4846D 03	0.4996D 03	0.5072D 03	0.5107D 03	0.5124D 03	0.5132D 03	0.5136D 03
18	0.5141D 03	0.5142D 03	0.5141D 03	0.5138D 03	0.5133D 03	0.5123D 03	0.5101D 03	0.5047D 03	0.4936D 03	0.4822D 03	0.4832D 03	0.4952D 03	0.5051D 03	0.5100D 03	0.5122D 03	0.5133D 03	0.5138D 03	0.5140D 03
19	0.5144D 03	0.5145D 03	0.5144D 03	0.5143D 03	0.5141D 03	0.5136D 03	0.5126D 03	0.5101D 03	0.5046D 03	0.4987D 03	0.4992D 03	0.5052D 03	0.5101D 03	0.5125D 03	0.5135D 03	0.5140D 03	0.5143D 03	0.5144D 03
20	0.5147D 03	0.5147D 03	0.5147D 03	0.5147D 03	0.5147D 03	0.5147D 03	0.5147D 03	0.5147D 03	0.5147D 03	0.5147D 03	0.5147D 03	0.5147D 03	0.5147D 03	0.5147D 03	0.5147D 03	0.5147D 03	0.5147D 03	0.5147D 03

****

****** FLUID FILM THICKNESS ******
(INCH)

R ↓ θ →

R									
1	1 0.3060D-04	2 0.3144D-04	3 0.3364D-04	4 0.3700D-04	5 0.4113D-04	6 0.4552D-04	7 0.4965D-04	8 0.5302D-04	9 0.5521D-04
	10 0.5598D-04	11 0.5521D-04	12 0.5302D-04	13 0.4965D-04	14 0.4552D-04	15 0.4113D-04	16 0.3700D-04	17 0.3364D-04	18 0.3144D-04
2	1 0.3060D-04	2 0.3114D-04	3 0.3248D-04	4 0.3453D-04	5 0.3705D-04	6 0.3973D-04	7 0.4225D-04	8 0.4430D-04	9 0.4564D-04
	10 0.4611D-04	11 0.4564D-04	12 0.4430D-04	13 0.4225D-04	14 0.3973D-04	15 0.3705D-04	16 0.3453D-04	17 0.3248D-04	18 0.3114D-04
3	1 0.3060D-04	2 0.3084D-04	3 0.3133D-04	4 0.3203D-04	5 0.3297D-04	6 0.3394D-04	7 0.3485D-04	8 0.3559D-04	9 0.3607D-04
	10 0.3624D-04	11 0.3607D-04	12 0.3559D-04	13 0.3485D-04	14 0.3394D-04	15 0.3297D-04	16 0.3201D-04	17 0.3133D-04	18 0.3084D-04
4	1 0.3498D-04	2 0.3485D-04	3 0.3448D-04	4 0.3391D-04	5 0.3320D-04	6 0.3246D-04	7 0.3175D-04	8 0.3118D-04	9 0.3081D-04
	10 0.3068D-04	11 0.3081D-04	12 0.3118D-04	13 0.3175D-04	14 0.3246D-04	15 0.3320D-04	16 0.3391D-04	17 0.3448D-04	18 0.3485D-04
5	1 0.4405D-04	2 0.4342D-04	3 0.4217D-04	4 0.4131D-04	5 0.3879D-04	6 0.3653D-04	7 0.3422D-04	8 0.3233D-04	9 0.3110D-04
	10 0.3068D-04	11 0.3110D-04	12 0.3233D-04	13 0.3422D-04	14 0.3653D-04	15 0.3899D-04	16 0.4131D-04	17 0.4319D-04	18 0.4442D-04
6	1 0.5472D-04	2 0.5399D-04	3 0.5191D-04	4 0.4871D-04	5 0.4478D-04	6 0.4061D-04	7 0.3669D-04	8 0.3349D-04	9 0.3140D-04
	10 0.3068D-04	11 0.3140D-04	12 0.3349D-04	13 0.3669D-04	14 0.4061D-04	15 0.4478D-04	16 0.4871D-04	17 0.5191D-04	18 0.5399D-04
7	1 0.6459D-04	2 0.6356D-04	3 0.6062D-04	4 0.5611D-04	5 0.5058D-04	6 0.4469D-04	7 0.3915D-04	8 0.3464D-04	9 0.3170D-04
	10 0.3068D-04	11 0.3170D-04	12 0.3464D-04	13 0.3915D-04	14 0.4469D-04	15 0.5058D-04	16 0.5611D-04	17 0.6062D-04	18 0.6356D-04
8	1 0.7446D-04	2 0.7314D-04	3 0.6933D-04	4 0.6351D-04	5 0.5637D-04	6 0.4876D-04	7 0.4162D-04	8 0.3580D-04	9 0.3200D-04
	10 0.3068D-04	11 0.3200D-04	12 0.3580D-04	13 0.4162D-04	14 0.4876D-04	15 0.5637D-04	16 0.6351D-04	17 0.6933D-04	18 0.7314D-04
9	1 0.8432D-04	2 0.8271D-04	3 0.7805D-04	4 0.7091D-04	5 0.6216D-04	6 0.5284D-04	7 0.4409D-04	8 0.3695D-04	9 0.3229D-04
	10 0.3068D-04	11 0.3229D-04	12 0.3695D-04	13 0.4409D-04	14 0.5284D-04	15 0.6216D-04	16 0.7091D-04	17 0.7805D-04	18 0.8271D-04
10	1 0.9419D-04	2 0.9228D-04	3 0.8676D-04	4 0.7831D-04	5 0.6795D-04	6 0.5692D-04	7 0.4656D-04	8 0.3811D-04	9 0.3259D-04
	10 0.3068D-04	11 0.3259D-04	12 0.3811D-04	13 0.4656D-04	14 0.5692D-04	15 0.6795D-04	16 0.7831D-04	17 0.8676D-04	18 0.9228D-04
11	1 0.1041D-03	2 0.1018D-03	3 0.9548D-04	4 0.8571D-04	5 0.7374D-04	6 0.6100D-04	7 0.4902D-04	8 0.3926D-04	9 0.3289D-04
	10 0.3068D-04	11 0.3289D-04	12 0.3926D-04	13 0.4902D-04	14 0.6100D-04	15 0.7374D-04	16 0.8571D-04	17 0.9548D-04	18 0.1018D-03
12	1 0.1139D-03	2 0.1114D-03	3 0.1042D-03	4 0.9312D-04	5 0.7953D-04	6 0.6507D-04	7 0.5149D-04	8 0.4041D-04	9 0.3319D-04
	10 0.3068D-04	11 0.3319D-04	12 0.4041D-04	13 0.5149D-04	14 0.6507D-04	15 0.7953D-04	16 0.9312D-04	17 0.1042D-03	18 0.1114D-03
13	1 0.1238D-03	2 0.1210D-03	3 0.1129D-03	4 0.1005D-03	5 0.8532D-04	6 0.6915D-04	7 0.5396D-04	8 0.4157D-04	9 0.3348D-04
	10 0.3068D-04	11 0.3348D-04	12 0.4157D-04	13 0.5396D-04	14 0.6915D-04	15 0.8532D-04	16 0.1005D-03	17 0.1129D-03	18 0.1210D-03
14	1 0.1337D-03	2 0.1306D-03	3 0.1216D-03	4 0.1079D-03	5 0.9111D-04	6 0.7323D-04	7 0.5642D-04	8 0.4272D-04	9 0.3378D-04
	10 0.3068D-04	11 0.3378D-04	12 0.4272D-04	13 0.5642D-04	14 0.7323D-04	15 0.9111D-04	16 0.1079D-03	17 0.1216D-03	18 0.1306D-03
15	1 0.1435D-03	2 0.1401D-03	3 0.1303D-03	4 0.1153D-03	5 0.9690D-04	6 0.7731D-04	7 0.5889D-04	8 0.4388D-04	9 0.3408D-04
	10 0.3068D-04	11 0.3408D-04	12 0.4388D-04	13 0.5889D-04	14 0.7731D-04	15 0.9690D-04	16 0.1153D-03	17 0.1303D-03	18 0.1401D-03
16	1 0.1534D-03	2 0.1497D-03	3 0.1390D-03	4 0.1227D-03	5 0.1027D-03	6 0.8138D-04	7 0.6136D-04	8 0.4503D-04	9 0.3438D-04
	10 0.3068D-04	11 0.3438D-04	12 0.4503D-04	13 0.6136D-04	14 0.8138D-04	15 0.1027D-03	16 0.1227D-03	17 0.1390D-03	18 0.1497D-03
17	1 0.1633D-03	2 0.1593D-03	3 0.1478D-03	4 0.1301D-03	5 0.1085D-03	6 0.8546D-04	7 0.6382D-04	8 0.4619D-04	9 0.3467D-04
	10 0.3068D-04	11 0.3467D-04	12 0.4619D-04	13 0.6382D-04	14 0.8546D-04	15 0.1085D-03	16 0.1301D-03	17 0.1478D-03	18 0.1593D-03
18	1 0.1731D-03	2 0.1688D-03	3 0.1565D-03	4 0.1375D-03	5 0.1143D-03	6 0.8954D-04	7 0.6629D-04	8 0.4734D-04	9 0.3497D-04
	10 0.3068D-04	11 0.3497D-04	12 0.4734D-04	13 0.6629D-04	14 0.8954D-04	15 0.1143D-03	16 0.1375D-03	17 0.1565D-03	18 0.1688D-03
19	1 0.1830D-03	2 0.1784D-03	3 0.1652D-03	4 0.1449D-03	5 0.1201D-03	6 0.9362D-04	7 0.6876D-04	8 0.4850D-04	9 0.3527D-04
	10 0.3068D-04	11 0.3527D-04	12 0.4850D-04	13 0.6876D-04	14 0.9362D-04	15 0.1201D-03	16 0.1449D-03	17 0.1652D-03	18 0.1784D-03
20	1 0.1929D-03	2 0.1880D-03	3 0.1739D-03	4 0.1523D-03	5 0.1259D-03	6 0.9769D-04	7 0.7123D-04	8 0.4965D-04	9 0.3557D-04
	10 0.3068D-04	11 0.3557D-04	12 0.4965D-04	13 0.7123D-04	14 0.9769D-04	15 0.1259D-03	16 0.1523D-03	17 0.1739D-03	18 0.1880D-03

Distribution List

Recipient	Number of Copies
Office of Naval Research 800 N. Quincy Street Arlington, Virginia 22217 Attn: M. Keith Ellingsworth, Code 473	(3)
Defense Documentation Center Building 5 Cameron Station Alexandria, Virginia 22314	(12)
Naval Research Laboratory 4555 Overlook Avenue Washington, DC 20390 Attn: Technical Information Division	
Code 2627	(6)
Dr. Ravner, Code 6170	(1)
U.S. Naval Postgraduate School Monterey, California 93940 Attn: Dept. of Mechanical Engineering	(1)
U.S. Naval Academy Annapolis, Maryland 21402 Attn: Dept. of Mechanical Engineering	(1)
Naval Air Systems Command Jefferson Plaza Washington, DC 20360 Attn: B. Poppert, Code 204E	(1)
Naval Sea Systems Command Crystal City, National Center #3 Washington, DC 20360 Attn: Frank Ventriglio, Code OSR14	(1)
Naval Ships R&D Center Annapolis, Maryland 21402 Attn: Friction and Wear Branch J. F. Dray	(1)
Naval Air Engineering Center Lakehurst, New Jersey 08733 Attn: Mr. P. Senholzi	(1)

Distribution List (continued)

Recipient	Number of Copies
Naval Air Propulsion Test Center Trenton, New Jersey 08628 Attn: Mr. R. Valori	(1)
Naval Air Development Center Warminster, Pennsylvania 18974 Attn: Mr. A. Conte	(1)
National Science Foundation 1800 G Street, NW Washington, DC 20550 Attn: Dr. C. J. Astill	(1)
National Bureau of Standards Washington, DC 20234 Attn: Dr. W. Ruff	(1)
NASA Lewis Research Center 21000 Brookpark Road Cleveland, Ohio 44135 Attn: R. L. Johnson	(1)
Air Force Office of Scientific Research Washington, DC 20333 Attn: Directorate of Engineering Sciences	(1)
Air Force Aeropropulsion Laboratory Wright-Patterson Air Force Base, Ohio 45433 Attn: AFAPL/POD-1, Dick Quigley, Jr.	(1)
Army Research Office Durham, North Carolina 27706 Attn: Dr. E. A. Saibel	(1)
Office of Naval Research Branch Office 1030 East Green Street Pasadena, California 91106	(1)
Assistant Chief for Technology Office of Naval Research, Code 200 Arlington, Virginia	(1)

Distribution List (continued)

Recipient	Number of Copies
Prof. H. S. Cheng Department of Mechanical Engineering Northwestern University Evanston, Illinois	(1)
Crane Packing Company 6400 Oakton Street Morton Grove, Illinois 60053 Attn: Art Zobens	(1)
Sealol, Inc. Box 2158 Providence, Rhode Island 02905 Attn: H. F. Greiner	(1)
Pure Carbon Company St. Marys, Pennsylvania 15857 Attn: R. R. Paxton	(1)
Franklin Research Institute 20th and Race Streets Philadelphia, Pennsylvania 19103 Attn: Harry C. Rippel	(1)
Naval Sea Systems Command Crystal City, National Center #3 Washington, DC 20360 Attn: Code 524, Dick Graham	(1)
Naval Ships R&D Center Annapolis, Maryland 21402 Attn: Al Harbaugh	(1)
Prof. Francis E. Kennedy, Jr. Thayer School of Engineering Dartmouth College Hanover, New Hampshire 03755	(1)
Mr. Clif Mussen PMS 396-223 Trident Submarine Ship Acquisition Project Naval Sea Systems Command Department of Navy Washington, DC 20362	(1)

4-83

DTI